UNIVERSITÉ DU LUXEMBOURG

PhD-FSTM-2022-093
The Faculty of Science, Technology and Medicine

DISSERTATION

Defence held on 29/07/2022 in Esch sur Alzette
to obtain the degree of

DOCTEUR DE L'UNIVERSITÉ DU LUXEMBOURG

EN BIOLOGIE

by

Michela BERNINI
Born on 14 November 1992 in Bergamo (Italy)

MULTI-SCALE CHARACTERISATION OF PARKINSON'S DISEASE DEVELOPMENT IN iPSCs DOPAMINERGIC DIFFERENTIATION

Dissertation defence committee

Dr Alexander Skupin, dissertation supervisor
Associate Professor, Université du Luxembourg

Dr Malte Spielmann
Direktor, Facharzt für Humangenetik, University Medical Center Schleswig-Holstein, Lübeck

Dr Anne Grünewald, Chair
Professor, Université du Luxembourg

Dr Alessandro Prigione
Professor, Heinrich Heine University Düsseldorf

Dr Carole Linster, Vice Chair
Assistant Professor, Université du Luxembourg,

Affidavit

I hereby confirm that the PhD thesis entitled “Multi-scale characterisation of Parkinson’s disease development in iPSCs dopaminergic differentiation” has been written independently and without any other sources than cited.

Luxembourg, _____ _____

Name

Acknowledgements

These PhD years have not only allowed me to experience a time of intense professional growth as a researcher, but they have also helped me develop a new deep awareness of who I am. The good and the bad, the highs and the lows, the feelings of indescribable joy, or misery, brought on by successful, or failed, experiments, the nights and weekends in the lab as well as the amazing fun times spent with an incredible team of wonderful people, they all shaped the person I am today, and inspired me to explore my goals, weaknesses, strength and ambitions. I feel grateful and blessed for everyone who contributed making this unforgettable experience a treasured opportunity for both personal and professional self-improvement.

I want to start by expressing my heartfelt gratitude to Alex, for believing in me from the start and for always making me feel respected, valued and appreciated all along this journey. I will never forget how motivated and protected I felt, both in the good times and the challenging ones. My "obsession for science" with the years blossomed into a true dedication, as a result of having such a motivating, kind and brilliant mentor. Thank you for all the hours you dedicated to me to discuss science, and life!

I also want to say a big thank you to my co-supervisors, Anne and Carole, for always making me feel encouraged in my research and being constructively critical about my progress during these years. Their treasured feedback has provided me a great chance to push beyond my limits, and the pleasant and nice environment they managed to establish during our meetings has always made me feel tremendously motivated and engaged.

Moreover, the support given by the Luxembourg National Research Found, particularly through the PRIDE CriTiCS Doctoral Training Unit, was crucial to make my PhD not only possible, but also exceptionally meaningful. I also want to express the deepest appreciation to the Fondation du Pélican for generously sponsoring my project and enabling me in getting through the uncertainties and troubles of the last, hectic years.

Without my incredible team of colleagues, of course, this journey wouldn't have been even somewhat similar. The passionate, collaborative spirit shared by all of the ICS group members, the diversity of their backgrounds and experiences, as well as their similar view

on life, make this group the best environment and family that I could ever wish to find here in my Luxembourg years. Thank you for the hundreds of insightful scientific chats, for all the times we pushed each other to step outside of our comfort zones and broaden our horizons, and for every wild, crazy moment we shared, which will always be with me.

I'm also extremely grateful for all my extraordinary, eccentric friends, here and around the world, who have shared with me thoughts, music, ideas, doubts, joy, projects, homes, tears, travels, cats, and a myriad of other things. They were there for me during all the changes and challenges of these years, I felt cherished and never alone because of them, and for this they deserve my everlasting love and appreciation.

Without my amazing family, however, who has always supported me and showed an active, genuine interest in my professional development, none of this would have been possible. I would like to thank my beloved parents Daniela and Alessandro for being my first life mentors, and my biggest inspiration. They showed me, first and foremost, that there are no impossible goals and that, with sincere desire and perseverance, we are all capable of achieving and creating amazing things. I consider myself truly lucky and blessed to have them by my side, as well as my incredible and gifted brother Lorenzo, my sweet uncle and aunt Giovanni and Mihaela, and the rest of the family. My grandma Anna, who has been, is and will always be by my side, deserves my sweetest, eternal gratitude.

I love you all so much.

Grazie!

Table of Content

Summary

Parkinson's disease (PD) is a neurodegenerative disease that predominantly affects dopaminergic (DA) neurons, which are progressively lost in the substantia nigra of the midbrain. No cure for PD has been found so far, as the mechanism of onset and progression of this disease remain still elusive. Most of PD cases are thought to be idiopathic, while only a small percentage of patients carry a known disease-related genetic mutation. Although most mutations have been strongly associated with mitochondrial activity, a comprehensive understanding of the underlying mechanisms of disease development is still lacking.

In this project, I addressed this gap by investigating the effect of a PD-related mutation in the PINK1 gene, on the differentiation dynamics of patient-derived induced pluripotent stem cells (iPSCs) into DA neurons to identify early processes of disease development.

For this purpose, I first established an optimised protocol for iPSCs differentiation to generate high-quality DA neurons. Based on the optimized protocol, the early phase of differentiation of a mutation-carrying and matched control cell line was characterized by single-cell RNA sequencing (sc-RNAseq) and complementary bulk proteomics analyses. This dynamic analysis of differentially expressed genes (DEGs) revealed a potential core network of PD development which linked known genetic risk factors of PD to mitochondrial and ubiquitination processes.

Based on these results, I subsequently performed a multiscale analysis of the differentiation processes including sc-RNAseq, proteomics and metabolomics measurements at 7 time points up to day 57 to investigate the establishment of PD phenotypes on the different biological levels. This multi-omics analysis allowed to highlight mechanisms of impaired neuronal development and further highlighted a subset of genes driving neurodegeneration. In particular, the dynamic analysis indicated that PD-related mutations may lead to faster maturation and aging as a potential driver of PD. Furthermore, many of the DEGs converged on mitochondrial activity and neuroinflammatory processes in agreement with the proteomics analysis. A targeted analysis of the metabolomics data supported the evidence of faster maturation of the PINK1 cell line by an earlier increase of mitochondrial metabolism compared to the control condition and indicated metabolic impairment at the later time points of differentiation.

Overall, my thesis provides a rather unique multi-omics data set of DA neuron differentiation and potential new mechanisms of PD development. These findings could eventually pave the way for a more comprehensive perspective on PD and may aid the development of new therapies.

List of Abbreviations

aCGH Array Comparative Genomic Hybridization
ATP adenosine triphosphate
CNS Central Nervous System
CTR Control
DA Dopamine
DAP Differentially Abundant Protein
DEGs Differentially Expressed Genes
ER Endoplasmic Reticulum
ESC Embryonic Stem Cell
ETC Electron Transport Chain
FC Fold Change
IMM Inner Mitochondrial Membrane
iPSCs Induced Pluripotent Stem Cells
L-DOPA L-3,4-dihydroxyphenylalanine
MAD Median-Absolute Deviation
MAM Mitochondrial-Associated Membrane
mDA neuron Midbrain Dopaminergic Neuron
MAO Monoamine Oxidase
MPP Mitochondria Processing Peptidase
MPTP 1-methyl-4-phenyl-1,2,3,6-tetrahydropyridine
MTS Mitochondrial Targeting Sequence
NOX NADPH Oxidase
OMM Outer Mitochondrial Membrane
PARL Presenilin-Associated Rhomboid-Like protein
PCA Principal Component Analysis
PCR Polymerase Chain Reaction
PD Parkinson's disease
PDMS Polydimethylsiloxane
PERK Protein kinase R-like Endoplasmic Reticulum Kinase
PINK1 PTEN-induced Putative Kinase 1
ROS Reactive Oxygen Species
RT-qPCR Quantitative Reverse Transcription Polymerase Chain Reaction
scRNA-seq Single Cell RNA sequencing
smNPCs Small Molecule Neural Precursor Cells
SN Substantia Nigra
TMD Transmembrane Domain
UPR Unfolded Protein Response
WT Wild Type

List of Figures

List of Tables

1. Introduction

1.1 Parkinson's disease: a general overview

Parkinson's disease (PD) is the second most common age-related neurodegenerative disease, affecting almost 10 million individuals worldwide. PD is most likely the consequence of a combination of genetic and environmental insults, as well as their interactions in the framework of brain aging (Chen and Ritz, 2018). In the following sections, I will give first a general overview on PD (Section 1) and subsequently summarize our current understanding of the disease in Sections 1.2 to 1.7 with a focus on the specific aims of the thesis detailed in Chapter 2.

1.1.1 PD pathogenic hallmarks

Only 5-10% of patients have familial Parkinson's disease due to the Mendelian inheritance of various genetic mutations, and common genetic polymorphisms that are believed to contribute to increase PD susceptibility have been discovered in the past few decades (Pang et al., 2019). According to pathological findings, the main symptoms of PD originate from the degradation of dopaminergic neurons in the *substantia nigra pars compacta* (SNpc) of the nigrostriatal pathway, which gradually diminishes during the progression of the disease (Giguère et al., 2018; Novak et al., 2022; Verschuur et al., 2019)[Fig. 1.1].

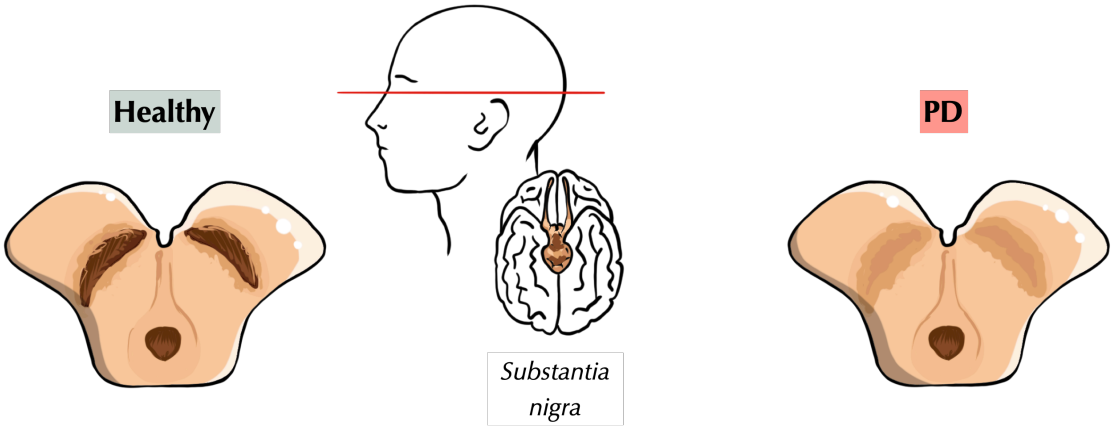

Figure 1.1 *PD is characterized by a diminished substantia nigra of the midbrain.*

On a smaller scale, affected midbrain dopaminergic (mDA) neurons exhibit a reduced release and exchange of dopamine (DA) vesicles. Since dopamine is the leading neurotransmitter for motor functions in the human body, dopamine depletion in the nigrostriatal pathway causes the typical motor symptoms of Parkinson's disease, such as bradykinesia, rigidity, resting tremor, and postural and gait difficulties (Fais et al., 2021)[Fig. 1.2].

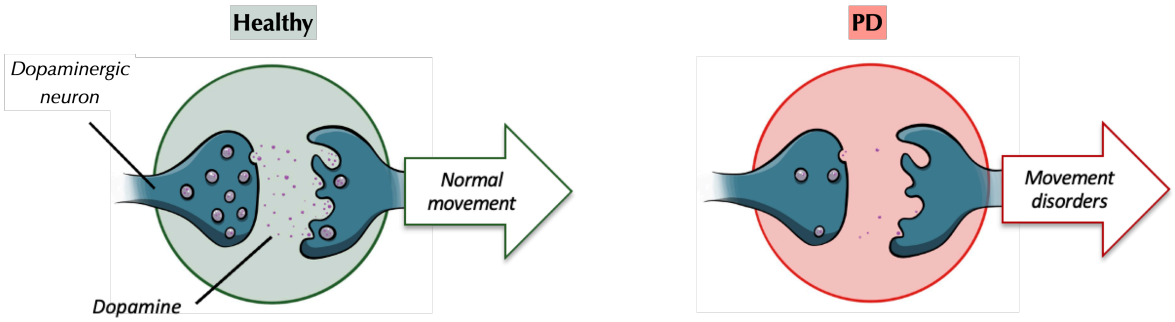

Figure 1.2 *An impaired exchange of dopamine between dopaminergic neurons leads to movement disorders.*

Indeed, motor cortical areas are normally involved in movement planning and execution. To execute smooth and desirable motor tasks, motor cortex areas communicate with deep brain circuits, and one of the fundamental circuits includes a group of nuclei commonly known as the basal ganglia (Mink, 1996). SNpc is a crucial part of the basal ganglia, together with the *globus pallidus externus* and *internus*, the *substantia nigra pars reticularis* and the *subthalamic nucleus* (Singh, 2018). The basal ganglia are critical components of cortical and subcortical circuits, connecting the cortex and the thalamus to form cortico-basal ganglia-thalamic (CBT) neural circuitry (DeLong and Wichmann, 2007). This complex network is made up of numerous loops and connections that converge primarily on two major pathways. These two paths (direct and indirect) arise from two distinct populations of striatal projection neurons, that eventually project to separate nuclei. Surprisingly, the direct and indirect circuits have opposite effects on mobility: the direct pathway stimulates movement, whereas the indirect one inhibits it (Kravitz et al., 2010). Therefore, the loss of nigrostriatal mDA neurons causes the bradykinetic or akinetic features that characterize PD, as indirect pathway inhibition of motor cortex predominates over direct pathway excitation of motor cortex, resulting in pathological global inhibition of motor cortical regions (Singh, 2018). This dopaminergic degeneration is also observed, even if less dramatic, in other brain areas, such as in the hippocampus, the prefrontal cortex and in the amygdala (Ray and Strafella, 2012).

Another fundamental pathological hallmark of PD is the presence of Lewy bodies, which are 8 to 30 mm intracytoplasmic inclusions characteristically found at sites of neurodegeneration. Since these inclusions are majorly constituted by aggregated and misfolded alpha-synuclein protein species, Parkinson's disease is also classified as a Synucleinopathy (Tolosa et al., 2021).

The precise causes and factors responsible for this pathology are still not completely understood. Ageing is considered as the biggest risk factor for PD because it affects many cellular processes that can accelerate or trigger neurodegeneration. However, a combination of both environmental and genetic causes is also believed to influence the disease onset and progression (Pang et al., 2019). Although recreating environmental factors and investigate their impact on the human brain development is rather complex, both causal and protective environmental traits have been associated to PD, as described in Subsection 1.1.3. As already mentioned, only a small percentage of total PD cases are caused by identified genetic mutations (Cherian and Divya, 2020); however, these represent valuable and reproducible experimental models which can clarify the underlying mechanisms of PD. Understanding the effects of different genetic defects could pave the way for a more complete understanding of the disease, potentially advancing hypothesis that could also explain the non-genetic cases and support the identification of personalized medicine approaches and novel therapies. A concise elucidation concerning the main genetic mutations that have been associated so far with PD can be found in Section 1.4.

1.1.2 Epidemiology of PD

Methodological differences between studies make it difficult to directly compare prevalence estimations, but it is largely acknowledged that PD affects 1% of the population above 60 years (Tysnes and Storstein, 2017). Notably, PD is twice as common in men than in women in most populations. This huge imbalance might be due to a protective effect of female sex hormones, sex-associated genetic mechanisms or sex-specific differences in exposure to environmental risk factors (Poewe et al., 2017).

Because the prevalence of PD has more than doubled over the past 30 years, PD is considered one of the leading causes of neurological disability. This rapid spread is thought to be a result of the overall increase of the elderly population, leading to longer disease duration, and of industrialization. Interestingly, the risk of PD is known to be associated with industrial chemicals

and pollutants such as pesticides, metals and various solvents (Abbas et al., 2018; Dorsey et al., 2018a). Therefore, demographic and other potential factors could substantially increase the future burden of PD, which is more and more acquiring the characteristics of a true pandemic, despite being non-infectious (Dorsey et al., 2018b; Morens et al., 2009). PD pandemics extend over large geographic areas and, as mentioned above, PD prevalence is constantly rising in every major region of the world. Moreover, pandemics tend to migrate, and the burden of this disease appears to be shifting following changes in ageing and industrialization. One study has indeed reported that, driven by demographic changes, PD pandemic is expected to move from the West to the East, especially towards China (Dorsey et al., 2007). Like other pandemics, PD is exhibiting exponential growth, and even if some protective factors (described in the next Paragraph) are now known, no individual is utterly invulnerable to the condition.

1.1.3 Environmental factors

In 1983, Langston and colleagues observed a specific form of parkinsonism occurrence in a group of people who used synthetic drugs containing traces of the neurotoxin 1-methyl-4-phenyl-1,2,3,6-tetrahydropyridine (MPTP). They specifically showed akinetic rigid syndrome with or without resting tremor within 7-14 days after the injection (Langston et al., 1983). Pesticides such as rotenone and paraquat were introduced after World War II as there was an urgent need of yielding enough food for a fast-growing population (Bloem et al., 2021). Interestingly, these compounds appeared to have a MPTP-similar chemical structure. This is the reason why, before the 1990s, the most widely accepted scenario was that PD was caused by the exposition to metals, toxins and environmental factors (Blesa and Przedborski, 2014).

MPTP itself is not neurotoxic, although, as a lipophilic compound, it is able to cross the blood-brain barrier. Once in the brain, MPTP is then metabolized to MPDP+ by the flavoenzyme monoamine oxidase B (MAO-B), which is present in the outer mitochondrial membrane in non-DA cells such as serotonin neurons, astrocytes and glial cells (Meredith and Rademacher, 2011). Then, MPDP+ is believed to spontaneously oxidize to the toxic radical 1-methyl-4-phenylpyridinium (MPP+) (Nagatsu, 2002). MPP+ is then specifically taken up by dopaminergic cells through the dopamine transporter (DAT) and can eventually destroy DA neurons by inhibiting their mitochondrial complex I and by generating high levels of reactive oxygen species (Jackson-Lewis and Przedborski, 2008). Exposure to the organochlorine insecticide dieldrin is also believed to represent a strong risk factor for PD. It has been demonstrated that DA neurons exposed to dieldrin present an increased level

of histone acetylation, which eventually leads to apoptotic cell death (Song et al., 2010). This evidence was particularly relevant as it emphasized that epigenetic modifications, induced by chemical exposure, might be involved in the pathogenesis of chronic neurodegenerative diseases (Migliore and Coppedè, 2009).
Accumulating evidence also correlates the risk of developing PD with traumatic brain injuries (TBI), particularly of greater severity. TBI had been already linked to several neurodegenerative diseases, but the strongest of these links appears to be its causative relationship with late onset PD. Following TBI, an acute immune and neuroinflammatory response is normally provoked as a neuroprotective reaction (Brett et al., 2022). Nevertheless, a prolonged state of neuroinflammation is most likely contributing to the course of PD pathogenesis (Delic et al., 2020).

A series of further risk factors for PD have also been identified. One of these, is the usage of methamphetamine, which binds to the presynaptic DA transporter and boosts its extracellular concentration. Importantly, it was shown that these compounds can damage the *substantia nigra* in animal models such as mice and rats, producing a similar phenotype to the one observed in brains affected by PD (Guilarte et al., 2003).
An increased risk of developing Parkinson's disease was also well documented among people with melanoma (Liu et al., 2011), and a correlation was also found with hypertension, diabetes, high cholesterol level and alcohol consumption. Interestingly, an elevated consumption of milk and dairy products is also now thought to be dangerous in this regard. The exact mechanism underlying this association is still unclear, but from multiple cohort case studies it was suggested that the increased PD risk is related to the urate-lowering effects of dairy products (Ascherio and Schwarzschild, 2016). Urate, in fact, was consistently showed to be protecting against DA neuron degeneration, most likely by stimulating Nrf2/antioxidant response. In addition to that, it was shown that an important intake of fonts of urate (such as fructose) reduces the risk of developing Parkinson's disease (Bakshi et al., 2015; Chen et al., 2013).

Among the list of protective factors, tobacco is one of the most discussed ones. It was shown that PD risk decreases up to 70% with increasing duration of smoking in several prospective investigations (Thacker et al., 2007). If this negative association was causal, the fast rise in PD incidence worldwide could also find a reasonable explanation in the statistical observation of the global tendency to smoke less and less (Rossi et al., 2018).
However, it is important to consider that smokers tend to show higher levels of dopamine, as it is involved in the reward mechanism. More specifically, when nicotine attaches to DA neurons, this

bond boosts their neuronal activity and therefore induces a more abundant release of dopamine, which eventually produces a feeling of pleasure and an inclination to repeat the action that led to it. For this reason, dopamine-mediate reward mechanism is thought to compensate the loss of dopamine that is expected when DA neurons are affected by PD.

Interestingly, caffeine consumption seems to protect from PD pathogenesis as well. Caffeine is in fact well-known for its neuroprotective effect in experimental PD models (Xu et al., 2010) by its adenosine receptor antagonist function. Not surprisingly, the negative correlation between a robust physical activity and the risk of Parkinson's disease has also been largely acknowledged from the scientific community (Fang et al., 2018).

1.2 Symptoms, diagnosis and current treatments

1.2.1 Symptoms

Motor symptoms such as bradykinesia, rigidity and tremor are a direct consequence of the progressive loss of mDA neurons, being dopamine the most crucial neurotransmitter coordinating motor control and executive functions in the human body. However, although Parkinson's disease has always been considered as a movement disorder, and clinical diagnosis relies on the presence of bradykinesia and the other motor features, this disease is now associated with many non-motor symptoms that add to overall disability (Poewe et al., 2017). These symptoms include rapid eye-movement sleep behaviour disorder, hyposmia or anosmia, constipation, daytime somnolence, symptomatic hypotension, erectile dysfunction, urinary dysfunction and depression, psychosis, depression, anxiety, fatigue and cognitive decline (Sivanandy et al., 2021; Tarakad and Jankovic, 2017).

Moreover, a recent study monitored for almost 40 years the outcome mortality of a large cohort of PD patients and has shown an additional bigger risk of dying from pneumonia or cardiovascular/cerebrovascular disease, emphasizing the importance of mobilization of PD patients, as one of the main factors leading to pneumonia is immobilization (Pinter et al., 2015).

1.2.2 Challenges in the diagnosis of PD

Since the first description of PD two centuries ago, our understanding of the disease has made huge progresses at different levels, from a more accurate definition of the clinical features and

pathophysiological mechanisms to the characterization of neuropathological hallmarks (Przedborski, 2017). Specific clinical criteria aimed to improve the diagnostic accuracy of PD cases, have been validated over the past 5 years. Nevertheless, PD diagnosis remains suboptimal since PD-associated clinical features often overlap with those of other neurodegenerative conditions (Tolosa et al., 2021).

The diagnosis is now mainly based on brain imaging, neurological signs, and clinical nonspecific clinical findings of rest tremor, cogwheel rigidity, and bradykinesia. However, as the confirmation of the diagnosis can only be obtained through neuropathology, several criteria and specific guidelines have been introduced in the last three decades (Marsili et al., 2018). The recently published criteria by the International Parkinson and Movement Disorder Society (MDS) task force (Postuma et al., 2015) encompass the two main previous sets of diagnostic criteria (United Kingdom PD Society Brain Bank and Gelb's criteria), introducing the use of non-motor symptoms as additional diagnostic features. Based on the assumption that the pathological process of PD may begin in non-dopaminergic structures of the brain or peripheral nervous system, these new guidelines have been implementing the concept of prodromal PD, which is considered to represent a true initial stage of PD. During this phase, non-motor symptoms, such as olfactory dysfunction, constipation, rapid eye movement behaviour disorder and depression, precede the motor signs of PD. For this reason, an early detection of prodromal phase of PD is becoming an important goal for determining the prognosis and choosing a suitable treatment strategy (Marino et al., 2012).
Methods for diagnosing PD are still very limited due to the lack of tissue diagnostic test or other more specific biomarker tests (Rajput and Rajput, 2014). By using neuropathologic findings of PD as the gold standard, Adler and colleagues have estimated only 26% accuracy for a clinical diagnosis of PD in untreated or not clearly responsive subjects, 53% accuracy in early PD responsive to medication (<5 years' duration), and >85% diagnostic accuracy of longer duration, medication-responsive PD, thus confirming the need to find a more distinct tissue or other diagnostic biomarkers (Adler et al., 2014).

1.2.3 Current treatments and clinical trials

Sadly, no cure for PD has been designed so far, but treatments to alleviate symptoms are available and, therefore, to improve the quality of life of PD patients.
Scientific breakthroughs such as the discovery of dopamine's crucial role as a neurotransmitter and its loss in PD patients, led to the development of Levodopa (L-DOPA, L-3,4-dihydroxyphenylalanine)

therapy. This drug was approved by the United States Food and Drug Administration back in 1970 and started to be commercialized 5 years later. Up to date, L-DOPA treatment remains the gold standard therapy for relieving PD symptoms.

L-DOPA is the metabolic precursor of dopamine. Hence, it can be used to restore the proper striatal concentration of dopamine in PD patients (Sharma et al., 2015). In the early stage of the treatment, the beneficial effect of this drug on all the signs and symptoms is undebatable. Nevertheless, it has been demonstrated that long-term use of L-DOPA provokes dramatic side effects that can be perceived as debilitating as PD symptoms themselves. First, this therapy lacks continued efficacy, as it becomes ineffective after 5 years of usage, in average (Nash and Brotchie, 2000). Furthermore, long-term administration of L-DOPA also causes a condition named LID (L-DOPA-induced-dyskinesia), characterized by critical motor complications (Jenner, 2008). Patients can start alternating "on" phases, with severe dyskinesia, and "off" phases, characterized by acute parkinsonian-features (Stocchi et al., 2008). Additionally, dopamine-agonist also cause another side effect, which is impulse control disorder. This psychiatric condition makes patients struggle in resisting resist urges and temptations, which can result in compulsive behaviours, including self-harm (Ephraty et al., 2007).

Because of all these Levodopa-induced dysfunctions, several clinical trials are currently being carried out to find alternative, less impacting treatments. These therapeutic trials are categorized into 15 main types, among which we find dopamine receptor agonists, anti-alpha-synuclein aggregation therapy, cell-based therapy, anti-apoptotic drugs and gene therapy (Prasad and Hung, 2021). In particular, after the identification of several mutations associated to familial monogenic PD, gene therapy gained a lot attention. However, recent studies proved that it can potentially cause adverse effects like inflammation, cancer and adverse immune system reactions (Goswami et al., 2019).

Non-pharmacologic surgical approaches are also possible, such as deep brain stimulation (DBS). DBS is mainly proposed to patients which are not responding to L-DOPA therapy and involves implanting electrodes in the brain to improve PD motor symptoms (Charles et al., 2012), but it is rather expensive and therefore not affordable for all PD patients in less industrialised countries (Dang et al., 2019). Furthermore, unlike pharmacological treatments, whose efficacy has been extensively studied, the effectiveness and long-term result of surgical approaches still remain rather elusive.

Especially because of the rapid rise of the rate of PD incidence, finding innovative, easily accessible and efficient drugs or therapies without severe consequences remains a huge challenge. In this regard, clarifying the molecular pathways behind PD pathogenesis and investigating the causes of the onset and progression of the disease, could allow considering the patient-to-patient variability and pave the way for finding new potential treatments for PD, or even a cure.

1.3 Mechanisms of Pathogenesis

Up to date, the molecular pathogenesis of PD has been associated to various pathways and mechanisms, such as α-synuclein proteostasis, mitochondrial function, oxidative stress, calcium homeostasis, axonal transport and neuroinflammation (Poewe et al., 2017). An overview of the most crucial discoveries and observations which progressively elucidated these mechanisms and their role in PD is provided in the following paragraphs.

1.3.1 Lewy pathology in PD

In 1817, James Parkinson firstly described the symptoms of the 'shaking palsy'. However, a clarification of the anatomical substrate of this condition could only be grasped after one century (Goedert et al., 2013). In fact, Lewy bodies were observed for the first time in 1912 by Friedrich H. Lewy. After a careful postmortem examination of brains of 85 PD patients, he identified these protein aggregates in cell bodies and extensions of neurons, in different brain areas such as the motor dorsal nucleus of the vagus, the basal nucleus of Meynert, the globus pallidus and the thalamus, but surprisingly not in the *substantia nigra* (Rouaud et al., 2021). It was Konstantin Trietakoff in 1919 who found similar inclusions in the substantia nigra, and because they were entirely like those described by Lewy a few years earlier, Trietakoff proposed to name them 'Lewy bodies and neurites' (Duyckaerts et al., 2018). He also observed a severe depigmentation of the area of the substantia nigra; only in 1960 Hornykiewicz indicated the correlation between this loss of dopamine-containing neurons in the substantia nigra and a massive dopaminergic denervation of the striatum, eventually leading to hypertonia and akinesia (Ehringer and Hornykiewicz, 1998).

1.3.2 Role of alpha-synuclein in PD

During the following decade, the role of alpha-synuclein in PD acquired more and more attention. First isolated and sequenced in 1988 from the electric organ of the Pacific electric ray *Torpedo*

californica (Maroteaux et al., 1988), this 143 amino acids-long protein is localized in presynaptic regions and in the nucleus, hence the name ‘‘synuclein’’ (SYNapse + NUCLEus). Human and rat homologues of this protein were subsequently sequenced (Maroteaux and Scheller, 1991; Uéda et al., 1993), and few years later the gene encoding alpha-synuclein (SNCA) was the first to be identified as a cause of autosomal-dominant PD (Polymeropoulos et al., 1997). The evidence that this protein is the main component of Lewy inclusions was provided from Goedert's team in Cambridge, which proved the Lewy bodies and neurites from brain of sporadic PD patients were highly immunoreactive for alpha-synuclein (Spillantini et al., 1997). Several neuropathology laboratories observed that Lewy pathology is much more widely distributed than previously thought; in the vast majority of patients, in fact, the inclusions can be found not only in the substantia nigra, but also in numerous structures of the central nervous system, such as in the olfactory bulb and the dorsal motor nucleus of the vagus (Adler et al., 2019; Beach et al., 2009; Braak et al., 2003; Gelpi et al., 2014).

Notably, Lewy bodies are also present throughout the peripheral autonomic networks, including sympathetic/parasympathetic ganglions (Braak et al., 2007), sympathetic innervation of the salivary glands (Beach et al., 2016; Del Tredici et al., 2010), autonomic innervation of heart and skin (Gelpi et al., 2014; Ikemura et al., 2008), and the enteric nervous system (Annerino et al., 2012; Lebouvier et al., 2010). This widespread neuroanatomical distribution of Lewy pathology could likely explain the non-motor and non-dopaminergic symptoms of PD (Adler and Beach, 2016).

Until now, the exact physiological functions of alpha-synuclein remain elusive, but it is thought to play a role in the regulation of neurotransmitter release, synaptic function and plasticity (Burré et al., 2018; Lashuel et al., 2013). Although alpha-synuclein is primarily monomeric in solution, it tends to aggregate in amyloid structures, starting from oligomers to fibrils and eventually into Lewy bodies (Wood et al., 1999); this aggregation can be triggered, for example, by overproduction of the protein, by defects in protein degradations or by mutations or truncations in the SNCA gene.

Originally, alpha-synuclein was thought to be only intracellular, but a first study carried out in 2005 showed that this protein can be secreted in cultured neuronal cells via unconventional exocytosis (Lee et al., 2005). This secretion was observed to occur also *in vivo* as alpha-synuclein was found in human plasma and cerebrospinal fluid (El-Agnaf et al., 2003). Another crucial remark for clarifying the pathogenesis of PD was published from Li and colleagues, who observed PD patients with long-term survival of transplanted foetal mesencephalic dopaminergic neurons: these hosts developed alpha-synuclein-positive Lewy bodies in the grafted neurons, implying that the Lewy inclusions (and therefore PD) can propagate from host to transplanted neurons (Li et al., 2008). Demonstrating this prion-like behaviour of alpha-synuclein became of vast relevance in the scientific community. It has

been shown that the accumulation of pathologic alpha-synuclein in the neurons is eventually causing a decrease in synaptic proteins, progressive impairments in neuronal excitability, and, ultimately, cell death (Volpicelli-Daley et al., 2011). Additional studies confirmed that alpha-synuclein has the ability to propagate the aggregation process between cells and tissues both *in vitro* and *in vivo* (Arotcarena et al., 2020; Masuda-Suzukake et al., 2013; Recasens et al., 2014).
In order to clarify the process of the alpha-synuclein propagation and consequently PD progression, Braak and colleagues proposed the dual-hit hypothesis, a theory which relies on the assumption that alpha-synuclein's misfolding and aggregation may in a first stage occur in the enteric nerves terminals and then spread through the vagus nerve (Braak et al., 2006). The second stage of the spread would then involve regions of the medulla and pontine tegmentum, then midbrain and basal forebrain would get affected (Stages 3 and 4) and eventually the propagation would reach the cerebral cortex in Stages 5 and 6. This assumption would also provide a mechanistic plausibility for a gut-to-brain transmission of alpha-synuclein pathology (Steiner et al., 2018).

1.3.3 Complex I deficiency, mitochondrial and oxidative stress

After the first identification of a mitochondrial defect in the *substantia nigra* of PD patients (Schapira et al., 1990), numerous studies have indicated that there is about a 35% complex I deficiency in PD substantia nigra (Dexter et al., 1994). Multiple proofs that a decrease in the complex I activity in this region is also accompanied by a severe oxidative stress damage were published in the next few years (Floor and Wetzel, 1998; Yoritaka et al., 1996). Oxidative stress is also associated with several other neurodegenerative disorders, such as Alzheimer's and Huntington's diseases and amyotrophic lateral sclerosis, despite they exhibit distinct pathological and clinical features, showing that it is a common mechanism contributing to general neurodegeneration (Andersen, 2004). Further studies have highlighted the presence of complex I deficiency in platelets mitochondria of PD patients (Benecke et al., 1993; Krige et al., 1992), enforcing the hypothesis that both mitochondrial dysfunction and oxidative stress are both triggering the cascade of events leading to PD pathogenesis (Beal, 2005; Parker et al., 2008).

1.3.3.1 Oxidative stress

Oxidative stress is defined as a disequilibrium between the levels of reactive oxygen species (ROS) produced and a biological system's ability to detoxify the reactive intermediates, resulting in a dangerous state that can contribute to cytotoxicity (Dias et al., 2013). The critical role of ROS in Parkinson's disease can be explained by the fact that the brain alone consumes about 20% of the

body's oxygen supply (Johnson et al., 2012), primarily from neurons and glial cells, and that a significant portion of this oxygen is converted to ROS with the mitochondrial electron transport chain (ETC) being the major contributor (Dumont and Beal, 2011; Yan et al., 2013). Monoamine oxidase (MAO), NADPH oxidase (NOX) and various other flavoenzymes are considered other important sources of ROS. It was proved that these reactive species are significant contributors to DA neuronal loss because they are produced in huge amount during the process of dopamine metabolism, and because there the substantia nigra presents high levels of iron and calcium, and low glutathione (GSH).

1.3.3.2 Mitochondrial dysfunction

A breakthrough for the progress of investigation of PD underlying molecular mechanisms occurred when it was observed that exposure to MPTP is causing rapid-onset of PD like symptoms, linking for the first time this disease with mitochondrial dysfunction (Gundogdu et al., 2021; Langston et al., 1983). Mitochondria are dynamical organelles which play a central role in energy generation despite being also closely involved in calcium homeostasis, stress response and cell death regulation.

The inner membrane of the mitochondria is composed of five enzymatic complexes: complex I (NADH dehydrogenase-ubiquinone oxidoreductase), complex II (succinate dehydrogenase-ubiquinone oxidoreductase), complex III (ubiquinone-cytochrome c oxidoreductase), complex IV (cytochrome c oxidase) and complex V (ATP synthase). These transmembrane complexes are all involved in the ETC and support the transfer of electrons from NADH and FADH2 to molecular oxygen, by creating a proton gradient across the mitochondrial membrane that ultimately drives the synthesis of ATP (Kühlbrandt, 2015). Complex I catalyses the first step in the ETC by oxidizing NADH and, as well as complex III and IV, is involved in the generation of the transmembrane electrochemical gradient itself (Brandt, 2006; Crofts, 2004; Johnson et al., 2021). Differently, complex II does not contribute to the proton gradient but links the TCA cycle to the ETC, as it releases electrons to complex III through ubiquinol (Votyakova and Reynolds, 2001). Finally, complex V acts as an ion channel that creates a proton flux back to the mitochondrial matrix where the loss of potential energy is transferred to the phosphorylation of ADP into ATP. As mentioned above, the ETC represents the major source of ROS in the mitochondria: during the process, in fact, superoxide anion is also produced (Turrens, 2003).
Mitochondrial dysfunction was first linked to Parkinson's disease after the discovery of MPTP-induced parkinsonism in some drug users (as described in detail in Subsection 1.1.3 about

environmental factors). MPP+ is a substrate for the dopamine transporter and is selectively taken up by dopaminergic neurons, where it inhibits complex I of the mitochondrial electron transport chain (Vila and Przedborski, 2003). Besides this effect, gene expression profiling in Parkinson's disease dopaminergic neurons revealed down-regulation of genes encoding mitochondrial proteins, providing further evidence of mitochondrial dysfunction (Elstner et al., 2011). In conclusion, it is widely accepted that mitochondrial functions are severely impaired in Parkinson's disease at multiple levels, ranging from organelle biogenesis to mitochondrial fusion/fission to mitophagy.

1.3.4 Ubiquitin-proteasome system (UPS)

Cells need to degrade all the damaged proteins which are not functioning properly. The ubiquitin-proteasome system (UPS) is the main pathway through which they can perform this task (Olanow and McNaught, 2006). Under physiological conditions, the ubiquitin-proteasome system is expected to recognize and ubiquitinate these abnormal proteins, thus targeting them for a definitive proteasomal degradation. The whole process requires of course an important amount of energy, both for the ubiquitination and for the protein disruption itself (Bragoszewski et al., 2017). Disorders in this balance due an excess of unwanted proteins, an inefficient protein degradation or maybe because not enough energy is available, leads to a state called proteolytic stress (Alfred L. Goldberg, 2003; McNaught et al., 2003). This becomes extremely relevant when it comes to oxidative stress, as removing unwanted proteins which tend to aggregate could avoid leading to cytotoxicity. Mutations in the genes *Parkin* and for ubiquitin carboxy-terminal hydrolase L1 (*UCH-L1*) have been associated to PD suggesting that UPS plays a crucial role in PD. Moreover, it was shown that UPS is involved in the degradation of defective mitochondria and could be therefore essential for minimizing the production of ROS (Collier et al., 2011).

1.3.5 Neuroinflammation

Recent studies showed that neuroinflammation is also a relevant feature of Parkinson’s disease and an essential contributor to pathogenesis. This hypothesis was reinforced by genome-wide studies which revealed that PD-associated genes, for example *LRRK2* (which is involved in autophagy by immune cells), often encode for proteins expressed in immune cells and involved in immune regulation (Pierce and Coetzee, 2017). Furthermore, it was shown that systemic inflammation

displays elevated proinflammatory cytokines, which appear to be related to the severity of motor symptoms (Williams-Gray et al., 2016).

Interestingly, the gastrointestinal tract has attracted a lot of attention among all the organs affected by neuroinflammation in PD. In fact, pro-inflammatory cytokines and glial markers, revealing enteric inflammation, are found in increased amount in colon biopsies from PD patients in respect to healthy controls (Devos et al., 2013). Further epidemiological studies have reported that patients with inflammatory bowel disease are statistically more exposed to develop PD. For example, a specific polymorphism in the *CARD15* gene, associated to Chron's disease, is also over expressed in PD patients (Bialecka et al., 2007). Furthermore, *LRRK2* (a PD-associated gene) has been identified as an important susceptibility gene for Chron's disease (Hui et al., 2018), and it was also reported that this disease is also exhibiting an over expression of enteric alpha-synuclein (Prigent et al., 2019). Hence, the hypothesis that systemic inflammation, more precisely chronic gut inflammation, could modulate pathogenesis in PD (Johnson et al., 2019; Rolli-Derkinderen et al., 2020).

All factors that have been identified as triggers, facilitators or aggravators of PD pathogenesis could partially clarify the clinical variability of PD cases, particularly referring to disease severity and phenotype, as well as the efficiency of treatments. This would support the recently proposed scenario that depicts PD not as a single, uniform disease, but rather as the combination of different but related diseases (Berg et al., 2014).

1.3.6 Selective vulnerability of mDA neurons

As illustrated above, there is now little doubt that alpha-synuclein spreads from neuron to neuron in different region of the body, most likely starting from the gut, and that it behaves like a prion. However, it is currently debated if this spread is sufficient to explain onset, progression, and clinical symptoms of PD, since up to date we are still lacking an explicit correlation between Lewy pathology, neuronal dysfunction and neuronal loss (Ma et al., 2019). A complementary mechanism, which was already proposed some years ago (Braak et al., 2004), could be that the formation of Lewy inclusions is driven by cell-autonomous mechanisms and not only by a single propagated pathogen (Engelender and Isacson, 2017; Surmeier et al., 2017a). This would lead to the conclusion that PD would not only evolve following the alpha-synuclein propagation but would also be influenced by the degeneration of specific, more sensitive regions of the brain. It was observed that the classes of neurons mostly affected in PD share a set of anatomical and physiological attributes. They have elongated, unmyelinated axons with many ramifications, they undergo an intense metabolic activity, and they are characterized by a weak capability to buffer the excess of

intracellular calcium (Surmeier et al., 2017b). Such specific phenotype is displayed in neurons of the dorsal motor nucleus of the *vagus, locus coeruleus* and the *substantia nigra pars compacta*, and appears to be particularly susceptible to neurodegeneration. Several theories have been proposed in order to find out why a longer and more branched axon makes neurons more vulnerable (Hunn et al., 2015). It is thought that this morphological phenotype can be associated with exceptionally high demands in ATP, which is needed in huge amount for supporting neurotransmission along abundant and complex axonal structures (Guzman et al., 2010). Moreover, it was shown that alpha-synuclein can accumulate more abundantly in unmyelinated axons, which are therefore more vulnerable to neurodegeneration rather than myelinated ones (Orimo et al., 2011; Sulzer and Surmeier, 2013). Recent screen studies furtherly confirmed that genes associated with alternations in neuroanatomy may significantly boost DA neurons vulnerability (Davis et al., 2021). Interestingly, it was also experimentally proven that the level of mitochondrial oxidative stress is directly proportional to the size of the arbor (Pacelli et al., 2015).

In conclusion, it is known that these cells have a large and complex axonal architecture and a pacemaking activity, which puts them under an extreme bioenergetic demand (Pissadaki and Bolam, 2013). This energy is needed for fulfilling different tasks, such as propagation of action potentials, synaptic transmission, and maintenance of a proper membrane potential.

1.3.7 Ageing

Ageing is considered the main risk factor for PD, as the occurrence of the disease increases exponentially above the age of 65. It is thought to be a rather stochastic process that can lead to accumulation of unrepaired cellular damage and to the weakening of compensatory mechanisms and cellular repair machineries (Kirkwood, 2003). It is reasonable to think that, with ageing, misfolded pathogenic proteins can in fact aggregate, until the threshold to incur neuronal damage is reached. Moreover, there is a physiological age-associated impairment of mitochondrial functions needed to protect the cell against cell damage, which can eventually lead to ROS production (Hindle, 2010).

Besides these more general aspects, recent reviews have specifically investigated the role of ageing in the selective vulnerability of mDA neurons in the *substantia nigra* (Reeve et al., 2014). As a result, high levels of mitochondrial DNA deletions have been found in these neurons when affected by PD, together with mutant forms of subunits of the electron transport chain which of course intensifies ROS production (Park and Larsson, 2011).

1.4 Genetics of PD

Following the identification of mutations in the alpha-synuclein encoding gene *SNCA* in 1997 (Polymeropoulos et al., 1997), genetic studies have led to the identification of several more genes involved in familial monogenic forms of PD, which account for 3-5% of PD cases; these genes have all been assigned a PARK number (*PARK1*, *PARK2*, etc) in order of their discovery. Age of onset (early- vs. late-onset PD), family history (familial vs. sporadic PD) and the existence of pathogenic mutations (monogenic vs idiopathic PD) are all common classification variables for PD (Day and Mullin, 2021). Up to date, 20 genetic loci have been associated to PD development (Blauwendraat et al., 2020), including the autosomal dominant alpha-synuclein (*SNCA*) and leucine-rich repeat kinase 2 (*LRRK2*), and the autosomal recessive *Parkin*, PTEN-induced putative kinase 1 (*PINK1*) and *DJ-1*. Many of these mutations have been unequivocally linked to impairments in mitochondrial homeostasis, more specifically in the regulation of mitophagy and electron transport chain. This observation emphasised the importance of mitochondria in PD neurodegeneration. The most recent identification of PD genes, such as DnaJ Heat Shock Protein Family Member C6 (*DNAJC6*) and *SYNJ1*, revealed that also vesicular traffic and endosomal pathway are critically involved in the progression of the disease (Cao et al., 2017; Sanchiz-Calvo et al., 2022). More details about PD-associated genes will be illustrated in the following paragraphs, with a focus on PINK1 which I mainly focused on during my PhD project.

1.4.1 PINK1 and Parkin

PINK1 (PTEN-induced putative kinase 1, identified under the name *PARK6*) is a tumour suppressor gene and was first noticed in 2001 when Unoki and Nakamura described its role in ovarian cancer (Unoki and Nakamura, 2001). Soon after its discovery, it got associated to numerous PD familial case studies (Valente et al., 2004, 2002, 2001). Mutations affecting this gene, which is localized on chromosome 1, represent the second most frequent cause of autosomal recessive early-onset PD after *Parkin* (a cytosolic E3 ubiquitin ligase, named *PARK2*), being associated to 1-9% of all genetic cases and to 15% of all early-onset cases (Klein and Schlossmacher, 2007).

Numerous mutations in *PINK1* have been reported, most of which are located in the protein kinase domain (Kawajiri et al., 2011). To date, 151 *PINK1* mutation loci have been identified and most of these reduce allelic expression, causing therefore haploinsufficiency or the protein which then impairs mitochondrial function (Grünewald et al., 2007; Kasten et al., 2018).

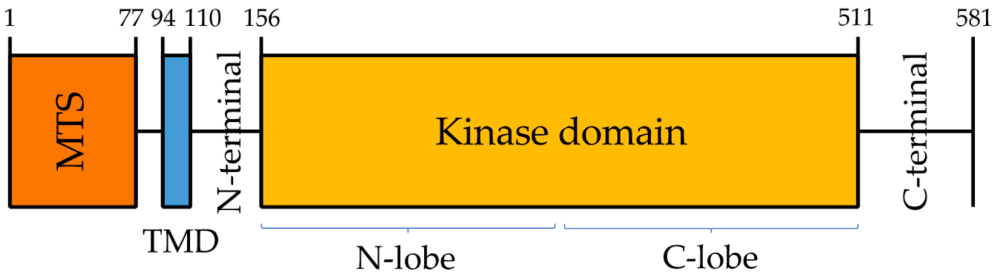

Figure 1.3 *Schematic representation of the domains of PINK1 gene (581 amino acids): mitochondrial targeting sequence (MTS, in orange) and transmembrane domain (TMD, in blue) (Vizziello et al., 2021).*

PINK1 encodes for a 581 amino acid-long protein kinase which is mainly localized in mitochondria [Fig. 1.3]. There, together with *Parkin*, coordinates a crucial feed-forward signalling pathway that supports the removal of damaged mitochondria via autophagic targeted digestion, a process called mitophagy (McWilliams and Muqit, 2017)(see paragraph below for details on the molecular mechanism).

As more than 130 mutations have been identified so far in patients with early onset PD, also *Parkin* is considered a hot spot for different signalling pathways associated to PD pathogenesis.

Aside from their essential role in mitophagy regulation, both *PINK1* and *Parkin* are known to prevent cell death in neurons which are exposed to different stress conditions (Voigt et al., 2016; Winklhofer, 2014). As an example, *PINK1* overexpression leads to a reduced toxin-induced cell death confirming the hypothesis of its pro-survival role (Klinkenberg et al., 2010).

1.4.2.1 PD and mitochondrial impairment: the PINK1/Parkin axis

As extensively described in the previous paragraphs, mitochondrial dysfunction plays a fundamental role in PD pathogenesis (Vizziello et al., 2021). PINK1, together with Parkin, is involved in mitochondrial dynamics and quality control, thus building a signalling pathway that is responsible for selective removal of damaged mitochondria. This supervision is crucial for maintaining a correct mitochondrial homeostasis (Narendra et al., 2008; Yamano et al., 2016). It was observed that DA neurons of PD and aged individuals show dysfunctional mitochondria and accumulate high level of mitochondrial DNA deletions (Bender et al., 2006).

In healthy mitochondria, a repression of the PINK1 protein occurs, because when it translocates to the inner mitochondrial membrane (IMM) its two domains MTS (mitochondrial targeting sequence) and TMD (transmembrane domain) [Fig. 1.3] are cleaved off by respectively MPP (mitochondria processing peptidase) and PARL (Presenilin-associated rhomboid-like protein) (Deas et al., 2011; Greene et al., 2012). At this stage, the processed PINK1 moves to the cytoplasm where it gets

degraded by the ubiquitin-proteasome system (Yamano and Youle, 2017). On the other hand, in response to severe stress or depolarization of mitochondria, the IMM can be altered and can prevent the cleavage of PINK1 domains, which therefore accumulates on the outer membrane (OMM). Here, the full-length protein can then form a multimeric structure (called TOM machinery) together with the outer membrane proteins, and eventually phosphorylates to activate its kinase domain (Lazarou et al., 2012). Activated PINK1 phosphorylates Parkin to stimulate its enzymatic functions, and it induces Parkin recruitment towards the OMM (Kondapalli et al., 2012). At the same time, PINK1 starts to phosphorylate ubiquitin itself, which binds to the RING1 domain of Parkin with high affinity, supporting its enzymatic activation (Kondapalli et al., 2012). PINK1/Parkin conjugated work ultimately causes the OMM to be coated with phosphorylated ubiquitin chains, which will finally trigger proteasome machine to start degradation of the damaged mitochondria (Koyano et al., 2014) [Fig. 1.4].

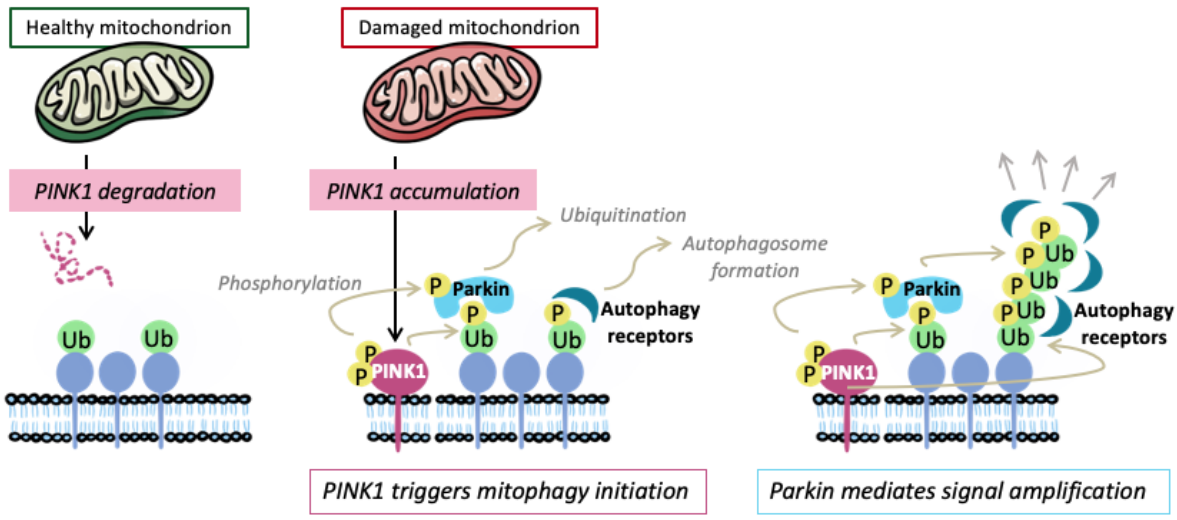

Figure 1.4 *Mechanism of PINK1/Parkin-induced mitophagy.*

Furthermore, a defective PINK1 can also affect complex I activity, causing an insufficiency in ATP production, hence reducing the mitochondrial membrane potential (Morais et al., 2014). This change of potential will push the recruitment of Parkin to the OMM, where it will promote mitophagy by driving the mechanism described above.

Interestingly, both PINK1 and Parkin have been observed to supervise mitochondria quality control also in an alternative way, completely independent from mitophagy. In fact, this process is based on the presence of cargo-selective mitochondria-derived vesicles (MDVs), which protrude from the

OMM and stimulate the degradation of damaged mitochondrial proteins and lipid cargo into peroxisomes and lysosomes (Soubannier et al., 2012).

Given the relevance of mitophagy and mitochondria dysfunction in PD, especially in *PINK1*-associated cases, targeting these PINK1/Parkin-regulated pathways is now considered among the most promising new therapeutic approaches. For example, several small molecules drugs which can enhance mitophagy are currently in preclinical development (Georgakopoulos et al., 2017; Palikaras et al., 2017). On the other hand, it could be possible to stimulate mitophagy also by using inhibitors (such as PTEN-L ones) which are able to prevent dephosphorylation of Parkin and ubiquitin on the OMM (L. Wang et al., 2018). However, an accurate investigation and monitoring of the therapeutic responses of patients exhibiting mitochondrial dysfunction is still needed, to develop therapies which could slow or potentially halt the pathological progression of PD.

1.4.2 PARK7, SNCA, LRRK2, GBA

PARK7 (previously identified as *DJ-1*) encodes for the DJ-1 protein, which has been found to interact with several proteins including tau, Parkin and PINK1 (Rizzu et al., 2004). These three proteins altogether form a ubiquitin ligase complex whose activity is obstructed by pathogenic mutations. The data shows that Parkin, DJ-1, and PINK1 interact within the ubiquitin-proteasome system and play a function in mitochondrial structure maintenance (Xiong et al., 2009).

Alpha-synuclein is a small cytosolic protein, encoded by the SNA gene on chromosome 4 found in several cellular compartments, such as nucleus, mitochondria, endoplasmic reticulum, synaptic vesicles, Golgi apparatus and lysosomes (Somayaji et al., 2021). As illustrated before, mutations and multiplications in *SNCA* gene are associated to the risk of dominantly inherited PD, as they intensify the tendency of alpha-synuclein to form cytotoxic protein aggregates (Ahn et al., 2008). The formation of these aggregates is known to be associated with increased oxidative stress and ROS production. Consequently, aggregated alpha-synuclein could undergo oxidative conjugation with dopamine, causing the accumulation of toxic soluble fibrils in DA neurons (Junn and Mouradian, 2002; Tabrizi et al., 2000). Several *in vitro* experiments have ultimately shown that ROS directly promote alpha-synuclein aggregation, which can then in turn increase ROS production, and therefore building a vicious cycle that eventually drives and aggravates neurodegeneration (Dias et al., 2013).

Mutations in both *LRRK2* and *GBA* have been associated to familial Parkinson's disease, however they are autosomal dominant pathogenic variations with incomplete penetrance. This implies that

they may also be classified as genetic risk factors, with the presence of specific variants conferring an increased chance of developing PD (Day and Mullin, 2021).

Several pathogenic *LRRK2* mutations have been identified so far. *LRRK2* encodes the leucine-rich repeat kinase 2 protein, and its physiological involvement is hypothesized to include autophagy, mitochondrial function, and microtubule stability (Berwick et al., 2019).

GBA gene variants can cause Gaucher disease, a lysosomal storage disorder caused by decreased activity of the *GBA*-encoded enzyme glucocerebrosidase (GCase). Its link to Parkinson's disease was originally recognized in 1996 when patients with Gaucher disease had abnormal levels of Parkinsonian symptoms. Similarly to *LRRK2*, environmental and genetic cofactors are proposed to explain variable penetrance of *GBA* variants (Day and Mullin, 2021).

1.5 Endoplasmic reticulum/mitochondria crosstalk in PD

1.5.1 ER and PD

The Endoplasmic Reticulum (ER) is the cellular compartment responsible for synthesis and post-translational modifications of proteins, and their final delivery to target sites (Perkins and Allan, 2021). Through a rigorous mechanism of proof-control, the correctly folded proteins are transported to the Golgi apparatus, whilst the misfolded ones can be retained for being properly folded or alternatively are targeted for autophagy.

Alterations in the proteins involved in regulating ER structure and activity have already been associated to Parkinson', Alzheimer's disease and amyotrophic lateral sclerosis. In PD, impairments in the ER and in mitochondria, as well as in their crosstalk at the MAM (mitochondrial-associated membrane), are known to be affecting crucial cellular pathways like protein secretion and metabolism [Fig. 1.5]. This can heavily destabilize the capability of the cell to maintain calcium homeostasis and to control oxidative stress levels (Sunanda et al., 2021).

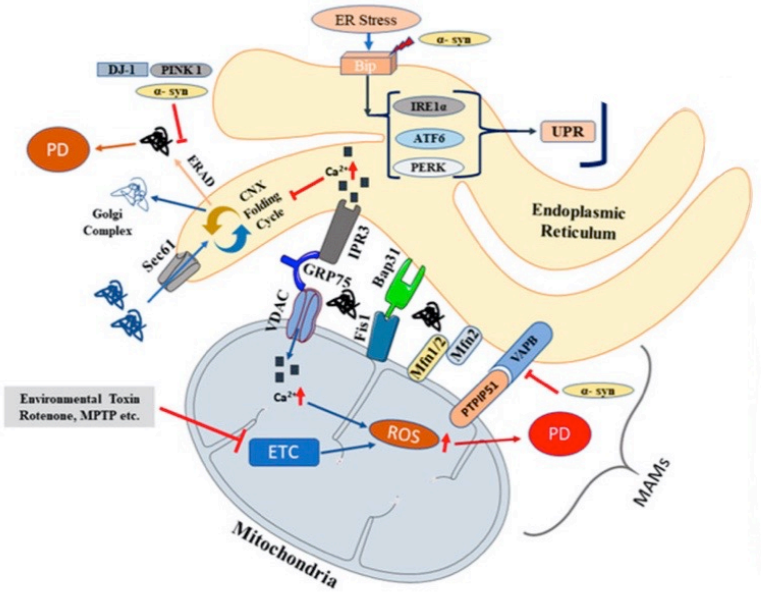

Figure 1.5 *Schematic representation of the contact site existing between ER and mitochondria (modified from (Sunanda et al., 2021)).*

If ER activity is deranged, this can lead to ER stress which eventually triggers the UPR (unfolded protein response) system, a signalling pathway regulated by various ER sensors [Fig. 1.6]. This pathway can halt the translation of misfolded protein, by activation of the ER chaperone proteins which are able to enable their degradation (Wang and Takahashi, 2007).

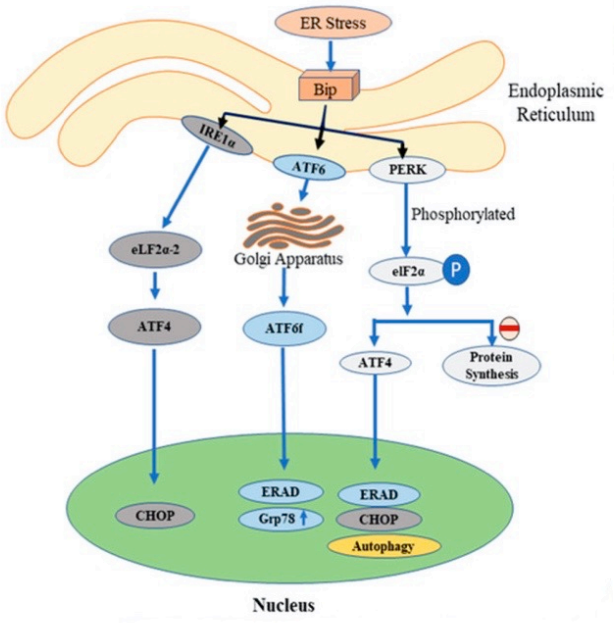

Figure 1.6 *The unfolded protein response (UPR) is activated in response to accumulation of proteins within the ER (modified from (Sunanda et al., 2021)).*

However, an unwanted accumulation of misfolded proteins for an extended period leads obstructs UPR's adaptive response, hence contributing to cellular death.

In 2007, it was observed that post-mortem brain samples of PD patients were strongly immunoreactive to phosphorylated PERK (a crucial component of the UPR system) in the DA neurons of the *substantia nigra* (Hoozemans et al., 2007). Moreover, the neurons which exhibit activated PERK also displayed more alpha-synuclein inclusions. These protein aggregations, in turn, trigger chronic ER stress, showing the dual correlation between these two parameters (Credle et al., 2015) and that PD pathology is associated with dysfunctions in the ER.

1.5.2 MAM in PD

The hypothesis that ER and mitochondria are actively communicating was suggested for the first time already in 1959 (Copeland and Dalton, 1959). Subsequent studies detected that 5-20% of the mitochondrial surface colocalizes with the surface of the ER, and that this apposition is formed by a lipid mitochondrial-associated membrane (MAM) (Rizzuto et al., 1998). The interaction of MAMs between ER and mitochondria helps the movement of biomolecules and supports the crosstalk signalling between the two compartments. The main functions which have been associated to this network, are metabolism of phospholipids and cholesterol, and maintenance of calcium homeostasis within the cell. Therefore, MAMs are believed to play a crucial role in degeneration of DA neurons, since these neurons depend on this structure for exchanging important metabolites and signalling molecules between ER and mitochondria (Arduíno et al., 2009). In particular, it was shown that under stress conditions the ER releases a net flux of calcium towards the mitochondrial matrix. This signalling pathway is particularly relevant as it has been implicated as a key event in many apoptotic biological systems, suggesting that it could induce mitochondria to prompt apoptotic cell death (Hayashi et al., 2009; Pinton et al., 2008). Consequently, alterations in the MAM affects movement of calcium across the organelles hence cause detrimental effects on the survival of neurons (Chan et al., 2007). PD-related genes have been identified as causes of pathological changes in the MAM, including *SNCA*, *DJ-1*, *Parkin* and *PINK1* (Guardia-Laguarta et al., 2015; Konovalova et al., 2015; Liu et al., 2019; Rieusset, 2018; Toyofuku et al., 2020).

1.6 Energy metabolism in PD

Recent research on innovative and successful PD therapies has focused on brain metabolism (Quansah et al., 2018; Yoshino et al., 2018). The rationale that ties neuronal energy metabolism to the regulation of aging of the human brain greatly supports the reason for this search. In humans, the massive metabolic requirement of the brain demands around 20% of the body's energy resources, in a process that is mostly glucose dependent (Braak et al., 2004). The energy generated by glucose oxidation is then utilized to produce ATP, which is the primary energy carrier in all living cells. Nicotinamide adenine dinucleotide (NAD^+) is required for ATP metabolism and hence intracellular energy metabolism. NAD^+ catalyses specific redox reactions during the glycolysis (Yoshino et al., 2018). Provided that cellular NAD+ levels drop with age, maintaining enough NAD^+ production is critical for neuron survival and function (Błaszczyk, 2018; Trammell et al., 2016).

Within the brain, neurons represent about 50% of all brain cells (Azevedo et al., 2009; Howarth et al., 2012). Remarkably, neuronal metabolism is strongly activity dependent and neurons' energy consumption is comparable to the one observed in muscle cells (Ames, 2000; Brown and Ransom, 2007; Sharp et al., 1975). Essential neuronal processes, such as axonal and dendritic transport, intracellular signalling and vegetative metabolism, account for about half of the brain's energy expenditure: consequently, the "baseline" energy demand is already very high. The other half of the energy required is utilised for maintenance of the resting potential in neurons (28%) and astrocytes (10%), while the actual signalling in the form of spike generation consumes 13% of the energy (Lennie, 2003).

Depending on the level of brain activity, neurons alone can consume for 86-88% of the total energy amount, whereas astrocytic processes are estimated to contribute with 12-14% to the overall consumption (Jolivet, 2009). As already mentioned, the human brain consumes staggering amounts of energy to fulfil its functions; it has been assessed that a single, resting neuron can consume even more than 4.7×10^9 ATP molecules per second, an estimation that evidently rises significantly during neuronal firing (Zhu et al., 2012).

Additional studies, which were carried out on macaques, showed that mitochondria in neurons are concentrated in glutamatergic synapses and unmyelinated axons; not surprisingly, glycolytic enzymes were found to be specifically located in nerve endings (Knull, 1978). These observations led to the assumption that neurons are capable to control their energy metabolism at an "exquisitely local level" (Wong-Riley, 1989). Due to their extraordinary morphology, characterised by a very small soma and long processes, the local control is crucial for a precise transport of metabolites, proteins and even whole organelles. Disruptions in this finely orchestrated pattern were shown to be related to various diseases, such as PD.

1.7 PD experimental models

In order to understand the processes underlying the disease and to assess new potential therapies or treatments, several models have been developed during the last decades, based on the main hallmarks of PD. Surely, the emergence of animal models has accelerated the research towards the comprehension of PD pathophysiology. Toxins that selectively target dopamine neurons were initially utilized to generate the first models, the most effective of which used MPTP, a toxin that causes parkinsonism in humans (see Section 1.1.3). Other toxins used on pharmacologic animal models are for example Paraquat, Rotenone and Manganese (Berry et al., 2010; Blesa et al., 2012; Bouabid et al., 2016, 2014). More recently, the discovery of alpha-synuclein aggregates caused by specific genetic mutations resulted in the development of alpha-synuclein transgenic animals such as mice, *Drosophila melanogaster* and primates (Beal, 2001). Feany and colleagues, in particular, created the first Drosophila model that overexpressed both mutant and wild-type alpha-synuclein, and they observed a selective loss of DA neurons as well as neuronal inclusions comparable to Lewy bodies (Feany and Bender, 2000).

Regarding transgenic animals, mice that have been genetically modified to develop loss of DA neurons in the SN are used in many studies (Devine et al., 2011). These mice exhibited the majority of PD features, such as motor impairment and DA neuron degeneration. They can also be used to investigate the involvement of mitochondria in the pathogenesis of this disease (Salari and Bagheri, 2019).

Remarkably, MPTP Parkinson's disease (PD) models in primates have been essential for the investigation of striatal circuitry involved in PD pathogenesis. As mentioned above, the basal ganglia is divided into sub-circuits that also include the thalamus and cerebral cortex. Electrophysiological experiments in the MPTP model have revealed that neurons in output pathways fire abnormally. Motor activity of neurons in the *external globus pallidus* is decreased after MPTP treatment, whereas it is dramatically amplified in the *subthalamic nucleus*, *internal globus pallidus*, and *substantia nigra pars reticulata* (Wichmann et al., 2001, 1999). It was also shown that lesions in these three areas improve motor symptoms of PD in MPTP-treated primates. These findings prompted renewed interest in surgical procedures for Parkinson's disease treatment (Beal, 2001).

In summary, while none of the currently available PD models entirely phenocopy the disorder, they have greatly contributed to our understanding of the disease so far. However, PD is a very complex, multifactorial disease and many different factors concur to its onset and progression. To tackle this complexity, *in vitro* models such as established cell lines and primary cell cultures may be used to recreate a controlled environment. Such experimental setup has the benefit of allowing researchers

to investigate single pathogenic processes and the genes and proteins implicated. The main advantages of cellular models over animal ones are that they generally develop diseases more quickly and at a lower cost (Falkenburger et al., 2016). The fact that they are less ethically objectionable also represents a significant benefit. Furthermore, while it is feasible to investigate a particular cell type to understand its precise contribution to PD pathogenesis, it is also critical to research the interaction between multiple cell types in order to comprehend the underlying mechanisms in a more realistic manner. In conclusion, these models enable for larger-scale testing in far less time, as well as precise genetic or pharmacologic manipulations, even when considerably invasive and impactful.

An example of cellular model to model PD *in vitro* are immortalized cell lines, such as Lund Human Mesencephalic (LUHMES), which were originally generated from a 8-week-old human ventral mesencephalic tissue. LUHMES cells can be differentiate very quickly and quite inexpensively (Lotharius, 2005). When converted into non-dividing neurons, these cells express neuronal markers, elongated neuronal connections, and even electrical properties mimicking the behavior of mDA neurons (Scholz et al., 2011). This method can be especially beneficial for electrophysiological or morphological investigations, rather than for obtaining a more genetic, reliable, patient-based perspective. Indeed, when compared to normal human cells, such cell lines frequently exhibit genetic and metabolic aberrations (Gordon et al., 2014).

Primary cultures have the potential to address many of the challenges associated with cell lines. However, collecting and growing primary dopaminergic neurons from adult/elderly patients' post-mortem brains is challenging. Consequently, primary DA neurons are often taken from embryonic mouse or rat brain tissue, particularly the central midbrain region, because these cells develop fast in culture and generate neurites and synapses (Gaven et al., 2014; Weinert et al., 2015). These cultures are frequently composed of different neuronal cell types, with 5–10% of them being dopaminergic neurons (Falkenburger et al., 2016). Glial cells are frequently the dominant cell type in this system, which turned out to be also beneficial. This method has been used, for example, to explore the therapeutic impact of microglial modulation in a mixed culture with primary neurons, indicating that microglia may influence neuronal function and survival under stressful conditions (Che et al., 2018).

Finally, with the introduction of human embryonic stem cells (ESCs) and, later, human induced pluripotent stem cells (iPSCs), researchers were able to generate several other differentiated cell types keeping the original genotype unaffected (Takahashi et al., 2007; Thomson et al., 1998). In particular, iPSCs can be derived directly from patients, thus providing a source of neurons carrying the same genetic variants associated with pathogenesis in a defined microenvironment. The first

PD-specific iPSC line was established from a sporadic type of the disease in a patient (Park et al., 2008). Since then, iPSC models of Parkinson's disease have been developed from patients with alterations in genes such as *LRRK2*, *PARKIN*, *SNCA*, *GBA*, *and PINK1* . These methods for converting human somatic cells into iPSCs using retroviral transduction and transcription factors like OCT4, SOX2, KLF4 and c-MYC have therefore unlocked new possibilities in the development of both 2D and 3D *in vitro* disease models (Slanzi et al., 2020). Innovative protocols for generating neural tube and neural crest lineages (including motor neurons and midbrain dopaminergic neurons) have been developed using only small molecule neural precursor cells (smNPCs), which are robust and undergo immortal expansion (Reinhardt et al., 2013). However, the smNPC purification steps are relatively energy- and time-consuming and may interfere with the natural gentle transition throughout this developmental stage, pushing the cells to retain residual stemness traits even at later stages. As a result, another differentiation strategy has been proposed that bypasses the intermediate prolonged phase of smNPCs purification (Kriks et al., 2011). More details on the cell culture protocols and their differences are provided in Section 3.5 of Materials and Methods.

2. Aims and Structure of the Thesis

2.1 General aims of the project

Parkinson's disease is a multifactorial, highly intricated disease that predominantly affects dopaminergic neurons in the *substantia nigra* of the midbrain. Despite intensive research over the last decades, our understanding of this disease is still limited and no disease reverting or disease modifying treatment is available. To address this challenge and investigate mechanisms of PD development, I mimicked the developmental process of DA neuronal differentiation during midbrain development in an iPSC model carrying the patient-based homozygous mutation ILE368ASN in the *PINK1* gene. The underlying strategy of this approach is that deep molecular phenotyping including single-cell sequencing, proteomics and metabolomics will thereby reveal essential early processes of disease development which can be followed up to the degeneration of DA neurons. For this purpose, I worked on the following 3 specific aims.

2.1.1 Comparison of DA neuron differentiation protocols

Different protocols have been optimized and published and can be used to differentiate dopaminergic neurons from human stem cells. For this reason, I compared two specific protocols for the “Indirect” (Reinhardt et al., 2013) and the “Direct” Differentiation (Kriks et al., 2011) during the first part of my PhD, as described in detail in Section 3.5. The main goal was to assess whether these two procedures allow to obtain midbrain specific DA neurons with the same phenotypes, and, if not, to identify the one which would be most appropriate to use for the following experiment and analyses which I planned for my research project.

2.1.2 Comparison between control and PINK1 cell lines by single-cell RNA-sequencing at early stages of differentiation

This part of the project was designated to the identification of a core group of genes which are differentially expressed (Differentially Expressed Genes, DEGs) in control and PINK1 cell lines, focusing on the early stages of differentiation (Day 0, 6, 15, 21) [Fig. 2.1]. At those points, the affected cells are not yet expected to display features typically associated to neurotoxicity, but are thought to show impairments in molecular pathways that could eventually lead to primary pathology of PD. This specific analysis was performed on a transcriptomic level, specifically through the Drop-seq single-cell RNA-sequencing and complemented with proteomics data. The results of

this comparison have been published in January 2022 in a paper that I co-authored (Novak et al., 2022).

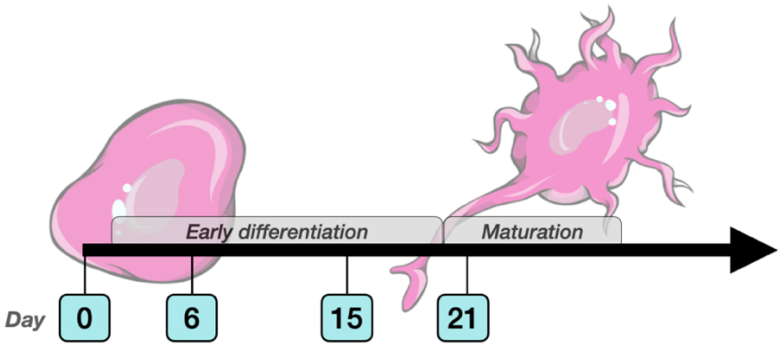

Figure 2.1 *Differentiation set up for single-cell transcriptomics comparison between control and PINK1 at early stages of neuronal differentiation.*

2.1.3 Multi-scale analysis of control and PINK1 mature and aged dopaminergic neurons

To elucidate even further the dynamics which are driving PD progression during neuronal differentiation, I investigated the PD-associated pathways and DEGs which were highlighted in the previous step of the project, but also at later stages of development, including the maturation and ageing phases (Day 0, 8, 18, 25, 32, 37, 57) [Fig. 2.2]. The same two cell lines (control and *PINK1* mutation) were differentiated simultaneously to minimize noise and batch effect during the analysis. For each time point, cells were then collected and, in addition to the transcriptomic sequencing, also metabolomics and proteomics analysis were performed for a broader, multi-scale overview on the differentiation dynamics. This big experimental set up represented the core of my PhD project, hence the results coming from this multi-omics analysis will be included in the first-author paper that I am currently drafting (Bernini et al., in preparation).

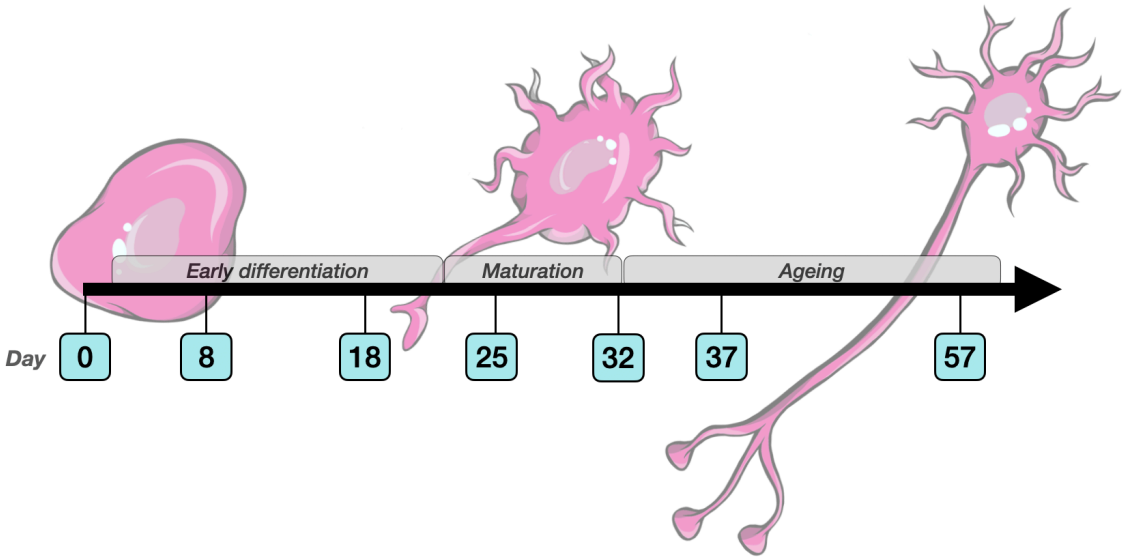

Figure 2.2 *Differentiation set up for multi-scale analysis of dopaminergic differentiation in control and PINK1 cell lines.*

2.2 Structure of the thesis

In the next chapters, I will present all essential material and methods used in my project. In the first section of the Results (Section 4.1), I will present the comparison between the different differentiation methods to address the first specific aim. Following that, in Section 4.2, I will present the findings of my co-authored paper (Novak et al., 2022), the goal of which was (i) to validate the efficacy of the chosen protocol at a single-cell level, (ii) to investigate the differences between the control and PINK1 cell lines in the early stages of neuronal development and (iii) to identify a network of key genes that could potentially interact to produce or aggravate neurodegeneration in Parkinson's disease. In Section 4.3, the results on the multiscale characterization of the differentiation will be presented in relation to the third specific aim. Finally, the results will be discussed in the broader scientific context including an outlook on future work in Chapter 5.

3. Materials and Methods

In the following chapter, I will list the reagents and factors that were used in this project and will describe the methodologies that were applied for the generation of iPSCs cell lines and their multi-scale characterization. Paragraphs in Sections 3.2 to 3.15 are extracted from one of the papers I co-authored (Novak et al., 2022), while the techniques discussed in Sections 3.16 and 3.17 are included in my first author paper (Bernini et al., in progress).

3.1 Chemicals and Reagents

Chemical Description	Manufacturer	Catalog Reference
Accutase	Gibco	A1110501
Advanced DMEM/F-12	Gibco	12634-010
Ascorbic Acid	Peprotech	5088177
ATP	Sigma-Aldrich	A18521VL
B-27 Supplement	Gibco	12587010
BDNF	StemCell Technologies	78005.3
cAMP	Sigma-Aldrich	D0627
CHIR	StemCell Technologies	73044
DAPT	R&D	2634/50
FgF-8b	StemCell Technologies	78008.1
Fibronectin	R&D	1918-FN-02M
Fluo4 Direct Calcium Assay Kit	Gibco	F10473
GDNF	StemCell Technologies	78058.3
Geltrex	Gibco	A1413202
KnockOut DMEM	Gibco	10829018
KnockOut Serum Replacement	Gibco	10828010
Laminin-521	StemCell Technologies	200-0117
LDN193189	StemCell Technologies	72147
GlutaMAX Supplement	Gibco	35050061
mTeSR1	StemCell Technologies	85850
N-2 Supplement (100X)	Gibco	17502001
NEAA MEM	Gibco	11140035
Neurobasal Medium	Gibco	21103049
NGF	Invitrogen	A42578
Poly-L-Ornithin	Sigma-Aldrich	P-3655
Puromorphamine	StemCell Technologies	72204

Puromycin	Peprotech	5855822
Rock Inhibitor	Abcam	ab10129
SAG	StemCell Technologies	73412
Shh	StemCell Technologies	78065.2
SB431542	StemCell Technologies	72234
Synth-a-freeze	Gibco	A1371301
TGFβ3	StemCell Technologies	78131

Table 3.1 *List of reagents used for iPSCs maintenance and neuronal differentiation.*

3.2 Generation and maintenance of iPSC cell lines

Fibroblasts isolated from a 64- year-old male with PD symptom onset at 33 years of age who carried a homozygous mutation ILE368ASN (P.I368N/P.I368N) in the *PINK1* gene were provided from the Coriell Institute (cat. No. ND40066).

Fibroblasts were cultured on gelatin-coated plates (10% gelatin in PBS, coated for 10 min at room temperature) in KO DMEM +10% FBS +1% Penicillin/Streptomycin at standard culture conditions (37 °C, 5% CO^2). Live adherent fibroblasts in culture media were sent to be karyotyped by Cell Line Genetics, Madison, WI, USA and confirmed to have a normal karyotype. The reprogramming of fibroblasts into pluripotent stem cells was done at Yale Human Embryonic Stem Cell Core (New Haven CT) using Sendai virus. The iPSC clone was again analyzed using Array Comparative Genomic Hybridization (aCGH), a high-resolution karyotype analysis for the detection of unbalanced structural and numerical chromosomal alterations and confirmed to be normal. To confirm the presence of homozygous *PINK1* (P.I368N/P.I368N) mutation, PCR was performed using GoTaq (Promega), Cycling: 95oC 30 s, 36x (95°C 15 s, 60°C 20 s, 68°C 15 s), 68°C 5 min. The PCR was confirmed by electrophoresis to produce only one band, the remaining reaction was cleaned using a PCR cleaning kit (Pure Link PCR Micro Kit cat. No. 310050). The PCR fragment was sequenced by Eurofins Genomics.

All the iPSC cell lines were maintained and expanded on Geltrex-coated plates (Gibco, cat. No. A1413302) in mTeSR™1 media (StemCell Technologies, cat. No. 85850) under standard incubator conditions of 5% CO_2 and humidity. The protocol was approved by the Committee on Human Research at the University of California San Francisco. The control stem cell line (WTSIi010-A) was obtained by EBISC (car. No. 66540080) and was reprogrammed from dermal fibroblasts of a healthy male donor aged 65-69 years.

3.3 Analysis of iPSC status and trilineage potential by TaqMan iPSC Scorecard assay

In order to confirm the iPSC status of reprogrammed donor fibroblasts, we performed a TaqMan iPSC Scorecard Assay (Tsankov et al., 2015), which also confirmed the cells' trilineage potential. We followed the protocol described by the manufacturer of the TaqMan hPSC Scorecard Assay (Thermo Fisher Scientific). Stem cells were cultured on Geltrex matrix (Gibco) in mTeSR™1 media (StemCell Technologies) under standard incubator conditions of 5% CO_2 and humidity. On the day of analysis, cells were dissociated using Accutase and pelleted by centrifugation. RNA was extracted using a Qiagen extraction kit and cDNA was synthesized as per Scorecard kit instructions. Embryonic bodies were generated as per Scorecard kit instructions, RNA was extracted, and cDNA synthesized in the same way as for iPSC pellets. The TaqMan hPSC Scorecard Kit 384w plate was amplified using Lightcycler 480 (Roche Diagnostics) and data were uploaded to the hPSC Scorecard analysis software available online from Thermo Fisher Scientific.

3.4 Immunocytochemistry

96-well cell culture plates were seeded with iPSCs, one or two wells per cell line, and the iPSCs were then allowed to form colonies. The adherent colonies were fixed in 4% PFA for 10 min, washed and permeabilized with 0.1% Triton X-100 in 1X PBS for 15 min, then washed and incubated in a blocking solution of 2% BSA in 1X PBS for 1 h. They were then incubated with a primary antibody for POU5F1 (also known as Oct 3/4, Santa Cruz Biotechnology, sc-5279) and TRA-1-60 (MAB4360, Merck Millipore) at 1/500 dilution in blocking solution, overnight at 4 °C. The next day, they were washed three times with PBS and a secondary antibody (AlexaFluor 488, Thermo Fisher) was applied at a 1/1000 dilution in blocking solution and incubated for 1 h at room temperature. The cells were then washed three times with PBS and imaged. Differentiated cells were stained for microtubule-associated protein 2 (MAP2, MAB3418, Merck Millipore), tyrosine hydroxylase (TH, Pel-Freez Biologicals P40101), PAX6 (901301, Imtec diagnostics) at 1/500 dilution, PITX3 (Sigma-Aldrich, HPA044639), LMX1A (Abcam, ab139726) and SLC6A3/DAT (Thermo fisher, PA1-4656). Images were captured using a confocal Zeiss Laser Scanning Microscope 710 with a 20x air objective and processed using ZEISS ZEN Microscope Software. The same preset parameters were used for the acquisition of images. Images were converted from czi-format to tiff-format and scale bars were added using Fiji open-source software (Schindelin et al., 2012).

3.5 Differentiation of iPSCs into dopaminergic neurons

Two different dopaminergic differentiation protocols were used to check the differences in the quality of the DA neurons obtained [Fig. 3.1].

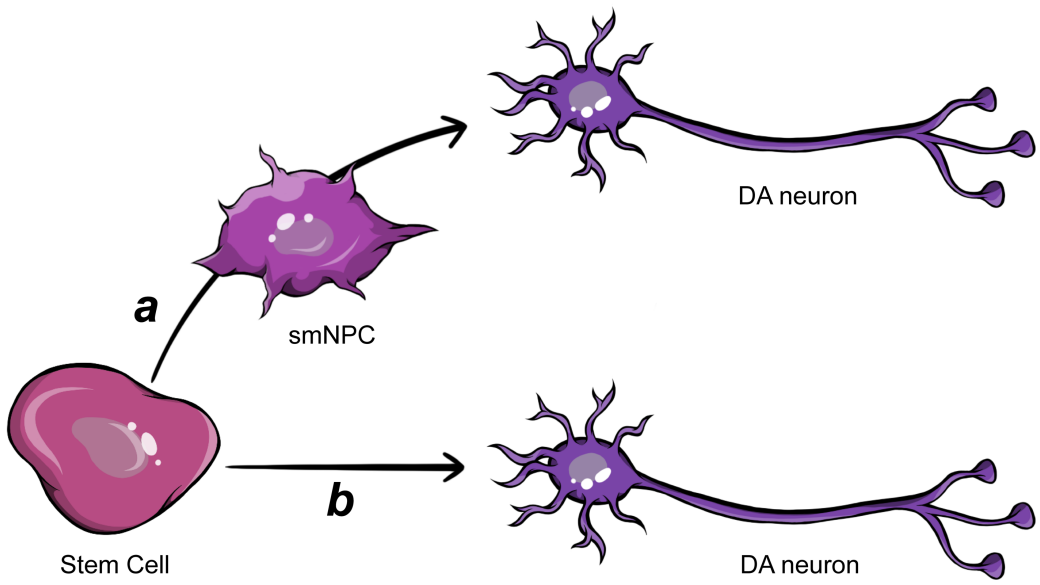

Figure 3.1 *Different approaches for dopaminergic neuronal differentiation: the "indirect" method (**a**) includes an intermediate step of smNPCs (Reinhardt et al., 2013), while the "direct" one (**b**) directly differentiates stem cells into dopaminergic neurons (Kriks et al., 2011).*

3.5.1 "Indirect" Differentiation Protocol

This differentiation was carried out by following the protocol described in (Reinhardt et al., 2013). This method allows to differentiate neuronal cell subtypes starting from human stem cells, by using only small molecules of neural progenitor cells (smNPCs). The protocol is in fact divided into two phases: (i) an initial conversion phase (from iPSCs to smNPCs) followed by expansion/purification of smNPCs, and (ii) the differentiation/maturation phase (from smNPCs to dopaminergic neurons)[Fig. 3.2]. In this protocol, cells were fed every second day. The purification steps were performed by manually picking the colonies which were forming the typical "rosette" structure of cells which are being exposed to neural induction. These colonies were collected and passaged more than 13 times before we could start to differentiate them into dopaminergic neurons.

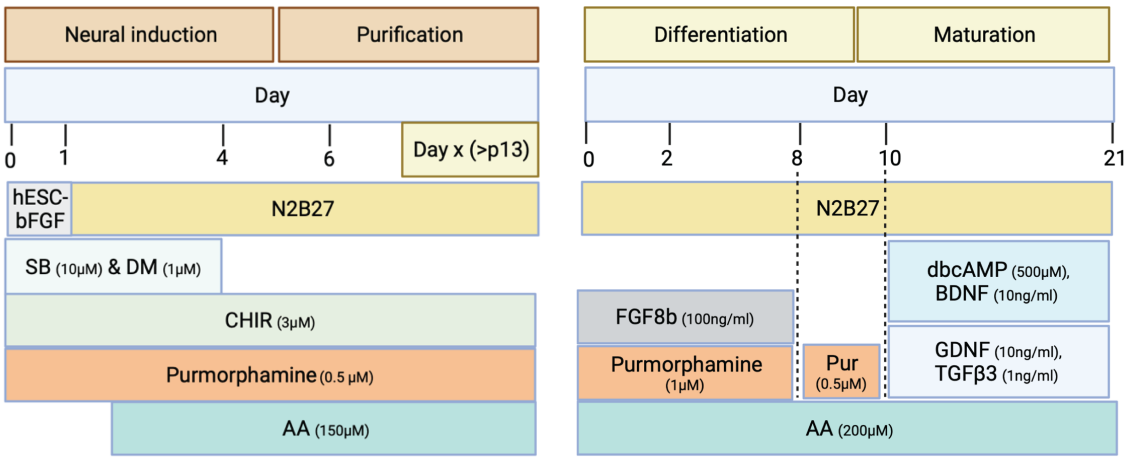

Figure 3.2 *Schematic representation of the Indirect Differentiation protocol described in (Reinhardt et al., 2013).*

3.5.2 "Direct" Differentiation Protocol

The protocol used to differentiate iPSCs into mDA neurons was modified from the Kriks et al. protocol (Kriks et al., 2011). This method allows to directly differentiate human iPSCs into midbrain dopaminergic neurons, without the smNPCs intermediate purification steps. The iPSCs were initially grown to 95% confluence, dissociated using accutase and then seeded in 12-well plates (1.4 x 10^6 cells/well). They were allowed to recover in the presence of ROCK inhibitor for 8 h and then put in mTeSR without ROCK inhibitor for the next 16 h. Subsequently, day 0 media were applied. All the cell lines were differentiated in parallel so that they would be exposed to the same conditions. Different timepoints were generated (from day 0 to day 57) by repeating the differentiation protocol on a later date. Cells were fed with fresh media daily with 3 ml per well using the appropriate media and factor mix described in the differentiation protocol [Fig. 3.3].

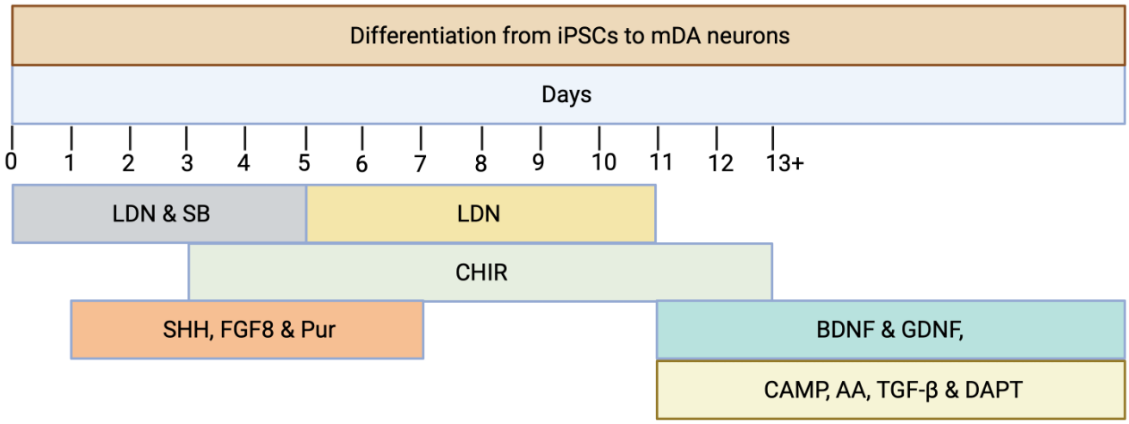

*Figure **3.3**. Schematic representation of the Indirect Differentiation protocol adapted from (Kriks et al., 2011).*

3.6 Real-time quantitative PCR (RT-qPCR) of mDA and non-mDA markers

Total RNA was extracted from a cell pellet of a 12-well plate well using the RNeasy Plus Universal Kit Mini (50) (cat. No. 73404) following the manufacturer's instructions. RNA concentration was determined through absorption at 260 nm using the Nanodrop instrument (Fisher Scientific). The Superscript IIITM First-Strand Synthesis Sys- tem for RT-PCR (Invitrogen) was used to prepare cDNA, using oligo(dT)20 and 2 µg of total RNA as per manufacturer instructions. The cDNA was stored at −20 °C.

Primers were designed using Primer Blast (Ye et al., 2012) and synthesized by Eurogentec Belgium. Standard templates of 90–150 bp in length were generated by PCR, purified using Invitrogen Pure Link PCR Micro Kit (K310050), and their concentration determined using NanoDrop Spectrophotometer. These were then diluted to generate a series of standards of known concentration, from 200 to 0.002 fg µl−1. cDNA levels within samples were determined using quantitative real-time PCR (QRT-PCR) on a Roche Lightcycler 480 using the Maxima® SYBR Green/ROX qPCR Master Mix (2×) (cat. No. #K0223) using absolute quantitation by generating a standard curve based on the standards of known concentration and extrapolating the concentration of the unknowns (samples). The parameters were: initial denaturation at 95 °C for 10 min., followed by 40 cycles of 95 °C for 15 s, 60 °C for 30 s, and 72 °C for 35 s. This was followed by a dissociation curve to confirm that only one PCR product was present. Each absolute concentration of a particular gene was then divided by the absolute concentration of a housekeeping gene, in this case *GAPDH*. In previous experiments, *GAPDH* has been identified as the most stable housekeeping gene in iPSCs and in iPSCs differentiating using our protocol. The values were, therefore, standardized per total RNA of the sample, since 2 µg of total RNA was used for every sample, as well as per expression *GAPDH*.

3.7 Statistics and reproducibility

In RT-qPCR graphs, each timepoint consists of at least three independently differentiated samples, seeded at the same time, hence representing biological replicates. Sample concentration was determined by absolute quantitation, comparing the sample concentration to a known concentration of a standard template identical to the one being amplified. The value was standardized to total RNA, by cDNA synthesizing each cDNA sample from a standard amount of total RNA for each sample. This value was then divided by the concentration of *GAPDH* obtained for that sample,

thus standardizing to *GAPDH* levels and generating a unitless number denoting expression relative to the expression of the housekeeping gene *GAPDH*. *GAPDH* was selected from among several possible housekeeping genes, as it showed the best ability to normalize gene expression in a population of untreated samples. Each of the samples was amplified in duplicates, and each sample value was an average of the experimental duplicate. Standard error was calculated as the standard deviation of the three biological replicates, divided by the square root of the number of samples. To allow for reproducibility through independent analysis, all datasets were made available and can be accessed from repositories listed at (https://r3lab.uni.lu/frozen/cca2-s098).

3.8 Single-cell RNA sequencing

On the day of collection, cells were dissociated using accutase. The single-cell suspension was spun down and cells were washed twice with PBS 2% BSA, then passed through a 40 µm filter to remove larger cell clumps. The sample was then counted, and viability was determined using Vi- CELL XR Cell Counter (Beckman Coulter). Cells were required to have at least a 95% viability. Samples were then diluted in PBS 2% BSA to a final concentration of 190,000 cells/ml. About 3 ml were used for single-cell analysis. Subsequently, cells were processed by the Drop-Seq approach (Macosko et al., 2015; Sousa et al., 2018; Trapnell et al., 2014) and sequenced.

3.9 Microfluidics fabrication for single-cell RNAseq

Microfluidics devices were generated on-site, using the technique described below, which is based on an earlier Drop-Seq protocol (Dirkse et al., 2019; Macosko et al., 2015). Soft lithography was performed using SU-8 2050 photoresist (MicroChem) on a 4" silicon substrate, to generate a 90 µm aspect depth feature. The wafer masks were subjected to silanization overnight using chlorotrimethylsilane (Sigma), before being used for the fabrication of microfluidics. Silicon-based polymerization chemistry was used to fabricate the Drop-Seq chips. In short, we prepared a 1:10 ration mix of polydimethylsiloxane (PDMS) base and cross-linker (Dow Corning), which was degassed and poured onto the Drop-Seq master template. PDMS was cured on the master template, at 70 °C for 2 h. After cooling, PDMS monoliths were cut, and 1.25 mm biopsy punchers (World Precision Instruments) were used to punch out the inlet/outlet ports. Using a Harrick plasma cleaner, the PDMS monolith was then plasma bonded to a clean microscope glass slide. After the

pairing of the PDMS monolith's plasma-treated surfaces with the glass slide, we subjected the flow channels to a hydrophobicity treatment using 1H,1H,2H,2H-perfluorodecyltri-chlorosilane (in 2% v/v in FC-40 oil; Alfa Aesar/Sigma) for 5 min of treatment. Excess silane was removed by being blown through the inlet/outlet ports. Chips were then incubated at 80 °C for 15 min.

3.10 Single-cell isolation and RNA capturing

We determined experimentally that, when using the microfluidics chips, a bead concentration of 180 beads/µl is optimal for an efficient co-encapsulation of the synthesized barcoded beads (ChemGenes Corp., USA) and cells, inside droplets containing lysis reagents in Drop-Seq lysis buffer medium. Barcoded oligo (dT) handles synthesized on the surface of the beads were used to capture cellular mRNA. For cell encapsulation, we loaded into one syringe each, 1.5 ml of bead suspensions (BD) and the cell suspension. Micro-stirrer was used (VP Scientific) to keep beads in homogenous suspension. For the droplet generation, a QX200 carrier oil (Bio-Rad) was loaded into a 20 ml syringe and used as a continuous phase. To create droplets, we used KD Scientific Legato Syringe Pumps to generate 2.5 and 11 ml/h flowrates for the dispersed and continuous phase flows, respectively. After the droplet formation was optimal and stable, the droplet suspension was collected into a 50 ml Falcon tube. In total, 1 ml of the single-cell suspension was collected. Bright-field microscopy using INCYTO C-Chip Disposable Hemacytometer (Thermo Fisher Scientific) was used to evaluate droplet consistency and stability. To avoid multiple beads per droplet, bead formation and occupancy within individual droplets was monitored throughout the collection process. The subsequent steps of droplet breakage, bead harvesting, reverse transcription and exonuclease treatment were carried out as described below, in accordance with the Drop-Seq protocol (Macosko et al., 2015). The RT buffer was premixed as follows, 1× Maxima RT buffer, 4% Ficoll PM-400 (Sigma), 1 µM dNTPs (Thermo Fisher Scientific), 1 U/ml RNase Inhibitor (Lucigen), 2.5 µM Template Switch Oligo, and 10 U/ml Maxima H-RT (Thermo Fisher Scientific). After Exo-I treatment, INCYTO C-Chip Disposable Hemacytometer was used to estimate the bead counts, and 10,000 beads were aliquoted in 0.2 ml Eppendorf PCR tubes. We then added 50 µl of PCR mix, consisting of 1× HiFi HotStart ReadyMix (Kapa Biosystems) and a 0.8 mM Template Switch PCR primer. The thermocycling program of the PCR was 95 °C (3 min), four cycles of 98 °C (20 s), 65 °C (45 s), 72 °C (3 min) and 9 cycles of 98 °C (20 s), 67 °C (20 s), 72 °C (3 min), and a final extension step of 72 °C for 5 min. After PCR amplification, 0.6× Agencourt AMPure XP beads (Beckman Coulter) were used for library purification according to the manufacturer's protocol. The purified libraries were eluted in

10 µl RNase/ DNase-free Molecular Grade Water. We used the Bioanalyzer High Sensitivity Chip (Agilent Technologies) to analyze the quality and concentration of the sequencing libraries.

3.11 NGS preparation for Drop-seq libraries

The 3' end-enriched cDNA libraries were prepared by tagmentation reaction of 600 pg cDNA library using the standard Nextera XT tagmentation kit (Illumina). Reactions were performed according to the manufacturer's instructions. The PCR amplification cycling program used was 95 °C (30 s), and 12 cycles of 95 °C (10 s), 55 °C (30 s), and 72 °C (30 s), followed by a final extension step of 72 °C (5 min). Libraries were purified twice to reduce primers and short DNA fragments with 0.6× and 1× Agencourt AMPure XP beads (Beckman Coulter), respectively, in accordance with the manufacturer's protocol. Finally, purified libraries were eluted in 10 µl Molecular Grade Water. Quality and quantity of the tagmented cDNA library were evaluated using Bioanalyzer High Sensitivity DNA Chip. The average size of the tagmented libraries prior to sequencing was between 400 and 700 bps. Purified Drop-seq cDNA libraries were sequenced using Illumina NextSeq 500 with the recommended sequencing protocol except for 6 pM of custom primer (GCCTGTCCGCGGAAGCAGTGGTATCAACGCAGAGTAC) applied for priming of read 1. Paired-end sequencing of 20 bases (covering the 1–12 bases of random cell barcode and the remaining 13–20 bases of random unique molecular identifier (UMI)) was performed for read 1, and of 50 bases of the genes for read 2.

3.12 Bioinformatics processing and data analysis

The FASTQ files were assembled from the raw BCL files using Illumina's bcl2fastq converter and run through the FASTQC codes (https://www.bioinformatics.babraham.ac.uk/projects/fastqc/) to check for consistency in library qualities. The monitored quality assessment parameters monitored were (i) per-base sequence quality (especially for the read 2 of the gene), (ii) per-base N content, (iii) per-base sequence content, and (iv) over-represented sequences. The FASTQ files were then merged and converted into binaries using PICARD's FastqToSam algorithm. The sequencing reads were converted into a digital gene expression matrix using the Drop-seq bioinformatics pipeline (Macosko et al., 2015).

3.13 Single-cell RNAseq data analysis

The identification of low-quality cells was done separately for each dataset. To select only the highest quality data, we sorted the cells by their cumulative gene expression. Only cells with the highest cumulative expression were considered for the analysis (James and Matteson, 2015). In addition to this filtering, we defined cells as low-quality based on three criteria for each cell. The number of expressed genes must be more than 200 and 2 median absolute-deviations (MADs) above the median; the total number of counts must be 2 MADs above or below the median, and the percentage of counts to mitochondrial genes must be 1.5 MADs above the median. Cells failing at least one criterion were considered as low-quality cells and filtered out from the further analysis. As for the cell filtering, we filtered out low-quality genes, identified by being expressed in less than ten cells in the data. The integration of the filtered matrices of the different datasets was performed using scTransform (Butler et al., 2018) on a Seurat object (Finak et al., 2015) based on the treatment. The final gene expression matrix, which was used for the downstream analysis, consisted of 4495 cells and 39,194 genes with a median total number of mRNA counts of 7,750 and a median number of expressed genes of 3,521. Principal component analysis (PCA) was computed using the 5,000 most variable genes of the integrated data. The clustering of data was performed using Louvain clustering. The resolution of the clustering was selected based on the best silhouette score of the different resolutions (Rousseeuw, 1987). A shortlist of manually curated markers was used to validate the different stages of the differentiation process. We then performed differential expression analysis between the two conditions (control and PINK1) at each timepoint. The differential expression analysis was done using MAST (Finak et al., 2015) (default parameters) on the normalized counts using the total number of transcripts in each cell as a covariate and the Bonferroni correction to correct for multiple hypothesis testing resulting in adjusted P-values (Padj). In addition, we tried to find conserved markers among the different timepoints using MAST again and the total number of transcripts in each cell used as a latent variable. Genes with fold changes of the same sign in the fold change were then identified across the different timepoints and the average fold change was calculated. The genes with average fold change >0.1 and maximum adjusted P-value <0.01 were selected as differentially expressed. The first analysis of pairwise differential expression at each timepoint (adjusted P-values (Padj) <0.01-fold changes (FC) >0.1) was performed to identify genes that were upregulated and downregulated in the PINK1 cell line compared to control (see Results Section 4.2). For the multi-scale analysis (Section 4.3), we applied different FC thresholds (|FC|>0.3 or >0.6) to allow for different scopes of the analyses. This analysis was carried out for all the time points. Then, we used the maximum adjusted P-value in a pairwise combination as an adjusted P-value, and the average fold change that occurred in the

pairwise comparison as fold change threshold hence retained only genes dysregulated in the same direction at all timepoints (Group B). We then took the mean of FC of the different timepoints to reduce the effect of the variability between pairs due to their different differentiation states. The analysis was performed for the four timepoints (iPSCs, D6, D15, and D21), considering only the absolute degree of change in iPSCs (Group C). The analysis was then repeated using only timepoints D6, D15, and D21 (Group D).

3.14 Network analysis

We extracted protein–protein interaction information between the DEGs from STRING (Szklarczyk et al., 2019) and from GeneMANIA (Warde-Farley et al., 2010). We excluded indirect association, such as text mining, co-occurrence, and neighborhood from STRING, and co-expression, colocalization, shared protein domains, and predicted interactions from GeneMANIA, retaining only genetic interactions, pathways, and physical interactions (2,122 interactions in total). We deleted any genes or interactions that were added by these databases, to only focus on DEGs and interactions among them. The network diameter was calculated and betweenness centrality was used to illustrate the relative importance of each node within the network. As a control, we selected the same number of genes at random, using the list of genes detected by our RNAseq analysis, excluding DEGs. This control set did not produce a network and led to a mostly disconnected array of genes. Networks were also generated using the STRING and GeneMANIA inputs independently. We constructed a correlation network based on the correlation of expression of DEGs (p value < 0.05, correlation > 0.1) and identify edges that are common to the two networks. This network consisted of 860 interactions. We next extracted shared interactions of these two networks, which amounted to 297 interactions. To validate the PPI network produced by STIRNGdb (v10), we created 50 PPI (protein–protein interaction) networks using 292 random genes (same as the number of DEGs). We then compared the number of detected proteins, the number of interactions between the genes, and the distribution of the node degrees. We performed the Wilcoxon test to access if the two-degree distributions are different from eachanother in a statistically significant manner, which showed a statistically significant difference ($p = 2.22e-16$).

3.15 Proteome analysis

Cell pellets were lysed in 1% sodium deoxycholate in 50 mM sodium bicarbonate pH8. After sonication, samples were incubated on ice for 30 min and centrifuged at 4 °C for 30 min at 16,000×g. Supernatants were recovered and quantified using PierceTM BCA Protein Assay Kit (23225, Thermo Scientific). Protein extracts (10 µg) were reduced with 10 mM DTT for 45 min at 37 °C, incubated for 15 min at room temperature, then alkylated with 25 mM iodoacetamide for 30 min at room temperature in darkness. Proteins were further digested overnight at 37 °C with 0.2 µg of trypsin/Lys-C Mix (V507A, Promega). Samples were acidified in 1% formic acid and centrifuged for 10 min at 12,000 × g. Supernatants were recovered, and peptides were desalted on Sep-Pak tC18 µElution Plates (Waters, 186002318), dried by vacuum centrifugation, and reconstituted in 25 µl of 1% Acetonitrile/0.05% trifluoroacetic acid. Following quantification by nanodrop, each sample (200 ng) was analyzed by mass spectrometry. The LCMS setup consisted of a Dionex Ultimate 3000 RSLC chromatography system configured in column switching mode. The mobile phases A and B consisted of0.1% formic acid in water and 0.1% formic acid in acetonitrile, respectively. The loading phase consisted of 0.05% trifluoroacetic acid and 1% acetonitrile in water. The LC system was operated with a Thermo pepmap100 C18 (2 µm particles) 75 µm × 15 cm analytical column (loading 5 ul min^{-1}; analytical 300 nl min^{-1}). The loading column consisted of Thermo pepmap100 C18 (3 µm particles) 75 µm × 2 cm. Samples were separated by a linear gradient ranging from 2% B to 35% B 66 min and sprayed into the mass spectrometer using a Nanospray Flex (Thermo Scientific) ion source. MS acquisition was performed on Q Exactive-HF (Thermo Scientific) operated in data-dependent acquisition mode. MS cycle (AGC MS1 3e6; AGC MS2 1e5) consisted of a high-resolution survey scan (60,000 at 200 m/z) followed by the fragmentation of the top 12 most intense peptides at a resolution of 15,000 at 200 m/z. Dynamic exclusion of already fragmented peptide ions was set to 20 s. Analysis was performed with the MaxQuant software package version 1.6.17.0(Cox and Mann, 2008). The minimum ratio for LFQ was set to 2. An FDR <1% was applied for peptides and proteins. A human Uniprot database (July 2018) was used to perform the Andromeda search (Cox et al., 2011). Oxidized methionine and acetylated N-termini were set as variable modifications while carbamidomethylation on cysteine was set as a fixed modification. Peptide tolerance was 20 ppm. MS intensities were normalized by the MaxLFQ algorithm (Cox et al., 2014) implemented in MaxQuant while using the match-between-runs feature.

3.16 Metabolome analysis

For the investigation of metabolic profiles and their potential impairment in Parkinson's disease cell lines, we used the available assays of the metabolomics platform at the LCSB headed by Dr. Carole Linster. This technique is based on liquid chromatography mass spectrometry (LC-MS) metabolomics to describe metabolomic alterations in mDA neurons *in vitro* (Anso et al., 2021). For each condition 3 samples have been analyzed on a Dionex UltiMate 3000 (Thermo Fisher Scientific) coupled to a Q Exactive Orbitrap mass spectrometer equipped with a HESI electrospray ion source (Thermo Fisher Scientific) at 15 °C. Extracellular glucose levels have been analysed by the YSI 2950D (Yellow Springs Instruments) biochemistry analyzer and lactate levels by quantified spectrophotometrically on a TECAN M200 Pro by changes of NADH absorption.

3.17 Live-cell calcium imaging, induction of calcium release and image analysis

For these imaging experiments, I used PhenoPlate™ 96-well microplates (Perkin Elmer, cat. No. 6055300) which are designed for cell culture and imaging with high-content screening systems. Cells were seeded in different concentrations, ranging from 50,000 to 250,000 cells/well, to be able to visualize neuronal structures but also to have a significant number of cells to analyze. To visualize intracellular calcium in my cultures of cells, I stained them by using the Fluo-4 Direct™ Calcium Assay Kit (Invitrogen, cat. No. F10471). The medium was initially removed from the wells, then a solution 1:1 (in this case 100 µL) of fresh medium and Fluo4 solution (according to the manufacturer's protocol) was added; the plates were then let in incubator for 30 to 45 minutes and were then immediately imaged. For images and videos acquisitions, I used the Leica SP8 Lightning super-resolution confocal microscope. During video acquisitions, the cells were perturbed by adding ATP solutions of different concentrations (from 30 µM to 1 mM) to the wells. All the videos were acquired with magnification 40x, emission wavelength 580nm, scan speed 600Hz and by using the filter CS2 UV Optics 1. For the analysis, cells were selected by manually running ROI manager on Fiji ImageJ and .csv files containing the mean of intensities for each single cell were generated (Schneider et al., 2012). Later, the .csv files were uploaded and processed on CaSiAn software (Moein et al., 2018) for manual adjustments of the automatic detection of intensity peaks and for generating the final plots.

4. Results

In this chapter, the main results obtained during my PhD for the specific aims detailed in Chapter 2 will be presented including the comparison of the differentiation protocols (Aim 1), the analysis of the early differentiation phase (Aim 2) and the multi-omics characterization for the long-term differentiation (Aim 3). Paragraph 4.1.3 and Section 4.2 are taken from the paper that I co-authored (Novak et al., 2022). This analysis focused on the early differentiation period and based on this the data and analysis I subsequently performed the core multi-omics experiment, which is described in detail in Section 4.3.

4.1 Comparison of DA neurons differentiation protocols

During embryonic development, different classes of neuronal progenitor cells can be identified in the neural tube where each class undergoes a precise spatio-temporal regulation which will eventually convert those precursor cells into a specific neuronal type. It is known from literature that the classes which are giving rise to midbrain dopaminergic neurons are the one identified as A8, A9 and A10, which are localized in a region called Floor Plate [Fig. 4.1]. The growth factors and regulators which can induce the right differentiation for each class, and their modification over time, have been widely studied and clarified in the last decades (Björklund and Dunnett, 2007).

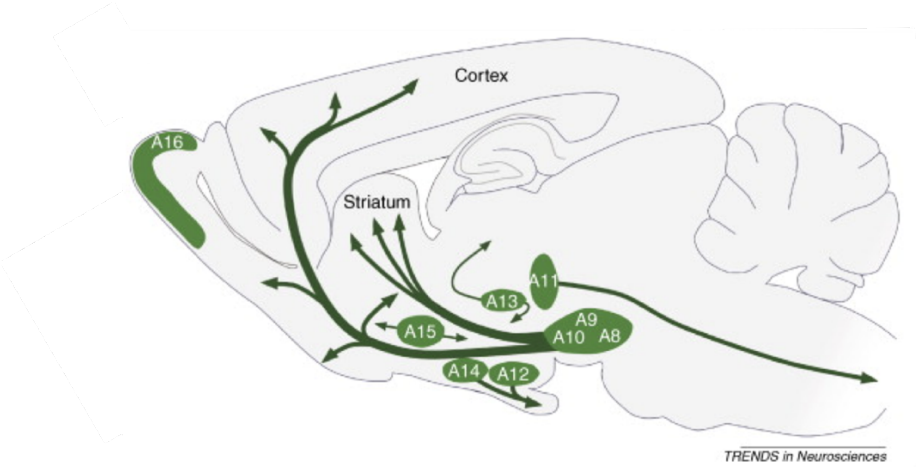

Figure 4.1 *A sagittal view of the adult rodent brain showing that dopamine neurons in the mammalian brain are localized in nine distinctive cell groups, distributed from the mesencephalon to the olfactory bulb; the primary projections of the DA cell groups are shown by the arrows (Björklund and Dunnett, 2007).*

As illustrated in Fig. 4.2, it was observed that PAX6 (Paired box protein-6) plays an important role in morphogenesis. In fact, its presence in the early stages of development will trigger a defined temporal expression of neuronal transcription factors; this cascade of gene expression will determine the growth of DA neurons specifically localized in the retina and in the olfactory bulb, whilst to develop into midbrain DA neurons the progenitor cells need to be completely unexposed to this factor [Fig.4.2].

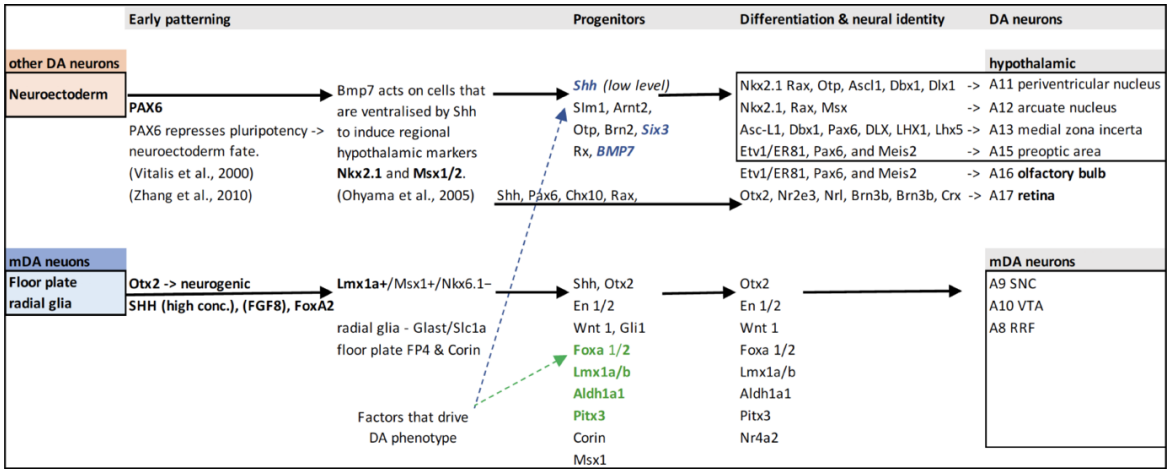

Figure 4.2 *Schematic overview of the temporal expression of neuronal transcription factors (image kindly provided by Gabriela Novak).*

Interestingly, additional embryological studies on the developing neural tube have shown that the region of the Floor Plate is characterized by the absence of PAX6 but also by the expression of Shh (Sonic hedgehog) which are mutually exclusive [Fig. 4.3] (Corbin et al., 2003). This patterning is therefore crucial for the region-specific development of different classes of neurons.

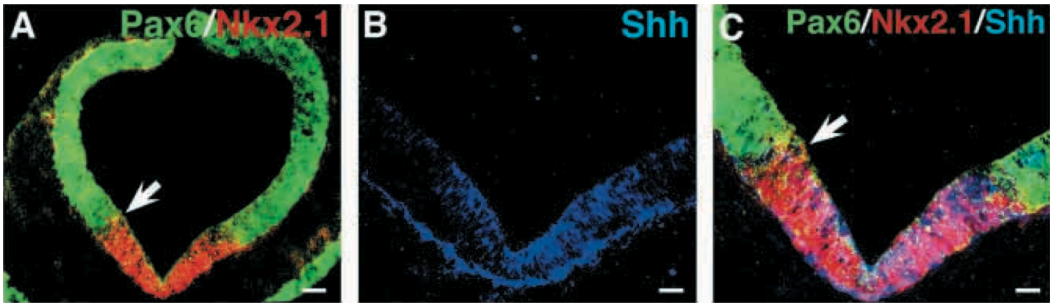

Figure 4.3 *Coronal section of developing neural tube, stained for early neuronal development markers, shows that the region of the Floor Plate is positive for Shh but negative for Pax6 (Corbin et al., 2003).*

For this reason, to assess the quality of dopaminergic neurons in respect to their midbrain characteristics obtained by the Direct and Indirect differentiation methods, I have been differentiating the same iPSC cell line by following both protocols and performed immunocytochemistry stainings on the developing cells at different time points. I checked for the presence of PAX6 and of Tyrosine Hydroxylase (TH), the rate-limiting enzyme that converts tyrosine into L-dopa, which is the dopamine precursor.

4.1.1 Indirect DA neurons are positive for TH and for PAX6 markers

A control cell line has been differentiated accordingly to the Indirect protocol for 30 days starting from smNPCs which had been previously derived and purified. Cells were then fixed and stained for TH and PAX6 at Day 0, 8, 20 and 30.

Cells at Day 0 and Day 8 showed a good PAX6 labelling. Subsequently, at Day 20 and Day 30, cells expressed TH, demonstrating their DA characteristics. The results of the immunostaining are illustrated in Fig. 4.4.

4.1.2 Direct DA neurons show TH labelling but not for PAX6

The same control cell line has been differentiated into neurons following the Direct protocol. Cells were again stained for TH and PX6 at Day 0, 15, 25, 30.

This time, cells at earlier stages of neuronal development (Day 0 and Day 15), did not show any labelling for PAX6. Nevertheless, at later time points (Day 25 and 30), cells expressed TH. The results of the immunostaining are illustrated in Fig. 4.5.

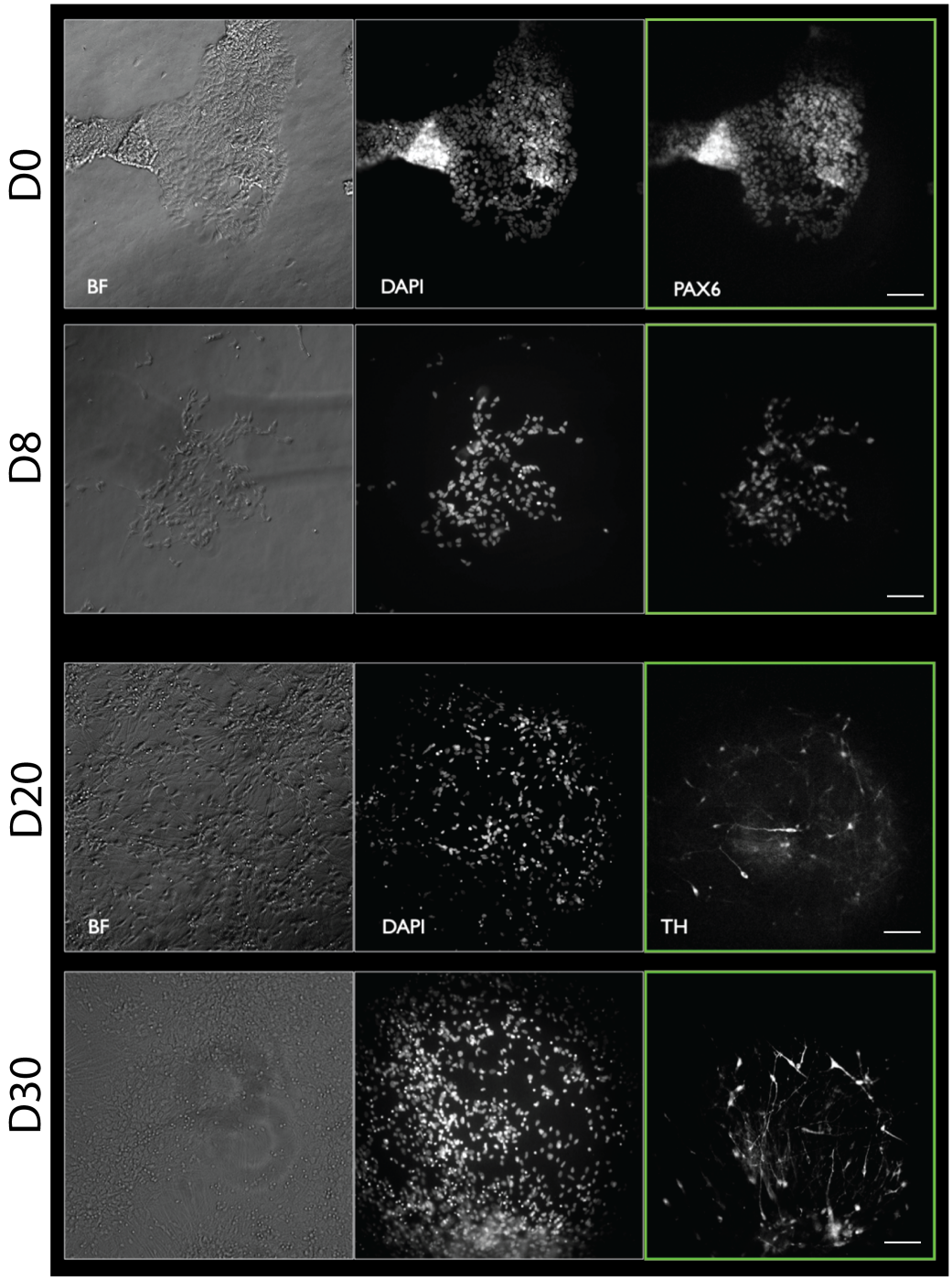

Figure 4.4 *Immunostaining on cells differentiated with the Indirect Protocol at Day 0, 8, 20 and 30. BF: Bright Field. DAPI: 4',6-diamidino-2-phenylindole, showing the nuclei of live cells. PAX6: Paired box protein-6. TH: Tyrosine Hydroxylase, the enzyme that converts L-tyrosine to L-DOPA, the precursor of dopamine. Scale bar: 100μM.*

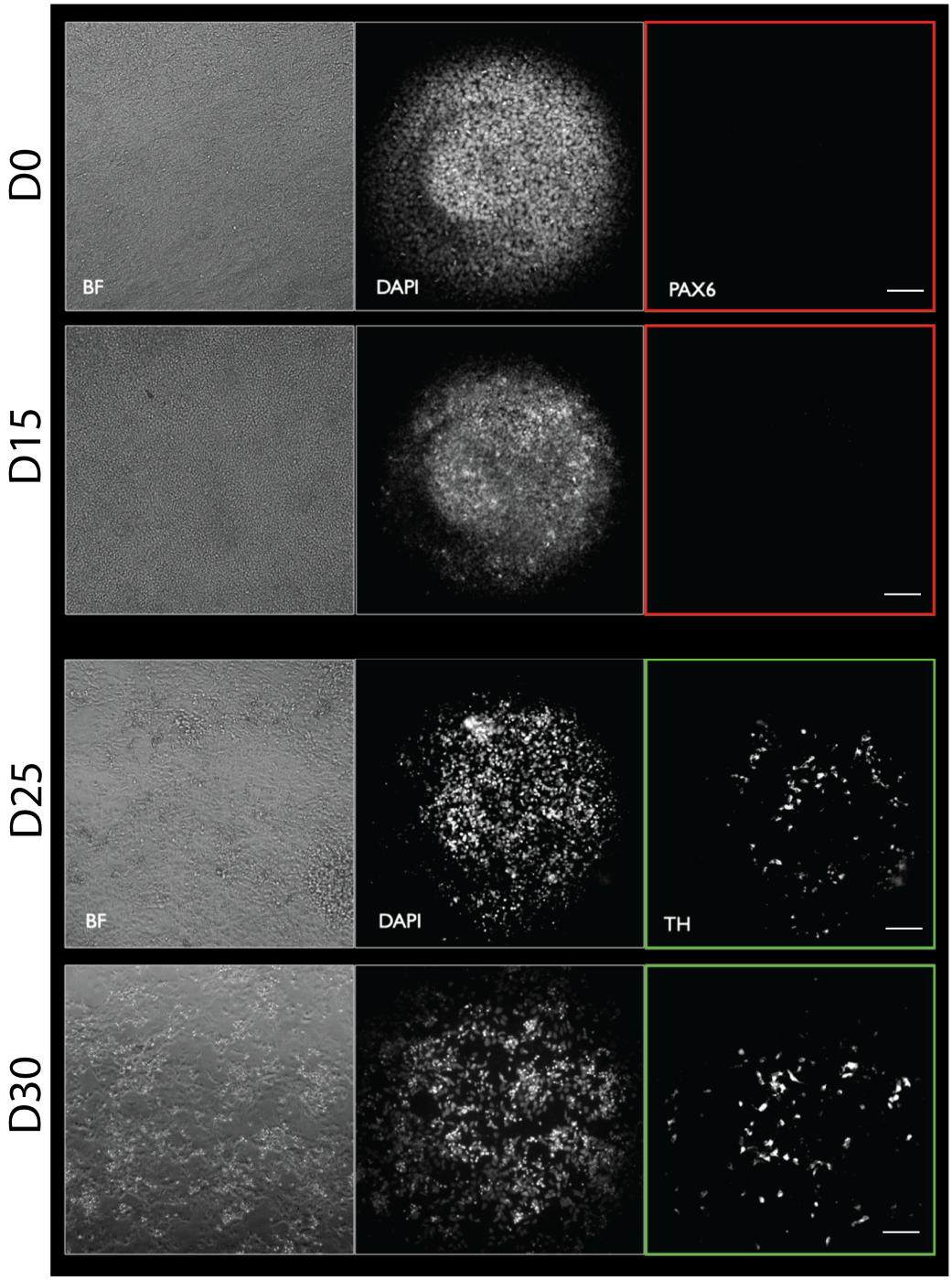

Figure 4.5 *Immunostaining on cells differentiated with the Direct Protocol at Day 0, 15, 25 and 30. BF: Bright Field. DAPI: 4',6-diamidino-2-phenylindole, showing the nuclei of live cells. PAX6: Paired box protein-6. TH: Tyrosine Hydroxylase, the enzyme that converts L-tyrosine to L-DOPA, the precursor of dopamine. Scale bar: 100μM.*

4.1.3 Single-cell transcriptomics shows that Direct DA Differentiation protocol recapitulates in vivo differentiation

As stated by Bjorklund & Dunnett, "expression of TH is not in itself sufficient to prove that a neuron is catecholaminergic, let alone dopaminergic". Hence, aside from the TH/PAX6 stainings, we made great effort to confirm that the neurons generated by the Direct protocol display a true midbrain DA (mDA) phenotype. To confirm that our differentiation protocol recapitulates the *in vivo* mDA differentiation path, we identified a group of genes that are essential and specific to the *in vivo* mDA differentiation process (OTX2, LMX1A, FOXA2, NR4A2, and others) and analysed their expression during the development of the control cell line at timepoints D0 (iPSCs), D6, D10, D15, D21, D26, D35, and D50, which represent the major developmental steps of the protocol [Fig. 4.6].

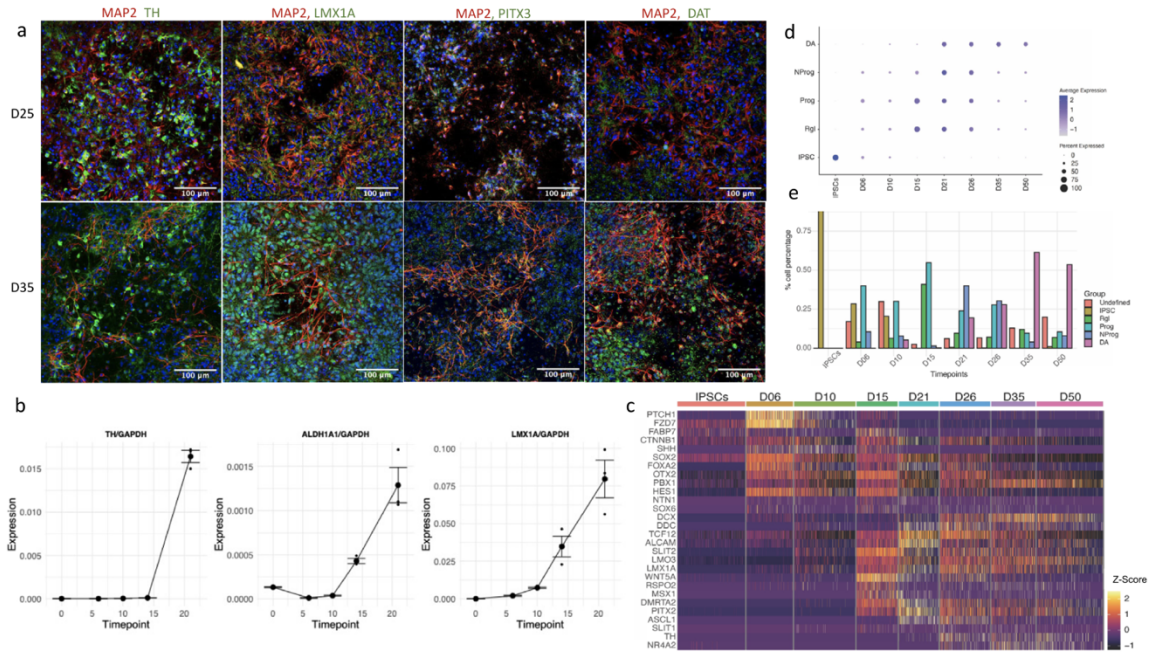

Figure 4.6 *In vitro differentiation of iPSC-derived mDA neurons recapitulates the in vivo process.* ***a:*** *To illustrate the maturation of neuronal morphology and mDA status, differentiated neurons were stained at D25 and D35 for a neuronal marker MAP2 (red) and mDA markers (green): TH, PITX3, LMX1A, and DAT. While D25 neurons show short processes and low expression of mDA markers, D35 neurons show much longer axons and well-defined expression of mDA markers (green/red overlap resulting on orange/yellow).* ***b:*** *Quantitation of mDA markers TH, ALDH1A1, and LMX1A, using absolute quantitation via qPCR. Each timepoint represents three independently differentiated biological replicates, amplified in duplicate. Standard error (SE) bars are the SE of biological replicates. The expression levels are standardized to total RNA and to the expression of the housekeeping gene GAPDH.* ***c:*** *Heatmap showing the expression of genes known from the literature to be involved and necessary for mDA neuron differentiation. Colors correlate to normalized counts (z-score, centered, and scaled) of the indicated genes.* ***d:*** *The mDA differentiation gene expression profile recently published by Ásgrímsdóttir and Arenas (Ásgrímsdóttir and Arenas, 2020) was used to show the progression during differentiation, from iPSCs to radial glia (Rgl), to progenitors (Prog) and neuroprogenitors (NProg), and to early mDA neurons (DA). The gene expression matrix obtained by SC-RNAseq used here consists of 4495 cells (see Methods section).* ***e:*** *Proportions of cells expressing the various phenotypes illustrated in (d).*

We first imaged cells at D25 and D35, as at this stage cells should have developed mDA characteristics. Staining for key mDA protein markers TH, PITX3, LMX1A, and DAT, with MAP2 as a neuronal marker, confirmed the mDA phenotype [Fig. 4.6a]. The co-expression of these mDA markers with TH is shown in Fig. 4.8a. At D25, neuronal cells possess only short processes and generally low mDA marker expression, but by D35 their axons are far longer and mDA marker expression is more defined and more robust. mRNA expression of TH, LMX1A, and ALDHA1A was further validated by qPCR, and the trajectory of these genes' expression indicated the development of mDA characteristics by D21 [Fig. 4.6b] in agreement with the imaging results at D25 [Fig. 4.6a]. To characterize the differentiation process more in detail, we performed single-cell RNA-sequencing (sc-RNAseq) analysis at eight timepoints during the differentiation process. Analysis of differentially expressed genes across timepoints revealed the expression of specific differentiation stage modules in accordance with known *in vivo* stage-specific expression patterns [Fig. 4.6c]. For example, the development of mDA phenotype *in vivo* depends on the early high expression of Sonic Hedgehog (SHH), followed by the induction of Wnt signaling and the expression mDA-specific downstream pathways [Fig. 4.6c]. Consistent with these *in vivo* differentiation steps, PTCH1, a receptor for SHH, and FZD7, a receptor for Wnt proteins [Fig. 4.6c] were among the highest-expressed genes at D6 of the differentiation protocol. The presence of EN1 as a key entity was also confirmed by qPCR, as its expression level was too low for detection by sc-RNAseq. The sc-RNAseq analysis again revealed that at Day 21 many factors that are specific to the mDA differentiation path, such as TCF12, ALCAM, PITX2, ASCL1, and DDC27, were among the most highly expressed genes [Fig. 4.6c]. Overall, these observations confirm that our *in vitro* differentiation protocol does indeed recapitulate the *in vivo* differentiation of mDA neurons and produces genuine mDA neurons (PAX6-, ALDH1A1+, PITX3+, KCNH6/GIRK2+, NR4A2/NURR1+, and LMX1A+), rather than other types of DA neurons (PAX6+ and ALDH1A3+).

However, the assessment of the differentiation process of human mDAs was mostly based on the pattern of mDA differentiation gene expression in murine brains. We, therefore, compared our data with the recently outlined pattern of gene expression during human mDA. The pattern of gene expression during our *in vitro* differentiation of human iPSCs into mDA neurons matched the pattern of human mDA differentiation more closely than that of murine neurons, confirming the validity of our differentiation protocol. Using the gene expression groups associated with different stages of maturation, from radial glia (Rgl), progenitors (Prog), to neural progenitors (NProg), and finally to mDA neurons (DA), we characterize the differentiation trajectory by the level of gene expression [Fig. 4.6d]. We then used these gene groups to characterize individual cells with respect to their most likely cell type and determined the population dynamics by the percentage of cell

types present at each timepoint [Fig. 4.6e]. The analysis showed fast differentiation from iPSC state to a neuronal lineage by D6, and the subsequent maturation towards an mDA phenotype starting at D21, accompanied by the increasing prevalence of DA phenotype, from 20% at D21, to 28% at D26, and 61% at D35, after which it seemed to stabilize [Fig. 4.6d]. This characterization further confirms that early mDA differentiation is achieved around D21.

Overall, this analysis demonstrates that the optimized Direct differentiation protocol leads to midbrain-specific DA neurons with an efficiency of above 60% after 21 days. While the Indirect differentiation protocol starting from smNPCs (Reinhardt et al., 2013) also generates DA neurons with an efficiency of around 50%, the here presented analysis indicates that they do not follow the midbrain specific path as indicated by PAX6 expression at early stages of differentiation which is not observed *in vivo*. Thus, following Aim 1, the results strongly suggest to use the Direct protocol for the detailed analysis of the effect of the *PINK1* mutation.

4.2 Single-cell transcriptomics of control and PINK1 cell lines differentiation dynamics reveal a core molecular network of PD

Based on the protocol establishment in the previous section, we next performed a systematic differential expression analysis at a single-cell resolution between the iPSC line carrying the PD-associated ILE368ASN mutation in the PINK1 gene and the age- and sex-matched control cell line during their parallel differentiation into mDA neurons using the Direct differentiation protocol. The initiated differentiation in the PINK1-ILE368ASN and the control cell line were analysed at three early different timepoints (D6, D15 and D21), to obtain cells which reach different stages of differentiation on the same collection day (generating four independent pairs). Samples were collected and processed for SC- RNAseq at the same time to avoid batch effects [Fig. 4.7]. After pre-processing and quality-filtering, we used 4495 cells and 18,097 genes in our downstream analysis of the SC-RNAseq data. For data integration, we then performed a network analysis to identify underlying key mechanisms of PD development.

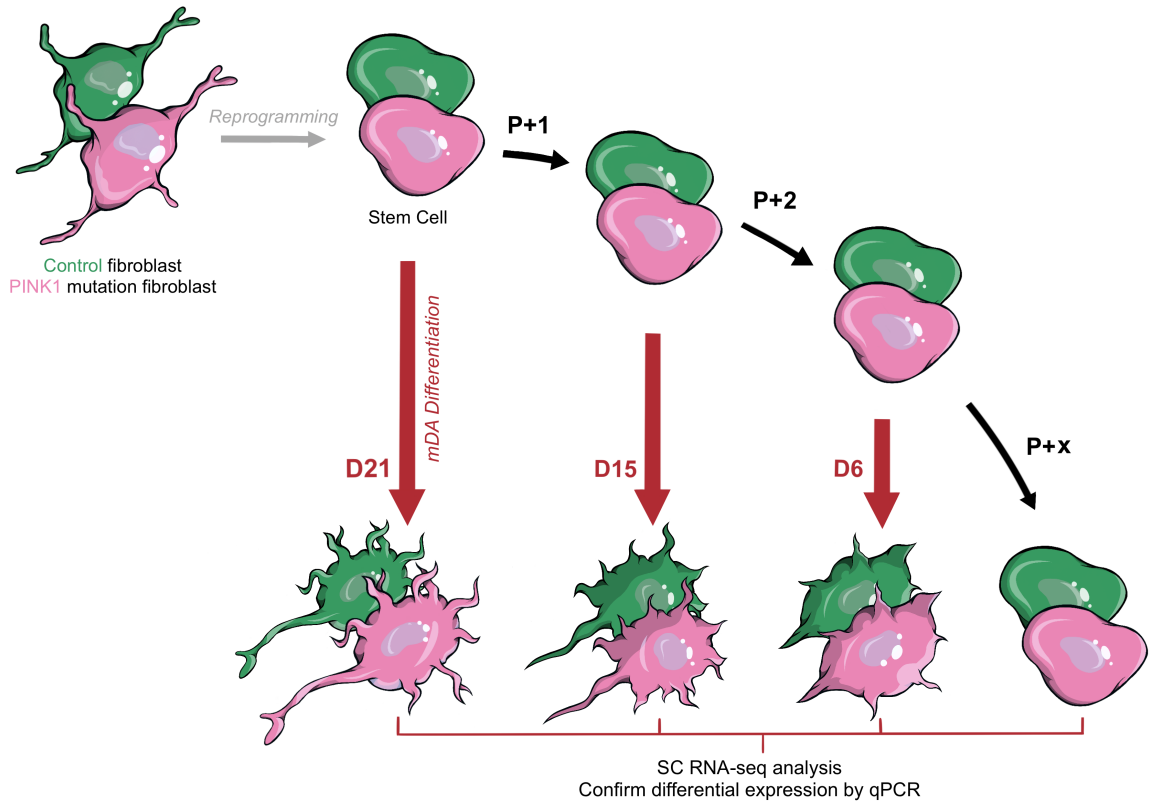

Figure 4.7 *Experimental design. Fibroblasts were used to generate human induced pluripotent stem cells (iPSCs), which were then differentiated until Day 6, 15 and 21. The cells were then collected at the same time; single cell RNA-seq, qPCR and proteomics analyses were performed "P + 1" indicates that the iPSCs were passaged before new differentiation was initiated.*

4.2.1 The PINK1-ILE368ASN mutation is associated with persistently dysregulated expression of nearly 300 loci

To investigate the effect of the PINK1 mutation on mDA development, we differentiated the control and the PINK1-ILE368ASN cell lines in parallel [Fig. 4.7] and focused on the early differentiation period, to increase our chances of finding the direct effects of the PINK1-ILE368ASN mutation as described below. Co-staining of TH positive neurons with the midbrain dopaminergic markers PITX3, LMX1A, and DAT in both the control and PINK1 cell lines identified neurons at day D21 as early post-mitotic mDA neurons with clearly neuronal morphology and no major differences between the cell lines [Fig. 4.8a].

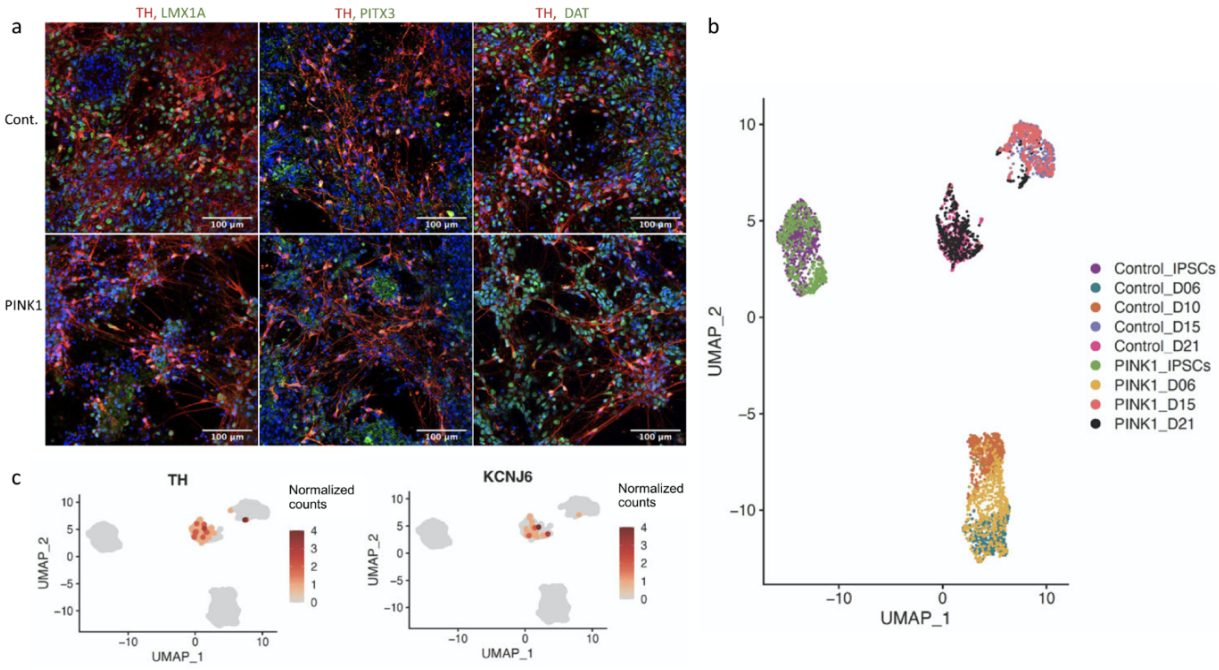

Figure 4.8 *Classification of mDA status.* ***a:*** *TH positive neurons co-express mDA markers PITX3, LMX1A, and DAT in control (top) and PINK1 cell line (bottom), at D35.* ***b:*** *Based on our SC-RNAseq data, cell lines cluster according to differentiation stage, indicating that gene expression is very homogenous between the control and the PINK1-ILE368ASN cell lines, which allows for the detection of even subtle alteration induced the presence of the PINK1 mutation.* ***c****: Trajectory of expression of TH and KCNJ6 (GIRK2), two mDA neuron markers. At D21 neurons begin to show TH expression, together with an expression of other mDA markers, which indicates that they are becoming early postmitotic mDA neurons. The scale represents normalized counts.*

To investigate potential underlying mechanisms of the PINK1 mutation, differential expression between the two simultaneously differentiated cell lines at each timepoint was determined. In addition to that, the genes defined as differentially expressed at all four timepoints were also identified. Each timepoint is an independent biological replicate, initiated at a different time and with cells of a different passage number. Control and PINK1-ILE368ASN cells co-clustered together based on their differentiation stage, from iPSCs, to day 6 (D6), D15, and D21 [Fig. 4.8b], indicating that overall RNA expression was specific to differentiation stages, and rather uniform between cell lines, which was amenable to the identification of subtle gene expression differences due to the presence of a mutation in the PINK1-ILE368ASN cell line. PINK1-ILE368ASN cells at D10 showed low viability, hence the D10 timepoint was not included in the pairwise analysis. After preprocessing and quality-filtering, a total of 4495 cells (2518 control and 1977 PINK1 cells) and 18,097 genes were included in our analysis. UMAP analysis of the single-cell data revealed that gene expression was rather similar between the cell lines and mainly defined by differentiation stage, rather than by cell line origin [Fig. 4.8b]. In accordance with the staining results, we observed the onset of expression of the mature mDA markers *TH* and *KCNH6* (also known as *GIRK2*) on D21 [Fig. 4.8c].

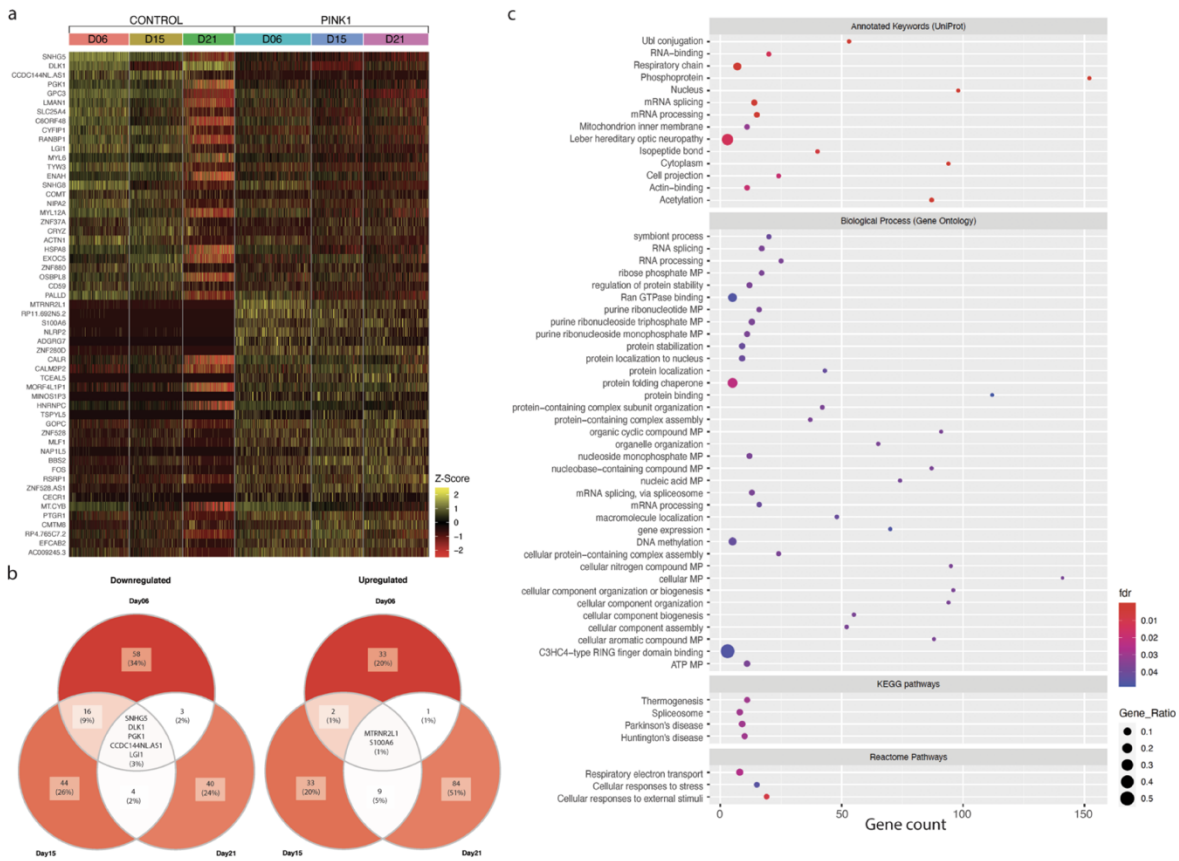

Figure 4.9 *Differentially expressed genes (DEGs) in a cell line homozygous for a mutation in the PINK1 gene, compared to a control cell line, at three timepoints during the differentiation of mDA neurons (D6, D15, and D21).* ***a:*** *Heatmap of the top DEGs. Each column corresponds to a timepoint for either control or PINK1 cells; each row shows the expression of one gene in individual cells. Colors correlate to normalized counts (z-score, centered, and scaled) of the indicated genes. For the complete list of DEGs identified, see Supplementary Fig. 10.* ***b:*** *Top DEGs. The minimum fold change was increased to highlight the top differentially expressed genes. We identified the top 56 genes as our group A; here we show the top five upregulated genes (left Venn diagram) and the top three downregulated genes (right Venn diagram).* ***c:*** *Enrichment analysis performed using the STRING database. The top KEGG pathway associated with this dataset is Parkinson's disease. The other three KEGG pathways identified were Spliceosome, Huntington's disease, and Thermogenesis. The gene expression matrix used for the downstream analysis consisted of 4495 cells (39,194 genes) and differential expression analysis resulted in 292 DEGs, which were used to perform the enrichment analysis. For better image resolution, see Supplementary Fig. S11.*

The analysis of pairwise differential expression at each timepoint (adjusted p values (padj) <0.01 fold changes (FC) >0.1) [Fig. 4.9a] identified 14 genes that were upregulated and 13 genes that were significantly downregulated in the PINK1- ILE368ASN cell line compared to control [Fig. 4.9b and Table 4.1, indicated by "X"]. Because iPSCs are very different from differentiating neuronal precursors, we next tested whether including iPSCs had disproportionately affected the results by excluding neuron-specific genes. Repeating the analysis on D6, D15 and D21 only identified 28

genes that were upregulated and 27 genes that were downregulated at all three timepoints, including all genes previously identified [Table 4.1]. As expected, excluding iPSCs resulted in the identification of a broader range of genes because genes that are differentially expressed only in the neuronal lineage were previously excluded due to the requirement that DEGs be dysregulated at all timepoints.

However, both sets are equally valuable, as genes dysregulated even in iPSCs are likely to participate in systemic PD pathology, regardless of cell type, and may be relevant to a broader spectrum of PD pathology than the death of mDA neurons. Interestingly, most of the differentially expressed genes are already linked to PD, other PD mutations, or neurodegeneration [Table 4.1].

Upregulated in PINK1					**Downregulated in PINK1**				
GENE	**incl. iPSCs**	**excl. in STRING**	**PD association**	**Ref.**	**GENE**	**incl. iPSCs**	**excl. in STRING**	**PD association**	**Ref.**
AC009245.3	X	Pseudogene			*ACTN1*			PD	145
ADGRG7	X		rare var., mito	146	*C6ORF48*	X			
BBS2					*CCDC144NL.AS1*	X	RNA		
CALM2P2	X	Pseudogene			*CD59*	X		PD	147
CALR			PD	148	*COMT*			PD	149
CECR1					*CRYZ*	X		GWAS, PD Gene	63
CMTM8			GWAS, PD	63	*CYFIP1*	X		(via mTOR)	150
EFCAB2	X		microarray	151	*DLK1*			PD	152
FOS			rat, L-DOPA	153	*ENAH*			GWAS, *LRRK2*	154
GOPC			*PARK7 (DJ-1)*	63	*EXOC5*			Parkinson Dis.Map	155
HNRNPC	X		binds Parkin	101	*GPC3*			reduced in *DJ-1* mut.	62
MALAT1			PD	156	*HSPA8*	X		PD, *LRRK2*	157
MINOS1P3	X	Pseudogene			*LGI1*			PD	119
MLF1			via *HTRA2*	158	*LMAN1*			Parkin transloc.	104
MORF4L1P1	X	Pseudogene			*MYL12A*			binds Parkin	101
MT-CYB			mito	159	*MYL6*	X		interacts with LRRK2	160
MTRNR2L1	X		binds Parkin	101	*NIPA2*	X		tremor	161
NAP1L5					*OSBPL8*			via ZNF746, Biogrid	162
NLRP2	X		inflammasome	163	*PALLD*			PD	164
PTGR1					*PGK1*	X		PD	165
RP11.692N5.2	X	Pseudogene			*RANBP1*				
RP4.765C7.2	X	Pseudogene			*SLC25A4*			binds Parkin	101
RSRP1					*SNHG5*	X	RNA	via miR-205, LRRK2	166
S100A6	X		PD	167	*SNHG8*		RNA		
TCEAL5	X				*TYW3*	X			
TSPYL5			Ubiquit.	168	*ZNF37A*	X			
ZNF280D	X		GWAS*	169	*ZNF880*	X			
ZNF528									
ZNF528.AS1		RNA Gene							

Pairwise differential expression analysis of each timepoint (iPSCs, D6, D15, and D21), resulted in 14 genes that were upregulated and 13 genes that were downregulated in the *PINK1*-ILE368ASN cell line, compared to control (p_val_adj <0.01 and abs(avg_logFC) >0.1); these genes are marked with "x" in column "Incl. iPSCs". Twenty-nine additional genes were identified in an analysis that included D6, D15, and D21, but not iPSCs. The "Excluded" column explains why a gene was not included in the protein-protein interaction network. These 56 top DEGs are later referred to as Group A. The gene expression matrix used for the downstream analysis consisted of 4495 cells (39,194 genes). * rs11060180.

Table 4.1 *Top genes dysregulated consistently in PINK1 vs. control cells across differentiation stages (Novak et al., 2022).*

For an alternative definition of differentially expressed genes (DEGs), we used the maximum adjusted p value in a pairwise combination as an adjusted p value, and the average fold change that occurred in the pairwise comparison as a fold change threshold. With this approach, we retained only genes dysregulated in the same direction at all timepoints. This analysis led to 151 DEGs (named Group B), which included the previously identified genes of Group A, and of which 65 were upregulated and 86 downregulated compared with controls (padj < 0.01 and FC > 0.1). Taking the mean of FC of the different timepoints enhanced the identification of DEGs because it reduced the effect of the variability between pairs due to their different differentiation states. Repeating the same analysis for the four timepoints (iPSCs, D6, D15, and D21), but taking into account only the absolute degree of change in iPSCs, yielded 172 genes (Group C). Repeating the analysis using only timepoints D6, D15, and D21 identified a total of 286 DEGs (Group D) [also see Fig. 4.10a]. Together, when all analyses were pooled, we obtained 292 DEGs (six genes in Group C depended on the inclusion of iPSCs and did not appear in Group D).

4.2.2 Enrichment analysis reveals a strong association with the KEGG Parkinson pathway

Enrichment analysis was performed using the STRING database [Fig. 4.9c]. The highest-associated KEGG pathways were the Parkinson's, Huntington's, and spliceosome pathways. Biological processes most strongly associated with the DEGs were C3HC4-type RING finger domain binding, Ran GTPase binding, and protein folding chaperones. Respiratory chain transport was the most strongly associated Reactome pathway.

4.2.3 Data integration reveals a common PD network

To integrate the expression analysis and identify underlying disease mechanisms, we generated a network of interactions between the DEGs by Gephi, using protein–protein interaction (PPI) information obtained from the STRING and GeneMANIA databases. The network we obtained includes 246 of the 292 DEGs, since pseudogenes and non-coding RNAs could not be integrated into a protein–protein interaction network [Fig. 4.10], and 2122 interactions. The curated network contains only DEGs and any genes that were automatically added by the databases were removed to ensure a reliable core network based solely on DEG data. Based on known protein–protein interactions, the DEGs integrate into a close-knit core network in which several DEGs form central nodes [Fig. 4.10]. To evaluate the importance of the DEG-based PPI network produced by STRINGdb (v10), we compared the DEG-based network with corresponding random networks generated from sets of 292 randomly chosen genes excluding DEGs. Based on 50 random networks, we show that the DEG-based network includes significantly more protein-coding genes and interactions than by chance and that the network structure in terms of degree distribution is significantly distinct as evaluated by the Wilcoxon test ($p = 2.22e-16$) and indicates the mechanistic character of the network.

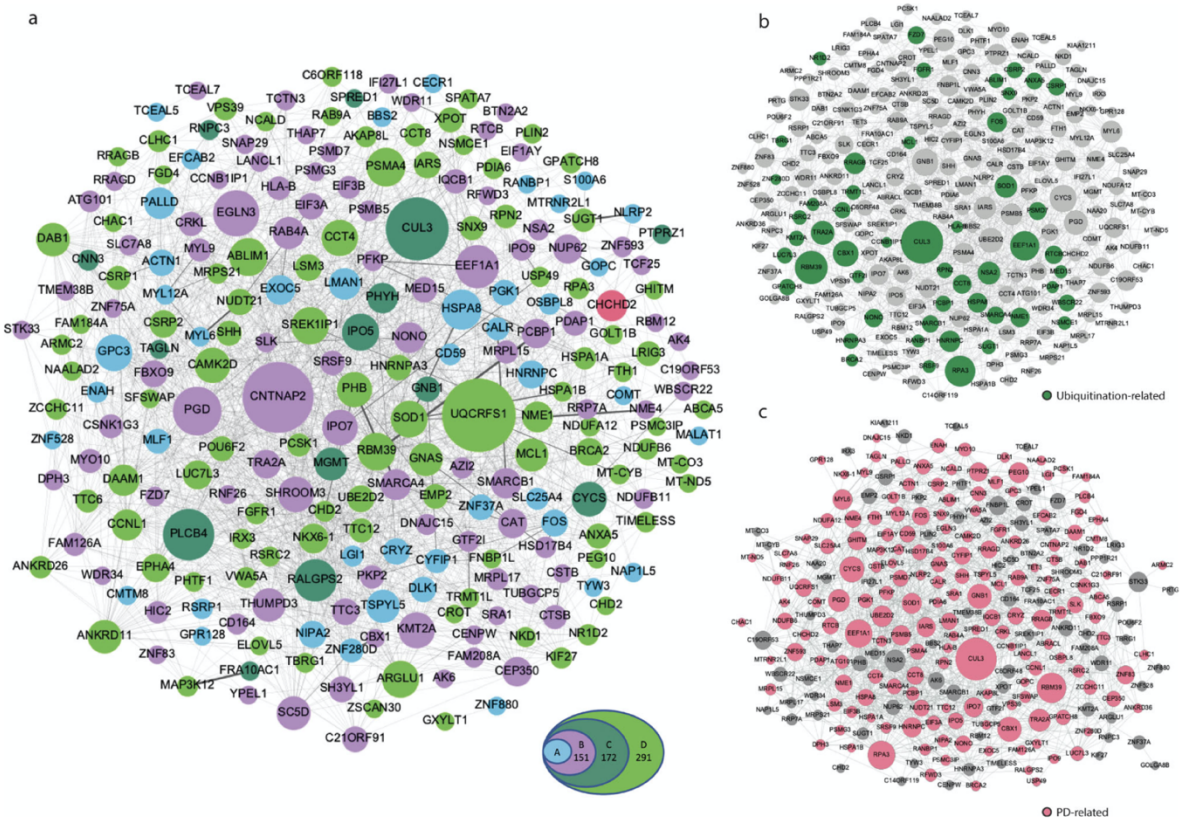

Figure 4.10 *Network analysis.* ***a:*** *Protein–protein interaction network based on known interactions available through the STRING and GeneMANIA databases. Only strong interactions were retained, predicted interactions or text associations were omitted. Betweenness centrality was used to illustrate the relative importance of each node within the network through the level of its connectedness to other proteins. The larger the circle, the more partners the node is connected to. The colors represent the four DEG sets, with the top 56 DEGs (group A) in light blue, group B in purple, group C in dark green, and group D in light green. Each set consists of genes of the previous set plus additional genes identified by the new parameters. CHCHD2 (pink, part of group B) is a DEG, which has recently been identified as a PARK gene. Random selection of genes from genes detected by sc-RNAseq did not lead to a network formation.* ***b:*** *DEGs which play a role in ubiquitination.* ***c*** *Based on the literature, 68% of the DEGs of this network are already known to be associated with PD. For better image resolution, see Supplementary Fig. S12.*

The network of genes dysregulated by the presence of the PINK1-ILE368ASN mutation includes genes related to other PD-associated pathways, which is intriguing since it was generally assumed that each PD-associated mutation leads to PD pathology via an independent, characteristic path. For example, two DEGs, GOPC, and GPC3 interact with the PD-associated gene DJ-1 (PARK7). The DEG network also includes genes of the LRRK2 (PARK8) network, namely ENAH, HSPA8, MYL6, MALAT1, and SNHG5. SNHG5 and MALAT1 interact with LRRK2 via miR-205-5p. DLK1 and MALAT1 mediate α-synuclein accumulation. In fact, the DLK1-NURR1 interaction involved in this process may be mDA neuron-specific, highlighting the necessity to use mDA neurons for the study of PD-related pathways. Additionally, MALAT1 was shown to increase α-synuclein protein expression. In short, this suggests that interactions leading to PD pathology are more complex than one mutation-

one path to PD, as generally thought. Moreover, this indicates that many druggable targets may be useful in treating PD and that these may be universally effective for PD caused by several different mutations, and perhaps even for idiopathic PD. For example, terazosin, which is already in clinical use, was found to be associated with slower disease progression, likely by enhancing the activity of phosphoglycerate kinase 1 (PGK1), one of the top DEGs identified in our study.

For the evaluation of the relative importance of each node within the network, we applied betweenness centrality [Fig. 4.10a], an approach that reveals the overall connectedness of each gene. Genes onto which several other genes converge are shown as large circles or nodes, their size being proportional to the number of interactions they form. Interestingly, the major nodes of this network are genes already known to play an important role in ubiquitination [Fig. 4.10b] and PD pathology [Fig. 4.10c and Table 4.2].

Node gene	Role in Parkinson's disease
HSPA8 (also known as *HSP73, HSC70*)	Disaggregation of α-synuclein amyloid fibrils[85] Autophagy, part of the catabolic pathway for α-synuclein[86] Mediates mitophagy by regulating the stability of PINK1 protein[87] Impaired gene expression in sporadic PD[88]
EEF1A1	Mediates activation of heat-shock transcription factor HSF1, prevents α-synuclein aggregation[90] Interacts with Parkin (PARK2)[82]
HNRNPC	Interacts with Parkin (PARK2)[82] Part of the poly ADP-ribose (PAR) cell death pathway accountable for selective dopaminergic neuronal loss[99]
PSMA4	Part of the Parkinson's disease KEGG pathway[92,93] Interacts with Parkin (PARK2) and FBX07 (PARK15)[82]
CYCS	Role in aggregation of alpha-synuclein[170] CTD gene-disease associations - Parkinson disease gene set[63]
ACTN1	Interacts with DJ-1 (PARK7)[82] It is a binding partner of mitochondrial-shaping proteins[171]
PGK1	PGK1 mutation causes vulnerability to parkinsonism[172] Activation of PGK1 partially restored motor function and slowed disease progression[69]
PHB	Regulates dopaminergic cell death in substantia nigra[173]
SHH	Play a role in neuroinflammatory response in the MPTP model of Parkinson's disease[174]
BRCA2	Deubiquitinase plays a role in neuronal inflammation[175]
VPS39	It is part of the endocytic membrane trafficking pathway involved in PD and its methylation rates are associated with Parkinson's disease risk[176] Plays complex functions in endocytic and autophagic pathways[177]
UQCRFS1	KEGG pathway, Parkinson disease[92,93]
CNTNAP2	Differentially expressed in the presence of *LRRK2* G2019S mutation, associated with PD[97] GWASdb SNP-disease associations, Parkinson's disease gene set[63] Plays a role in the formation of protein aggregates and PD[95,96]
CUL3	Ubiquitin ligase, a potential drug target for Parkinson's disease[84]
PLCB4	GWAS - Parkinson's disease[63] Motor defect consistent with ataxia in Plcb4-null mice[100]
EGLN3	GEO signatures of differentially expressed genes for diseases—Parkinson's Disease_Substantia Nigra[63] Prolyl hydroxylase targets substrates for ubiquitination[178]
RALGPS2	Targets include Nurr1, which is associated with Parkinson disease[63]

Central nodes were determined using the Gephi visualization platform. They represent points of convergence of the network (Supplementary Fig. 5). Since these nodes have already been linked to PD pathways, many more DEGs might also contribute to PD pathology through these pathways. These nodes not only provide a point of convergence for DEGs identified in our study, but they also interact with several PARK genes, suggesting that PARK proteins may also converge on the pathways identified here (Supplementary Fig. 7).

*Table **4.2** Central nodes of the DEG network are associated with PD [Fig. 4.10c].*

Next, we built a correlation network (p value < 0.05, r > 0.1) of the 246 DEGs based on the normalized counts. By extracting the common interactions of these two networks, we obtained a network with 297 interactions, which highlights protein–protein connections that correlate with differential expression of the genes. This analysis further supports the role of the connections between these genes in mediating the resulting differential expression in the presence of the PINK1-ILE368ASN mutation. STRING was subsequently used to highlight functional pathways represented within the DEG network. Several pathways known to play a role in PD pathology are strongly represented within the network, notably ubiquitination, mitochondrial pathways, cellular response to stress, lysoso- mal proteins, protein metabolism (localization, modification, transport, folding, and stability), RNA processing, aromatic compound metabolism, vesicle-mediated transport and exocytosis, and cellular catabolic processes. Importantly, the strongest-associated pathway is the KEGG-PD pathway. The CHCHD2 gene was identified as a dysregulated gene through our analysis, but it was also recently identified as a PD-associated gene and named PARK22 [Fig. 4.10a].

Further analysis revealed that a large number of the DEGs interact with genes associated with mitochondria or ubiquitination [Fig. 4.10b]. For this analysis, we used BioGRID to identify interactions with mitochondrial or ubiquitination proteins for the top 172 DEGs (groups A–C). These interactions were used to create a network illustrating that many of the DEGs in our study directly interact with genes involved in mitochondrial function and in ubiquitination. Only direct DEG to mitochondrial gene or DEG to ubiquitination gene interactions were included and PARK genes were added for reference. Based on manual literature search, we determined that at least 68% of the DEGs (174 of 255 genes, not including pseudogenes and RNA genes) are already directly associated with PD, either experimentally, or linked through GWAS-PD, or by PD expression studies [Fig. 4.10c.] This is particularly true for the major nodes of the network [Table 4.2 and Fig. 4.10c].

4.2.4 Proteomics analysis confirms impaired neuronal phenotype in PINK1-ILE368ASN mutant cell line

To investigate how the identified transcriptional modifications manifest in the neuronal phenotypes, we performed proteomics analysis at an early (day 25) and later maturation stage (day 40). The analysis identified 39 differentially abundant proteins in PINK1-ILE368ASN cells as compared to controls, based on biological duplicates with a log2 fold change larger than 1 [Fig. 4.11a]. Of these, four differ at both timepoints (D25 and D40). Overall, 31 proteins were differentially abundant at D25, including CSRP2 and VWASA, which were also identified by sc-RNAseq as differentially expressed at the mRNA level at D6, D15, and D21 [Fig. 4.11b]. At D40, 12 proteins were found to be differentially abundant, including four also identified at D25, namely TH, DDC, NES, and VIM. We performed a network analysis based on the differentially abundant proteins [Fig. 4.11b]. The resulting network again connects PD-related nodes and exhibits a good overlap with the transcriptional-derived network. This consistent result indicates that the observed transcriptional modification led to an impaired neuronal phenotype, despite the subtle differences in expression, and further highlights the importance of the proposed PD Core network.

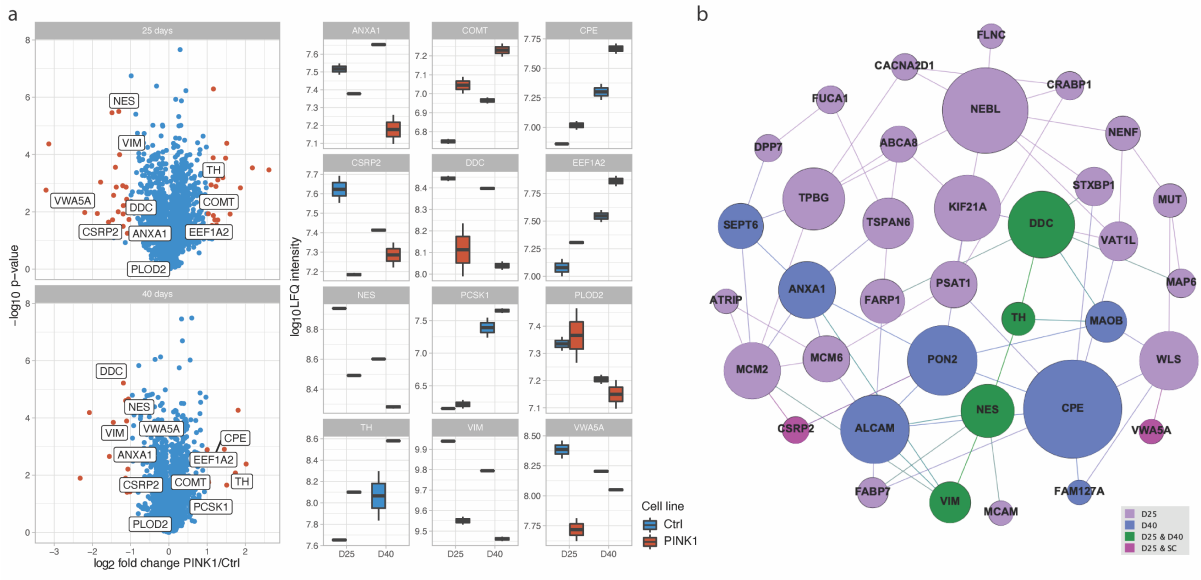

Figure 4.11 *Comparative proteomics analysis between CTRL and PINK1-ILE368ASN cell line at D25 and D40 validates the manifestation of the transcriptional phenotype. Results of proteomic analysis at D25 and D40 of the differentiation protocol.* ***a:*** *The volcano plot shows significantly differentially abundant proteins (FDR <0.05, fold change larger than 2 or −2) as red points, with remaining datapoints shown in blue. The names of proteins that were detected as both top differentially abundant at the protein level by the proteomics analysis and as differentially expressed at the mRNA level by SC-RNAseq are highlighted using a textbox. The data shows results at two timepoints, D25 and D40, in two biological replicates per timepoint. Box plots further highlight the expression of genes shown in textboxes of the volcano plot (interquartile range, showing the expression at D25 and D40, in the PINK1 cell line and in control (IQR, 25–75% q1–q3), with bars indicating Q1 ± 1.5 IQR).* ***b:*** *This*

figure shows a network of proteins differentially expressed between a control and a PINK1 mutation-carrying cell line, at D25 and D40. Proteins which are differentially expressed at both D25 and D40 are highlighted in green and point to a dysfunction of the dopaminergic system. D25 differentially abundant proteins are in purple, D40 in blue, proteins also identified as by SC-RNAseq differentially expressed at the mRNA level are in pink. Betweenness centrality was used to illustrate the relative connectedness of each node within the network, the greater the number of documented interactions with other nodes, the larger the circle.

4.3 Multi-scale analysis of control and PINK1 mature and aged dopaminergic neurons

Based on the assessment that Direct differentiation protocol allows to obtain high quality mDA neurons (Section 4.1) and on the characterization of the early differentiation period (Section 4.2) which led to the identification of a core PD-related gene network, I subsequently performed a multi-OMICs characterization including single-cell differential expression, proteomics, and metabolomics analysis to monitor the mDA differentiation process up to day 57. For this purpose, the same two cell lines as the previous experiment were used (the age- and sex-matched control and the ILE368AS PINK1 mutation cell lines). This time, the cells were differentiated until complete maturation and seven different time points were considered (Day 0, 8, 18, 25, 32, 37 and 57) [Fig. 4.12]. Moreover, cells from the same differentiation were collected for transcriptomic, proteomic, and metabolomic analysis at each time point to explore the underlying disease dynamics on multiple levels of organization. The iPSCs cell lines were differentiated into mature mDA neurons by using the Direct differentiation protocol (see Subsection 3.5.2).

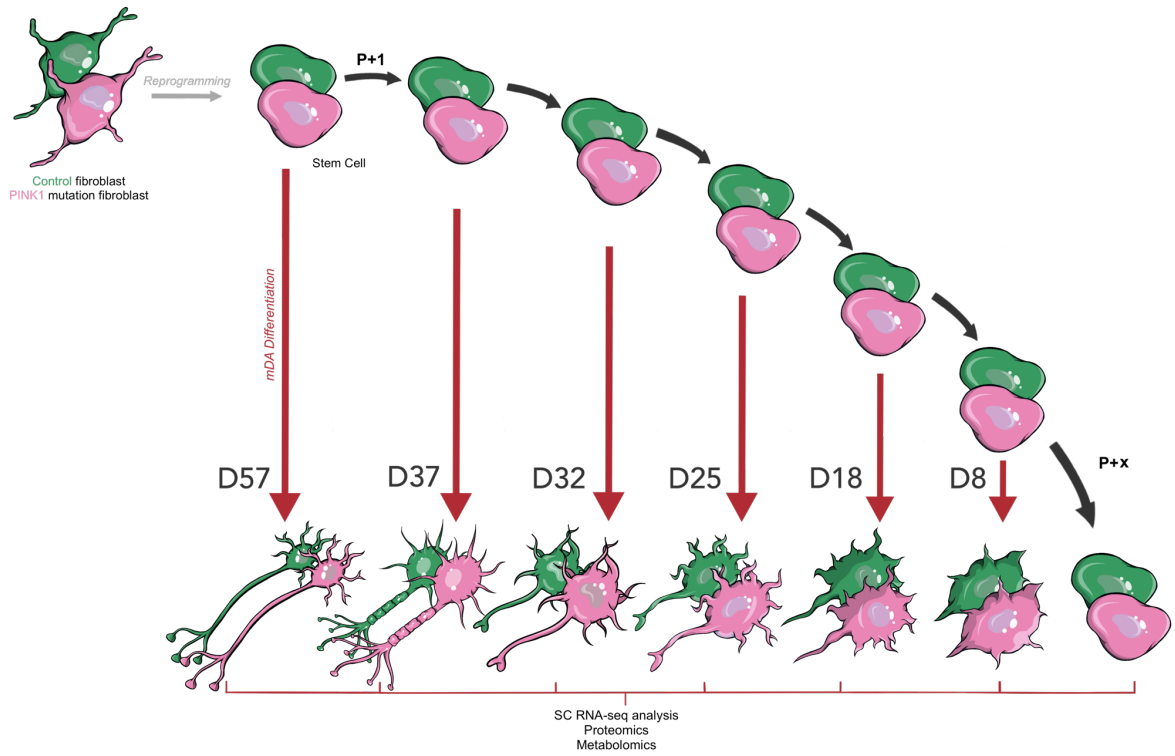

Figure 4.12 *Experimental design. Fibroblasts from a healthy individual and a PINK1 patient were used to generate iPSCs, which were then differentiated until Day 8, 18, 25, 32, 37 and 57. The cells were then collected at the same time; single cell RNA-seq, Proteomics and Metabolomics analyses were performed.*

4.3.1 Verifying the compatibility between the two transcriptomic datasets

To ensure that the results from this new experimental setup could be combined with the previous analysis later on, we compared the two datasets and established that the expression profiles of the cell lines during development were overlapping in the independent experiments. For this comparison, we looked at the correlation between the whole gene expression profile of both control and PINK1 cell lines in the two experiments (cell lines from the previous datasets are named CTR and PINK1; the ones from the new one are labelled as WT and ND). Because the time points of the collection were slightly different, we looked at the correlation between the time points that were almost analogous (previous data: D0, D6, D15, 21; new data: D0, D8, D18). As illustrated in the two correlation plots shown in Fig. 4.13, both controls and PD cell lines exhibited highly correlated profiles during development (i.e. WT_D0 and CTR_D0 scored a correlation of 0.94, WT_D8 and CTR_D6 score was 0.89, WT_18 scored 0.98 with CTR_D15 and 0.96 with CTR_D21).

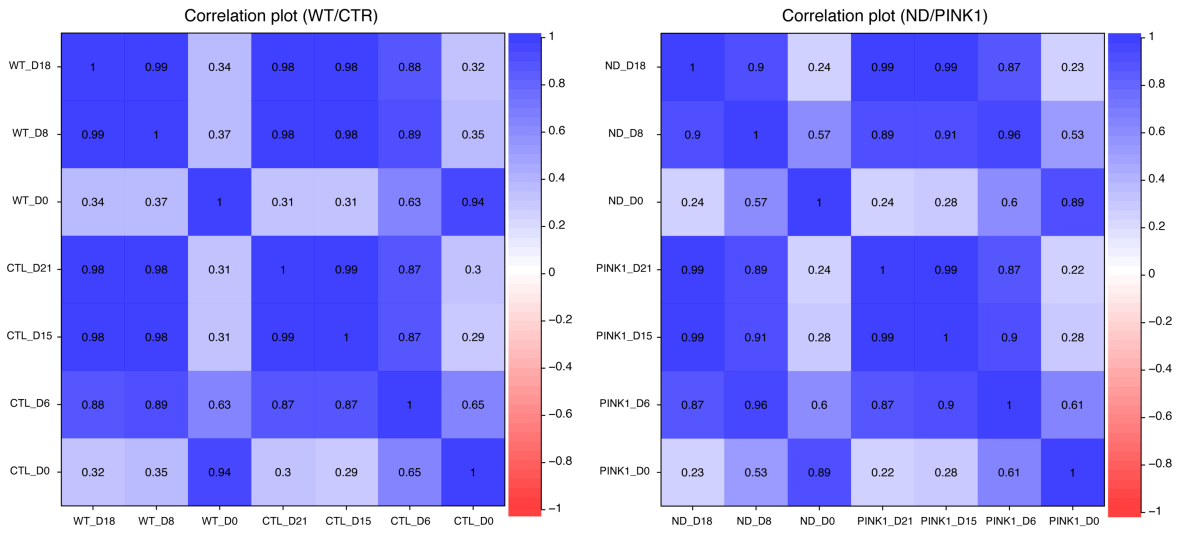

Figure 4.13 *Correlation analysis between the new dataset (WT, wild type; ND, PINK1-mutated cell line) and the previous one (CTR, control cell line; PINK1) for the control cell line (left) and the PINK1 mutation-carrying cell line (right).*

4.3.2 Single-cell RNA-sequencing confirms the correct development of both control and PINK1 cell lines from iPSCs to mature neurons

To verify that the cells had developed in the expected neuronal differentiation trajectory, we examined their entire gene expression profile and validated that they clustered according to the appropriate time point. By applying dimensionality reduction by UMAP, we could confirm that the control and PINK1 cell lines belonging to the same time point (Day 0, 8, 18, 25, 32, 37 and 57) formed homogeneous clusters as illustrated in Fig. 4.14. This indicates that the two populations were undergoing the transition towards the same cell type.

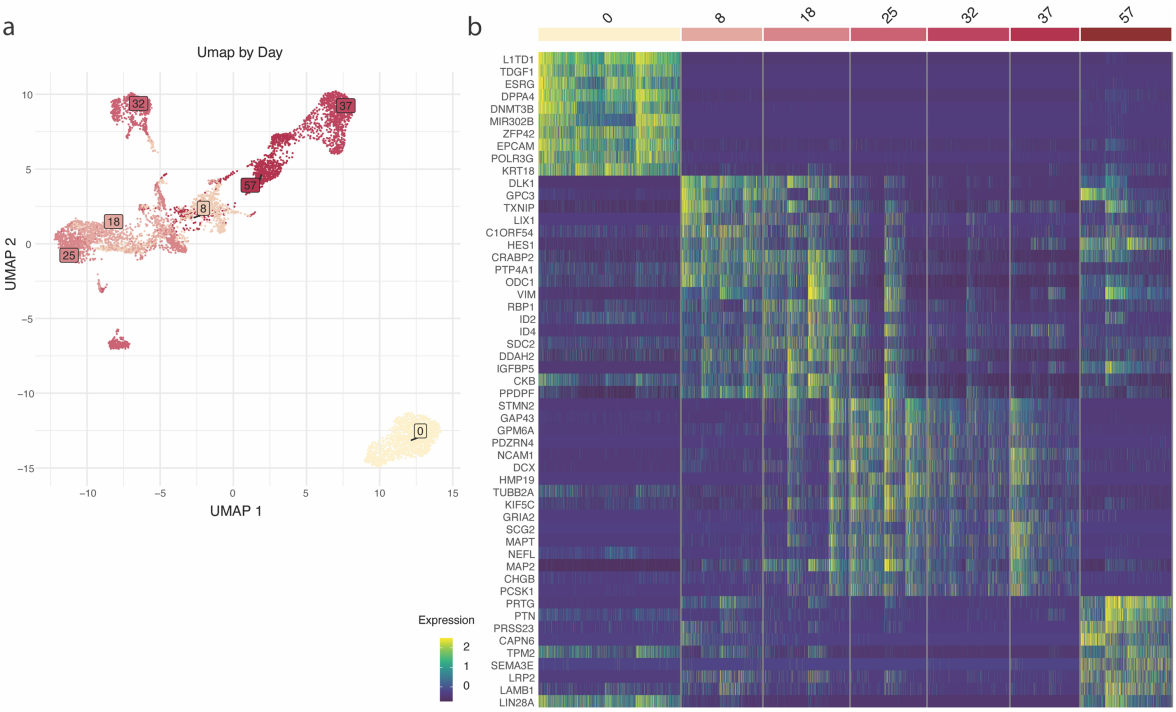

Figure 4.14 *PINK1 and control cell lines differentiated towards the same neuronal cell type.* ***a:*** *Based on our SC-RNAseq data, control and PINK1 cell lines both cluster depending on the different time points, indicating that their gene expression is very homogenous, which enables for the identification of even minor changes caused by the PINK1 mutation.* ***b:*** *Heatmap of the top DEGs which uniquely characterize each time point, considering control and PINK1 cell lines altogether. Each column corresponds to a timepoint (D0, 8, 18, 25, 32, 37, 57) and each row indicates the expression of the specified gene in individual cells. Colors correlate to the normalized expression of the indicated gene.*

To check that before the differentiation both control and PD cell lines were exhibiting the appropriate stemness phenotype, we checked for the expression of genes which we had been identified in the previous analysis as stemness markers (POU5F1, L1TD1, TDGF1, POLR3G, TERF1, USP44, LIN28A) (Novak et al., 2022) [Fig. 4.15 and Supplementary Fig. S1]. As shown in Fig. 4.15, all these genes were highly expressed in all the cells associated to the D0 cluster (control and PINK1 cell lines combined). Interestingly, we detected that LIN28A was also expressed at the latest time point of the differentiation, more specifically in the D37 and 57 clusters (see Discussion chapter).

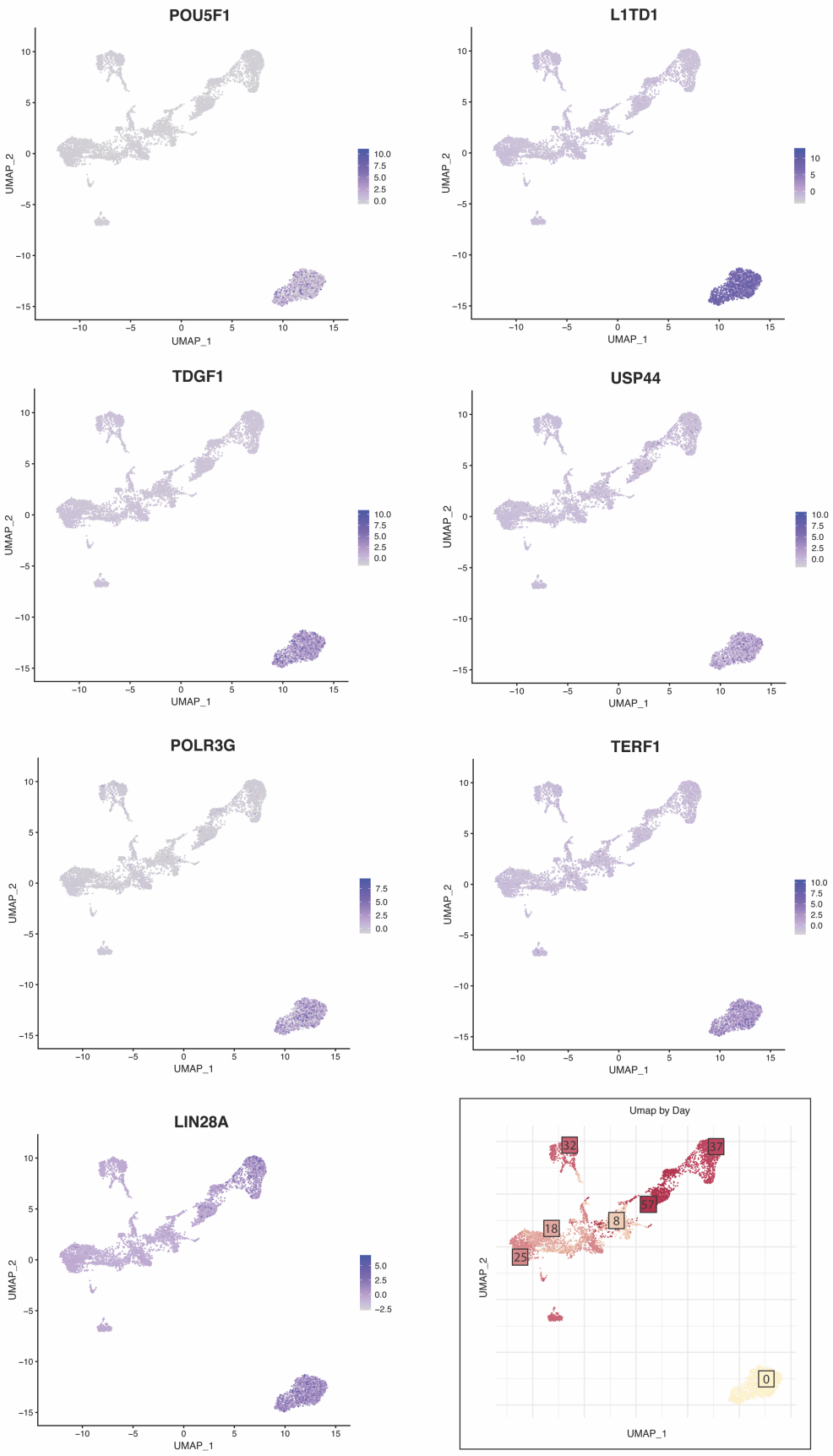

Figure 4.15 *Expression of stemness markers over time. Trajectory of expression of POU5F1, L1TD1, TDGF1, POLR3G, TERF1, USP44, LIN28A. All these genes resulted highly expressed only in the cluster corresponding to D0, even if LIN28A was also expressed in D37 and D57 cluster [see Fig. 4.14]. The color scale represents the normalized expression for that specific gene.*

The same analysis was then performed on a set of selected genes which could confirm that the developmental trajectory was going towards the intended mDA neuronal cell type where we specifically selected both early and late mDA differentiation markers (OTX2, LMX1A, FOXA2, MSX1, NR4A2, TH, MAP2, PITX2, DCX, SLIT1, DDC) (Novak et al., 2022). All the genes followed the expected trends of expression over development. The results of these analysis are illustrated in the Figure 4.16 [also see Supplementary Fig. S2].

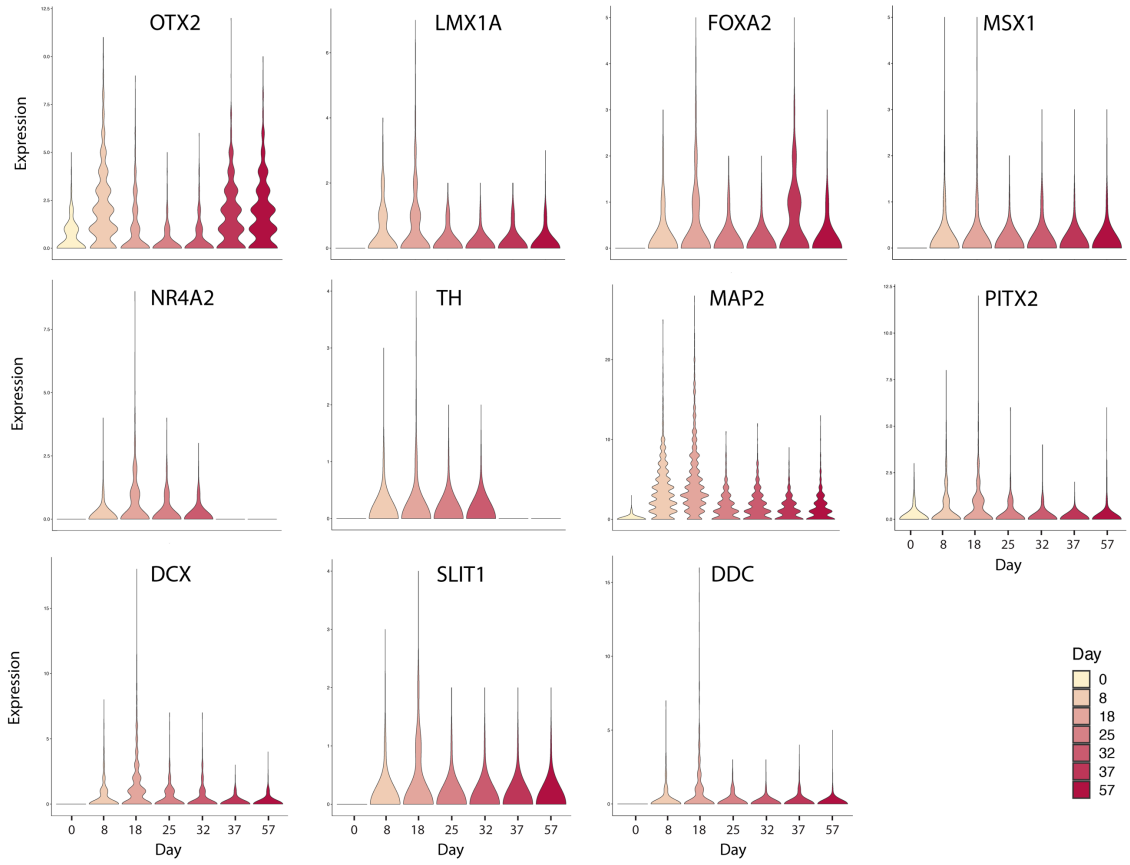

Figure 4.16 *Expression of early and late neuronal markers over time. Violin plots showing the normalized expression at all the different time points of neuronal markers OTX2, LMX1A, FOXA2, MSX1, NR4A2, TH, MAP2, PITX2, DCX, SLIT1 and DDC, for control and PINK1 combined.*

4.3.3 Gene function analysis reveals the main cellular functions associated to each specific time points

The next objective was to assess the distinctive features of each time point to emphasize the dynamical changes in the cellular processes throughout the developmental process. For this purpose, the gene expression profiles of both the control and PINK1 cell lines were again combined, and each individual time point was compared to all other time points. Next the 100 most differentially expressed genes (DEGs) for each of the time point were investigated on GeneMANIA to determine the major pathways in which these genes are implicated [Table 4.3]. All the Top 100 DEGs for each time point are reported in Supplementary Fig. S3. As shown in the table below, the cells were following the expected neuronal development since most of these DEGs, especially after Day 18, were involved in cytoskeleton reorganization, neuronal growth, axonal transport and eventually to synaptic activity. For more details, see Discussion.

Time Point	Genes functions
Day 0 	*chromosome separation* *nuclear DNA replication* *cell cycle DNA replication* *mitotic nuclear division* *spindle assembly* *DNA recombination*
Day 8 	*stem cell population maintenance* *stem cell differentiation* *gland development* *forebrain development* *ovulation cycle* *regulation of epithelial cell proliferation* *gliogenesis* *brain development* *regulation of neuron differentiation*
Day 18 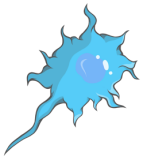	*regulation of organelle organization* *regulation of neuron projection development* *supramolecular fiber organization* *cytoskeleton organization* *axonogenesis* *dendrite development*
Day 25 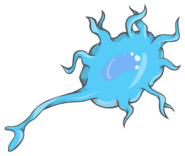	*axonogenesis* *post-synapse activity* *intracellular transport* *glutamate receptor activity* *microtubule polymerization* *organelle transport along microtubule* *neurotransmitter receptor activity* *axonal transport* *membrane depolarization*

Day 32 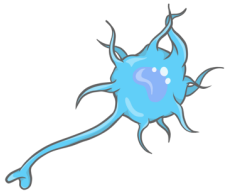	*axonogenesis* *axonal transport* *axo-dendritic transport* *membrane depolarization* *transport along microtubule* *organelle transport along microtubule*
Day 37 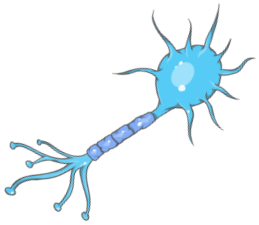	*neurotransmitter receptor activity* *transmitter-gated ion channel activity* *postsynapse* *axonal transport* *axonogenesis* *regulation of protein deacetylation* *organelle transport along microtubule*
Day 57 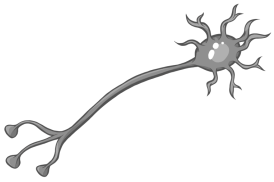	*DNA conformation change* *chromatin assembly/disassembly* *cellular component disassembly* *nuclear chromosome segregation* *apoptotic nuclear changes* *chromatin silencing* *regulation of gene silencing* *actin-mediated cell contraction* *execution phase of apoptosis*

Table 4.3 *Summary of the main gene functions associated to the highest ranked DEGs characterizing each time point.*

4.3.4 Identification of key DEGs between control and PINK1 cell lines highlights the main impaired pathways at each time point

To further investigate potential key mechanisms of PD development and establishment, the most differentially expressed genes between the control and PINK1 cell lines have been identified for each of the seven time points. This enabled us to determine which pathways or processes are severely hampered by this PD-associated mutation, and at what stage of neuronal development this impairment starts to occur. An overview of the most differentially expressed genes for each time point between the *PINK1* (ND) and control (WT) lines are shown in the heatmap in Fig. 4.17.

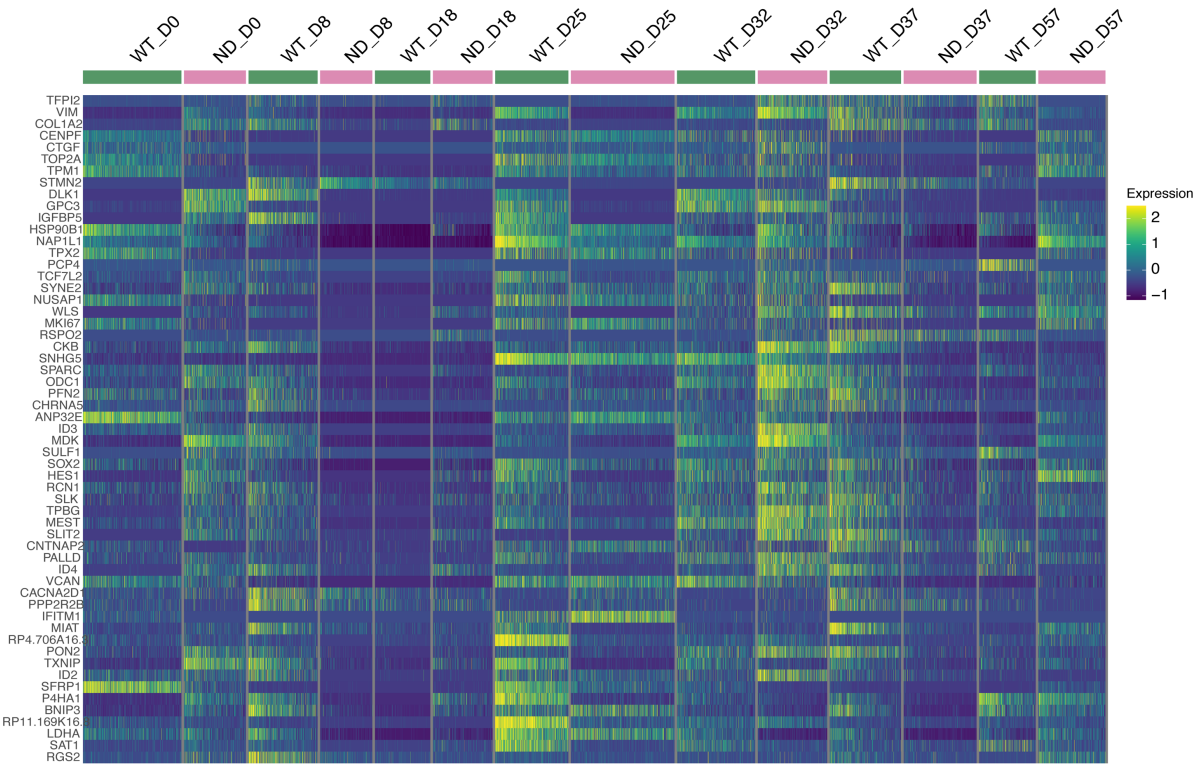

Figure 4.17 *Top DEGs between control and PINK1 at each time point of the differentiation. Colors correlate to the normalized expression of the indicated gene.*

After filtering the DEGs with pValue < 0.05 and FC > +0.3 or < -0.3, we analysed the top 100 DEGs (with the smallest adjusted P-value) for each time point and run the gene function analysis in GeneMANIA to highlight the main differences between control and PINK1 development over time [Table 4.4]. Because the total amount of DEGs identified for the later time points D37 and D57 was significantly smaller compared to the others, we included the entire list of DEGs (not only the top 100) for the gene function analysis of these two days. For the complete set of DEGs between the two conditions at each time point see Supplementary Fig. S4. As illustrated in Table 4.4, the first noticeable impairment appeared at Day 18 and it was related to protein synthesis, being most of the DEGs involved in ribosomal activity. Remarkably, a significant difference in neurogenesis was then observed at Day 32 and 37. For more detailed interpretation of these results, see Discussion.

Time Point	Genes functions
Day 0 	*actin cytoskeleton* *muscle contraction* *actin filament-based movement* *actin-mediated cell contraction* *regulation of G1/S transition of mitotic cell cycle* *G1/S transition of mitotic cell cycle* *actin-myosin filament sliding*
Day 8 	*cytosolic ribosome* *protein targeting to ER* *cell division* *establishment of protein localization to endoplasmic reticulum* *protein targeting to membrane* *ribosomal subunit* *nuclear-transcribed mRNA catabolic process* *DNA biosynthetic process* *ribonucleoprotein complex assembly* *regulation of cellular response to growth factor stimulus*
Day 18 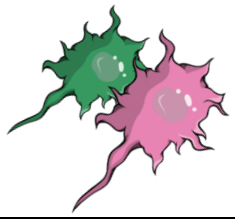	*ribosomal subunit* *nuclear-transcribed mRNA catabolic process* *ribonucleoprotein complex subunit organization* *regulation of translation* *ubiquitin-like protein ligase binding* *negative regulation of proteolysis involved in cellular protein catabolic process* *ribosomal large subunit biogenesis* *ribosomal small subunit biogenesis* *regulation of neuron migration*
Day 25 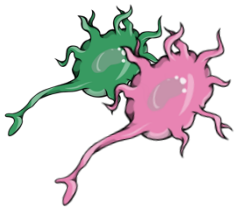	*mitotic nuclear division* *chromosome segregation* *sister chromatid segregation* *negative regulation of mitotic cell cycle* *microtubule cytoskeleton organization involved in mitosis* *condensed chromosome* *spindle organization* *ATP metabolic process* *glucose catabolic process to pyruvate* *neuron death* *NADH metabolic process* *glycolytic process* *glucose metabolic process*
Day 32 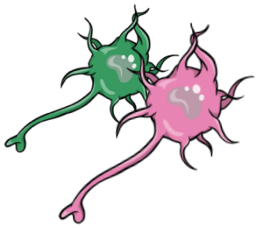	*mitotic nuclear division* *positive regulation of cell cycle* *mitotic cell cycle checkpoint* *aminoglycan catabolic process* *brain development* *gliogenesis* *forebrain development* *glial cell differentiation* *positive regulation of neurogenesis* *forebrain neuron differentiation*
Day 37 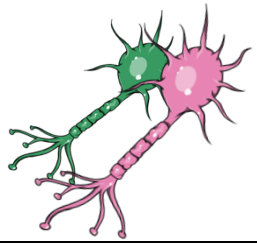	*brain development* *regulation of neurogenesis* *regulation of nervous system development* *positive regulation of gliogenesis* *glial cell differentiation* *stem cell population maintenance* *microtubule-based movement* *actin-based cell projection*

Day 57	*regulation of neuron projection development* *transmembrane receptor protein serine/threonine kinase signaling pathway* *axonogenesis* *cell-cell junction* *regulation of actin cytoskeleton organization* *response to hypoxia* *postsynapse* *regulation of apoptotic signaling pathway* *presynapse* *glucose catabolic process to pyruvate* *glycolytic process through fructose-6-phosphate* *NADH regeneration*

Table 4.4 *Summary of the main gene functions associated to the DEGs between control and PINK1 at each stage of neuronal differentiation.*

4.3.5 Identification of the consistently significant DEGs in control versus PINK1 cell lines during neuronal differentiation

To further study the effect of PINK1 mutation on differentiating neurons during mDA development, we identified the genes that are consistently substantially differentially expressed in the PD cell line compared to the control line at all time points. However, at Day 0, the cells still have to activate the differentiation transcription program, and at Day 57, they exhibited already rather extreme signs of apoptotic profiles potentially linked to neurodegeneration. Consequently, the transcriptomic profiles of these two points differ dramatically from those of the other days. For this reason, Day 0 and Day 57 were excluded from the overall investigation of DEGs during development.

In particular, the DEG identification and interpretation have been performed on three different sets of time points. First, we identified the DEGs from day 8 up to day 37 including all the intermediate time points (Set 1, 76 DEGs). However, after Day 21 the differentiating cells show an abrupt change in their gene expression, as at this stage they start their actual neuronal maturation. Therefore, we performed the analogous DEG analysis on two smaller sub-sets of Set 1: on Set 2 covering the period before maturation (Day 8-18, resulting in 183 consistently DEGs) and Set 3 covering the maturation period (Day 25-32-37, resulting in 61 consistently DEGs). We then performed an Enrichment Analysis on the three sets independently to identify the biological processes which involve the identified DEGs [Fig. 4.18-4.20]. The list of all significant DEGs for each set is reported in Figure S5 in the Supplementary Material section.

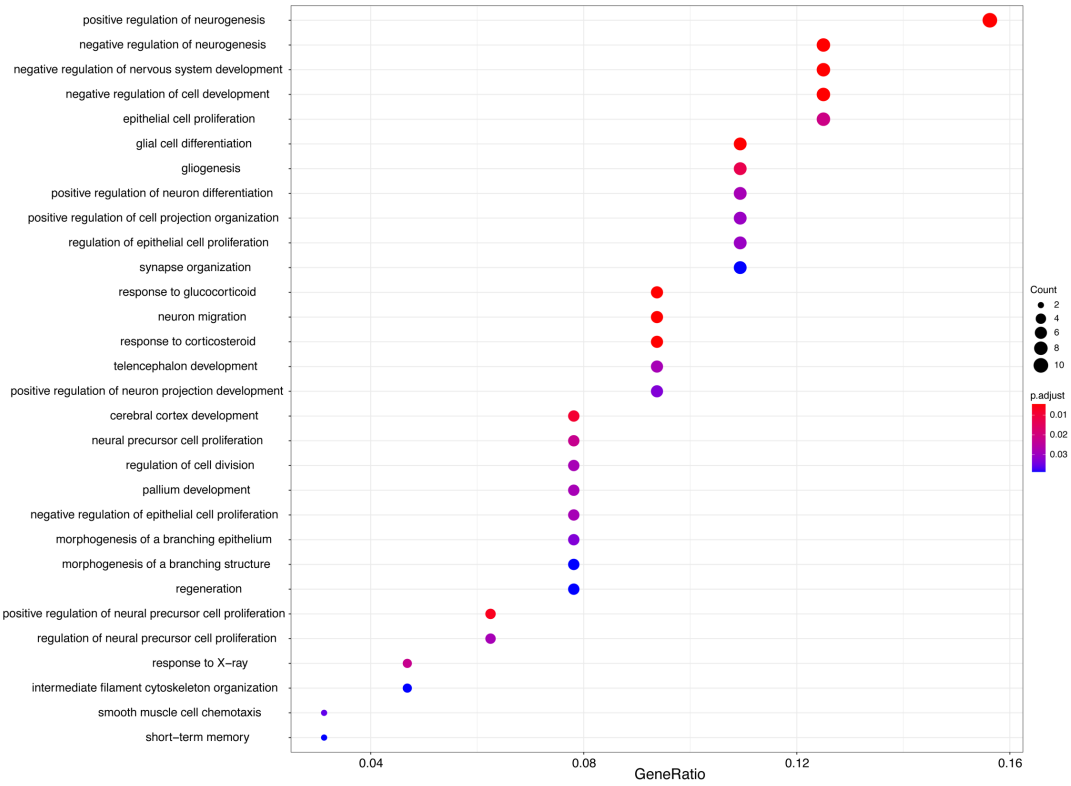

Figure 4.18 *Enrichment analysis on Gene Set 1 (common DEGs between Day 8, 18, 25, 32, 37).*

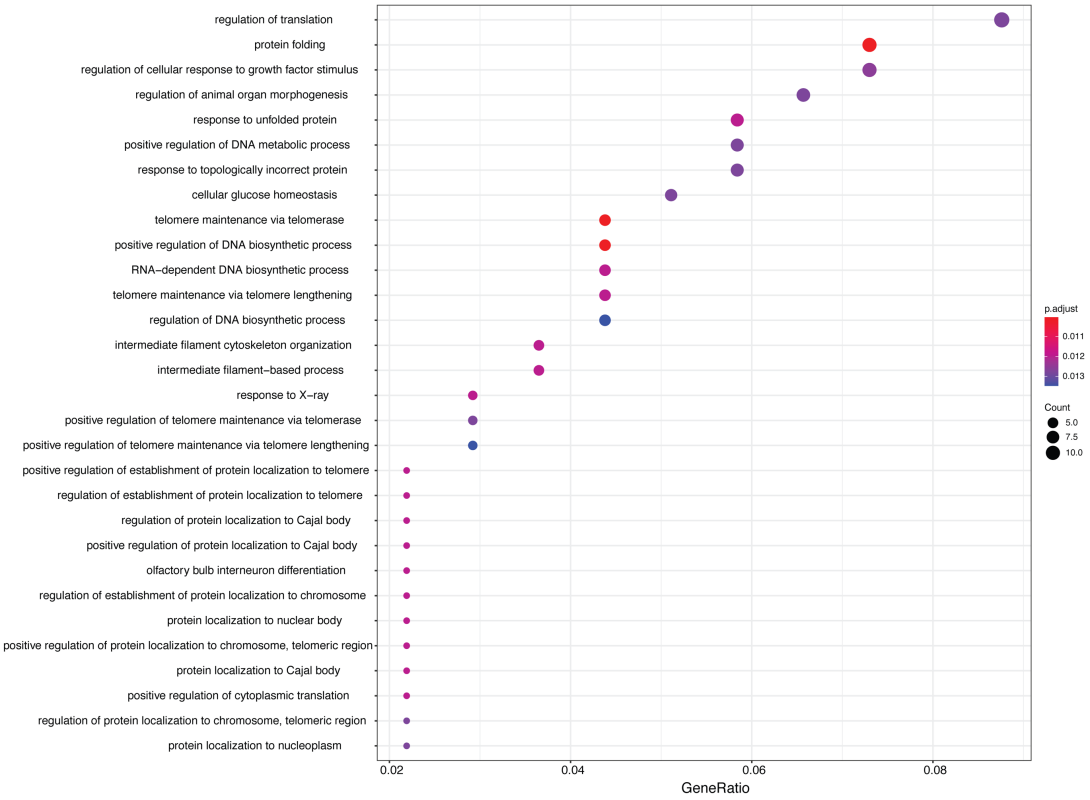

Figure 4.19 *Enrichment analysis on Gene Set 2 (common DEGs between Day 8 and 18).*

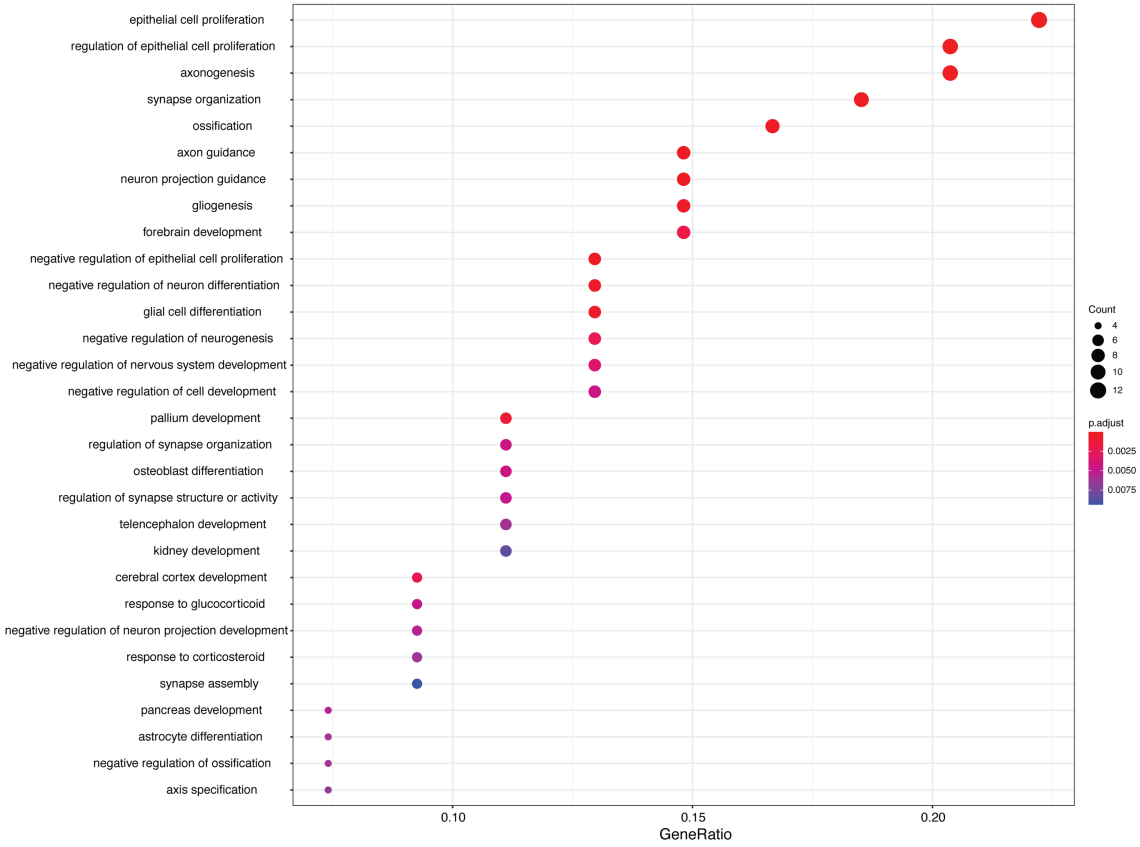

Figure 4.20 *Enrichment analysis on Gene Set 3 (common DEGs between Day 25, 32 and 37).*

To narrow down our investigation further, we next sought for the subset of DEGs shared by all these three sets. This approach finally led to the identification of a central core of 13 DEGs (*CCND1*, *MDK*, *MT.RNR2*, *NEFL*, *SNHG5*, *NAP1L1*, *VIM*, *EIF1AY*, *RP4.765C7.2*, *VCAN*, *FAM162A*, *LIX1*, *SLIT2*) that were persistently impaired in the PINK1 cell line compared to the control line [Fig. 4.21]. The key cellular pathways which involve this subgroup of genes is reported in Fig. S6 (Supplementary Material).

Figure 4.21 *Core set of DEGs.* ***a:*** *Venn diagram showing the overlap between the three sets of DEGs identified by comparing PINK1 and control cell lines. Set 1 (purple) includes all the time points (Day8-18-25-32-37); Set 2 (violet) corresponds to the early differentiation stage (Day8-18); Set 3 (light blue) corresponds to the neuronal maturation phase (Day25-32-37). For each Set, all the statistically significant DEGs between PINK1 and control at the desired time points were considered.* ***b:*** *Violin plots illustrating the distribution at the various stages of the differentiation of the core set of 13 DEGs.*

4.3.6 Proteomics analysis reflects the transcriptomic dysregulation

The proteomics analysis identified a total of 1837 Differentially Abundant Proteins (DAPs, adjusted P-value < 0.05 and FC > +1 and < -1), many of which were found dysregulated at more than one time point. As a first step, we checked for the overlap between this list and the total number of DEGs identified in the DEGs analysis (including all time points, P-value < 0.05 and FC > +0.3 and < -0.3, for a total of 2911 genes). This revealed that 609 genes were dysregulated in both lists, indicating that the impairment in gene expression was also mirrored substantially on the proteome scale by 21% [Fig. 4.22]. The volcano plots showing the most differentially abundant proteins at the different time points are reported in Fig. 4.23.

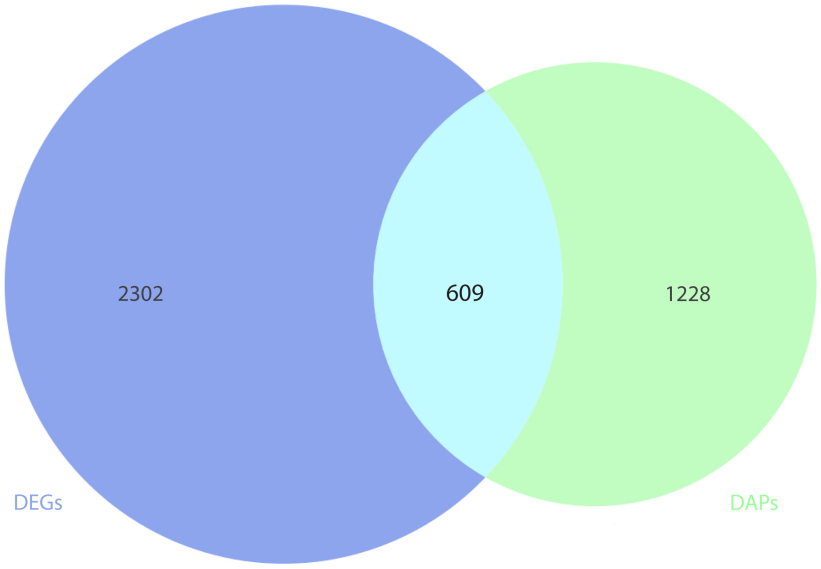

*Figure **4.22** Overlap between total amount of DEGs (light blue) and DAPs (light green) (all time points combined).*

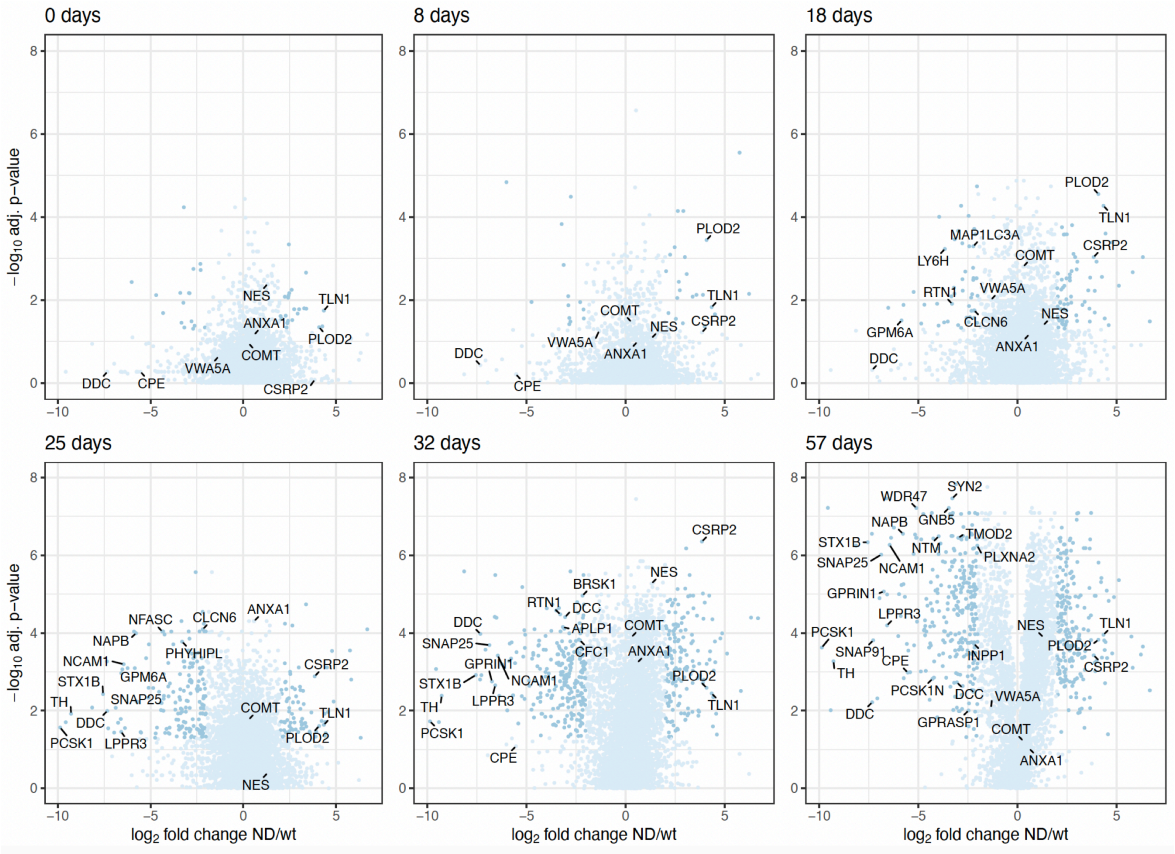

Figure 4.23 *Volcano plots showing the most differentially abundant proteins between PINK1 and control at Day 0, 8, 18, 25, 32 and 57.*

In order to understand which cellular pathways are linking this group of protein-coding genes, we run the gene function analysis on GeneMANIA. For computational limitations, we doubled the FC filtering (0.6 for DEGs and 2 for DAPs) and run the functional analysis on this narrower subset of 90 genes [see Figure S7 in Supplementary Material]. We next checked how many of these shared genes were also included in the 13 key DEGs persistently dysregulated during differentiation [Fig. 4.21]. Out of 609 (with FC +1/-1), 6 DAPs were also in our subset of key DEGs (FAM162A, MDK, NAP1L1, NEFL, SLIT2, VIM), with NEFL and SLIT2 being the most dysregulated proteins and were persisting in the group of the 90 genes obtained by doubling the FC.

4.3.7 Proteomics analysis shows a significant accumulation of DAPs over time

Subsequently, we looked at the top DAPs for each time point. Because the number of proteins measured for Day 37 was not very high for technical limitations, we decided to exclude this time point from this analysis. Figure 4.24 shows the comparison between the number of DEGs (with FC=0 (FC0), and FC > +0.3 and < -0.3 (FC0.3), and P-value < 0.05) and of DAPs (with FC > +2 and < -2 (FC2),

and FC > +1 and < -1 (FC1), and P-value < 0.05) for each time point. Based on this comparison, we decided to continue the analysis by considering the DEGs with FC > +0.3 and < -0.3, and the DAPs with FC > +1 and < -1. From the graph, it is visible that the amount of DAPs accumulates massively over time potentially mirroring the establishment of the PD phenotype.

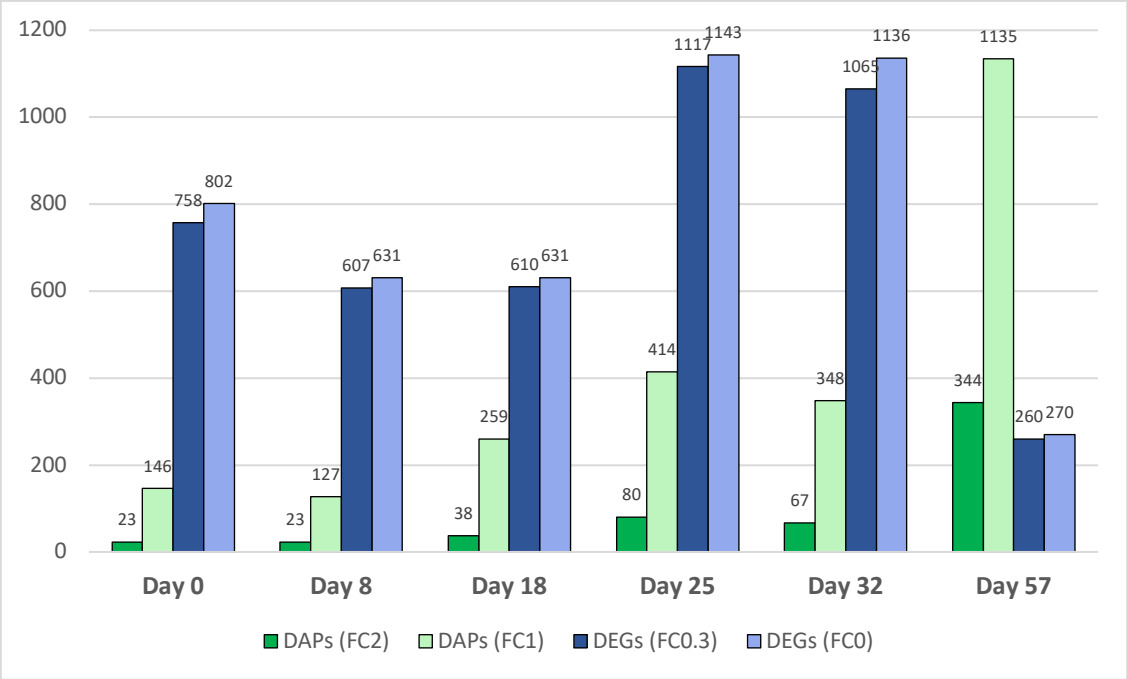

Figure 4.24 *Time point-based total amount of DEGs/DAPs considering two different FC filtering (FC = Fold Change).*

In analogy to the DEG analysis, we investigated the main biological processes on GeneMANIA for the sets of DAPs for each time point (adjusted P-value < 0,05; FC > +2 and < -2). Moreover, we counted how many of those DAPs are also present in the DEGs for that specific time point. The results of this analysis are reported in Table 4.5 [also see Fig. S8 in Supplementary Material]. This functional analysis revealed that most of DAPs were involved in synaptic signalling activity, neurotransmitter regulation and several metabolic processes. For more exhaustive conclusions and observations, see the Discussion Section.

	DAPs Functional Analysis	**Common with DEGs**
Day 0	*apoptotic signaling pathway; cell proliferation; regulation of cell cycle G1/S phase transition; actin-mediated cell contraction*	ANP32A, ANP32E, ASRGL1, CALB1, CASP3, CDK6, CENPF, DSP, EPB41L2, FAM162A, GDF3, GULP1, L1TD1, LARP7, MFGE8, MT1H, PEG10, PFDN5, PLOD2, SCRN1, SEMA6A, SPG20, TES, TMSB10, TUBB6, UFC1, ZNF281 (**19%**)

Day 8	*DNA methylation or demethylation; histone methylation; central nervous system neuron axonogenesis*	ALCAM, CAPN6, EPCAM, EXOC5, GPC3, L1TD1, MT1F, OTX2, PTPN13, SLC2A1, STK39, WLS (**9%)**
Day 18	*axonogenesis; neuron projection organization; long-chain fatty acid metabolic processes; amino acid metabolism*	ALCAM, CENPF, CENPH, EPHA4, FNDC3A, GJA1, GULP1, HELLS, LAMB1, LIN28A, MT1X, MTHFD2, NACA, PALLD, PBX1, PEG10, PGK1, PLOD2, RBP1, SH3BGRL, SLIT2, SNRPD1, SNRPD2, SPARC, SPATS2L, SYNE2 (**10%)**
Day 25	*DNA replication; protein-DNA complex; DNA conformation change; G1/S phase transition of mitotic cycle; helicase activity; double-strand break repair*	ACTN1, ALCAM, ANXA1, APOE, ARL6IP5, CACNA2D1, CADM1, CDK6, CHD1, CNN2, COL4A5, COLEC12, DNAJC9, DNMT1, DPYSL3, EIF4EBP1, ELAVL4, ENO2, EPB41L2, EVL, FAM136A, FAM162A, FAM84B, GADD45GIP1, GAP43, GGH, GJA1, GMPS, GPI, HMGB3, INA, KIF4A, KIF5C, KPNA2, KRT18, LDHA, LSAMP, MAP1B, MCM3, MCM4, MCM7, MTHFD2, NBEA, NCAM1, NOVA1, OTX2, PAFAH1B1, PALLD, PCNA, PHGDH, PLIN2, PLOD2, PSMD1, PTPN13, RAB2A, RRM2, RTN1, RTN4, SEPT10, SMC2, SMC4, SOX2, TAGLN, TCEA1, TERF2IP, TPI1, TPM2, UTRN, VPS13C, VRK1, WARS, ZNF503 (**17%)**
Day 32	*axonogenesis; transport along microtubule; presynapse; regulation of neurotransmitter levels; neuron projection guidance; synapse organization; synaptic vesicle cycle; developmental cell growth*	ABCA8, ANP32E, CACNA2D1, CALB1, CD99, CHGA, CRABP1, GAP43, GPM6A, ITGA6, MDK, NCAM1, NEFL, NRXN1, OSBPL3, PAPSS2, PCNA, PCSK1, PLXDC2, PON2, POU2F2, QKI, RAB13, SCG2, SSFA2, STK33, SYNE2, SYT4, TJP1, TMEM2, TPBG, TUBB2A, WLS (**9%**)
Day 57	*presynapse; axonogenesis; neuron projection development; postsynapse; neurotransmitter transport; synaptic membrane; regulation of membrane potential; axonal transport*	AKAP12, AP3B1, APLP2, BASP1, CA2, CALD1, CNN3, DCX, EZR, FTH1, GAP43, GLO1, GSTP1, NAP1L1, NCAM1, NEFL, NQO1, P4HA1, PCSK1, PDIA6, PEG10, PFKP, PLS3, RTN4, SDC2, STMN1, STMN2, SYNE2, SYT1, TFPI2, TMSB10, VCL (**3%**)

Table 4.5 *Functional analysis on the DAPs of each time point (first column, with FC > +2 and < -2). In the second column, the genes shared in both DAPs and DEGs lists for that time point (to compare a similar number of elements, we decreased the minimum FC for the DAPs to +1/-1 where DEGs were filtered with P-value<0,05 and FC > +1 and < -1). The percentage represents the fraction of DAPs which is overlapping with DEGs at each time point. Genes marked in red were also present in the subset of the 13 key DEGs which were observed to be persistently dysregulated during development [Fig. 4.21].*

Eventually, we identified the overlap between DEGs and DAPs at each time point in order to check how much the impairments on the transcriptomic level were also mirrored on the protein scale [Fig. 4.25].

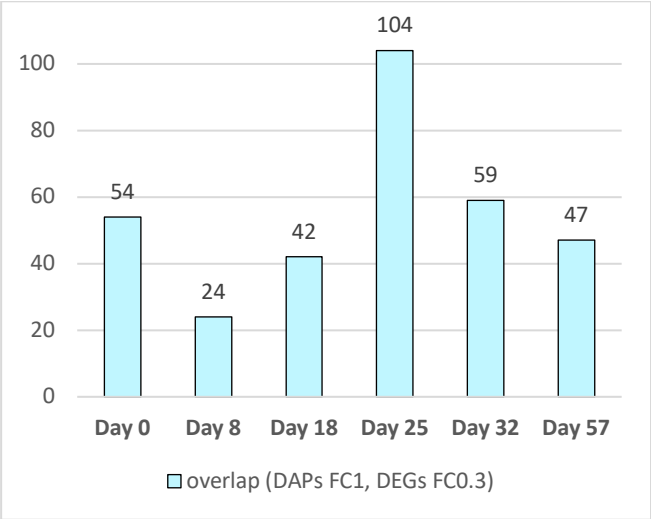

Figure 4.25 *Overlap between the identified DEGs and DAPs at each time point of the neuronal differentiation.*

4.3.8 Metabolomics analysis indicates metabolic dysfunctions

In parallel, we generated metabolomics data for each time point [Methods]. For each of them, we identified 152 metabolites. Based on the transcriptomic and proteomic data we looked through a targeted approach to these metabolomic data, with a focus on mitochondrial activity. For this purpose, we included in the analysis an isogenic cell pair that was differentiated simultaneously to allow for a more coherent analysis. This cell line pair consists of a PINK1 patient-derived cell line, carrying a c.1366C>T mutation, and a CRISPR-Cas9 corrected control (see Discussion). In line with the previous results, we excluded Day 57 from this analysis as neurons at that stage exhibited strong apoptotic and stress-related phenotypes.

Remarkably, a-Ketoglutarate (AKG) exhibited an interesting time-dependent difference [Fig. 4.26 and 4.27]. AKG is a crucial component in the Krebs cycle and hence can modulate the organism's citric acid cycle activity (Wu et al., 2016). It serves as a nitrogen scavenger and a source of glutamate and glutamine, which then promote the synthesis of new proteins. The increase of this metabolite in PINK1 cell lines at Day 18 and 25 compared to the controls, suggests that the PD cell lines are undergoing a faster maturation characterized by a higher mitochondrial activity compared to higher glycolysis activity in iPSC status. This more intense metabolic activity in the early maturation stage is followed by a saturation of this mechanism which can be deduced from the decrease amount of AKG in later stages. This may indicate that the PINK1 cell lines are then affected by a mitochondrial dysfunction which can lead to a severe metabolic impairment.

Moreover, an intriguing time-dependent variation was also observed in the metabolite Sedoheptulose-7-phosphate [Fig. 4.26 and 4.28]. This molecule is associated to the pentose phosphate pathway (PPP). A recent study showed that it forms and accumulates during PPP activity in response to prolonged oxidative stress (Cheng et al., 2019). Therefore, its increase in PINK1 cell lines during the late neuronal maturation stages might support further the hypothesis that PD neurons are progressively impacted by oxidative stress caused by a gradual mitochondrial failure.

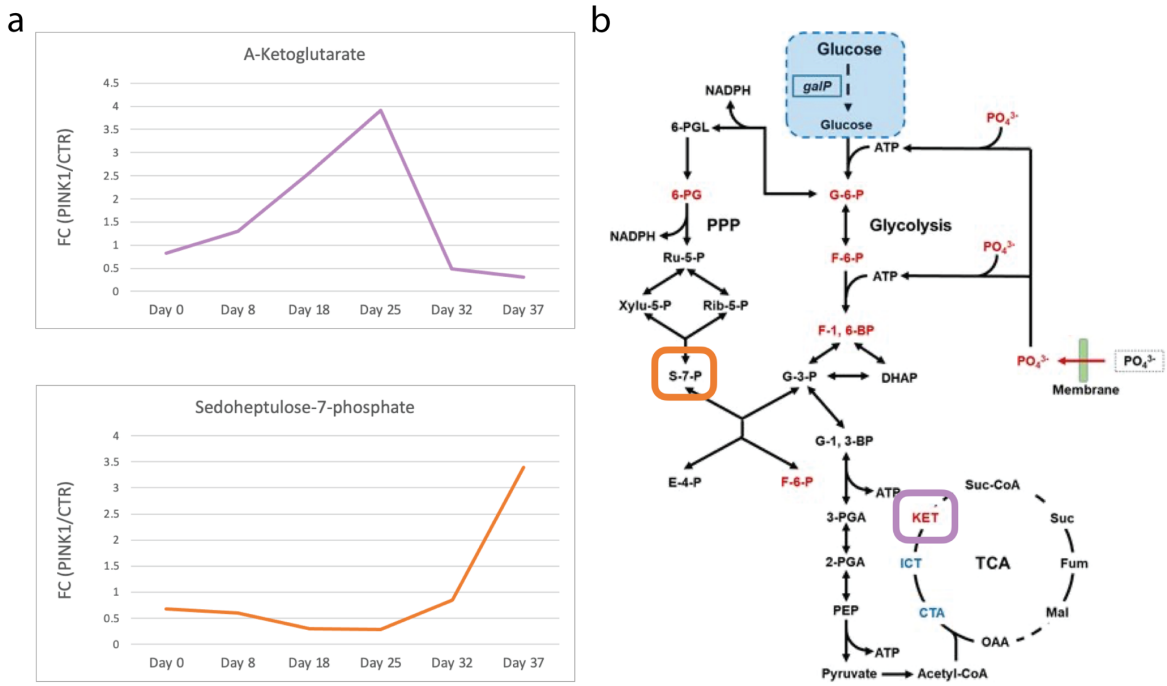

Figure 4.26 a: *Fold-change plots of a-Ketoglutarate and Sedoheptulose-7-phosphate of PINK1 compared to Control over time.* ***b:*** *Schematic representation of the metabolic processes of Glycolysis, Pentophosphate pathway (PPP) and Tricarboxylic acid cycle (TCA).*

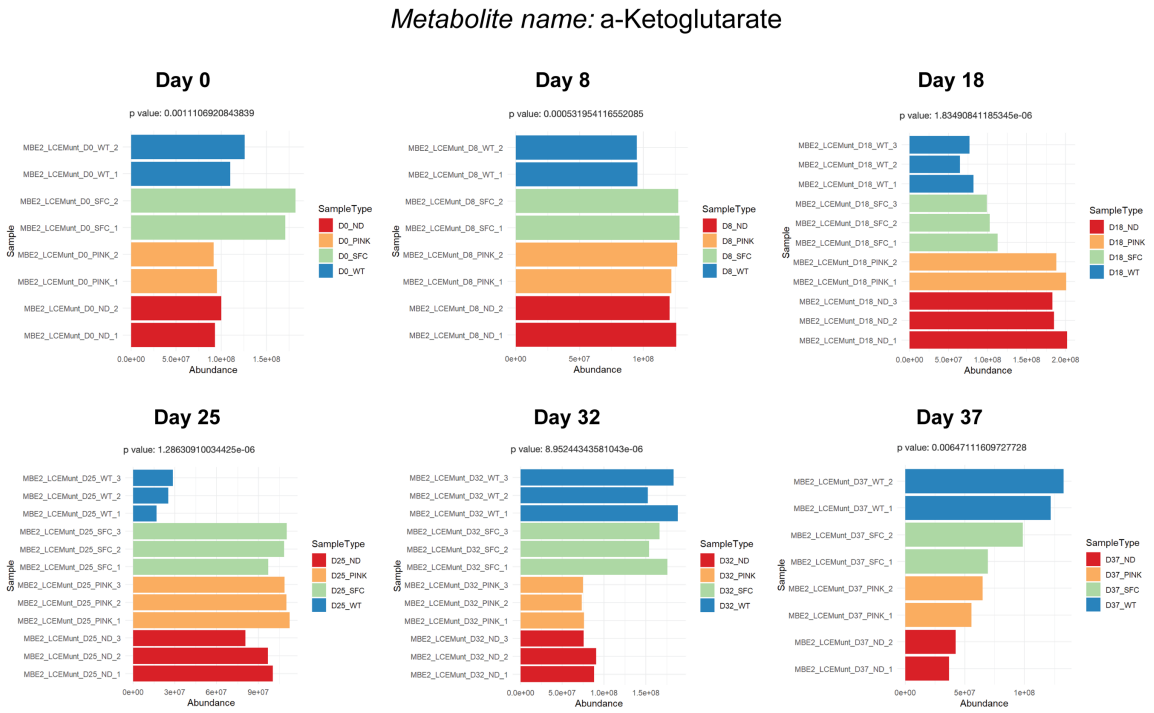

Figure 4.27 *a-Ketoglutarate abundance in PINK1 and control cell lines, at Day 0, 8, 18, 25, 32 and 37. In blue, data related to the normal control cell line which was paired with the PINK1 cell line in red. The other two colors refer to the isogenic cell line (in green the second PINK1-mutation cell line, in orange the CRISPR-Cas9 corrected isogenic control).*

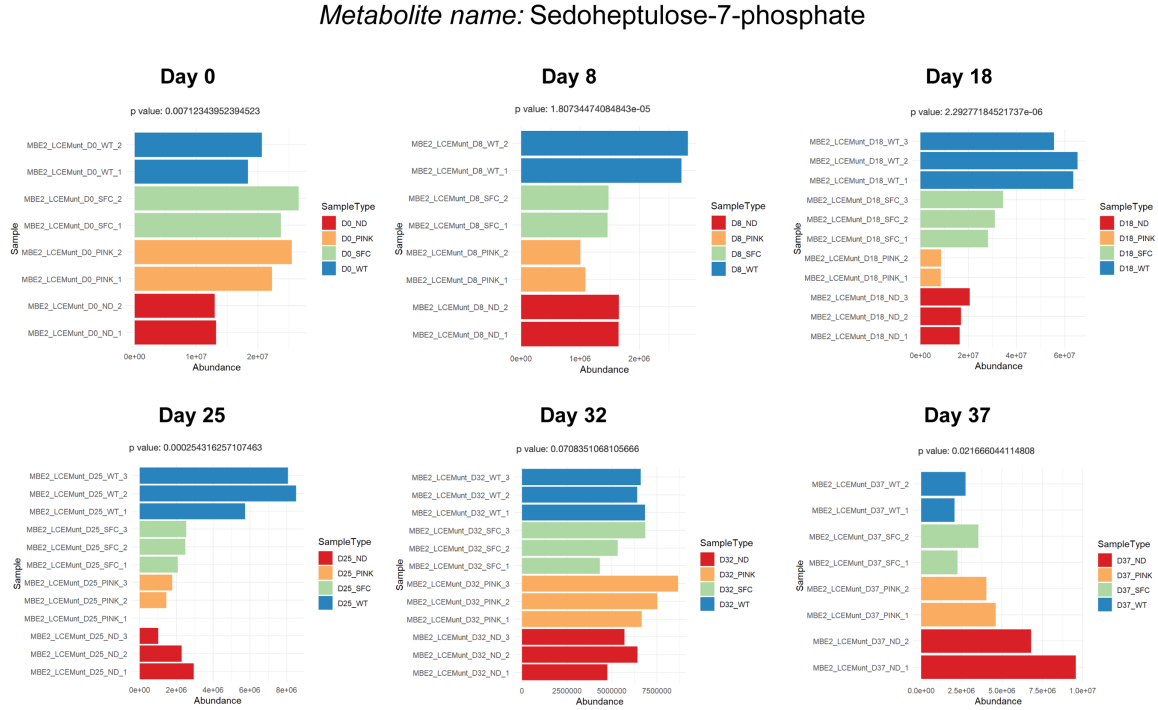

Figure 4.28 *Sedoheptulose-7-phosphate abundance in PINK1 and control cell lines, at Day 0, 8, 18, 25, 32 and 37. In blue, data related to the normal control cell line which was paired with the PINK1 cell line in red. The other two colors refer to the isogenic cell line (in green the second PINK1-mutation cell line, in orange the CRISPR-Cas9 corrected isogenic control).*

5. Discussion and Outlook

Parkinson's disease is a complex neurodegenerative pathology whose precise aetiology remains elusive, although several genetic risk factors, as well as various genes which cause rare familial forms of PD, have now been identified (see Section 1.4) (Blauwendraat et al., 2020). Likewise, different environmental factors such as smoking, exposure to toxins or pesticides, and caffeine consumption are known to alter the risk of developing PD (Subsection 1.1.3) (Zanon et al., 2018). The movement disorder is caused by the progressive death of dopaminergic neurons in the *substantia nigra pars compacta*, with intracellular aggregation of alpha-synuclein in the form of Lewy bodies and Lewy neurites being the pathogenic hallmark (Subsection 1.1.1) (Tolosa et al., 2021). To date, numerous processes have been linked to Parkinson's disease, including mitochondrial dysfunction, defective protein clearance systems, and neuroinflammation (Section 1.3), but the details regarding how these parameters interact are still elusive due to the underlying complexity. To address this challenge in my PhD project, I applied current cutting-edge technologies to investigate mechanisms of PD development by characterizing the differentiation dynamics of patient-based iPSCs carrying a mutation in the *PINK1* gene into dopaminergic neurons, by deep phenotyping including single cell RNA-sequencing, proteomics, metabolomics, and imaging.

During the last decades, scientific advances in developmental, cellular, and molecular biology led to the understanding of how to obtain dopaminergic neurons from patient-derived fibroblasts, previously reprogrammed into stem cells. Today, there are different methods available that allow for this *in vitro* neuronal development. Consequently, the first step in my project was to compare two principal approaches to determine which protocol would be best to adopt for our investigation (Kriks et al., 2011; Reinhardt et al., 2013). Specifically, Reinhardt's protocol allows an "indirect" differentiation from iPSCs to DA neurons by passing through the stage of smNPCs, which are expanded and purified for several days or weeks. Contrarily, Kriks' protocol avoids this intermediate step and permits a "direct" differentiation from iPSCs to DA neurons. For our comparison, I initially differentiated the same cell line following the two protocols until neuronal maturation (Day 30) and performed immunostainings at different stages of the development (Section 4.1). These experiments were based on the evidence from literature that the presence of PAX6 in the early stage of maturation leads to the generation of dopaminergic neurons typically found in the retina and the olfactory bulb, and therefore to non-specific midbrain DA neurons. On the other hand, the absence of PAX6 triggers a cascade of gene expressions which eventually leads to differentiation of

midbrain-specific DA neurons, which are the ones mostly affected in PD (Corbin et al., 2003). In these experiments, differentiating cells were stained for PAX6 and for TH (as a marker for dopaminergic neurons). From our results, both protocols eventually allowed the generation of TH positive neuronal populations with the expected yield of around 50%-60%. However, the cells differentiated with the Indirect protocol exhibited PAX6 signal for the early stage of differentiation (Day 0 and 8), which was not the case for the Direct protocol where cells derived with this approach never showed a signal for PAX6 [Fig. 4.4 and 4.5]. This suggests that the Direct method was generating exactly the type of DA neurons affected in PD. To validate this, we set up a separate experiment to perform a deeper analysis on the cells differentiated with the Direct method by analysing their transcriptome by single-cell RNA-sequencing at different time points of the differentiation until Day 50 [Fig. 4.6]. This investigation highlighted that both stemness and early/late maturation markers were expressed following the expected trends and timing, confirming that the Direct differentiation protocol allows to generate high-quality midbrain-specific DA neurons. This transcriptomic analysis was subsequently used as the foundation to investigate changes in gene expression in the context of a mutation in the *PINK1* gene which is a PD-associated (Subsection 1.4.1).

In the first characterization (Section 4.2), we focused on the analysis of early timepoints of the differentiation protocol, during which cells undergo neural differentiation up to the state of early postmitotic mDA neurons (D21). The underlying hypothesis is that these cells are not expected to display already strong neurotoxicity features but are likely to reveal central pathways that lead to the early pathology of PD which might be hidden in analyses of later stages and may provide new entry points for therapeutic intervention. We chose a cell line homozygous for the ILE368ASN-PINK1 mutation since the genetic background can impact severity and progression of the disease (Zanon et al., 2018). *PINK1* mutations are typically characterized of a full penetrance and early onset of PD. Hence its very strong influence is expected to mitigate the effect of the genetic background. The limitation of using an early time period is of course that we could not identify pathways associated with PD pathology in mature and aging neurons. Instead, as mentioned above, we wanted to focus on the identification of pathways prior to damage onset, in order to eliminate the identification of pathways secondary to the disease, like those induced by damage and associated with the process of cell death. The single-cell transcriptomic comparison between the PINK1 and a control cell line, led to the identification of 285 DEGs, which were persistently dysregulated during development. Creating a protein–protein interaction network based on these groups of DEGs demonstrated that genes of all groups formed important nodes within the interaction network.

Furthermore, genes of all groups were frequently associated with PD. Notably, analysis of the network showed that certain DEGs are points of convergence within the protein network and form major nodes, namely CUL3, HSPA8, EEF1A1, UQCRFS1, CNTNAR2, PSMA4, HNRNPC, and PLCB4 [Fig. 4.10]. CUL3 has been linked to PD by GWAS studies and is considered a potential PD drug target (Canning and Bullock, 2014). HSPA8 (also known as HSP73 and HSC70) disaggregates alpha-synuclein amyloid fibrils and plays a role in autophagy and the catabolic pathway for alpha-synuclein, controls mitophagy by modulating the stability of the PINK1 protein, and its expression has been reported to be impaired in sporadic PD (Zheng et al., 2018). Indeed, HSPA8 was by far the most important node in our network, and it is also one of the most highly dysregulated genes in our dataset. EEF1A1 Translation Elongation Factor mediates activation of the heat-shock transcription factor HSF1, a key player in PD, and prevents α-synuclein aggregation, as well as interacting with Parkin (PARK2) and HTRA2 (PARK13) (Ekimova et al., 2018). UQCRFS1 is a mitochondrial electron transport chain ubiquinol-cytochrome c reductase, a member of the KEGG-PD pathway (Entry K00411), and has been identified as a PD risk gene (Feng and Wang, 2017; Hernandez et al., 2020; Kanehisa et al., 2019). CNTNAP2, which belongs to the neurexin superfamily, plays a role in triggering protein aggregates, was found to be differentially expressed in the blood of PD patients with *LRRK2* mutation, and was also associated with PD by GWAS (La Cognata et al., 2017; Varea et al., 2015). PSMA4, a proteasome subunit, is part of the KEGG-PD pathway (hsa05012, bta05012, and K02728) and participates in the ubiquitin-proteasomal pathway, which plays a key role in PD (Chung et al., 2001). HNRNPC interacts with both PARK2 and members of the Poly (ADP-ribose)-dependent cell death pathway implicated in PD (Lee et al., 2014). PLCB4 has been linked to PD and knock-out mice show motor defects consistent with ataxia (Kim et al., 1997; Rouillard et al., 2016). However, many of the less conspicuous nodes are also known to play a role in PD, including EGLN3, IPO5, IPO7, PALLD, PGD, RALGPS2, CYCS, SHH, BRCA2, and others. Hence, the network derived from our analysis of the ILE368ASN-PINK1 mutation is revealing the convergence of many known key PD-associated pathways.

This convergence suggests that different mutations may feed into the same PD pathology-associated routes and that each mutation can act through several pathways. A strength of our network analysis is that it might shed light on PD-associated genes whose function is so far poorly understood. Another line of supporting evidence for this network's role in PD is that, based on the STRING database search, the most strongly associated KEGG pathway of this dataset is the Parkinson's disease KEGG pathway [Fig. 4.9].

A surprising finding from our investigation is that pathways known to play a role in Parkinson's disease are profoundly and consistently dysregulated at all timepoints examined, far before the onset of PD pathology. This is consistent with current research, which indicates that the disease is likely to occur long before the onset of mDA neuron cell death and evident PD motor symptoms (Chaudhuri et al., 2011; Le et al., 2014). Many of the DEGs identified in our study are involved in more than one pathway and thus connect the various pathways known to play a role in Parkinson's disease, such as stress and catabolic processes, aromatic compound metabolism, vesicle-mediated transport and exocytosis, RNA metabolism, protein transport, localization, folding, stability, and ubiquitination (Ebanks et al., 2020; Garcia-Esparcia et al., 2015; Lin et al., 2019; Martin, 2016; Walden and Muqit, 2017). This confirms the hypothesis that PD pathology involves many different pathways and suggests that the final disease phenotype is the result of long-term untreated pathology (Agarwal et al., 2020). It also points to possible early alterations which may be detectable and used as a diagnostic tool, as well as to targets for early treatment and prevention of the disease.

In order to assess how persistent these dysregulations are, and how the late maturation affects them, I proceeded with a new experimental set up which would include later time points and a deeper phenotyping (Section 4.3). For this purpose, this experiment included also a rigorous proteomics and metabolomics analysis at several time points of the neuronal differentiation, aside the single-cell RNA-sequencing. In fact, performing an investigation on multiple scales given by the biological levels and combining them to achieve a broader picture might clarify the pathology's complexity and the underlying mechanism causing the onset and progression. Such a multi-scale approach has already been adopted in the last years. An example is the international FOUNDIN-PD project, which aims to create foundational multi-omics data for PD (www.foundinpd.org). In this project, they included 95 different PD patients-derived iPSCs cell lines including from idiopathic cases, from which DNA, RNA and proteins were isolated and subsequently processed.

However, even if this important initiative has a broader approach which includes more cell lines, my project led to a deeper understanding of the dynamics of PINK1-cell lines differentiation, since I considered more time points and, for each of them, I collected data on the transcriptomic, proteomic and metabolomic levels whereas the FOUNDIN-PD project had only complete phenotyping for the endpoint and therefore miss some essential dynamic properties. For this experiment, I differentiated cells of the same PINK1 and control cell lines of the previous project up to Day 57 with the Direct differentiation protocol (Kriks et al., 2011). In this case, cells were

collected and analysed at Day 0, 8, 18, 25, 32, 37 and 57. To support the hypothesis that the PINK1 mutation causes persistent dysregulation of a subset of genes, resulting in impairment in a variety of specific cellular functions, we initially compared our identified DEGs with those found in the previous analysis (Section 4.2.1). Because the other analysis was limited to early time points of the differentiation (Day 6-15-21), we only considered Day 8 and 18 of our new dataset. The DEGs comparison highlighted 8 genes which were common to both datasets: SNHG5, EIF1AY, PGK1, PSMB5, LMAN1, PSMC3IP, RP11.298C3.2, PGD. The more limited overlap is probably caused by the not perfectly aligned time points of analysis which were adapted in the multiscale experiments to cover the most essential differentiation steps during the more long-term analysis. Notably, running the GeneMANIA gene function analysis on this group of 8 genes revealed that they collectively play a role in cellular response to hypoxia, in the proteasome complex activity as well as in the regulation of several metabolic processes. The analysis of the overlap between the two datasets was carried out only after a precise correlation analysis, which revealed that these two datasets were derived from cell populations with gene expression profiles that were significantly close enough to be comparable [Fig. 4.13].

After this comparison, we analysed deeper the new single-cell RNA-sequencing data. As a first approach, we selected a list of stemness and neuronal markers and checked for their expression in the two cell lines, control and PINK1, combined. All the markers were expressed in the expected time points. Interestingly, we noticed that LIN28A, which is considered a stemness marker for its activity as regulator of embryogenesis timing and progenitor self-renewal (Copley et al., 2013), was also highly expressed at Day 37 and 57 and not just at Day 0 [Figs. 4.15 and 5.1].

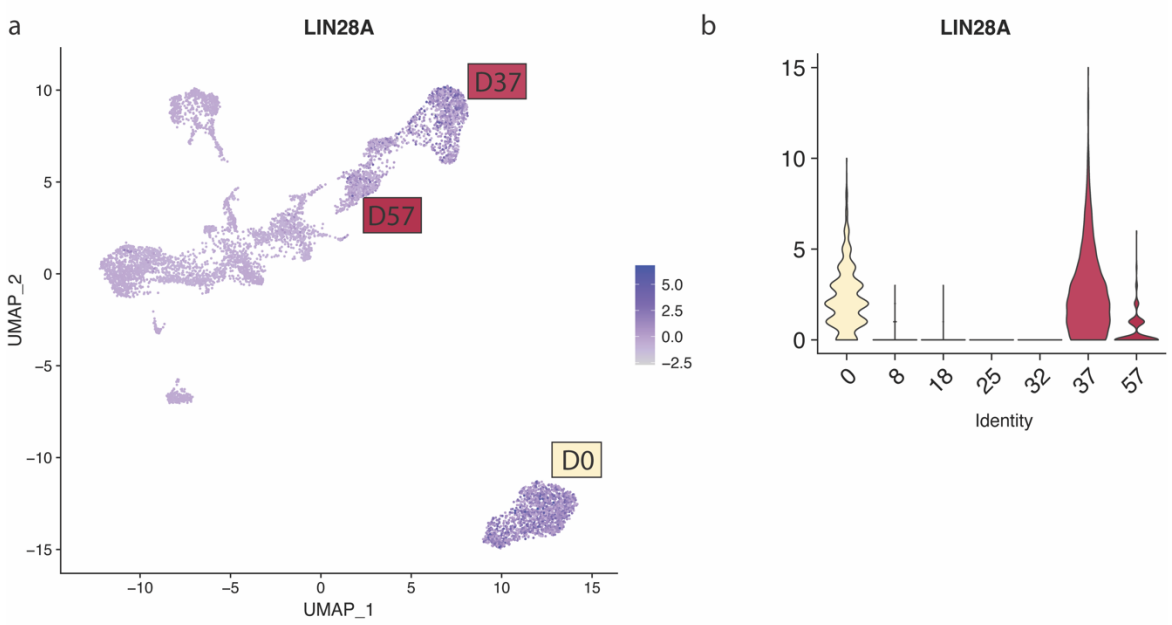

Figure 5.1 *LIN28A expression in control and PINK1 combined [taken from Fig. 4.15 and S1].*

From literature, it is also known that the overexpression of this gene significantly increases the rate of glycolysis, and, combined with a reduced oxygen consumption, is specifically affecting the mitochondrial complex IV activity. This suggests that LIN28A plays a crucial role in cellular metabolic plasticity by promoting a more glycolytic phenotype through mediating enhanced mitochondrial recycling which reducing oxidative phosphorylation (Docherty et al., 2016). This observation highlighted the fact that neurons in the later stages of the differentiation most likely are undergoing intense changes in their metabolic profiles, as expected, which is probably indicating stress conditions.

In order to further characterize the differentiation dynamics of mDA neurons development, we initially combined the PINK1 and control conditions and identified the DEGs which were uniquely defining each time point in comparison to all others. We next performed a functional analysis via GeneMANIA on the top DEGs for each time point in order to highlight the main biological processes which are representative of that specific developmental stage [Table 4.3].

For Day 0, the main functions were associated with DNA replication, spindle assembly, DNA recombination and nuclear division, suggesting that at this stage the cells are still actively proliferating. At Day 8, several DEGs were still involved in stemness-related functions, such as stem cell population maintenance and regulation of cell proliferation. However, some of them also were

associated with early stages of neuronal differentiation, forebrain development and gliogenesis. Cells at the next stage (Day 18) appeared to be strongly associated to a more specific and functional neuronal differentiation because the main DEGs characterizing this time point compared to the other days were associated to specific changes in the cytoskeleton organization – most likely indicating neuronal projection growth, such as for dendrites and axons. The same trend, but even more intensified, was observed at Days 25 and 32. Interestingly, these two time points are also characterized by the presence of DEGs associated with membrane depolarization and axonal transport. At Day 37, all DEGs were again found to be strongly related to neuronal characteristics with more specific functions related to the neurotransmitter synaptic activity. Neurons collected at the last time point (Day 57) were thought to be considerable as an "aged" population of neurons, potentially in an already stressful conditions, to which the cells are exposed after two months of culture that might have partly triggered physiological biological processes linked to ageing processes *in vivo*. Indeed, the analysis of the main DEGs for this time point visibly showed that some cells exhibited signs of apoptotic nuclear changes.

Once we validated that both control and PINK1 cell lines were following the expected neuronal differentiation path, we next looked for the DEGs at each time point between the two populations to detect the intrinsic more subtle differences which were caused by the presence of the *PINK1* mutation. Again, we identified the list of the top DEGs for each time point and run the function analysis on GeneMANIA to highlight the main functions affected [Table 4.4].

This investigation revealed that the first relevant impairment appeared around Day 18 where a huge difference in the protein synthesis capability is observed since most dysregulated functions are related to ribosomal-associated activities. At Day 25 a substantial difference in the cell division of these two cell lines was detected, indicating a significant difference in active proliferation. Furthermore, the biggest differences observed at Days 32 and 37 were associated with the process of neurogenesis (such as axon development), suggesting that the control and PINK1 populations were branching into two separate phases of neuronal differentiation.
This is in line with our hypothesis that the presence of a mutation in *PINK1* gene might induce a faster maturation, and therefore faster ageing, of the neurons. In fact, it was noticeable already during the differentiation of the cells, that the PINK1 cell line was maturing faster compared to the control based on their morphological changes [Fig. 5.2]. As shown in Fig. 5.2, at Day 24 the PINK1 cell line had already started developing neuronal projections, while it was visible that the control was still intensively proliferating.

This finding supports the evidence that PD-related mutations lead to faster differentiation and maturation, like in the context of *LRRK2* (Walter et al., 2021) where impairment of metabolism might drive the faster aging and subsequent cell death.

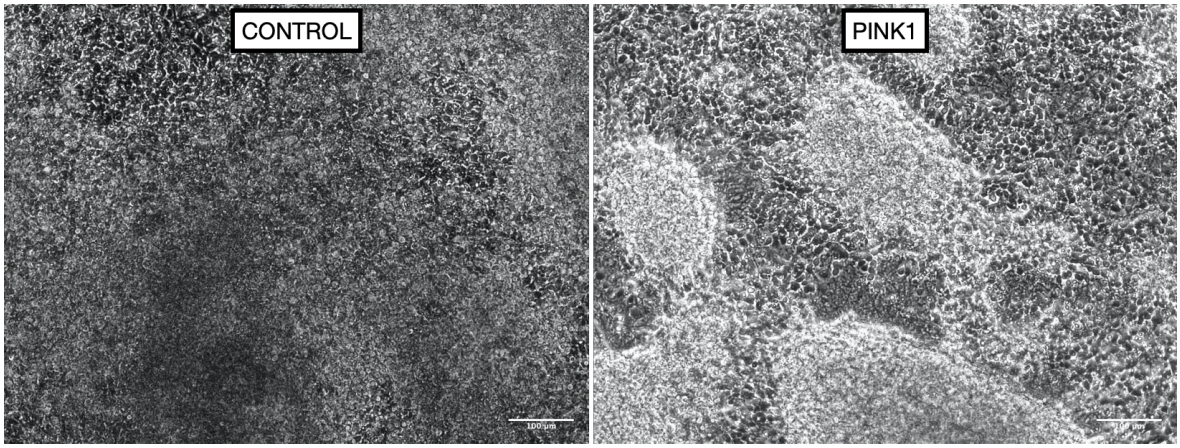

Figure 5.2 *Differentiating neurons at Day 24 from the control (left) and PINK1 (right) cell lines.*

In order to identify genes which were persistently dysregulated between the PINK1 and control cell lines during the whole differentiation process, we run the DEGs analysis on different combinations of time points together. We initially considered all time points between Day 8 and 37 (Set 1), excluding Day 0 and 57 as they highly differ from the other time points in terms of transcriptional profiles. Then, we performed the same analysis on Set 2 (Day 8-18), as representative of the early maturation phase, and on Set 3 (Day 25-32-37) which corresponds complementary to the late developmental maturation phase. The enrichment analysis for these three different sets highlighted a list of major biological processes that were significantly impaired [Fig. 4.18-4.20]. More specifically, the main processes identified for Set 1 were regulation of neurogenesis, nervous system development, neuron differentiation, synapse organization and neuron projection development. Because Set 1 included all the central time points of differentiation, this result suggested that these were the major impaired functions in the overarching big picture of the process. To unveil more specific impairments, which were taking place either before or after the maturation, we run the same analysis on Set 2 and 3. For Set 2, the key processes involved were related to unfolded protein response, regulation of translation, DNA metabolic and biosynthetic processes, and cellular glucose homeostasis. This is in line with what we observed before, in the time point-based comparison which highlighted a severe impairment in the ribosomal activity of

the cells at Day 18 which most likely would trigger a change in the principal maintenance activity of cells such as metabolism and growth. Finally, the enrichment analysis on the after-maturation time points revealed that the main impaired processes between PINK1 and control are more specifically related to axonogenesis, synapse organization, axon guidance, forebrain development and cell proliferation. This indicates that the cells are at already significantly different phases of the differentiation at this stage, again supporting our hypothesis that the *PINK1* mutation induces a faster ageing of neurons, hence causing metabolic impairments and less efficient responses to stress.

To narrow down our analysis even more, we looked at the DEGs which were common to all three lists of DEGs for Set 1, 2 and 3. The result was a small group of 13 DEGs (*CCND1*, *MDK*, *MT.RNR2*, *NEFL*, *SNHG5*, *NAP1L1*, *VIM*, *EIF1AY*, *RP4.765C7.2*, *VCAN*, *FAM162A*, *LIX1*, *SLIT2*) which were therefore identified as the most persistently differentially expressed ones [Fig. 4.21 and Supplementary Fig. S9]. Having identified the small central set of DEGs of interest, we also looked at the single gene functions and link them to their potential role in PD-associated impairments.

CCND1 (Cyclin D1) is a regulator of cell cycle progression by controlling the G1/S phase transition. CCDN1 was already linked to PD as it was observed that its overexpression generally results in oncogenic development or apoptotic-related neurodegeneration in *post-mitotic* neurons (Höglinger et al., 2007). More recently, it was also shown that CCDN1 is specifically involved in alpha-synuclein related cell death (Santos-Lobato et al., 2021).

MDK (Midkine) is a growth factor that act as a reparative neurotrophic factor (Sakakima et al., 2009). From literature, it is known that this gene plays a role as survival factor for neurons and that it is a crucial factor for neurogenesis *in vivo* (Reiff et al., 2011; Winkler and Yao, 2014). Moreover, Prediger et al. showed that Mdk deficient mice exhibited preclinical features of PD, such as reduced dopamine levels in both olfactory bulb and striatum (Prediger et al., 2011).

NEFL (Neurofilament Light Chain) is one of the three main components of the neurofilament of axons in dopaminergic neurons, and it is therefore involved in crucial neuronal functions such as neuron projection morphogenesis and axonal transport. It was proven that a dysregulation in this gene leads to an abnormal development of neuronal projections, axonal hypotrophy and therefore causes a slower signal conduction (Yum et al., 2009). Furthermore, it is also known that it also interacts with *VIM* (encoding for Vimentin), which is also one of our key DEGs. Vimentin is an intermediate filament protein of the cytoskeleton which plays a critical role in cell structure and dynamics. It was recently demonstrated that a decreased amount of this protein in PD-patient

derived fibroblasts contributes to PD pathogenesis, probably due to oxidative stress and increased cellular calcium level (Papa et al., 2009; Siciliano et al., 2020; Tanzarella et al., 2019). Interestingly, our experiments showed a significant decreased expression of VIM in the PINK1 cell line compared to the control line already in the first phases of the differentiation [Fig. 4.21b].

SNHG5 (Small Nucleolar RNA Host Gene 5) was also identified as one of the most persistently downregulated DEGs in our previous project [Table 4.1] (Novak et al., 2022). In the network analysis we performed in the previous experiment, we found that *SNHG5* is already specifically related to PD, based on its strong association to LRRK2 mutation. *SNHG5* produces a long non-coding RNA function of which is still under debate. However, numerous studies have linked these RNAs with the occurrence of a variety of diseases, especially neurodegenerative ones such as Parkinson's, Alzheimer's, and Huntington's diseases, as well as with amyotrophic lateral sclerosis (D.-Q. Wang et al., 2018). For this reason, the severe SNHG5 under expression that we observed in the PINK1 line compared to the control condition might be interesting to analyse further in order to clarify the mechanisms through which this gene interferes with the normal neuronal development [Fig. 4.21b].

MT.RNR2 (Mitochondrially Encoded 16S rRNA) encodes for the small mitochondrial-derived polypeptide Humanin. Humanin is involved in several processes such as in the negative regulation of cell death, playing a role as a neuroprotective factor in several cell types including germ cells, neurons and leukocytes, and for this reason has already been largely investigated as it could hold an exciting therapeutic potential (Hazafa et al., 2021; Zuccato et al., 2019). Notably, this gene was severely lower expressed in the PINK1 line suggesting that this cell line was less protected against neuronal apoptosis. This gene was also identified in our previous analysis (Novak et al., 2022) demonstrating its potential essential role in PD development.

NAP1L1 encodes for the Nucleosome assembly protein 1-like 1, which is a histone chaperone that also participates in several important DNA repair mechanisms. Interestingly for our study, this protein was also associated to the regulation of neurogenesis, as it seems to actively promote the proliferation of neuronal progenitors (from UniProt.org). According to our analysis, this gene is less expressed in the PINK1 cell line [Fig. 4.21b] promoting the hypothesis that the mutation induces the corresponding cells to stop proliferating earlier than the control cells, hence accelerating maturation and ageing of neurons.

EIF1AY is a crucial gene for protein biosynthesis, by enhancing ribosome dissociation into subunits and stabilizing the initiator factor Met-tRNA(I) to 40S ribosomal subunits (UniProt.org). Consequently, the severe reduced expression of this gene in PINK1 cells [Fig. 4.21b] is in line with

the impairment in ribosomal-associated activities at day 8 and 18 highlighted in the functional analysis [Table 4.4].

RP4.765C7.2 is a pseudogene that was already identified as highly upregulated in the PINK1 cell line in our previous analysis [Table 4.1], in agreement with the results from the multiscale experiment [Fig. 4.21b]. However, its function remains quite elusive, and further research should definitely focus on its potential role in PD.

VCAN is the gene responsible for encoding Versican, a large proteoglycan found in the extracellular matrix, which plays a role in intercellular signalling, regulation of growth, differentiation, and inflammation. Because this proteoglycan modulates the immune cell trafficking and activation, also in neuronal cells, thereby regulating neuroinflammation, it represents an emerging potential target in the control of inflammation in several diseases (Wight et al., 2020). Once again, from our recent investigation, we could observe a faster drop in the expression of this gene in the PINK1 compared to the control cell line, followed by a sudden increase at the later time points. This suggests that the *PINK1* mutation might decrease cells' capability to respond appropriately to external stress during development, and that under extremely stressful conditions, such as in the late stage of neuronal differentiation, neurons may try to compensate for this prolonged impairment by activating an intense emergency response.

FAM162A is thought to be involved in the regulation of apoptosis, probably through hypoxia-induced cell death. It is believed that FAM162A transmits hypoxic signals to the mitochondria and when over-expressed causes programmed cell death via mitochondrial-regulated apoptosis (Kim et al., 2006; Mazzio and Soliman, 2012).

LIX1 is a protein-coding gene which is predicted to be involved in autophagosome maturation. High-throughput screenings analysis revealed that this gene is highly more expressed in neurons in the *substantia nigra* compared to the other regions of the brain (Chung et al., 2005). Interestingly, further analysis suggested that LIX1 seems to be highly downregulated in PD dopaminergic neurons compared to healthy ones (Verma et al., 2020). These findings support our observation that LIX1 is severely lower expressed in the PINK1 cell line compared to the control line, especially in the first time points. This could indicate the selective vulnerability of mDA neurons in the region of the *substantia nigra* of the brain, even if the precise mechanism underlying this link is still unclear.

SLIT2 (Slit Guidance Ligand 2) encodes a member of the slit family of secreted glycoproteins. This family of proteins is known for playing a crucial role in axon guidance and neuronal migration. Together with SLIT1, SLIT2 appears to be essential for forebrain development by impeding inappropriate midline crossing by axons projecting from the olfactory bulb. Moreover, this gene seems to be crucially involved in the inflammatory response process in the brain, and recent studies

have shown that it works as a neuroprotective factor as it reduces the impact of ageing in mouse brains by regulating the correct growth of axons and neuronal projections (Dugan et al., 2011; Li et al., 2018). As shown in Fig. 4.21b, *SLIT2* was severely lower expressed in PINK1 compared to the control cell line.

Overall, the functional analysis of the persistently dysregulated genes has indicated a set of promising new candidates mediating the development of PD based on their already known biological function. Future research will focus on the validation and detailed analysis of the interplay between these potentially essential entities in the context of PD.

The next step of the analysis was then to look at the proteomics data. More specifically, we searched for the most differentially abundant proteins (DAPs) between the PINK1 and control cell line for each time point. Next, we again looked at the main gene-gene interactions and their related functions [Table 4.5]. This highlighted that at Day 0 the most differentially abundant proteins were involved in apoptotic signalling pathways, cell proliferation and G1/S cell cycle phase transition. At Day 8, most of DAPs were involved in histone methylation/demethylation, axonogenesis and central nervous system development, suggesting that already at this early stage the two populations were undergoing different developmental-related conformational changes. This trend intensifies dramatically at Day 18, when aside axonogenesis and neuron projection development, the dysregulated proteins were involved in amino acid and fatty acid metabolism. DAPs at Day 25 resulted to be involved in DNA replication, protein-DNA complex, helicase activity and DNA double strand break repair. The protein functions of the DAPs for Day 32 were instead showing an important difference in the neuronal activity (presynaptic activity, transport along microtubule, synaptic vesicle cycle), even if not as severe as for Day 57, when DAPs are also participating in the processes of neurotransmitter transport and regulation of membrane potential.

Interestingly, these findings were in line with preliminary proteomics results that we obtained from the analysis of the early differentiation period [Fig. 4.11]. These preliminary observations were only limited to Day 25 (early postmitotic neurons) and Day 40 (mature neurons) and had already shown dysregulation of dopaminergic metabolism at both time points of differentiation. These DAPs exhibited an overlap with the DEGs identified in the previous DEGs analysis, and many of these proteins were already known to be involved in the pathology of PD – the most evident ones were TH and DDC, which are key enzymes involved in dopamine metabolism and therefore closely associated to the disease (Burkhard et al., 2001; Clark et al., 2021; Tabrez et al., 2012). Overall, the

data showed a consistent abnormality in the levels of enzymes needed for DA metabolism, which indicates that cells carrying the PINK1-ILE368ASN mutation have a functional deficit of the DA metabolic pathway that eventually can lead to neuronal loss of mDAs. Notably, both TH and DDC (together with PLOD2 and PCSK1) were also identified in the proteomics datasets of the more long-term differentiation. This overlap is supporting the idea that this metabolic impairment is a key feature in PINK1-associated PD progression. However, the proteomics analysis of the multiscale experiment included more time points and showed that the impairment in the protein scale were already observable in the early time points suggesting that there are early disease-related mechanisms happening even before the visible PD phenotype appearance also at the proteome level.

In a second approach, we checked if the specific impairments on the proteomic level was reflecting the dysregulation of the gene expression. For this purpose, we analysed for how many DEGs we could find the correspondent encoded protein in our proteomics dataset in time-point specific manner [Table 4.5]. Notably, among these lists, we could also identify some of the core 13 DEGs persistently dysregulated during differentiation. Furthermore, these datasets could be also supporting the investigation of the potential delay between the effect of the transcriptomic dysregulation and the proteomic level, and thereby better understand the causality relations between these two scales. In this respect, the metabolomics data represent an a very valuable resource as it seems to indicate consistent metabolic impairments for *PINK1* mutations (Section 4.3.8) which may allow for better phenotype mapping also by more holistic data integration (Gligorijević and Pržulj, 2015). This will be the topic of future analysis.

Such a high-throughput multi-scale analysis provides a huge amount of data whose integration can pave the way to the understanding of PD pathophysiology. However, these results are coming from an “artificial” set up which can just simplify and mimic the *in vivo* process of neuronal differentiation. For addressing this issue I had already included in this project a second iPSCs cell line carrying a *PINK1* mutation (72-year-old female, AAO47, c.1366C>T) and the corresponding isogenic control (generated by using CRISPR-Cas9) which was provided by the Institute of Neurogenetics of University of Lübeck in addition to the above-described control and PINK1 cell lines. The corresponding parallel experiments were carried out with the aim of clarifying the role of the genetic background in the context of mutation-associated PD pathogenesis but could not yet fully integrated in the analysis due to time limitations. But a targeted analysis of the data allowed already for a first validation approach of the previously identified PD network of genes. Some

preliminary results already showed that there is a significant overlap between the DEGs from the PINK1 line and control line of both cell pairs, at each time point of the neuronal differentiation [Fig. 5.3].

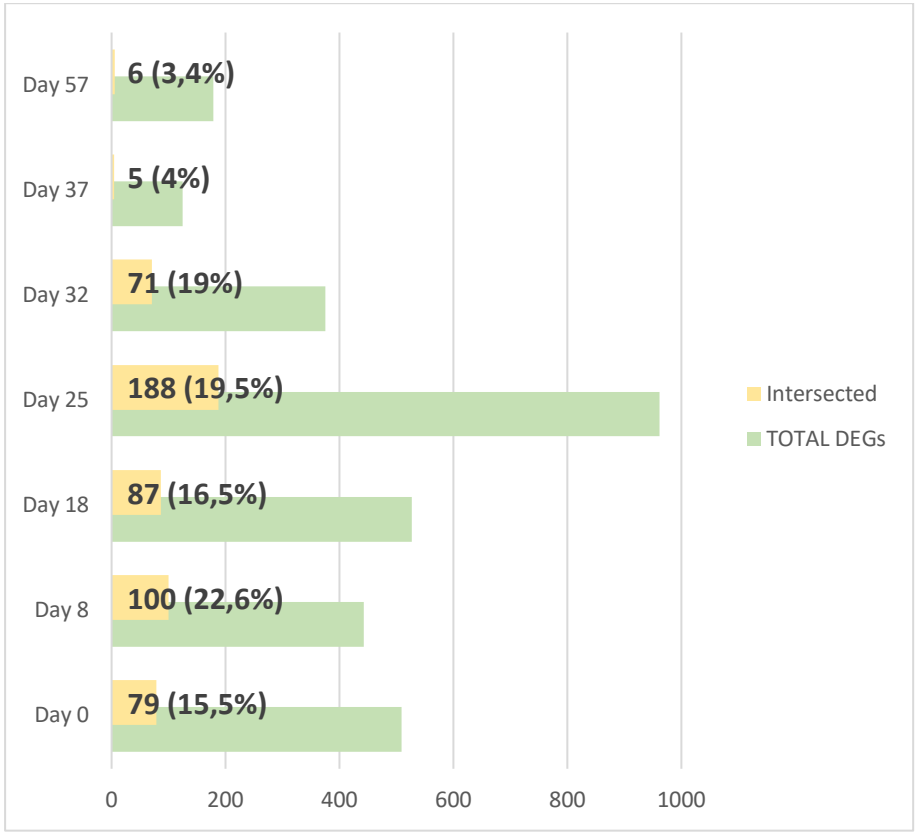

Figure 5.3 *Comparison between the DEGs identified in the PINK1/control cell pair and in the isogenic PINK1/control pair. In green, the total amount of DEGs found in both pairs, and in yellow the number and percentage of these DEGs which are shared from the two lists.*

Further analysis on the comparison of these two cell line pairs will clarify the role of the genetic background and its influence on the disease mechanisms. Furthermore, this approach will also provide an independent validation of the core genes which are key to PD pathophysiology, and which are conserved even in different experimental set ups or genetic contexts.

In conclusion, this project has generated new insights into the underlying mechanisms of PD development by a dynamic multi-omics approach from the underlying hypothesis that disease development can be investigated by following the differentiation dynamics of patient-based iPSCs into dopaminergic neurons. For this purpose, I focused on the ILE368ASN mutation in the *PINK1* gene and first characterized different differentiation protocols (Section 4.1) and subsequently used

the Direct protocol from iPSC to mDAs to identify transcriptional modification during the early differentiation phase by sc-RNAseq and proteomics data revealing a potential core network of PD (Section 4.2). Based on these findings, I subsequently performed a parallel multi-omics characterization of the long-term differentiation dynamics which confirmed the previous findings and identified new pathway candidates of disease development (Section 4.3).
In particular, the multi-omics data sets represent currently a rather unique resource since it allows for analysis across the biological levels and thereby for ranking the identified targets based on their establishment on the phenotype. In this regard, this approach complements other recent multi-omics approaches (www.foundinpd.org) by providing time point coherent data sets that allow for more systematic data integration. Here, we mainly applied a linear data analysis strategy by starting from the transcriptional level at single cell resolution, identifying key DEGs by a network analysis approach and subsequently linked the proteomics and metabolomics data in a targeted manner.

While this approach allowed for a validated and ranked network description, it may miss some essential connections between the individual biological levels. To address this potential gap, more holistic data integration strategies like non-negative matrix factorization (NMF) (Bredikhin et al., 2022; Gligorijević and Pržulj, 2015) will be adapted to these data sets and compared to our results. This might reveal additional insights into PD development.

Another essential next step is a functional validation of the identified candidates. For this purpose, we will target specific candidates of key players in PD progression by monitoring functional changes in knock-out/down cell lines for metabolic related genes identified in our analysis such as LIN28A and try to modulate the metabolic impairment during differentiation. For an ultimate translational step, these results must be subsequently validated in *in vivo* models. However, at the current stage, this project has already demonstrated the appropriateness and potential of such a dynamic multi-scale analysis which will be extended to further patient-based iPSC lines either from idiopathic cases or carrying different PD-related mutations. Eventually, such a cross-condition integration might lead to common key pathways in PD. A potentially unifying approach might be given by the major PD hallmarks of impaired mitochondrial homeostasis and related calcium dynamics in accordance with the selective vulnerability analysis (Subsections 1.3.3 and 1.3.6). In this regard, PINK*1* might represent an important model system due to it central role in mitochondria quality control and degradation and link to calcium homeostasis (Subsections 1.3.3.2 and 1.3.6). Interestingly, preliminary experiments with the PINK1 and control cell lines have actually indicated differences in their calcium dynamics. In particular, the control cell line seemed to be less responsive to ATP

external stimulation. This, combined with a super-resolution imaging analysis of mitochondrial morphology in differentiated mDA neurons, is currently under further investigation.

6. References

Abbas, M.M., Xu, Z., Tan, L.C.S., 2018. Epidemiology of Parkinson's Disease-East Versus West. Mov. Disord. Clin. Pract. 5, 14–28. https://doi.org/10.1002/mdc3.12568

Adler, C.H., Beach, T.G., 2016. Neuropathological basis of nonmotor manifestations of Parkinson's disease. Mov. Disord. Off. J. Mov. Disord. Soc. 31, 1114–9. https://doi.org/10.1002/mds.26605

Adler, C.H., Beach, T.G., Shill, H.A., Caviness, J.N., Sue, L.I., Jacobson, S.A., Belden, C.M., Dugger, B.N., 2014. Low clinical diagnostic accuracy of early vs advanced Parkinson disease. Neurology 83, 406–412.

Adler, C.H., Beach, T.G., Zhang, N., Shill, H.A., Driver-Dunckley, E., Caviness, J.N., Mehta, S.H., Sabbagh, M.N., Serrano, G.E., Sue, L.I., Belden, C.M., Powell, J., Jacobson, S.A., Zamrini, E., Shprecher, D., Davis, K.J., Dugger, B.N., Hentz, J.G., 2019. Unified Staging System for Lewy Body Disorders: Clinicopathologic Correlations and Comparison to Braak Staging. J. Neuropathol. Exp. Neurol. 78, 891–899. https://doi.org/10.1093/jnen/nlz080

Agarwal, D., Sandor, C., Volpato, V., Caffrey, T.M., Monzón-Sandoval, J., Bowden, R., Alegre-Abarrategui, J., Wade-Martins, R., Webber, C., 2020. A single-cell atlas of the human substantia nigra reveals cell-specific pathways associated with neurological disorders. Nat. Commun. 11, 4183. https://doi.org/10.1038/s41467-020-17876-0

Ahn, T.-B., Kim, S.Y., Kim, J.Y., Park, S.-S., Lee, D.S., Min, H.J., Kim, Y.K., Kim, S.E., Kim, J.-M., Kim, H.-J., Cho, J., Jeon, B.S., 2008. alpha-Synuclein gene duplication is present in sporadic Parkinson disease. Neurology 70, 43–9. https://doi.org/10.1212/01.wnl.0000271080.53272.c7

Alfred L. Goldberg, 2003. Protein degradation and protection against misfolded or damaged proteins. Nature 426, 895–899.

Ames, A., 2000. CNS energy metabolism as related to function. Brain Res. Rev. 34, 42–68. https://doi.org/10.1016/S0165-0173(00)00038-2

Andersen, J.K., 2004. Oxidative stress in neurodegeneration: cause or consequence? Nat. Med. 10, S18–S25. https://doi.org/10.1038/nrn1434

Annerino, D.M., Arshad, S., Taylor, G.M., Adler, C.H., Beach, T.G., Greene, J.G., 2012. Parkinson's disease is not associated with gastrointestinal myenteric ganglion neuron loss. Acta Neuropathol. (Berl.) 124, 665–80. https://doi.org/10.1007/s00401-012-1040-2

Anso, I., Basso, L.G.M., Wang, L., Marina, A., Páez-Pérez, E.D., Jäger, C., Gavotto, F., Tersa, M., Perrone, S., Contreras, F.-X., Prandi, J., Gilleron, M., Linster, C.L., Corzana, F., Lowary, T.L., Trastoy, B., Guerin, M.E., 2021. Molecular ruler mechanism and interfacial catalysis of the integral membrane acyltransferase PatA. Sci. Adv. 7, eabj4565. https://doi.org/10.1126/sciadv.abj4565

Arduíno, D.M., Esteves, A.R., Cardoso, S.M., Oliveira, C.R., 2009. Endoplasmic reticulum and mitochondria interplay mediates apoptotic cell death: relevance to Parkinson's disease. Neurochem. Int. 55, 341–8. https://doi.org/10.1016/j.neuint.2009.04.004

Arotcarena, M.-L., Dovero, S., Prigent, A., Bourdenx, M., Camus, S., Porras, G., Thiolat, M.-L., Tasselli, M., Aubert, P., Kruse, N., Mollenhauer, B., Trigo Damas, I., Estrada, C., Garcia-Carrillo, N., Vaikath, N.N., El-Agnaf, O.M.A., Herrero, M.T., Vila, M., Obeso, J.A., Derkinderen, P., Dehay, B., Bezard, E., 2020. Bidirectional gut-to-brain and brain-to-gut propagation of synucleinopathy in non-human primates. Brain 143, 1462–1475. https://doi.org/10.1093/brain/awaa096

Ascherio, A., Schwarzschild, M.A., 2016. The epidemiology of Parkinson's disease: risk

factors and prevention. Lancet Neurol. 15, 1257–1272. https://doi.org/10.1016/S1474-4422(16)30230-7
Ásgrímsdóttir, E.S., Arenas, E., 2020. Midbrain Dopaminergic Neuron Development at the Single Cell Level: In vivo and in Stem Cells. Front. Cell Dev. Biol. 8, 463. https://doi.org/10.3389/fcell.2020.00463
Azevedo, F.A.C., Carvalho, L.R.B., Grinberg, L.T., Farfel, J.M., Ferretti, R.E.L., Leite, R.E.P., Filho, W.J., Lent, R., Herculano-Houzel, S., 2009. Equal numbers of neuronal and nonneuronal cells make the human brain an isometrically scaled-up primate brain. J. Comp. Neurol. 513, 532–541. https://doi.org/10.1002/cne.21974
Bakshi, R., Zhang, H., Logan, R., Joshi, I., Xu, Y., Chen, X., Schwarzschild, M.A., 2015. Neuroprotective effects of urate are mediated by augmenting astrocytic glutathione synthesis and release. Neurobiol. Dis. 82, 574–579. https://doi.org/10.1016/j.nbd.2015.08.022
Beach, T.G., Adler, C.H., Serrano, G., Sue, L.I., Walker, D.G., Dugger, B.N., Shill, H.A., Driver-Dunckley, E., Caviness, J.N., Intorcia, A., Filon, J., Scott, S., Garcia, A., Hoffman, B., Belden, C.M., Davis, K.J., Sabbagh, M.N., 2016. Prevalence of Submandibular Gland Synucleinopathy in Parkinson's Disease, Dementia with Lewy Bodies and other Lewy Body Disorders. J. Park. Dis. 6, 153–163. https://doi.org/10.3233/JPD-150680
Beach, T.G., White, C.L., Hladik, C.L., Sabbagh, M.N., Connor, D.J., Shill, H.A., Sue, L.I., Sasse, J., Bachalakuri, J., Henry-Watson, J., Akiyama, H., Adler, C.H., 2009. Olfactory bulb α-synucleinopathy has high specificity and sensitivity for Lewy body disorders. Acta Neuropathol. (Berl.) 117, 169–174. https://doi.org/10.1007/s00401-008-0450-7
Beal, M.F., 2005. Mitochondria take center stage in aging and neurodegeneration. Ann. Neurol. 58, 495–505. https://doi.org/10.1002/ana.20624
Beal, M.F., 2001. EXPERIMENTAL MODELS OF PARKINSON'S DISEASE 8.
Bender, A., Krishnan, K.J., Morris, C.M., Taylor, G.A., Reeve, A.K., Perry, R.H., Jaros, E., Hersheson, J.S., Betts, J., Klopstock, T., Taylor, R.W., Turnbull, D.M., 2006. High levels of mitochondrial DNA deletions in substantia nigra neurons in aging and Parkinson disease. Nat. Genet. 38, 515–517. https://doi.org/10.1038/ng1769
Benecke, R., Strümper, P., Weiss, H., 1993. Electron transfer complexes I and IV of platelets are abnormal in parkinson's disease but normal in parkinson-plus syndromes. Brain 116, 1451–1463. https://doi.org/10.1093/brain/116.6.1451
Berg, D., Postuma, R.B., Bloem, B., Chan, P., Dubois, B., Gasser, T., Goetz, C.G., Halliday, G.M., Hardy, J., Lang, A.E., Litvan, I., Marek, K., Obeso, J., Oertel, W., Olanow, C.W., Poewe, W., Stern, M., Deuschl, G., 2014. Time to redefine PD? Introductory statement of the MDS Task Force on the definition of Parkinson's disease. Mov. Disord. Off. J. Mov. Disord. Soc. 29, 454–62. https://doi.org/10.1002/mds.25844
Berry, C., La Vecchia, C., Nicotera, P., 2010. Paraquat and Parkinson's disease. Cell Death Differ. 17, 1115–1125. https://doi.org/10.1038/cdd.2009.217
Berwick, D.C., Heaton, G.R., Azeggagh, S., Harvey, K., 2019. LRRK2 Biology from structure to dysfunction: research progresses, but the themes remain the same. Mol. Neurodegener. 14, 49. https://doi.org/10.1186/s13024-019-0344-2
Bialecka, M., Kurzawski, M., Klodowska-Duda, G., Opala, G., Juzwiak, S., Kurzawski, G., Tan, E.-K., Drozdzik, M., 2007. CARD15 variants in patients with sporadic Parkinson's disease. Neurosci. Res. 57, 473–6. https://doi.org/10.1016/j.neures.2006.11.012
Björklund, A., Dunnett, S.B., 2007. Dopamine neuron systems in the brain: an update. Trends Neurosci. 30, 194–202. https://doi.org/10.1016/j.tins.2007.03.006
Błaszczyk, J.W., 2018. The Emerging Role of Energy Metabolism and Neuroprotective Strategies in Parkinson's Disease. Front. Aging Neurosci. 10, 301. https://doi.org/10.3389/fnagi.2018.00301
Blauwendraat, C., Nalls, M.A., Singleton, A.B., 2020. The genetic architecture of

Parkinson's disease. Lancet Neurol. 19, 170–178. https://doi.org/10.1016/S1474-4422(19)30287-X
Blesa, J., Phani, S., Jackson-Lewis, V., Przedborski, S., 2012. Classic and New Animal Models of Parkinson's Disease. J. Biomed. Biotechnol. 2012, 1–10. https://doi.org/10.1155/2012/845618
Blesa, J., Przedborski, S., 2014. Parkinson's disease: animal models and dopaminergic cell vulnerability. Front. Neuroanat. 8, 1–12. https://doi.org/10.3389/fnana.2014.00155
Bloem, B.R., Okun, M.S., Klein, C., 2021. Parkinson's disease. The Lancet 397, 2284–2303. https://doi.org/10.1016/S0140-6736(21)00218-X
Bouabid, S., Delaville, C., De Deurwaerdère, P., Lakhdar-Ghazal, N., Benazzouz, A., 2014. Manganese-Induced Atypical Parkinsonism Is Associated with Altered Basal Ganglia Activity and Changes in Tissue Levels of Monoamines in the Rat. PLoS ONE 9, e98952. https://doi.org/10.1371/journal.pone.0098952
Bouabid, S., Tinakoua, A., Lakhdar-Ghazal, N., Benazzouz, A., 2016. Manganese neurotoxicity: behavioral disorders associated with dysfunctions in the basal ganglia and neurochemical transmission. J. Neurochem. 136, 677–691. https://doi.org/10.1111/jnc.13442
Braak, H., de Vos, R.A.I., Bohl, J., Del Tredici, K., 2006. Gastric alpha-synuclein immunoreactive inclusions in Meissner's and Auerbach's plexuses in cases staged for Parkinson's disease-related brain pathology. Neurosci. Lett. 396, 67–72. https://doi.org/10.1016/j.neulet.2005.11.012
Braak, H., Del Tredici, K., Rüb, U., de Vos, R.A.I., Jansen Steur, E.N.H., Braak, E., 2003. Staging of brain pathology related to sporadic Parkinson's disease. Neurobiol. Aging 24, 197–211. https://doi.org/10.1016/s0197-4580(02)00065-9
Braak, H., Ghebremedhin, E., Rüb, U., Bratzke, H., Del Tredici, K., 2004. Stages in the development of Parkinson's disease-related pathology. Cell Tissue Res. 318, 121–34. https://doi.org/10.1007/s00441-004-0956-9
Braak, H., Sastre, M., Bohl, J.R.E., de Vos, R.A.I., Del Tredici, K., 2007. Parkinson's disease: lesions in dorsal horn layer I, involvement of parasympathetic and sympathetic pre- and postganglionic neurons. Acta Neuropathol. (Berl.) 113, 421–429. https://doi.org/10.1007/s00401-007-0193-x
Bragoszewski, P., Turek, M., Chacinska, A., 2017. Control of mitochondrial biogenesis and function by the ubiquitin-proteasome system. Open Biol. 7, 170007. https://doi.org/10.1098/rsob.170007
Brandt, U., 2006. Energy converting NADH:quinone oxidoreductase (complex I). Annu. Rev. Biochem. 75, 69–92. https://doi.org/10.1146/annurev.biochem.75.103004.142539
Bredikhin, D., Kats, I., Stegle, O., 2022. MUON: multimodal omics analysis framework. Genome Biol. 23, 42. https://doi.org/10.1186/s13059-021-02577-8
Brett, B.L., Gardner, R.C., Godbout, J., Dams-O'Connor, K., Keene, C.D., 2022. Traumatic Brain Injury and Risk of Neurodegenerative Disorder. Biol. Psychiatry 91, 498–507. https://doi.org/10.1016/j.biopsych.2021.05.025
Brown, A.M., Ransom, B.R., 2007. Astrocyte glycogen and brain energy metabolism. Glia 55, 1263–1271. https://doi.org/10.1002/glia.20557
Burkhard, P., Dominici, P., Borri-Voltattorni, C., Jansonius, J.N., Malashkevich, V.N., 2001. Structural insight into Parkinson's disease treatment from drug-inhibited DOPA decarboxylase. Nat. Struct. Biol. 8, 5.
Burré, J., Sharma, M., Südhof, T.C., 2018. Cell Biology and Pathophysiology of α-Synuclein. Cold Spring Harb. Perspect. Med. 8, a024091. https://doi.org/10.1101/cshperspect.a024091
Butler, A., Hoffman, P., Smibert, P., Papalexi, E., Satija, R., 2018. Integrating single-cell transcriptomic data across different conditions, technologies, and species. Nat. Biotechnol. 36, 411–420. https://doi.org/10.1038/nbt.4096
Canning, P., Bullock, A.N., 2014. New strategies to inhibit KEAP1 and the Cul3-based E3

ubiquitin ligases. Biochem. Soc. Trans. 42, 103–107. https://doi.org/10.1042/BST20130215

Cao, M., Wu, Y., Ashrafi, G., McCartney, A.J., Wheeler, H., Bushong, E.A., Boassa, D., Ellisman, M.H., Ryan, T.A., De Camilli, P., 2017. Parkinson Sac Domain Mutation in Synaptojanin 1 Impairs Clathrin Uncoating at Synapses and Triggers Dystrophic Changes in Dopaminergic Axons. Neuron 93, 882-896.e5. https://doi.org/10.1016/j.neuron.2017.01.019

Charles, D., Tolleson, C., Davis, T.L., Gill, C.E., Molinari, A.L., Bliton, M.J., Tramontana, M.G., Salomon, R.M., Kao, C., Wang, L., Hedera, P., Phibbs, F.T., Neimat, J.S., Konrad, P.E., 2012. Pilot Study Assessing the Feasibility of Applying Bilateral Subthalamic Nucleus Deep Brain Stimulation in Very Early Stage Parkinson's Disease: Study Design and Rationale. J. Park. Dis. 2, 215–223. https://doi.org/10.3233/JPD-2012-012095

Chaudhuri, K.R., Odin, P., Antonini, A., Martinez-Martin, P., 2011. Parkinson's disease: The non-motor issues. Parkinsonism Relat. Disord. 17, 717–723. https://doi.org/10.1016/j.parkreldis.2011.02.018

Che, Y., Hou, L., Sun, F., Zhang, C., Liu, X., Piao, F., Zhang, D., Li, H., Wang, Q., 2018. Taurine protects dopaminergic neurons in a mouse Parkinson's disease model through inhibition of microglial M1 polarization. Cell Death Dis. 9, 435. https://doi.org/10.1038/s41419-018-0468-2

Chen, H., Ritz, B., 2018. The Search for Environmental Causes of Parkinson's Disease: Moving Forward. J. Park. Dis. 8, S9–S17. https://doi.org/10.3233/JPD-181493

Chen, X., Burdett, T.C., Desjardins, C.A., Logan, R., Cipriani, S., Xu, Y., Schwarzschild, M.A., 2013. Disrupted and transgenic urate oxidase alter urate and dopaminergic neurodegeneration. Proc. Natl. Acad. Sci. 110, 300–305. https://doi.org/10.1073/pnas.1217296110

Cheng, M.-L., Lin, J.-F., Huang, C.-Y., Li, G.-J., Shih, L.-M., Chiu, D.T.-Y., Ho, H.-Y., 2019. Sedoheptulose-1,7-bisphospate Accumulation and Metabolic Anomalies in Hepatoma Cells Exposed to Oxidative Stress. Oxid. Med. Cell. Longev. 2019, 1–12. https://doi.org/10.1155/2019/5913635

Cherian, A., Divya, K.P., 2020. Genetics of Parkinson's disease. Acta Neurol. Belg. 120, 1297–1305. https://doi.org/10.1007/s13760-020-01473-5

Chung, C.Y., Seo, H., Sonntag, K.C., Brooks, A., Lin, L., Isacson, O., 2005. Cell type-specific gene expression of midbrain dopaminergic neurons reveals molecules involved in their vulnerability and protection. Hum. Mol. Genet. 14, 1709–1725. https://doi.org/10.1093/hmg/ddi178

Chung, K.K.K., Dawson, V.L., Dawson, T.M., 2001. The role of the ubiquitin-proteasomal pathway in Parkinson's disease and other neurodegenerative disorders 8.

Clark, E.H., Vázquez de la Torre, A., Hoshikawa, T., Briston, T., 2021. Targeting mitophagy in Parkinson's disease. J. Biol. Chem. 296, 100209. https://doi.org/10.1074/jbc.REV120.014294

Collier, T.J., Kanaan, N.M., Kordower, J.H., 2011. Ageing as a primary risk factor for Parkinson's disease: evidence from studies of non-human primates. Nat. Rev. Neurosci. 12, 359–366. https://doi.org/10.1038/nrn3039

Copeland, D.E., Dalton, A.J., 1959. An Association between Mitochondria and the Endoplasmic Reticulum in Cells of the Pseudobranch Gland of a Teleost. J. Biophys. Biochem. Cytol. 5, 393–396. https://doi.org/10.1083/jcb.5.3.393

Copley, M.R., Babovic, S., Benz, C., Knapp, D.J.H.F., Beer, P.A., Kent, D.G., Wohrer, S., Treloar, D.Q., Day, C., Rowe, K., Mader, H., Kuchenbauer, F., Humphries, R.K., Eaves, C.J., 2013. The Lin28b–let-7–Hmga2 axis determines the higher self-renewal potential of fetal haematopoietic stem cells. Nat. Cell Biol. 15, 916–925. https://doi.org/10.1038/ncb2783

Corbin, J.G., Rutlin, M., Gaiano, N., Fishell, G., 2003. Combinatorial function of the homeodomain proteins Nkx2.1 and Gsh2 in ventral telencephalic patterning. Dev. Camb. Engl. 130, 4895–906. https://doi.org/10.1242/dev.00717

Cox, J., Hein, M.Y., Luber, C.A., Paron, I., Nagaraj, N., Mann, M., 2014. Accurate Proteome-wide Label-free Quantification by Delayed Normalization and Maximal Peptide Ratio Extraction, Termed MaxLFQ. Mol. Cell. Proteomics 13, 2513–2526. https://doi.org/10.1074/mcp.M113.031591

Cox, J., Mann, M., 2008. MaxQuant enables high peptide identification rates, individualized p.p.b.-range mass accuracies and proteome-wide protein quantification. Nat. Biotechnol. 26, 1367–1372. https://doi.org/10.1038/nbt.1511

Cox, J., Neuhauser, N., Michalski, A., Scheltema, R.A., Olsen, J.V., Mann, M., 2011. Andromeda: A peptide search engine integrated into the MaxQuant environment. J. Proteome Res. 10, 1794–1805. https://doi.org/10.1021/pr101065j

Credle, J.J., Forcelli, P.A., Delannoy, M., Oaks, A.W., Permaul, E., Berry, D.L., Duka, V., Wills, J., Sidhu, A., 2015. α-Synuclein-mediated inhibition of ATF6 processing into COPII vesicles disrupts UPR signaling in Parkinson's disease. Neurobiol. Dis. 76, 112–125. https://doi.org/10.1016/j.nbd.2015.02.005

Crofts, A.R., 2004. The cytochrome bc1 complex: function in the context of structure. Annu. Rev. Physiol. 66, 689–733. https://doi.org/10.1146/annurev.physiol.66.032102.150251

Dang, T.T.H., Rowell, D., Connelly, L.B., 2019. Cost-Effectiveness of Deep Brain Stimulation With Movement Disorders: A Systematic Review. Mov. Disord. Clin. Pract. 6, 348–358. https://doi.org/10.1002/mdc3.12780

Day, J.O., Mullin, S., 2021. The Genetics of Parkinson's Disease and Implications for Clinical Practice. Genes 12, 1006. https://doi.org/10.3390/genes12071006

Deas, E., Plun-Favreau, H., Gandhi, S., Desmond, H., Kjaer, S., Loh, S.H.Y., Renton, A.E.M., Harvey, R.J., Whitworth, A.J., Martins, L.M., Abramov, A.Y., Wood, N.W., 2011. PINK1 cleavage at position A103 by the mitochondrial protease PARL. Hum. Mol. Genet. 20, 867–879. https://doi.org/10.1093/hmg/ddq526

Del Tredici, K., Hawkes, C.H., Ghebremedhin, E., Braak, H., 2010. Lewy pathology in the submandibular gland of individuals with incidental Lewy body disease and sporadic Parkinson's disease. Acta Neuropathol. (Berl.) 119, 703–13. https://doi.org/10.1007/s00401-010-0665-2

Delic, V., Beck, K.D., Pang, K.C.H., Citron, B.A., 2020. Biological links between traumatic brain injury and Parkinson's disease. Acta Neuropathol. Commun. 8, 45. https://doi.org/10.1186/s40478-020-00924-7

DeLong, M.R., Wichmann, T., 2007. Circuits and Circuit Disorders of the Basal Ganglia. Arch. Neurol. 64, 20. https://doi.org/10.1001/archneur.64.1.20

Devine, M.J., Plun-Favreau, H., Wood, N.W., 2011. Parkinson's disease and cancer: two wars, one front. Nat. Rev. Cancer 11, 813–823. https://doi.org/10.1038/nrc3150

Devos, D., Lebouvier, T., Lardeux, B., Biraud, M., Rouaud, T., Pouclet, H., Coron, E., Bruley des Varannes, S., Naveilhan, P., Nguyen, J.-M., Neunlist, M., Derkinderen, P., 2013. Colonic inflammation in Parkinson's disease. Neurobiol. Dis. 50, 42–48. https://doi.org/10.1016/j.nbd.2012.09.007

Dexter, D.T., Sian, J., Rose, S., Hindmarsh, J.G., Mann, V.M., Cooper, J.M., Wells, F.R., Daniel, S.E., Lees, A.J., Schapira, A.H.V., Jenner, P., Marsden, C.D., 1994. Indices of oxidative stress and mitochondrial function in individuals with incidental Lewy body disease. Ann. Neurol. 35, 38–44. https://doi.org/10.1002/ana.410350107

Dias, V., Junn, E., Mouradian, M.M., 2013. The role of oxidative stress in Parkinson's disease. J. Park. Dis. 3, 461–91. https://doi.org/10.3233/JPD-130230

Dirkse, A., Golebiewska, A., Buder, T., Nazarov, P.V., Muller, A., Poovathingal, S., Brons, N.H.C., Leite, S., Sauvageot, N., Sarkisjan, D., Seyfrid, M., Fritah, S., Stieber, D., Michelucci, A., Hertel, F., Herold-Mende, C., Azuaje, F., Skupin, A., Bjerkvig, R., Deutsch, A., Voss-Böhme, A., Niclou, S.P., 2019. Stem cell-associated heterogeneity in Glioblastoma results from intrinsic tumor plasticity shaped by the microenvironment. Nat. Commun. 10, 1787. https://doi.org/10.1038/s41467-019-09853-z

Docherty, C.K., Salt, I.P., Mercer, J.R., 2016. Lin28A induces energetic switching to glycolytic metabolism in human embryonic kidney cells. Stem Cell Res. Ther. 7, 78. https://doi.org/10.1186/s13287-016-0323-2

Dorsey, E.R., Constantinescu, R., Thompson, J.P., Biglan, K.M., Holloway, R.G., Kieburtz, K., Marshall, F.J., Ravina, B.M., Schifitto, G., Siderowf, A., Tanner, C.M., 2007. Projected number of people with Parkinson disease in the most populous nations, 2005 through 2030. Neurology 68, 384–386. https://doi.org/10.1212/01.wnl.0000247740.47667.03

Dorsey, E.R., Elbaz, A., Nichols, E., Abbasi, N., Abd-Allah, F., Abdelalim, A., Adsuar, J.C., Ansha, M.G., Brayne, C., Choi, J.-Y.J., Collado-Mateo, D., Dahodwala, N., Do, H.P., Edessa, D., Endres, M., Fereshtehnejad, S.-M., Foreman, K.J., Gankpe, F.G., Gupta, R., Hamidi, S., Hankey, G.J., Hay, S.I., Hegazy, M.I., Hibstu, D.T., Kasaeian, A., Khader, Y., Khalil, I., Khang, Y.-H., Kim, Y.J., Kokubo, Y., Logroscino, G., Massano, J., Mohamed Ibrahim, N., Mohammed, M.A., Mohammadi, A., Moradi-Lakeh, M., Naghavi, M., Nguyen, B.T., Nirayo, Y.L., Ogbo, F.A., Owolabi, M.O., Pereira, D.M., Postma, M.J., Qorbani, M., Rahman, M.A., Roba, K.T., Safari, H., Safiri, S., Satpathy, M., Sawhney, M., Shafieesabet, A., Shiferaw, M.S., Smith, M., Szoeke, C.E.I., Tabarés-Seisdedos, R., Truong, N.T., Ukwaja, K.N., Venketasubramanian, N., Villafaina, S., gidey Weldegwergs, K., Westerman, R., Wijeratne, T., Winkler, A.S., Xuan, B.T., Yonemoto, N., Feigin, V.L., Vos, T., Murray, C.J.L., 2018a. Global, regional, and national burden of Parkinson's disease, 1990–2016: a systematic analysis for the Global Burden of Disease Study 2016. Lancet Neurol. 17, 939–953. https://doi.org/10.1016/S1474-4422(18)30295-3

Dorsey, E.R., Sherer, T., Okun, M.S., Bloem, B.R., 2018b. The Emerging Evidence of the Parkinson Pandemic. J. Park. Dis. 8, S3–S8. https://doi.org/10.3233/JPD-181474

Dugan, J.P., Stratton, A., Riley, H.P., Farmer, W.T., Mastick, G.S., 2011. Midbrain dopaminergic axons are guided longitudinally through the diencephalon by Slit/Robo signals. Mol. Cell. Neurosci. 46, 347–356. https://doi.org/10.1016/j.mcn.2010.11.003

Duyckaerts, C., Sazdovitch, V., Ando, K., Seilhean, D., Privat, N., Yilmaz, Z., Peckeu, L., Amar, E., Comoy, E., Maceski, A., Lehmann, S., Brion, J.-P., Brandel, J.-P., Haïk, S., 2018. Neuropathology of iatrogenic Creutzfeldt–Jakob disease and immunoassay of French cadaver-sourced growth hormone batches suggest possible transmission of tauopathy and long incubation periods for the transmission of Abeta pathology. Acta Neuropathol. (Berl.) 135, 201–212. https://doi.org/10.1007/s00401-017-1791-x

Ebanks, K., Lewis, P.A., Bandopadhyay, R., 2020. Vesicular Dysfunction and the Pathogenesis of Parkinson's Disease: Clues From Genetic Studies. Front. Neurosci. 13, 1381. https://doi.org/10.3389/fnins.2019.01381

Ehringer, H., Hornykiewicz, O., 1998. Distribution of noradrenaline and dopamine (3-hydroxytyramine) in the human brain and their behavior in diseases of the extrapyramidal system. Parkinsonism Relat. Disord. 4, 53–57. https://doi.org/10.1016/S1353-8020(98)00012-1

Ekimova, I.V., Plaksina, D.V., Pastukhov, Y.F., Lapshina, K.V., Lazarev, V.F., Mikhaylova, E.R., Polonik, S.G., Pani, B., Margulis, B.A., Guzhova, I.V., Nudler, E., 2018. New HSF1 inducer as a therapeutic agent in a rodent model of Parkinson's disease. Exp. Neurol. 306, 199–208. https://doi.org/10.1016/j.expneurol.2018.04.012

El-Agnaf, O.M.A., Salem, S.A., Paleologou, K.E., Cooper, L.J., Fullwood, N.J., Gibson, M.J., Curran, M.D., Court, J.A., Mann, D.M.A., Ikeda, S.-I., Cookson, M.R., Hardy, J., Allsop, D., 2003. α-Synuclein implicated in Parkinson's disease is present in extracellular biological fluids, including human plasma. FASEB J. 17, 1–16. https://doi.org/10.1096/fj.03-0098fje

Engelender, S., Isacson, O., 2017. The Threshold Theory for Parkinson's Disease. Trends Neurosci. 40, 4–14. https://doi.org/10.1016/j.tins.2016.10.008

Ephraty, L., Porat, O., Israeli, D., Cohen, O.S., Tunkel, O., Yael, S., Hatano, Y., Hattori, N., Hassin-Baer, S., 2007. Neuropsychiatric and cognitive features in autosomal-recessive early parkinsonism due to PINK1 mutations. Mov. Disord. 22, 566–569. https://doi.org/10.1002/mds.21319

Falkenburger, B.H., Saridaki, T., Dinter, E., 2016. Cellular models for Parkinson's disease. J. Neurochem. 139, 121–130. https://doi.org/10.1111/jnc.13618

Fang, X., Han, D., Cheng, Q., Zhang, P., Zhao, C., Min, J., Wang, F., 2018. Association of Levels of Physical Activity With Risk of Parkinson Disease. JAMA Netw. Open 1, e182421. https://doi.org/10.1001/jamanetworkopen.2018.2421

Feany, M.B., Bender, W.W., 2000. A Drosophila model of Parkinson's disease. Nature 404, 394–398. https://doi.org/10.1038/35006074

Feng, Y., Wang, X., 2017. Systematic analysis of microarray datasets to identify Parkinson's disease-associated pathways and genes. Mol. Med. Rep. 15, 1252–1262. https://doi.org/10.3892/mmr.2017.6124

Finak, G., McDavid, A., Yajima, M., Deng, J., Gersuk, V., Shalek, A.K., Slichter, C.K., Miller, H.W., McElrath, M.J., Prlic, M., Linsley, P.S., Gottardo, R., 2015. MAST: a flexible statistical framework for assessing transcriptional changes and characterizing heterogeneity in single-cell RNA sequencing data. Genome Biol. 16, 278. https://doi.org/10.1186/s13059-015-0844-5

Floor, E., Wetzel, M.G., 1998. Increased protein oxidation in human substantia nigra pars compacta in comparison with basal ganglia and prefrontal cortex measured with an improved dinitrophenylhydrazine assay. J. Neurochem. 70, 268–75. https://doi.org/10.1046/j.1471-4159.1998.70010268.x

Garcia-Esparcia, P., Hernández-Ortega, K., Ansoleaga, B., Carmona, M., Ferrer, I., 2015. Purine metabolism gene deregulation in Parkinson's disease: Purine in PD. Neuropathol. Appl. Neurobiol. 41, 926–940. https://doi.org/10.1111/nan.12221

Gaven, F., Marin, P., Claeysen, S., 2014. Primary Culture of Mouse Dopaminergic Neurons. J. Vis. Exp. 51751. https://doi.org/10.3791/51751

Gelpi, E., Navarro-Otano, J., Tolosa, E., Gaig, C., Compta, Y., Rey, M.J., Martí, M.J., Hernández, I., Valldeoriola, F., Reñé, R., Ribalta, T., 2014. Multiple organ involvement by alpha-synuclein pathology in Lewy body disorders. Mov. Disord. 29, 1010–1018. https://doi.org/10.1002/mds.25776

Georgakopoulos, N.D., Wells, G., Campanella, M., 2017. The pharmacological regulation of cellular mitophagy. Nat. Chem. Biol. 13, 136–146. https://doi.org/10.1038/nchembio.2287

Giguère, N., Burke Nanni, S., Trudeau, L.-E., 2018. On Cell Loss and Selective Vulnerability of Neuronal Populations in Parkinson's Disease. Front. Neurol. 9, 455. https://doi.org/10.3389/fneur.2018.00455

Gligorijević, V., Pržulj, N., 2015. Methods for biological data integration: perspectives and challenges. J. R. Soc. Interface 12, 20150571. https://doi.org/10.1098/rsif.2015.0571

Goedert, M., Spillantini, M.G., Del Tredici, K., Braak, H., 2013. 100 years of Lewy pathology. Nat. Rev. Neurol. 9, 13–24. https://doi.org/10.1038/nrneurol.2012.242

Gordon, K., Clouaire, T., Bao, X.X., Kemp, S.E., Xenophontos, M., de Las Heras, J.I., Stancheva, I., 2014. Immortality, but not oncogenic transformation, of primary human cells leads to epigenetic reprogramming of DNA methylation and gene expression. Nucleic Acids Res. 42, 3529–3541. https://doi.org/10.1093/nar/gkt1351

Goswami, R., Subramanian, G., Silayeva, L., Newkirk, I., Doctor, D., Chawla, K., Chattopadhyay, S., Chandra, D., Chilukuri, N., Betapudi, V., 2019. Gene Therapy Leaves a Vicious Cycle. Front. Oncol. 9, 1–25. https://doi.org/10.3389/fonc.2019.00297

Greene, A.W., Grenier, K., Aguileta, M.A., Muise, S., Farazifard, R., Haque, M.E., McBride, H.M., Park, D.S., Fon, E.A., 2012. Mitochondrial processing peptidase regulates PINK1 processing, import and Parkin recruitment. EMBO Rep. 13, 378–

385. https://doi.org/10.1038/embor.2012.14
Grünewald, A., Breedveld, G.J., Lohmann-Hedrich, K., Rohé, C.F., König, I.R., Hagenah, J., Vanacore, N., Meco, G., Antonini, A., Goldwurm, S., Lesage, S., Dürr, A., Binkofski, F., Siebner, H., Münchau, A., Brice, A., Oostra, B.A., Klein, C., Bonifati, V., 2007. Biological effects of the PINK1 c.1366C>T mutation: Implications in Parkinson disease pathogenesis. Neurogenetics 8, 103–109. https://doi.org/10.1007/s10048-006-0072-y
Guardia-Laguarta, C., Area-Gomez, E., Schon, E.A., Przedborski, S., 2015. A new role for α-synuclein in Parkinson's disease: Alteration of ER-mitochondrial communication. Mov. Disord. 30, 1026–1033. https://doi.org/10.1002/mds.26239
Guilarte, T.R., Nihei, M.K., McGlothan, J.L., Howard, A.S., 2003. Methamphetamine-induced deficits of brain monoaminergic neuronal markers: distal axotomy or neuronal plasticity. Neuroscience 122, 499–513. https://doi.org/10.1016/S0306-4522(03)00476-7
Gundogdu, M., Tadayon, R., Salzano, G., Shaw, G.S., Walden, H., 2021. A mechanistic review of Parkin activation. Biochim. Biophys. Acta Gen. Subj. 1865, 129894. https://doi.org/10.1016/j.bbagen.2021.129894
Guzman, R.E., Schwarz, Y.N., Rettig, J., Bruns, D., 2010. SNARE force synchronizes synaptic vesicle fusion and controls the kinetics of quantal synaptic transmission. J. Neurosci. Off. J. Soc. Neurosci. 30, 10272–81. https://doi.org/10.1523/JNEUROSCI.1551-10.2010
Hayashi, T., Rizzuto, R., Hajnoczky, G., Su, T.-P., 2009. MAM: more than just a housekeeper. Trends Cell Biol. 19, 81–88. https://doi.org/10.1016/j.tcb.2008.12.002
Hazafa, A., Batool, A., Ahmad, S., Amjad, M., Chaudhry, S.N., Asad, J., Ghuman, H.F., Khan, H.M., Naeem, M., Ghani, U., 2021. Humanin: A mitochondrial-derived peptide in the treatment of apoptosis-related diseases. Life Sci. 264, 118679. https://doi.org/10.1016/j.lfs.2020.118679
Hernandez, S.M., Tikhonova, E.B., Karamyshev, A.L., 2020. Protein-Protein Interactions in Alpha-Synuclein Biogenesis: New Potential Targets in Parkinson's Disease. Front. Aging Neurosci. 12, 72. https://doi.org/10.3389/fnagi.2020.00072
Hindle, J.V., 2010. Ageing, neurodegeneration and Parkinson's disease. Age Ageing 39, 156–61. https://doi.org/10.1093/ageing/afp223
Höglinger, G.U., Breunig, J.J., Depboylu, C., Rouaux, C., Michel, P.P., Alvarez-Fischer, D., Boutillier, A.-L., DeGregori, J., Oertel, W.H., Rakic, P., Hirsch, E.C., Hunot, S., 2007. The pRb/E2F cell-cycle pathway mediates cell death in Parkinson's disease. Proc. Natl. Acad. Sci. 104, 3585–3590. https://doi.org/10.1073/pnas.0611671104
Hoozemans, J.J.M., van Haastert, E.S., Eikelenboom, P., de Vos, R.A.I., Rozemuller, J.M., Scheper, W., 2007. Activation of the unfolded protein response in Parkinson's disease. Biochem. Biophys. Res. Commun. 354, 707–11. https://doi.org/10.1016/j.bbrc.2007.01.043
Howarth, C., Gleeson, P., Attwell, D., 2012. Updated Energy Budgets for Neural Computation in the Neocortex and Cerebellum. J. Cereb. Blood Flow Metab. 32, 1222–1232. https://doi.org/10.1038/jcbfm.2012.35
Hui, K.Y., Fernandez-Hernandez, H., Hu, J., Schaffner, A., Pankratz, N., Hsu, N.-Y., Chuang, L.-S., Carmi, S., Villaverde, N., Li, X., 2018. Functional variants in LRRK2 confer pleiotropic effects on risk for Crohn's disease and Parkinson's disease. Sci. Transl. Med. 10. https://doi.org/10.1126/scitranslmed.aai7795.Functional
Hunn, B.H.M., Cragg, S.J., Bolam, J.P., Spillantini, M.-G., Wade-Martins, R., 2015. Impaired intracellular trafficking defines early Parkinson's disease. Trends Neurosci. 38, 178–88. https://doi.org/10.1016/j.tins.2014.12.009
Ikemura, M., Saito, Y., Sengoku, R., Sakiyama, Y., Hatsuta, H., Kanemaru, K., Sawabe, M., Arai, T., Ito, G., Iwatsubo, T., Fukayama, M., Murayama, S., 2008. Lewy body pathology involves cutaneous nerves. J. Neuropathol. Exp. Neurol. 67, 945–53. https://doi.org/10.1097/NEN.0b013e318186de48

Jackson-Lewis, V., Przedborski, S., 2008. The MPTP Mouse Model of Parkinson's Disease: the True, the False, and the Unknown, in: Parkinson's Disease. Elsevier, pp. 147–158. https://doi.org/10.1016/B978-0-12-374028-1.00011-7
James, N.A., Matteson, D.S., 2015. ecp: An R package for nonparametric multiple change point analysis of multivariate data. J. Stat. Softw. 62, 1–25. https://doi.org/10.18637/jss.v062.i07
Jenner, P., 2008. Molecular mechanisms of L-DOPA-induced dyskinesia. Nat. Rev. Neurosci. 9, 665–677. https://doi.org/10.1038/nrn2471
Johnson, J., Mercado-Ayon, E., Mercado-Ayon, Y., Dong, Y.N., Halawani, S., Ngaba, L., Lynch, D.R., 2021. Mitochondrial dysfunction in the development and progression of neurodegenerative diseases. Arch. Biochem. Biophys. 702, 108698. https://doi.org/10.1016/j.abb.2020.108698
Johnson, M.E., Stecher, B., Labrie, V., Brundin, L., Brundin, P., 2019. Triggers, Facilitators, and Aggravators: Redefining Parkinson's Disease Pathogenesis. Trends Neurosci. 42, 4–13. https://doi.org/10.1016/j.tins.2018.09.007
Jolivet, R., 2009. Deciphering neuron-glia compartmentalization in cortical energy metabolism. Front. Neuroenergetics 1. https://doi.org/10.3389/neuro.14.004.2009
Junn, E., Mouradian, M.M., 2002. Human α-Synuclein over-expression increases intracellular reactive oxygen species levels and susceptibility to dopamine. Neurosci. Lett. 320, 146–150. https://doi.org/10.1016/S0304-3940(02)00016-2
Kanehisa, M., Sato, Y., Furumichi, M., Morishima, K., Tanabe, M., 2019. New approach for understanding genome variations in KEGG. Nucleic Acids Res. 47, D590–D595. https://doi.org/10.1093/nar/gky962
Kasten, M., Hartmann, C., Hampf, J., Schaake, S., Westenberger, A., Vollstedt, E.-J., Balck, A., Domingo, A., Vulinovic, F., Dulovic, M., Zorn, I., Madoev, H., Zehnle, H., Lembeck, C.M., Schawe, L., Reginold, J., Huang, J., König, I.R., Bertram, L., Marras, C., Lohmann, K., Lill, C.M., Klein, C., 2018. Genotype-Phenotype Relations for the Parkinson's Disease Genes Parkin , PINK1 , DJ1: MDSGene Systematic Review. Mov. Disord. 33, 730–741. https://doi.org/10.1002/mds.27352
Kawajiri, S., Saiki, S., Sato, S., Hattori, N., 2011. Genetic mutations and functions of PINK1. Trends Pharmacol. Sci. 32, 573–580. https://doi.org/10.1016/j.tips.2011.06.001
Kim, D., Jun, K.S., Lee, S.B., Kang, N.-G., Min, D.S., Kim, Y.-H., Ryu, S.H., Suh, P.-G., Shin, H.-S., 1997. Phospholipase C isozymes selectively couple to specific neurotransmitter receptors. Nature 389, 290–293. https://doi.org/10.1038/38508
Kim, J.-Y., Kim, S.-M., Ko, J.-H., Yim, J.-H., Park, Jin-Hae, Park, Jae-Hoon, 2006. Interaction of pro-apoptotic protein HGTD-P with heat shock protein 90 is required for induction of mitochondrial apoptotic cascades. FEBS Lett. 580, 3270–3275. https://doi.org/10.1016/j.febslet.2006.05.001
Kirkwood, T.B.L., 2003. The most pressing problem of our age. BMJ 326, 1297–1299. https://doi.org/10.1136/bmj.326.7402.1297
Klein, C., Schlossmacher, M.G., 2007. Parkinson disease, 10 years after its genetic revolution: multiple clues to a complex disorder. Neurology 69, 2093–104. https://doi.org/10.1212/01.wnl.0000271880.27321.a7
Klinkenberg, M., Thurow, N., Gispert, S., Ricciardi, F., Eich, F., Prehn, J.H.M., Auburger, G., Kögel, D., 2010. Enhanced vulnerability of PARK6 patient skin fibroblasts to apoptosis induced by proteasomal stress. Neuroscience 166, 422–34. https://doi.org/10.1016/j.neuroscience.2009.12.068
Knull, H.R., 1978. Association of glycolytic enzymes with particulate fractions from nerve endings. Biochim. Biophys. Acta BBA - Enzymol. 522, 1–9. https://doi.org/10.1016/0005-2744(78)90316-9
Kondapalli, C., Kazlauskaite, A., Zhang, N., Woodroof, H.I., Campbell, D.G., Gourlay, R., Burchell, L., Walden, H., MacArtney, T.J., Deak, M., Knebel, A., Alessi, D.R., Muqit, M.M.K., 2012. PINK1 is activated by mitochondrial membrane potential depolarization and stimulates Parkin E3 ligase activity by phosphorylating Serine

65. Open Biol. 2. https://doi.org/10.1098/rsob.120080
Konovalova, E.V., Lopacheva, O.M., Grivennikov, I.A., Lebedeva, O.S., Dashinimaev, E.B., Khaspekov, L.G., Fedotova, E.Y., Illarioshkin, S.N., 2015. Mutations in the Parkinson's Disease-Associated PARK2 Gene Are Accompanied by Imbalance in Programmed Cell Death Systems. Acta Naturae 7, 146–149. https://doi.org/10.32607/20758251-2015-7-4-146-149
Koyano, F., Okatsu, K., Kosako, H., Tamura, Y., Go, E., Kimura, M., Kimura, Y., Tsuchiya, H., Yoshihara, H., Hirokawa, T., Endo, T., Fon, E.A., Trempe, J.F., Saeki, Y., Tanaka, K., Matsuda, N., 2014. Ubiquitin is phosphorylated by PINK1 to activate parkin. Nature 510, 162–166. https://doi.org/10.1038/nature13392
Kravitz, A.V., Freeze, B.S., Parker, P.R.L., Kay, K., Thwin, M.T., Deisseroth, K., Kreitzer, A.C., 2010. Regulation of parkinsonian motor behaviours by optogenetic control of basal ganglia circuitry. Nature 466, 622–626. https://doi.org/10.1038/nature09159
Krige, D., Carroll, M.T., Cooper, J.M., Marsden, C.D., Schapira, A.H.V., 1992. Platelet mitochondria function in Parkinson's disease. Ann. Neurol. 32, 782–788. https://doi.org/10.1002/ana.410320612
Kriks, S., Shim, J.-W., Piao, J., Ganat, Y.M., Wakeman, D.R., Xie, Z., Carrillo-Reid, L., Auyeung, G., Antonacci, C., Buch, A., Yang, L., Beal, M.F., Surmeier, D.J., Kordower, J.H., Tabar, V., Studer, L., 2011. Dopamine neurons derived from human ES cells efficiently engraft in animal models of Parkinson's disease. Nature 480, 547–51. https://doi.org/10.1038/nature10648
Kühlbrandt, W., 2015. Structure and function of mitochondrial membrane protein complexes. BMC Biol. 13, 89. https://doi.org/10.1186/s12915-015-0201-x
La Cognata, V., Morello, G., D'Agata, V., Cavallaro, S., 2017. Copy number variability in Parkinson's disease: assembling the puzzle through a systems biology approach. Hum. Genet. 136, 13–37. https://doi.org/10.1007/s00439-016-1749-4
Langston, J., Ballard, P., Tetrud, J., Irwin, I., 1983. Chronic Parkinsonism in Humans due to a Product of Meperidine-Analog Synthesis. Science 219, 979–980.
Lashuel, H.A., Overk, C.R., Oueslati, A., Masliah, E., 2013. The many faces of α-synuclein: from structure and toxicity to therapeutic target. Nat. Rev. Neurosci. 14, 38–48. https://doi.org/10.1038/nrn3406
Lazarou, M., Jin, S.M., Kane, L.A., Youle, R.J., 2012. Role of PINK1 Binding to the TOM Complex and Alternate Intracellular Membranes in Recruitment and Activation of the E3 Ligase Parkin. Dev. Cell 22, 320–333. https://doi.org/10.1016/j.devcel.2011.12.014
Le, W., Sayana, P., Jankovic, J., 2014. Animal Models of Parkinson's Disease: A Gateway to Therapeutics? Neurotherapeutics 11, 92–110. https://doi.org/10.1007/s13311-013-0234-1
Lebouvier, T., Neunlist, M., Bruley des Varannes, S., Coron, E., Drouard, A., N'Guyen, J.-M., Chaumette, T., Tasselli, M., Paillusson, S., Flamand, M., Galmiche, J.-P., Damier, P., Derkinderen, P., 2010. Colonic biopsies to assess the neuropathology of Parkinson's disease and its relationship with symptoms. PloS One 5, e12728. https://doi.org/10.1371/journal.pone.0012728
Lee, H.J., Patel, S., Lee, S.J., 2005. Intravesicular localization and exocytosis of α-synuclein and its aggregates. J. Neurosci. 25, 6016–6024. https://doi.org/10.1523/JNEUROSCI.0692-05.2005
Lee, Y., Kang, H.C., Lee, B.D., Lee, Y.-I., Kim, Y.P., Shin, J.-H., 2014. Poly (ADP-ribose) in the pathogenesis of Parkinson's disease. BMB Rep. 47, 424–432. https://doi.org/10.5483/BMBRep.2014.47.8.119
Lennie, P., 2003. The Cost of Cortical Computation. Curr. Biol. 13, 493–497. https://doi.org/10.1016/S0960-9822(03)00135-0
Li, G., He, X., Li, H., Wu, Y., Guan, Y., Liu, S., Jia, H., Li, Y., Wang, L., Huang, R., Pei, Z., Lan, Y., Zhang, Y., 2018. Overexpression of Slit2 improves function of the paravascular pathway in the aging mouse brain. Int. J. Mol. Med. https://doi.org/10.3892/ijmm.2018.3802

Li, J.-Y., Englund, E., Holton, J.L., Soulet, D., Hagell, P., Lees, A.J., Lashley, T., Quinn, N.P., Rehncrona, S., Björklund, A., Widner, H., Revesz, T., Lindvall, O., Brundin, P., 2008. Lewy bodies in grafted neurons in subjects with Parkinson's disease suggest host-to-graft disease propagation. Nat. Med. 14, 501–503. https://doi.org/10.1038/nm1746

Lin, K.-J., Lin, K.-L., Chen, S.-D., Liou, C.-W., Chuang, Y.-C., Lin, H.-Y., Lin, T.-K., 2019. The Overcrowded Crossroads: Mitochondria, Alpha-Synuclein, and the Endo-Lysosomal System Interaction in Parkinson's Disease. Int. J. Mol. Sci. 20, 5312. https://doi.org/10.3390/ijms20215312

Liu, R., Gao, X., Lu, Y., Chen, H., 2011. Meta-analysis of the relationship between Parkinson disease and melanoma. Neurology 76, 2002–2009. https://doi.org/10.1212/WNL.0b013e31821e554e

Liu, Y., Ma, X., Fujioka, H., Liu, J., Chen, S., Zhu, X., 2019. DJ-1 regulates the integrity and function of ER-mitochondria association through interaction with IP3R3-Grp75-VDAC1. Proc. Natl. Acad. Sci. 116, 25322–25328. https://doi.org/10.1073/pnas.1906565116

Lotharius, J., 2005. Progressive Degeneration of Human Mesencephalic Neuron-Derived Cells Triggered by Dopamine-Dependent Oxidative Stress Is Dependent on the Mixed-Lineage Kinase Pathway. J. Neurosci. 25, 6329–6342. https://doi.org/10.1523/JNEUROSCI.1746-05.2005

Ma, J., Gao, J., Wang, J., Xie, A., 2019. Prion-Like Mechanisms in Parkinson's Disease. Front. Neurosci. 13, 552. https://doi.org/10.3389/fnins.2019.00552

Macosko, E.Z., Basu, A., Satija, R., Nemesh, J., Shekhar, K., Goldman, M., Tirosh, I., Bialas, A.R., Kamitaki, N., Martersteck, E.M., Trombetta, J.J., Weitz, D.A., Sanes, J.R., Shalek, A.K., Regev, A., McCarroll, S.A., 2015. Highly Parallel Genome-wide Expression Profiling of Individual Cells Using Nanoliter Droplets. Cell 161, 1202–1214. https://doi.org/10.1016/j.cell.2015.05.002

Marino, S., Ciurleo, R., di Lorenzo, G., Barresi, M., de Salvo, S., Giacoppo, S., Bramanti, A., Lanzafame, P., Bramanti, P., 2012. Magnetic resonance imaging markers for early diagnosis of Parkinson's disease. Neural Regen. Res. 7, 611–619. https://doi.org/10.3969/j.issn.1673-5374.2012.08.009

Maroteaux, L., Campanelli, J., Scheller, R., 1988. Synuclein: a neuron-specific protein localized to the nucleus and presynaptic nerve terminal. J. Neurosci. 8, 2804–2815. https://doi.org/10.1523/JNEUROSCI.08-08-02804.1988

Maroteaux, L., Scheller, R.H., 1991. The rat brain synucleins; family of proteins transiently associated with neuronal membrane. Mol. Brain Res. 11, 335–343. https://doi.org/10.1016/0169-328X(91)90043-W

Marsili, L., Rizzo, G., Colosimo, C., 2018. Diagnostic Criteria for Parkinson's Disease: From James Parkinson to the Concept of Prodromal Disease. Front. Neurol. 9, 1–10. https://doi.org/10.3389/fneur.2018.00156

Martin, I., 2016. Decoding Parkinson's Disease Pathogenesis: The Role of Deregulated mRNA Translation. J. Park. Dis. 6, 17–27. https://doi.org/10.3233/JPD-150738

Masuda-Suzukake, M., Nonaka, T., Hosokawa, M., Oikawa, T., Arai, T., Akiyama, H., Mann, D.M.A., Hasegawa, M., 2013. Prion-like spreading of pathological α-synuclein in brain. Brain 136, 1128–1138. https://doi.org/10.1093/brain/awt037

Mazzio, E., Soliman, K.F.A., 2012. Whole genome expression profile in neuroblastoma cells exposed to 1-methyl-4-phenylpyridine. NeuroToxicology 33, 1156–1169. https://doi.org/10.1016/j.neuro.2012.06.009

McNaught, K.S.P., Olanow, C.W., Schapira, Jenner, Isacson, Hunot, Tatton, Beal, 2003. Proteolytic stress: A unifying concept for the etiopathogenesis of Parkinson's disease. Ann. Neurol. 53, 73–86. https://doi.org/10.1002/ana.10512

McWilliams, T.G., Muqit, M.M., 2017. PINK1 and Parkin: emerging themes in mitochondrial homeostasis. Curr. Opin. Cell Biol. 45, 83–91. https://doi.org/10.1016/j.ceb.2017.03.013

Meredith, G.E., Rademacher, D.J., 2011. MPTP Mouse Models of Parkinson's Disease:

An Update. J. Park. Dis. 1, 19–33. https://doi.org/10.3233/JPD-2011-11023
Migliore, L., Coppedè, F., 2009. Environmental-induced oxidative stress in neurodegenerative disorders and aging. Mutat. Res. Toxicol. Environ. Mutagen. 674, 73–84. https://doi.org/10.1016/j.mrgentox.2008.09.013
Mink, J.W., 1996. THE BASAL GANGLIA: FOCUSED SELECTION AND INHIBITION OF COMPETING MOTOR PROGRAMS. Prog. Neurobiol. 50, 381–425. https://doi.org/10.1016/S0301-0082(96)00042-1
Moein, M., Grzyb, K., Gonçalves Martins, T., Komoto, S., Peri, F., Crawford, A.D., Fouquier d'Herouel, A., Skupin, A., 2018. CaSiAn: a Calcium Signaling Analyzer tool. Bioinforma. Oxf. Engl. 34, 3052–3054. https://doi.org/10.1093/bioinformatics/bty281
Morais, V.A., Haddad, D., Craessaerts, K., De Bock, P.-J., Swerts, J., Vilain, S., Aerts, L., Overbergh, L., Grünewald, A., Seibler, P., Klein, C., Gevaert, K., Verstreken, P., De Strooper, B., 2014. PINK1 Loss-of-Function Mutations Affect Mitochondrial Complex I Activity via NdufA10 Ubiquinone Uncoupling. Science 344, 203–207. https://doi.org/10.1126/science.1249161
Morens, D.M., Folkers, G.K., Fauci, A.S., 2009. What Is a Pandemic? J. Infect. Dis. 200, 1018–1021. https://doi.org/10.1086/644537
Nagatsu, T., 2002. Amine-related neurotoxins in Parkinson's disease Past, present, and future. Neurotoxicol. Teratol. 5.
Narendra, D., Tanaka, A., Suen, D.-F., Youle, R.J., 2008. Parkin is recruited selectively to impaired mitochondria and promotes their autophagy. J. Cell Biol. 183, 795–803. https://doi.org/10.1083/jcb.200809125
Nash, J.E., Brotchie, J.M., 2000. A Common Signaling Pathway for Striatal NMDA and Adenosine A 2a Receptors: Implications for the Treatment of Parkinson's Disease. J. Neurosci. 20, 7782–7789. https://doi.org/10.1523/JNEUROSCI.20-20-07782.2000
Novak, G., Kyriakis, D., Grzyb, K., Bernini, M., Rodius, S., Dittmar, G., Finkbeiner, S., Skupin, A., 2022. Single-cell transcriptomics of human iPSC differentiation dynamics reveal a core molecular network of Parkinson's disease. Commun. Biol. 5, 49. https://doi.org/10.1038/s42003-021-02973-7
Olanow, C.W., McNaught, K.S.P., 2006. Ubiquitin–proteasome system and Parkinson's disease. Mov. Disord. 21, 1806–1823. https://doi.org/10.1002/mds.21013
Orimo, S., Uchihara, T., Kanazawa, T., Itoh, Y., Wakabayashi, K., Kakita, A., Takahashi, H., 2011. Unmyelinated axons are more vulnerable to degeneration than myelinated axons of the cardiac nerve in Parkinson's disease: Unmyelinated axon of cardiac nerve in PD. Neuropathol. Appl. Neurobiol. 37, 791–802. https://doi.org/10.1111/j.1365-2990.2011.01194.x
Pacelli, C., Giguère, N., Bourque, M.-J., Lévesque, M., Slack, R.S., Trudeau, L.-É., 2015. Elevated Mitochondrial Bioenergetics and Axonal Arborization Size Are Key Contributors to the Vulnerability of Dopamine Neurons. Curr. Biol. 25, 2349–2360. https://doi.org/10.1016/j.cub.2015.07.050
Palikaras, K., Daskalaki, I., Markaki, M., Tavernarakis, N., 2017. Mitophagy and age-related pathologies: Development of new therapeutics by targeting mitochondrial turnover. Pharmacol. Ther. 178, 157–174. https://doi.org/10.1016/j.pharmthera.2017.04.005
Pang, S.Y.-Y., Ho, P.W.-L., Liu, H.-F., Leung, C.-T., Li, L., Chang, E.E.S., Ramsden, D.B., Ho, S.-L., 2019. The interplay of aging, genetics and environmental factors in the pathogenesis of Parkinson's disease. Transl. Neurodegener. 8, 23. https://doi.org/10.1186/s40035-019-0165-9
Papa, S., Sardanelli, A.M., Capitanio, N., Piccoli, C., 2009. Mitochondrial respiratory dysfunction and mutations in mitochondrial DNA in PINK1 familial Parkinsonism. J. Bioenerg. Biomembr. 41, 509–516. https://doi.org/10.1007/s10863-009-9252-4
Park, C.B., Larsson, N.-G., 2011. Mitochondrial DNA mutations in disease and aging. J. Cell Biol. 193, 809–818. https://doi.org/10.1083/jcb.201010024

Park, I.-H., Arora, N., Huo, H., Maherali, N., Ahfeldt, T., Shimamura, A., Lensch, M.W., Cowan, C., Hochedlinger, K., Daley, G.Q., 2008. Disease-Specific Induced Pluripotent Stem Cells. Cell 134, 877–886. https://doi.org/10.1016/j.cell.2008.07.041

Parker, W.D., Parks, J.K., Swerdlow, R.H., 2008. Complex I deficiency in Parkinson's disease frontal cortex. Brain Res. 1189, 215–8. https://doi.org/10.1016/j.brainres.2007.10.061

Perkins, H.T., Allan, V., 2021. Intertwined and Finely Balanced: Endoplasmic Reticulum Morphology, Dynamics, Function, and Diseases. Cells 10, 2341. https://doi.org/10.3390/cells10092341

Pierce, S., Coetzee, G.A., 2017. Parkinson's disease-associated genetic variation is linked to quantitative expression of inflammatory genes. PloS One 12, e0175882. https://doi.org/10.1371/journal.pone.0175882

Pinter, B., Diem-Zangerl, A., Wenning, G.K., Scherfler, C., Oberaigner, W., Seppi, K., Poewe, W., 2015. Mortality in Parkinson's disease: A 38-year follow-up study. Mov. Disord. 30, 266–269. https://doi.org/10.1002/mds.26060

Pinton, P., Giorgi, C., Siviero, R., Zecchini, E., Rizzuto, R., 2008. Calcium and apoptosis: ER-mitochondria Ca2+ transfer in the control of apoptosis. Oncogene 27, 6407–18. https://doi.org/10.1038/onc.2008.308

Pissadaki, E.K., Bolam, J.P., 2013. The energy cost of action potential propagation in dopamine neurons: clues to susceptibility in Parkinson's disease. Front. Comput. Neurosci. 7, 1–17. https://doi.org/10.3389/fncom.2013.00013

Poewe, W., Seppi, K., Tanner, C.M., Halliday, G.M., Brundin, P., Volkmann, J., Schrag, A.-E., Lang, A.E., 2017. Parkinson disease. Nat. Rev. Dis. Primer 3, 17013. https://doi.org/10.1038/nrdp.2017.13

Polymeropoulos, M.H., Lavedan, C., Leroy, E., Ide, S.E., Dehejia, A., Dutra, A., Pike, B., Root, H., Rubenstein, J., Boyer, R., Stenroos, E.S., Chandrasekharappa, S., Athanassiadou, A., Papapetropoulos, T., Johnson, W.G., Lazzarini, A.M., Duvoisin, R.C., Di Iorio, G., Golbe, L.I., Nussbaum, R.L., 1997. Mutation in the alpha-synuclein gene identified in families with Parkinson's disease. Science 276, 2045–7. https://doi.org/10.1126/science.276.5321.2045

Postuma, R.B., Berg, D., Stern, M., Poewe, W., Olanow, C.W., Oertel, W., Obeso, J., Marek, K., Litvan, I., Lang, A.E., Halliday, G., Goetz, C.G., Gasser, T., Dubois, B., Chan, P., Bloem, B.R., Adler, C.H., Deuschl, G., 2015. MDS clinical diagnostic criteria for Parkinson's disease. Mov. Disord. 30, 1591–1601. https://doi.org/10.1002/mds.26424

Prasad, E.M., Hung, S.-Y., 2021. Current Therapies in Clinical Trials of Parkinson's Disease: A 2021 Update. Pharmaceuticals 14, 717. https://doi.org/10.3390/ph14080717

Prediger, R.D.S., Rojas-Mayorquin, A.E., Aguiar, A.S., Chevarin, C., Mongeau, R., Hamon, M., Lanfumey, L., Del Bel, E., Muramatsu, H., Courty, J., Raisman-Vozari, R., 2011. Mice with genetic deletion of the heparin-binding growth factor midkine exhibit early preclinical features of Parkinson's disease. J. Neural Transm. 118, 1215–1225. https://doi.org/10.1007/s00702-010-0568-3

Prigent, A., Lionnet, A., Durieu, E., Chapelet, G., Bourreille, A., Neunlist, M., Rolli-Derkinderen, M., Derkinderen, P., 2019. Enteric alpha-synuclein expression is increased in Crohn's disease. Acta Neuropathol. (Berl.) 137, 359–361. https://doi.org/10.1007/s00401-018-1943-7

Przedborski, S., 2017. The two-century journey of Parkinson disease research. Nat. Rev. Neurosci. 18, 251–259. https://doi.org/10.1038/nrn.2017.25

Quansah, E., Peelaerts, W., Langston, J.W., Simon, D.K., Colca, J., Brundin, P., 2018. Targeting energy metabolism via the mitochondrial pyruvate carrier as a novel approach to attenuate neurodegeneration. Mol. Neurodegener. 13, 28. https://doi.org/10.1186/s13024-018-0260-x

Rajput, A.H., Rajput, A., 2014. Accuracy of Parkinson disease diagnosis unchanged in 2

decades. Neurology 83, 386–7. https://doi.org/10.1212/WNL.0000000000000653
Ray, N.J., Strafella, A.P., 2012. The neurobiology and neural circuitry of cognitive changes in Parkinson's disease revealed by functional neuroimaging. Mov. Disord. 27, 1484–1492. https://doi.org/10.1002/mds.25173
Recasens, A., Dehay, B., Bove, J., Caraballo, I., Dovero, S., Perez, A., Fernagut, P., Blesa, J., Parent, A., Perier, C., Fariñas, I., Obeso, J., Berzard, E., Vila, M., 2014. Lewy Body extracts from Parkinson's Disease Brains trigger α-Synuclein Pathology. Ann. Neurol. 75, 351–362.
Reeve, A., Simcox, E., Turnbull, D., 2014. Ageing and Parkinson's disease: Why is advancing age the biggest risk factor? Ageing Res. Rev. 14, 19–30. https://doi.org/10.1016/j.arr.2014.01.004
Reiff, T., Huber, L., Kramer, M., Delattre, O., Janoueix-Lerosey, I., Rohrer, H., 2011. Midkine and Alk signaling in sympathetic neuron proliferation and neuroblastoma predisposition. Development 138, 4699–4708. https://doi.org/10.1242/dev.072157
Reinhardt, P., Glatza, M., Hemmer, K., Tsytsyura, Y., Thiel, C.S., Höing, S., Moritz, S., Parga, J.A., Wagner, L., Bruder, J.M., Wu, G., Schmid, B., Röpke, A., Klingauf, J., Schwamborn, J.C., Gasser, T., Schöler, H.R., Sterneckert, J., 2013. Derivation and expansion using only small molecules of human neural progenitors for neurodegenerative disease modeling. PloS One 8, e59252. https://doi.org/10.1371/journal.pone.0059252
Rieusset, J., 2018. The role of endoplasmic reticulum-mitochondria contact sites in the control of glucose homeostasis: an update. Cell Death Dis. 9, 388. https://doi.org/10.1038/s41419-018-0416-1
Rizzu, P., Hinkle, D.A., Zhukareva, V., Bonifati, V., Severijnen, L.-A., Martinez, D., Ravid, R., Kamphorst, W., Eberwine, J.H., Lee, V.M.-Y., Trojanowski, J.Q., Heutink, P., 2004. DJ-1 colocalizes with tau inclusions: A link between parkinsonism and dementia. Ann. Neurol. 55, 113–118. https://doi.org/10.1002/ana.10782
Rizzuto, R., Pinton, P., Carrington, W., Fay, F.S., Fogarty, K.E., Lifshitz, L.M., Tuft, R.A., Pozzan, T., 1998. Close Contacts with the Endoplasmic Reticulum as Determinants of Mitochondrial Ca 2+ Responses. Science 280, 1763–1766. https://doi.org/10.1126/science.280.5370.1763
Rolli-Derkinderen, M., Leclair-Visonneau, L., Bourreille, A., Coron, E., Neunlist, M., Derkinderen, P., 2020. Is Parkinson's disease a chronic low-grade inflammatory bowel disease? J. Neurol. 267, 2207–2213. https://doi.org/10.1007/s00415-019-09321-0
Rossi, A., Berger, K., Chen, H., Leslie, D., Mailman, R.B., Huang, X., 2018. Projection of the prevalence of Parkinson's disease in the coming decades: Revisited. Mov. Disord. 33, 156–159. https://doi.org/10.1002/mds.27063
Rouaud, T., Corbillé, A.-G., Leclair-Visonneau, L., de Guilhem de Lataillade, A., Lionnet, A., Preterre, C., Damier, P., Derkinderen, P., 2021. Pathophysiology of Parkinson's disease: Mitochondria, alpha-synuclein and much more\ldots. Rev. Neurol. (Paris) 177, 260–271. https://doi.org/10.1016/j.neurol.2020.07.016
Rouillard, A.D., Gundersen, G.W., Fernandez, N.F., Wang, Z., Monteiro, C.D., McDermott, M.G., Ma'ayan, A., 2016. The harmonizome: a collection of processed datasets gathered to serve and mine knowledge about genes and proteins. Database 2016, baw100. https://doi.org/10.1093/database/baw100
Rousseeuw, P.J., 1987. Silhouettes: A graphical aid to the interpretation and validation of cluster analysis. J. Comput. Appl. Math. 20, 53–65. https://doi.org/10.1016/0377-0427(87)90125-7
Sakakima, H., Yoshida, Y., Yamazaki, Y., Matsuda, F., Ikutomo, M., Ijiri, K., Muramatsu, H., Muramatsu, T., Kadomatsu, K., 2009. Disruption of the midkine gene (Mdk) delays degeneration and regeneration in injured peripheral nerve. J. Neurosci. Res. 87, 2908–2915. https://doi.org/10.1002/jnr.22127
Salari, S., Bagheri, M., 2019. In vivo, in vitro and pharmacologic models of Parkinson's disease. Physiol. Res. 17–24. https://doi.org/10.33549/physiolres.933895

Sanchiz-Calvo, M., Bentea, E., Baekelandt, V., 2022. Rodent models based on endolysosomal genes involved in Parkinson's disease. Curr. Opin. Neurobiol. 72, 55–62. https://doi.org/10.1016/j.conb.2021.09.004

Santos-Lobato, B.L., Vidal, A.F., Ribeiro-dos-Santos, Â., 2021. Regulatory miRNA–mRNA Networks in Parkinson's Disease. Cells 10, 1410. https://doi.org/10.3390/cells10061410

Schapira, A.H.V., Cooper, J.M., Dexter, D., Clark, J.B., Jenner, P., Marsden, C.D., 1990. Mitochondrial Complex I Deficiency in Parkinson's Disease. J. Neurochem. 54, 823–827. https://doi.org/10.1111/j.1471-4159.1990.tb02325.x

Schindelin, J., Arganda-Carreras, I., Frise, E., Kaynig, V., Longair, M., Pietzsch, T., Preibisch, S., Rueden, C., Saalfeld, S., Schmid, B., Tinevez, J.-Y., White, D.J., Hartenstein, V., Eliceiri, K., Tomancak, P., Cardona, A., 2012. Fiji: an open-source platform for biological-image analysis. Nat. Methods 9, 676–82. https://doi.org/10.1038/nmeth.2019

Schneider, C.A., Rasband, W.S., Eliceiri, K.W., 2012. NIH Image to ImageJ: 25 years of image analysis. Nat. Methods 9, 671–5. https://doi.org/10.1038/nmeth.2089

Scholz, D., Pöltl, D., Genewsky, A., Weng, M., Waldmann, T., Schildknecht, S., Leist, M., 2011. Rapid, complete and large-scale generation of post-mitotic neurons from the human LUHMES cell line: LUHMES as widely applicable neuronal model system. J. Neurochem. 119, 957–971. https://doi.org/10.1111/j.1471-4159.2011.07255.x

Sharma, S., Singh, S., Sharma, V., Singh, V.P., Deshmukh, R., 2015. Neurobiology of l-DOPA induced dyskinesia and the novel therapeutic strategies. Biomed. Pharmacother. 70, 283–293. https://doi.org/10.1016/j.biopha.2015.01.029

Sharp, F.R., Kauer, J.S., Shepherd, G.M., 1975. Local sites of activity-related glucose metabolism in rat olfactory bulb during olfactory stimulation. Brain Res. 98, 596–600. https://doi.org/10.1016/0006-8993(75)90377-7

Siciliano, R.A., Mazzeo, M.F., Ferretta, A., Pacelli, C., Rosato, A., Papa, F., Scacco, S., Papa, S., Cocco, T., Lippolis, R., 2020. Decreased amount of vimentin N-terminal truncated proteolytic products in parkin-mutant skin fibroblasts. Biochem. Biophys. Res. Commun. 521, 693–698. https://doi.org/10.1016/j.bbrc.2019.10.154

Singh, A., 2018. Oscillatory activity in the cortico-basal ganglia-thalamic neural circuits in Parkinson's disease. Eur. J. Neurosci. 48, 2869–2878. https://doi.org/10.1111/ejn.13853

Sivanandy, P., Leey, T.C., Xiang, T.C., Ling, T.C., Wey Han, S.A., Semilan, S.L.A., Hong, P.K., 2021. Systematic Review on Parkinson's Disease Medications, Emphasizing on Three Recently Approved Drugs to Control Parkinson's Symptoms. Int. J. Environ. Res. Public. Health 19, 364. https://doi.org/10.3390/ijerph19010364

Slanzi, A., Iannoto, G., Rossi, B., Zenaro, E., Constantin, G., 2020. In vitro Models of Neurodegenerative Diseases. Front. Cell Dev. Biol. 8, 328. https://doi.org/10.3389/fcell.2020.00328

Somayaji, M., Lanseur, Z., Choi, S.J., Sulzer, D., Mosharov, E.V., 2021. Roles for α-Synuclein in Gene Expression. Genes 12, 1166. https://doi.org/10.3390/genes12081166

Soubannier, V., McLelland, G.-L., Zunino, R., Braschi, E., Rippstein, P., Fon, E.A., McBride, H.M., 2012. A Vesicular Transport Pathway Shuttles Cargo from Mitochondria to Lysosomes. Curr. Biol. 22, 135–141. https://doi.org/10.1016/j.cub.2011.11.057

Sousa, C., Golebiewska, A., Poovathingal, S.K., Kaoma, T., Pires-Afonso, Y., Martina, S., Coowar, D., Azuaje, F., Skupin, A., Balling, R., Biber, K., Niclou, S.P., Michelucci, A., 2018. Single-cell transcriptomics reveals distinct inflammation-induced microglia signatures. EMBO Rep. 19, 1–17. https://doi.org/10.15252/embr.201846171

Spillantini, M.G., Schmidt, M.L., Lee, V.M.-Y., Trojanowski, J.Q., Jakes, R., Goedert, M., 1997. a -Synuclein in Lewy bodies. Nature 388, 839–840.

Steiner, J.A., Quansah, E., Brundin, P., 2018. The concept of alpha-synuclein as a prion-

like protein: ten years after. Cell Tissue Res. 373, 161–173. https://doi.org/10.1007/s00441-018-2814-1
Stocchi, F., Tagliati, M., Olanow, C.W., 2008. Treatment of levodopa-induced motor complications. Mov. Disord. 23, S599–S612. https://doi.org/10.1002/mds.22052
Sulzer, D., Surmeier, D.J., 2013. Neuronal vulnerability, pathogenesis, and Parkinson's disease: Neuronal Vulnerability, Pathogenesis, and PD. Mov. Disord. 28, 41–50. https://doi.org/10.1002/mds.25095
Sunanda, T., Ray, B., Mahalakshmi, A.M., Bhat, A., Rashan, L., Rungratanawanich, W., Song, B.-J., Essa, M.M., Sakharkar, M.K., Chidambaram, S.B., 2021. Mitochondria-Endoplasmic Reticulum Crosstalk in Parkinson's Disease: The Role of Brain Renin Angiotensin System Components. Biomolecules 11, 1669. https://doi.org/10.3390/biom11111669
Surmeier, D.J., Obeso, J.A., Halliday, G.M., 2017a. Parkinson's Disease Is Not Simply a Prion Disorder. J. Neurosci. Off. J. Soc. Neurosci. 37, 9799–9807. https://doi.org/10.1523/JNEUROSCI.1787-16.2017
Surmeier, D.J., Obeso, J.A., Halliday, G.M., 2017b. Selective neuronal vulnerability in Parkinson disease. Nat. Rev. Neurosci. 18, 101–113. https://doi.org/10.1038/nrn.2016.178
Szklarczyk, D., Gable, A.L., Lyon, D., Junge, A., Wyder, S., Huerta-Cepas, J., Simonovic, M., Doncheva, N.T., Morris, J.H., Bork, P., Jensen, L.J., von Mering, C., 2019. STRING v11: protein-protein association networks with increased coverage, supporting functional discovery in genome-wide experimental datasets. Nucleic Acids Res. 47, D607–D613. https://doi.org/10.1093/nar/gky1131
Tabrez, S., R. Jabir, N., Shakil, S., H. Greig, N., Alam, Q., M. Abuzenadah, A., A. Damanhouri, G., A. Kamal, M., 2012. A Synopsis on the Role of Tyrosine Hydroxylase in Parkinson's Disease. CNS Neurol. Disord. - Drug Targets 11, 395–409. https://doi.org/10.2174/187152712800792785
Tabrizi, S.J., Orth, M., Wilkinson, J.M., Taanman, J.W., Warner, T.T., Cooper, J.M., Schapira, A.H., 2000. Expression of mutant alpha-synuclein causes increased susceptibility to dopamine toxicity. Hum. Mol. Genet. 9, 2683–9. https://doi.org/10.1093/hmg/9.18.2683
Takahashi, K., Tanabe, K., Ohnuki, M., Narita, M., Ichisaka, T., Tomoda, K., Yamanaka, S., 2007. Induction of Pluripotent Stem Cells from Adult Human Fibroblasts by Defined Factors. Cell 131, 861–872. https://doi.org/10.1016/j.cell.2007.11.019
Tanzarella, P., Ferretta, A., Barile, S., Ancona, M., De Rasmo, D., Signorile, A., Papa, S., Capitanio, N., Pacelli, C., Cocco, T., 2019. Increased Levels of cAMP by the Calcium-Dependent Activation of Soluble Adenylyl Cyclase in Parkin-Mutant Fibroblasts. Cells 8, 250. https://doi.org/10.3390/cells8030250
Tarakad, A., Jankovic, J., 2017. Diagnosis and Management of Parkinson's Disease. Semin. Neurol. 37, 118–126.
Thacker, E.L., O'Reilly, E.J., Weisskopf, M.G., Chen, H., Schwarzschild, M.A., McCullough, M.L., Calle, E.E., Thun, M.J., Ascherio, A., 2007. Temporal relationship between cigarette smoking and risk of Parkinson disease. Neurology 68, 764–768. https://doi.org/10.1212/01.wnl.0000256374.50227.4b
Thomson, J.A., Itskovitz-Eldor, J., Shapiro, S.S., Waknitz, M.A., Swiergiel, J.J., Marshall, V.S., Jones, J.M., 1998. Embryonic Stem Cell Lines Derived from Human Blastocysts. Sci. New Ser. 282, 1145–1147.
Tolosa, E., Garrido, A., Scholz, S.W., Poewe, W., 2021. Challenges in the diagnosis of Parkinson's disease. Lancet Neurol. 20, 385–397. https://doi.org/10.1016/S1474-4422(21)00030-2
Toyofuku, T., Okamoto, Y., Ishikawa, T., Sasawatari, S., Kumanogoh, A., 2020. LRRK2 regulates endoplasmic reticulum-mitochondrial tethering through the PERK-mediated ubiquitination pathway. EMBO J. 39, e100875. https://doi.org/10.15252/embj.2018100875
Trammell, S.A., Yu, L., Redpath, P., Migaud, M.E., Brenner, C., 2016. Nicotinamide

Riboside Is a Major NAD+ Precursor Vitamin in Cow Milk. J. Nutr. 146, 957–963. https://doi.org/10.3945/jn.116.230078

Trapnell, C., Cacchiarelli, D., Grimsby, J., Pokharel, P., Li, S., Morse, M., Lennon, N.J., Livak, K.J., Mikkelsen, T.S., Rinn, J.L., 2014. The dynamics and regulators of cell fate decisions are revealed by pseudotemporal ordering of single cells. Nat. Biotechnol. 32, 381–386. https://doi.org/10.1038/nbt.2859

Tsankov, A.M., Akopian, V., Pop, R., Chetty, S., Gifford, C.A., Daheron, L., Tsankova, N.M., Meissner, A., 2015. A qPCR ScoreCard quantifies the differentiation potential of human pluripotent stem cells. Nat. Biotechnol. 33, 1182–92. https://doi.org/10.1038/nbt.3387

Turrens, J.F., 2003. Mitochondrial formation of reactive oxygen species. J. Physiol. 552, 335–344. https://doi.org/10.1113/jphysiol.2003.049478

Tysnes, O.-B., Storstein, A., 2017. Epidemiology of Parkinson's disease. J. Neural Transm. 124, 901–905. https://doi.org/10.1007/s00702-017-1686-y

Uéda, K., Fukushima, H., Masliah, E., Xia, Y.U., Iwai, A., Yoshimoto, M., Otero, D.A.C., Kondo, J., Ihara, Y., Saitoh, T., 1993. Molecular cloning of cDNA encoding an unrecognized component of amyloid in Alzheimer disease (neurodegeneration/chaperone/amyloid P/A4 protein/neuritic plaque). Proc Natl Acad Sci USA 90, 11282–11286.

Unoki, M., Nakamura, Y., 2001. Growth-suppressive effects of BPOZ and EGR2, two genes involved in the PTEN signaling pathway. Oncogene 20, 4457–65. https://doi.org/10.1038/sj.onc.1204608

Valente, E.M., Abou-Sleiman, P.M., Caputo, V., Muqit, M.M.K., Harvey, K., Gispert, S., Ali, Z., Del Turco, D., Bentivoglio, A.R., Healy, D.G., Albanese, A., Nussbaum, R., González-Maldonado, R., Deller, T., Salvi, S., Cortelli, P., Gilks, W.P., Latchman, D.S., Harvey, R.J., Dallapiccola, B., Auburger, G., Wood, N.W., 2004. Hereditary Early-Onset Parkinson's Disease Caused by Mutations in PINK1. Science 304, 1158–1160. https://doi.org/10.1126/science.1096284

Valente, E.M., Bentivoglio, A.R., Dixon, P.H., Ferraris, A., Ialongo, T., Frontali, M., Albanese, A., Wood, N.W., 2001. Localization of a Novel Locus for Autosomal Recessive Early-Onset Parkinsonism, PARK6, on Human Chromosome 1p35-p36. Am. J. Hum. Genet. 68, 895–900. https://doi.org/10.1086/319522

Valente, E.M., Brancati, F., Ferraris, A., Graham, E.A., Davis, M.B., Breteler, M.M.B., Gasser, T., Bonifati, V., Bentivoglio, A.R., De Michele, G., Dürr, A., Cortelli, P., Wassilowsky, D., Harhangi, B.S., Rawal, N., Caputo, V., Filla, A., Meco, G., Oostra, B.A., Brice, A., Albanese, A., Dallapiccola, B., Wood, N.W., European Consortium on Genetic Susceptibility in Parkinson's Disease, 2002. PARK6-linked parkinsonism occurs in several European families. Ann. Neurol. 51, 14–8. https://doi.org/10.1002/ana.10053

Varea, O., Martin-de-Saavedra, M.D., Kopeikina, K.J., Schürmann, B., Fleming, H.J., Fawcett-Patel, J.M., Bach, A., Jang, S., Peles, E., Kim, E., Penzes, P., 2015. Synaptic abnormalities and cytoplasmic glutamate receptor aggregates in contactin associated protein-like 2 */Caspr2* knockout neurons. Proc. Natl. Acad. Sci. 112, 6176–6181. https://doi.org/10.1073/pnas.1423205112

Verma, A., Suresh, P., Gnanabharathi, B., Hirsch, E.C., Ravindranath, V., 2020. Genes critical for development and differentiation of dopaminergic neurons are downregulated in Parkinson's disease (preprint). Neuroscience. https://doi.org/10.1101/2020.03.21.001552

Verschuur, C.V.M., Suwijn, S.R., Boel, J.A., Post, B., Bloem, B.R., van Hilten, J.J., van Laar, T., Tissingh, G., Munts, A.G., Deuschl, G., Lang, A.E., Dijkgraaf, M.G.W., de Haan, R.J., de Bie, R.M.A., 2019. Randomized Delayed-Start Trial of Levodopa in Parkinson's Disease. N. Engl. J. Med. 380, 315–324. https://doi.org/10.1056/NEJMoa1809983

Vizziello, M., Borellini, L., Franco, G., Ardolino, G., 2021. Disruption of Mitochondrial Homeostasis: The Role of PINK1 in Parkinson's Disease. Cells 10, 3022.

https://doi.org/10.3390/cells10113022
Voigt, A., Berlemann, L.A., Winklhofer, K.F., 2016. The mitochondrial kinase PINK1: functions beyond mitophagy. J. Neurochem. 139, 232–239. https://doi.org/10.1111/jnc.13655
Volpicelli-Daley, L.A., Luk, K.C., Patel, T.P., Tanik, S.A., Riddle, D.M., Stieber, A., Meaney, D.F., Trojanowski, J.Q., Lee, V.M.-Y., 2011. Exogenous α-synuclein fibrils induce Lewy body pathology leading to synaptic dysfunction and neuron death. Neuron 72, 57–71. https://doi.org/10.1016/j.neuron.2011.08.033
Votyakova, T.V., Reynolds, I.J., 2001. DeltaPsi(m)-Dependent and -independent production of reactive oxygen species by rat brain mitochondria. J. Neurochem. 79, 266–77. https://doi.org/10.1046/j.1471-4159.2001.00548.x
Walden, H., Muqit, M.M.K., 2017. Ubiquitin and Parkinson's disease through the looking glass of genetics. Biochem. J. 474, 1439–1451. https://doi.org/10.1042/BCJ20160498
Walter, J., Bolognin, S., Poovathingal, S.K., Magni, S., Gérard, D., Antony, P.M.A., Nickels, S.L., Salamanca, L., Berger, E., Smits, L.M., Grzyb, K., Perfeito, R., Hoel, F., Qing, X., Ohnmacht, J., Bertacchi, M., Jarazo, J., Ignac, T., Monzel, A.S., Gonzalez-Cano, L., Krüger, R., Sauter, T., Studer, M., de Almeida, L.P., Tronstad, K.J., Sinkkonen, L., Skupin, A., Schwamborn, J.C., 2021. The Parkinson's-disease-associated mutation LRRK2-G2019S alters dopaminergic differentiation dynamics via NR2F1. Cell Rep. 37, 109864. https://doi.org/10.1016/j.celrep.2021.109864
Wang, D.-Q., Fu, P., Yao, C., Zhu, L.-S., Hou, T.-Y., Chen, J.-G., Lu, Y., Liu, D., Zhu, L.-Q., 2018. Long Non-coding RNAs, Novel Culprits, or Bodyguards in Neurodegenerative Diseases. Mol. Ther. - Nucleic Acids 10, 269–276. https://doi.org/10.1016/j.omtn.2017.12.011
Wang, H., Takahashi, R., 2007. Expanding insights on the involvement of endoplasmic reticulum stress in Parkinson's disease. Antioxid. Redox Signal. 9, 553–61. https://doi.org/10.1089/ars.2006.1524
Wang, L., Cho, Y.-L., Tang, Y., Wang, J., Park, J.-E., Wu, Yajun, Wang, C., Tong, Y., Chawla, R., Zhang, Jianbin, Shi, Y., Deng, S., Lu, G., Wu, Yihua, Tan, H.W.-S., Pawijit, P., Lim, G.G.-Y., Chan, H.-Y., Zhang, Jingzi, Fang, L., Yu, H., Liou, Y.-C., Karthik, M., Bay, B.-H., Lim, K.-L., Sze, S.-K., Yap, C.T., Shen, H.-M., 2018. PTEN-L is a novel protein phosphatase for ubiquitin dephosphorylation to inhibit PINK1-Parkin-mediated mitophagy. Cell Res. 28, 787–802. https://doi.org/10.1038/s41422-018-0056-0
Warde-Farley, D., Donaldson, S.L., Comes, O., Zuberi, K., Badrawi, R., Chao, P., Franz, M., Grouios, C., Kazi, F., Lopes, C.T., Maitland, A., Mostafavi, S., Montojo, J., Shao, Q., Wright, G., Bader, G.D., Morris, Q., 2010. The GeneMANIA prediction server: biological network integration for gene prioritization and predicting gene function. Nucleic Acids Res. 38, W214-20. https://doi.org/10.1093/nar/gkq537
Weinert, M., Selvakumar, T., Tierney, T.S., Alavian, K.N., 2015. Isolation, Culture and Long-Term Maintenance of Primary Mesencephalic Dopaminergic Neurons From Embryonic Rodent Brains. J. Vis. Exp. 52475. https://doi.org/10.3791/52475
Wichmann, T., Bergman, H., Starr, P.A., DeLong, M.R., Watts, R.L., Subramanian, T., 1999. Comparison of MPTP-induced changes in spontaneous neuronal discharge in the internal pallidal segment and in the substantia nigra pars reticulata in primates. Exp. Brain Res. 125, 397–409. https://doi.org/10.1007/s002210050696
Wichmann, T., Kliem, M.A., DeLong, M.R., 2001. Antiparkinsonian and Behavioral Effects of Inactivation of the Substantia Nigra Pars Reticulata in Hemiparkinsonian Primates. Exp. Neurol. 167, 410–424. https://doi.org/10.1006/exnr.2000.7572
Wight, T.N., Kang, I., Evanko, S.P., Harten, I.A., Chang, M.Y., Pearce, O.M.T., Allen, C.E., Frevert, C.W., 2020. Versican—A Critical Extracellular Matrix Regulator of Immunity and Inflammation. Front. Immunol. 11, 512. https://doi.org/10.3389/fimmu.2020.00512

Williams-Gray, C.H., Wijeyekoon, R., Yarnall, A.J., Lawson, R.A., Breen, D.P., Evans, J.R., Cummins, G.A., Duncan, G.W., Khoo, T.K., Burn, D.J., Barker, R.A., 2016. Serum immune markers and disease progression in an incident Parkinson's disease cohort (ICICLE-PD). Mov. Disord. 31, 995–1003. https://doi.org/10.1002/mds.26563

Winkler, C., Yao, S., 2014. The midkine family of growth factors: diverse roles in nervous system formation and maintenance: Midkine and neurogenesis. Br. J. Pharmacol. 171, 905–912. https://doi.org/10.1111/bph.12462

Winklhofer, K.F., 2014. Parkin and mitochondrial quality control: toward assembling the puzzle. Trends Cell Biol. 24, 332–41. https://doi.org/10.1016/j.tcb.2014.01.001

Wong-Riley, M.T.T., 1989. Cytochrome oxidase: an endogenous metabolic marker for neuronal activity. Trends Neurosci. 12, 94–101. https://doi.org/10.1016/0166-2236(89)90165-3

Wood, S.J., Wypych, J., Steavenson, S., Louis, J.-C., Citron, M., Biere, A.L., 1999. α-Synuclein Fibrillogenesis Is Nucleation-dependent. J. Biol. Chem. 274, 19509–19512. https://doi.org/10.1074/jbc.274.28.19509

Wu, N., Yang, M., Gaur, U., Xu, H., Yao, Y., Li, D., 2016. Alpha-Ketoglutarate: Physiological Functions and Applications. Biomol. Ther. 24, 1–8. https://doi.org/10.4062/biomolther.2015.078

Xiong, H., Wang, D., Chen, L., Choo, Y.S., Ma, H., Tang, C., Xia, K., Jiang, W., Ronai, Z., Zhuang, X., Zhang, Z., 2009. Parkin, PINK1, and DJ-1 form a ubiquitin E3 ligase complex promoting unfolded protein degradation. J. Clin. Invest. 119, 650–660. https://doi.org/10.1172/JCI37617

Xu, K., Xu, Y.-H., Chen, J.-F., Schwarzschild, M.A., 2010. Neuroprotection by caffeine: time course and role of its metabolites in the MPTP model of Parkinson's disease. Neuroscience 167, 475–481. https://doi.org/10.1016/j.neuroscience.2010.02.020

Yamano, K., Matsuda, N., Tanaka, K., 2016. The ubiquitin signal and autophagy: an orchestrated dance leading to mitochondrial degradation. EMBO Rep. 17, 300–16. https://doi.org/10.15252/embr.201541486

Yamano, K., Youle, R.J., 2017. PINK1 is degraded through the N-end rule pathway. Autophagy 8627, 1758–1769.

Yoritaka, A., Hattori, N., Uchida, K., Tanaka, M., Stadtman, E.R., Mizuno, Y., 1996. Immunohistochemical detection of 4-hydroxynonenal protein adducts in Parkinson disease. Proc. Natl. Acad. Sci. 93, 2696–2701. https://doi.org/10.1073/pnas.93.7.2696

Yoshino, J., Baur, J.A., Imai, S., 2018. NAD+ Intermediates: The Biology and Therapeutic Potential of NMN and NR. Cell Metab. 27, 513–528. https://doi.org/10.1016/j.cmet.2017.11.002

Yum, S.W., Zhang, J., Mo, K., Li, J., Scherer, S.S., 2009. A novel recessive *Nefl* mutation causes a severe, early-onset axonal neuropathy. Ann. Neurol. 66, 759–770. https://doi.org/10.1002/ana.21728

Zanon, A., Pramstaller, P.P., Hicks, A.A., Pichler, I., 2018. Environmental and Genetic Variables Influencing Mitochondrial Health and Parkinson's Disease Penetrance. Park. Dis. 2018, 1–8. https://doi.org/10.1155/2018/8684906

Zheng, Q., Huang, C., Guo, J., Tan, J., Wang, C., Tang, B., Zhang, H., 2018. Hsp70 participates in PINK1-mediated mitophagy by regulating the stability of PINK1. Neurosci. Lett. 662, 264–270. https://doi.org/10.1016/j.neulet.2017.10.051

Zhu, X.-H., Qiao, H., Du, F., Xiong, Q., Liu, X., Zhang, X., Ugurbil, K., Chen, W., 2012. Quantitative imaging of energy expenditure in human brain. NeuroImage 60, 2107–2117. https://doi.org/10.1016/j.neuroimage.2012.02.013

Zuccato, C.F., Asad, A.S., Nicola Candia, A.J., Gottardo, M.F., Moreno Ayala, M.A., Theas, M.S., Seilicovich, A., Candolfi, M., 2019. Mitochondrial-derived peptide humanin as therapeutic target in cancer and degenerative diseases. Expert Opin. Ther. Targets 23, 117–126. https://doi.org/10.1080/14728222.2019.1559300

7. Appendix A: Supplementary Material

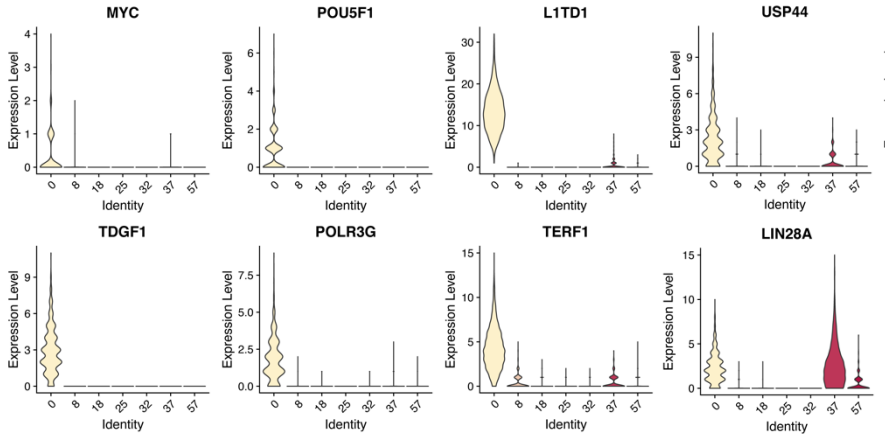

Figure S1 *Violin plots showing the normalized expression of stemness markers MYC, POU5F1, L1TD1, TDGF1, POLR3G, TERF1, USP44, LIN28A, in PINK1 and control cell lines combined, at the different time points of the differentiation.*

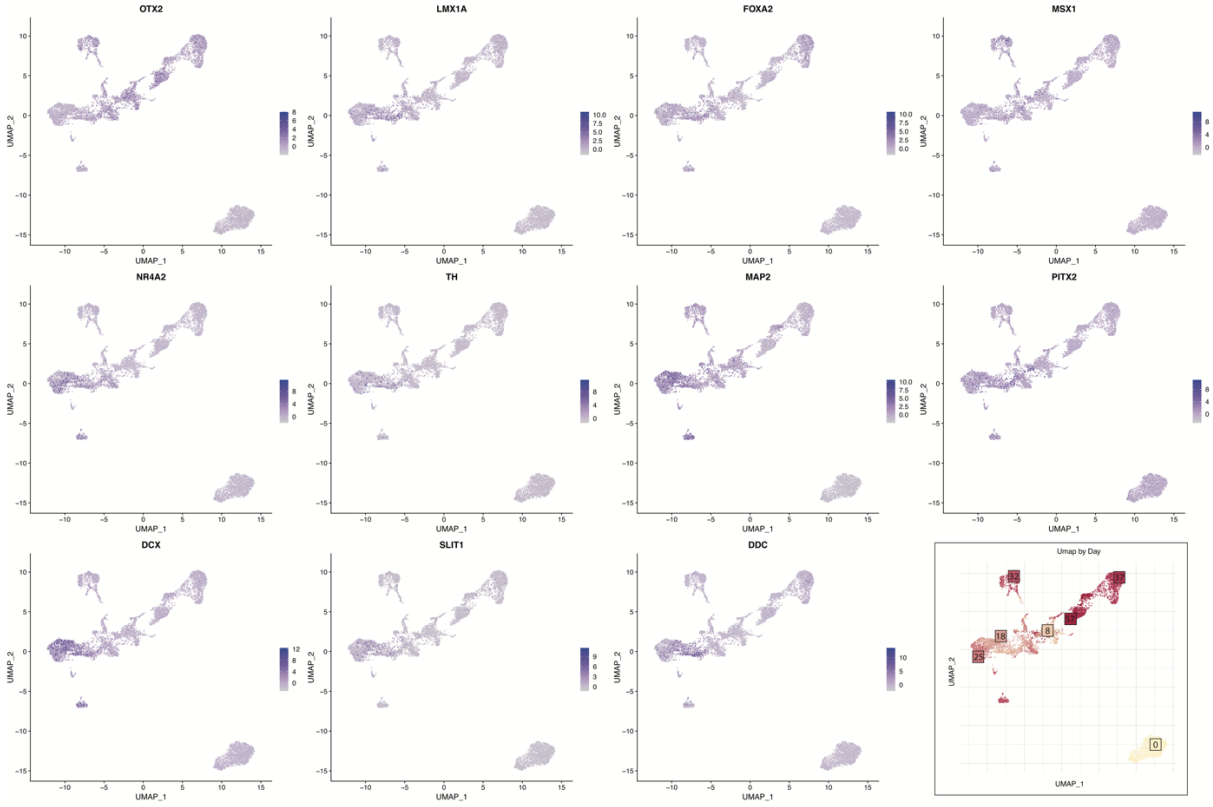

Figure S2 *Trajectory of expression of neuronal markers OTX2, LMX1A, FOXA2, MSX1, NR4A2, TH, MAP2, PITX2, DCX, SLIT1 and DDC, in PINK1 and control combined. The color scale represents the normalized expression for that specific gene.*

Day 0		Day 8		Day 18		Day 25		Day 32		Day 37		Day 57	
HIST1H1D	MT2A	TAOK1	FTLP3	MALAT1	CENPF	MT.RNR2	MT.CO1	MALAT1	RAD21	MALAT1	GAP43	MALAT1	TMSB10
MT.RNR2	MT.CO3	MT.RNR2	SFRP1	VIM	HSP90B1	GSTP1	TPX2	PEG10	HMGCS1	TTR	MT.ND4	TTR	IGFBP5
FTL	HSP90B1	GAPDH	MT.ND1	FTL	HDAC2	HIST1H4C	HMGCS1	TMSB10	IGFBP5	MT.RNR2	HNRNPC	MT.RNR2	CANX
HSP90AB1	DNAJA1	HSP90AB1	MT.CO3	MT2A	ZC3H13	CALM2	HNRNPM	MT.RNR2	MATR3	HSP90AA1	SYT1	PTN	APP
HSPA5	HINT1	VIM	GPC3	CALD1	RGS2	FTH1	ACTB	FTL	UBB	HSP90AB1	SCG2	CXCL14	APLP2
MALAT1	KMT2E	FTL	UBE2C	TTR	VCAN	TPM1	UBE2C	AP000769.1	NAP1L1	VIM	TTC3	PABPC1	IGFBP3
MT.ND1	RP11.475C16.1	HSP90AA1	NUCKS1	ENO1	RAD21	VIM	MEST	MAP1B	GAPDH	PEG10	PTGES3	VIM	HSPA5
NUCKS1	IDI1	MT1E	SNRPD2	AP000769.1	NCL	SULF1	HIST1H1D	TFPI2	DDX5	TCF7L2	DYNLL1	TPM1	MACF1
CCT3	ANP32E	CALD1	RP11.371A22.1	RP11.234A1.1	AKAP12	HTATSF1	NEFM	VIM	KIF5C	MAP1B	MT.CO2	TPT1	RP11.234A1.1
MT1G	ARPC5	HMGB2	WSB1	SULF1	HIST1H4C	CENPF	TRIM24	TPT1	SYT1	MT.CO3	PDIA3	TFPI2	MORF4L2
HNRNPA2B1	PTMA	MT.CO1	PARP1	PTN	IFT57	HNRNPA2B1	EEF2	ACTG1	TCF7L2	CALM2	GSTP1	SAT1	SPATS2L
H2AFZ	CALR	GAS5	MLEC	DLK1	LRRC75A.AS1	CTGF	NUSAP1	NEFM	DST	CHGB	CHGA	TPH1	CD24
FABP7	FDPS	DLK1	PDIA3	HNRNPA2B1	RACK1	TOP2A	NREP	HIST1H4C	MIAT	HSP90B1	IGFBP5	TMSB4X	PDIA3P1
HNRNPU	AC016739.2	RACK1	TAF1D	TMSB4X	APLP2	HMGB2	AC016739.2	NEFL	GNAS	CALM1	CANX	COL1A2	HNRNPA2B1
MT.RNR1	SMARCA5	NPM1	RP4.604A21.1	PEG10	TUBA1B	CRH	AP000769.1	COL1A2	ALCAM	HIST1H4C	MT.CYB	PCP4	TPM4
CASP3	PDIA6	PTMA	DSP	SEPT11	HIST1H1E	H1F0	IGFBP5	TUBA1A	FNBP1L	STMN2	APLP2	TAOK1	PDIA3
CALM2	SSBP1	TMSB4X	ID2	ALCAM	NAP1L1	TMSB4X	ID3	HMGB2	SYNE2	ALCAM	FAU	AP000769.1	RP11.475C16.1
MT.CO2	C11ORF58	IGFBP5	ACTB	SNHG5	EEF2	ALCAM	NEFL	HSP90AB1	MAP2	CENPF	BEX3	MAP1B	RP11.864N7.2
GNAS	TPM1	H3F3B	GSTP1	COL3A1	AC004453.8	ENO1	MKI67	GPC3	MT.CO1	TUBA1A	C11ORF88	PDIA4	HSPH1
TPM3	LAPTM4B	SNHG5	FAM60A	MAP1B	MT.RNR2	PEG10	COLEC12	TPH1	PTMA	TMSB4X	SEC62	FTH1	NQO1
HIST1H4C	RP11.234A1.1	RP11.475C16.1	LDHB	RP11.466H18.1	CHML	DYNLL1	ID4	CENPF	ONECUT2	STMN1	PTMA	CALB1	PABPC1P3
MLEC	TXN	ACTG1	PRRC2C	H3F3B	RP11.864N7.2	STMN2	KIF21A	HSP90AA1	EPB41	SOX4	ACTB	AKAP12	CP
PGK1	MIR302B	NACA	TOP2A	TPM1	RP11.425L10.1	CALM1	PABPC1	HSPA5	ACTB	SULF1	NPM1	SULF1	ANXA1
LDHA	SPP1	AC090498.1	CALM2	MT.CO1	VCL	CRABP1	MT.CO2	STMN2	RP11.234A1.1	HMGB2	CALM2P2	SCG2	PCSK1
BNIP3	RTN4	EEF2	UBB	PTMA	YBX1	TAGLN	TPT1	TMSB4X	MT.CYB	TRH	NUCKS1	HSP90AA1	CNTNAP2
UCHL1	FAU	HNRNPA2B1	HNRNPCP2	ZFAS1	SSFA2	H3F3B	RP11.466H18.1	TOP2A	MT.CO3	MT.CO1	COX6C	CTSV	CLU
ACAT2	MT1X	PTN	ENO1	PABPC1	HSBP1	TRH	SPARC	CALM2	UBE2C	CALB1	NEFL	H3F3B	PDIA6
SNHG5	MDH2	TPM4	LIN28A	NEFM	ARL6IP1	DLK1	LDHB	H3F3B	TRH	TMSB10	ID3	GAPDH	CHGB
PSMA7	PSIP1	SAT1	EEF1A1	MEST	NACA	SFRP2	CALD1	SOX4	MACF1	NEFM	NCL	NEAT1	SPARCL1
FTH1	MYL6	XRCC5	RP11.466H18.1	CANX	GSTP1	RGS2	NUCKS1	TUBB2B	FTLP3	NAP1L1	TUBA1B	ID4	CPE
PSAT1	MT1H	SOX4	HSPA5	CALM2	MACF1	TPH1	POSTN	CALM1	LMO4	TFPI2	TUBB2B	FTL	GSTP1
HSPA8	MT.ATP6	YBX1	CNBP	CRABP1	NUCKS1	HSP90AA1	GNAS	FTH1	PABPC1	AC016739.2	PIK3R1	HSP90B1	PTMA
VIM	MT.ND2	PABPC1	FAU	COL1A2	HSPD1	TPM4	SERF2	SCG2	PNISR	YWHAE	MDK	AC016739.2	MAP2
SFRP1	SKIL	AP000769.1	HSP90B1	MDK	TLE4	COL11A1	GJA1	NUCKS1	RGS16	FTL	IK	PON2	NAP1L1
BEX3	BTF3	HNRNPC	CALR	AC016739.2	KPNA2	AKAP12	NCL	HNRNPA2B1	WLS	SRP14	HNRNPU	PEG10	ANKRD12
NES	ELOVL6	P4HA1	MT.ND3	GAS5	SFRP2	MDM2	RACK1	TFF3	APLP2	ACTG1	RP11.234A1.1	ALCAM	TXN
NASP	GAS5	NCL	MT1X	PRRC2C	WSB1	PMEL	HSPH1	TTR	EIF1	DLK1	RTN4	TCF7L2	GNG11
CCT2	ILF2	CENPF	LDHA	SOX4	CALM1	ANXA1	S100A10	TUBA1B	MT.CO2	MT.ND5	MT.RNR1	ENO1	RP11.543P15.1
HNRNPDL	S100A10	UBA52	RP11.864N7.2	ACTG1	PTTG1	GPC3	AKAP9	MT.ND4	MT.ND5	HSP90AB3P	MATR3	NEFL	DSTN
HSPD1	NDUFS5	TPM1	FAM162A	HSP90AA1	PSIP1	H2AFZ	FTL	MYL6	YWHAE	AKAP9	SOX2	P4HA1	SYT4
HSP90AA1	SRSF10	ZFAS1	RGS2	PRDX6	KCNQ1OT1	ARL6IP1	PTP4A1	GAP43	CRABP1	ARL6IP1	RSPO2	CALD1	TUBA1A
RACK1	RSL1D1	LMAN1	PDIA6	TMSB10	PRDX1	CANX	LDHA	ARL6IP1	HSP90B1	RSPH1	ATP5E	MT2A	GAP43
HMGCS1	THRAP3	AC016739.2	SERBP1	TAOK1	CKAP2	WLS	NAP1L1	WSB1	RSPO2	NNAT	CNTNAP2	ATP11A	LDHA
SNRPD2	HNRNPR	HIST1H1D	CCT3	TPT1	H2AFZ	PRDX6	NASP	NNAT	TUBB	HNRNPA2B1	GAPDH	RP11.466H18.1	CALM2
HNRNPM	UBB	STMN1	HNRNPU	UCHL1	SAT1	SYT1	HES1	MKI67	HNRNPU	AP000769.1	SSB	BNIP3	ACTG1
CD24	FAM162A	TUBB	MATR3	MT1X	PGK1	GAPDH	CALM2P2	DLK1	AKAP9	WLS	LUC7L3	KCNQ1OT1	HMGCS1
NPM1	AKAP12	RP11.169K16.8	TPI1	NREP	RP11.146N23.1	TFPI2	PSMA4	CANX	CEP63	H3F3B	EID1	GNAS	CFAP43
CCT6A	UBA52	MT.RNR1	RP11.234A1.1	STMN1	HMMR	WSB1	HNRNPD	STMN1	CKB	KIF5C	YBX1	RTN4	HNRNPU
ENO1	TARS	TMSB10	CANX	LMAN1	ANP32A	TUBA1B	PTTG1	RTN4	NREP	TPT1	ENKUR	ACTB	KTN1
NOP58	PRRC2C	PGK1	YBX1P10	TPM4	PABPC3	HNRNPU	MT.CO3	NCL	LUC7L3	FTH1	UBB	NEFM	MAP1LC3B

Figure S3 *List of the 100 most DEGs for each time point of the differentiation (control + PINK1 cell lines together) compared to all the other time points.*

Day 0	SNHG5	TUBB6	BEX1	APLP2	REST
	RP4.765C7.2	AKAP12	TRIML2	ZNF676	FAM136A
	BNIP3	CCT3	NUCB2	ZNF880	ZNF729
	IFITM1	L1TD1	NODAL	CHGA	SEC11C
	RP11.69I8.2	RP11.267L5.1	MECOM	BNIP3P1	NNAT
	MT.RNR2	CENPU	FTL	CNTNAP2	ZIC1
	NLRP2	INPP5F	ACTG1	CLIC4	CTSV
	SFRP1	CCND1	CXXC5	FAU	DNAJC15
	ESRG	KIAA0101	SKIL	PRDM14	LAMB1
	MLEC	SEPT11	CDK6	MRPS21	ASRGL1
	ID1	SCGB3A2	SYNE2	BEX2	USP44
	DSP	TPM3	ATP5E	ZNF208	BNIP3L
	CASP3	GDF3	TXLNGY	TPM1	CALB1
	PGK1	NEFL	SCRN1	NOP10	FTH1
	GNAS	HSPA5	TMEM123	GSTO1	NUCKS1
	LAPTM4B	LDHA	MFGE8	SLC25A24	SNRPE
	SPG20	ZNF770	MYL6	PITX2	ARPC5
	BEX3	NASP	AC016739.2	HDAC2	TXN
	MTRNR2L1	RP11.343H5.4	FAM162A	RBM8A	PMAIP1
	SEMA6A	MT1E	RIPPLY3	TRMT112	KCNMB4

Day 8	MT.RNR2	ADSS	ID2	RGS2	SIX6
	NPM1	MT.ND3	LHX5.AS1	LDHB	SULF2
	GAPDH	FTL	DDC	FTLP3	FOXP1
	RP4.765C7.2	MALAT1	PTMAP5	SNRPD2	SLC2A1
	HSP90AB1	RP11.475C16.1	TPI1P1	RP11.314A20.1	CBX3P9
	RP11.169K16.8	PTPN13	SAT1	MYH10	SRP14
	SNHG5	GAPDHP65	VIM	HES1	SFRP2
	CALM2	RP3.417G15.1	CALM1	YWHAE	CRABP1
	RACK1	GAS5	CCT3	ALCAM	RAC1P2
	DLK1	FAM60A	MT.ATP8	FGFBP3	RP1.102E24.1
	AC090498.1	SFRP1	UBA52	ATP5E	TXNIP
	CDH2	HMGN1	HNRNPC	PLOD2	BSG
	RP4.706A16.3	HMGN1P38	CCT8	ZNF385D	CHD1
	PGK1	AC144530.1	RP11.40C6.2	MT.CO1	NR2F2
	L1TD1	CCND1	H3F3B	EEF2	NREP
	CALM2P2	RP4.604A21.1	SKAP2	DOCK10	NME2
	WLS	MDK	RP11.114H7.1	CPE	BTG1
	RP11.641D5.1	YBX1P10	RP11.371A22.1	VCAN	TTC6
	TMSB10	FRMD4B	RP11.244J10.1	PABPC1P3	MEST
	IFITM1	SLIT2	NLRP2	HNRNPCP2	RP11.422P24.9
Day 18	SNHG5	HTR2C	TMSB10	CCND1	NREP
	RP4.765C7.2	RP11.371A22.1	MAB21L2	SNRPD2	ID4
	GAS5	PEG10	TOP2A	L1TD1	EEF1B2P3
	PABPC1	TXNIP	CENPU	CHCHD2	LMO4
	ZFAS1	TLE4	UBA52	PRIM1	NASP
	RP11.466H18.1	YBX1	VCAN	MAMDC2	EIF3H
	MAP1B	PTN	GULP1	PAX6	SEMA3A
	RP11.425L10.1	TUBA1B	TFPI	EGFL6	TBX3
	RP11.234A1.1	COL3A1	NEFL	HIST1H4C	SLC39A8
	LRRC75A.AS1	RBP1	WSB1	JUN	SESN3
	COL1A2	SNHG6	CENPF	RP11.343H5.4	LMO3
	AC016739.2	MDK	LAMB1	NUSAP1	MKI67
	RACK1	HMGA1	NR3C1	ZNF711	CNTN1
	TPT1	SC22CB.1E7.1	PITX2	NRG1	YBX1P6
	PABPC3	HSPD1	CENPH	RP11.169K16.8	CRABP1
	RP11.864N7.2	FAM13C	ZIC1	DIO2	CLSPN
	PGK1	PIEZO2	PRTG	FAU	VIM
	NAP1L1	CNTNAP2	MTRNR2L1	HSP90AB1	EEF2
	EEF1B2	PDK4	LIN28A	NR5A2	TYMS
	MT.RNR2	AC004453.8	AP000769.1	RP11.333E13.2	GCNT1

Day 25	LDHA	TOP2A	NR3C1	CDK1	RP11.834C11.4
	BNIP3	COL1A2	PDZRN4	STMN4	H2AFZ
	ENO1	CTGF	NREP	TPX2	HIST1H4C
	MT.RNR2	GAPDH	UBE2C	TERF2IP	TPH1
	RP4.765C7.2	CENPF	ASCL1	DDC	NDC80
	WSB1	HMGA2	BIRC5	SPARC	KIF5C
	RGS2	LGI1	CLSPN	MAPT	ADCYAP1
	VIM	CACNA2D1	FAM162A	ENO2	GAP43
	TXNIP	CENPU	EVL	SYT4	GPI
	P4HA1	KIAA0101	SCG3	PLOD2	SCG2
	PPP2R2B	CCND1	TUBA1B	LMO4	PKIB
	HNRNPM	SYT1	ALDOA	HMP19	FNBP1L
	MIAT	CHGA	HNRNPA2B1	ETFB	ATAD2
	SNHG5	HRC	SMC4	PSAT1	CDK6
	STMN2	DLK1	CCNB1	CDCA8	TPM4
	H3F3B	TPI1	BNIP3P1	KIF11	KIF23
	GPC3	TGFB2	HMGA1	AC016739.2	NASP
	MKI67	IGFBP5	NUF2	ASPM	TYMS
	MAP1B	SRSF3	POSTN	PALLD	RP11.672L10.2
	NUSAP1	ATF5	CYR61	TPBG	NAP1L1
Day 32	SOX2	SLC39A8	CCDC144NL.AS1	ANXA2	MKI67
	RSPO2	LRP2	ABCA8	PDLIM5	PON2
	GAP43	ARX	TMEM2	RAB13	VRK1
	HES1	CENPF	CCND1	QKI	PTPRZ1
	TPBG	HDAC1	MECOM	C3ORF58	GGH
	TCF7L2	ID2	DSP	SYNE2	CENPU
	STMN1	WLS	MYO10	SNHG5	KIF5C
	COL1A2	TMEM123	GNG5	PAPSS2	PLTP
	SCG2	OTX2	SMC4	C1ORF54	UTRN
	GPC3	PLS3	ASCL1	RCN1	CEP135
	STMN2	MEST	GNG11	SPAG17	DDIT4
	LIX1	GLUL	REEP3	COL4A5	METRN
	ID3	CDK6	TSPAN6	LHX5.AS1	MAF
	VCAN	ANP32E	ADAMTS9	ZNF880	RFX4
	WNT5A	IGFBP5	TOP2A	PLXDC2	CCDC173
	COL4A6	PTTG1	RP11.574K11.24	ZIC1	GPM6A
	SLIT2	PCNA	NAP1L5	CCNG1	HTR2C
	ZFP36L1	DECR1	PAX6	LINC00461	TXLNGY
	TFPI2	SPARC	QPRT	NEFL	PTP4A1
	EMX2	PRTG	LIMCH1	PTPRG	PCSK1

Day 37	SOX2	OTX2	IQCG	RSPH1	PAPSS2
	RSPO2	HMP19	DMD	MAF	SLC25A24
	RP4.765C7.2	CCDC144NL.AS1	OSBPL1A	ARL13B	TUBB2A
	TPBG	SYNE2	ATP6V0E1	IFI27L2	SNHG5
	SCG2	LIX1	SNHG8	NTM	ID3
	IGFBP5	CCND1	PAX6	MAPT	FAM162A
	GNG11	CHRNA5	CNTNAP2	NTNG1	CDK6
	SPARC	NAP1L5	CITED2	CHKA	TMEM14DP
	WLS	CALB1	ENKUR	GPC3	CENPF
	DECR1	LHX5.AS1	EZR	ADD3	RTN3P1
	GNG5	PLS3	NEFL	LINC00467	GAP43
	PCSK1	VCAN	CFAP70	PTTG1IP	SERPINE2
	VIM	TFPI2	COL4A6	EFNB2	CFAP43
	HES1	HSPB1	TEX9	GPM6A	MT.RNR2
	SULF1	REST	VGLL4	EMX2	CLINT1
	MDK	CROT	NCAM1	AURKAIP1	CD99
	STMN2	CHGB	COL4A5	TRPM3	PPP4C
	LMO3	TTR	RTN1	CCDC173	C1ORF54
	SSR3	TMEM97	CDO1	FTL	JUN
	RTN4	UGP2	TM2D1	POLR2H	NSG1
Day 57	PEG10	TPM1	ZIC4	TMBIM4	SAT1
	MT.RNR2	CXCL14	GNG11	MT.CO2	DCX
	MAP1B	MDK	LGALS1	HNRNPA2B1	NNAT
	PCP4	C11ORF88	CTSV	HTR2C	SLC5A3
	XIST	CP	ZFYVE16	TMSB10P1	NCAM1
	CPE	MT.CO3	NQO1	PAPSS2	AC007405.6
	MT.ND5	IL17RD	MAF	MIAT	TMBIM6
	MT.ND4	CHGB	KRT18	MYL12A	CHCHD2
	SYT1	MALAT1	GRIK1	BNIP3	PLEKHA4
	MT.CO1	FTH1	ATP11A	PDIA3	DSP
	SULF1	CA2	CLIC6	IGFBP5	FAM60A
	CNTNAP2	ZIC1	TRPM3	PDIA6	GAPDH
	STMN2	TPT1	RP11.169K16.8	IGFBP7	CFAP43
	IER3	TIMP3	PALLD	CCDC39	SLC7A8
	TTR	DDX3Y	ENO1	MT.ATP6	PAX6
	FAM81B	ANXA1	CFAP126	SAMD15	C1ORF194
	TMSB10	CNN3	RTN4	TFPI2	SPARCL1
	VIM	GRIA2	TTTY15	AP000769.1	VAMP2
	MT.CYB	AC016739.2	COLEC12	AKAP12	EZR
	MT.RNR1	COL4A6	SPAG17	RAB8A	ERICH2

Figure S4 *List of Top 100 DEGs for each time point (PINK1 vs control, P-val <0,05, |FC|>0,3).*

Set 1 (D 8-18-25-32-37)	Set 2 (D 8-18)		Set 3 (S 25-32-37)
CCND1	CCND1	RP11.146N23.1	CCND1
MDK	MDK	ZNF711	MDK
MT.RNR2	MT.RNR2	TGIF1	MT.RNR2
NEFL	NEFL	MALAT1	NEFL
SNHG5	SNHG5	PBX1	SNHG5
NAP1L1	NAP1L1	FAM60A	NAP1L1
VIM	VIM	MT.ND5	VIM
EIF1AY	TMSB10	SNHG8	P4HA1
RP4.765C7.2	EIF1AY	EIF3K	EIF1AY
VCAN	RP4.765C7.2	EIF3H	RP4.765C7.2
FAM162A	VCAN	MORF4L1P1	VCAN
LIX1	FAM162A	RP11.112J1.1	FAM162A
SLIT2	LIX1	LGALS1	LIX1
GAP43	SLIT2	FBL	SLIT2
PAX6	LMO3	GOPC	CCDC144NL.AS1
RP11.343H5.4	RP11.169K16.8	UBE2C	IGFBP5
HELLS	SAT1	XBP1	GAP43
KIF11	RP11.343H5.4	EEF1B2P3	PAX6
RP11.543P15.1	FTL	CCT5	CENPF
NAP1L5	HELLS	LSM4	ANP32E
PRTG	KIF11	DANCR	EFNB2
SERPINF1	MT.CO1	EEF1B2	NAP1L5
SPARC	TPM1	RACK1	SPARC
SHMT2	RP11.543P15.1	RP11.36C20.1	CHGB
SMC4	PRTG	RSL1D1	COL4A6
ZIC1	MEST	SPATS2L	ELAVL4
KRT18	NEFM	SRP14	NCAM1
CHGB	PGK1	TUBB	TFPI2
COL4A6	PRDX6	L1TD1	TRPM3
ELAVL4	SERPINF1	SERINC5	GNG11
GNG11	SHMT2	CTD.2287O16.1	GRIA2
GRIA2	SMC4	MT2A	NRXN1
NRXN1	KRT18	MT1X	PCSK1
PCSK1	ADAMTS9	GAS5	SCG2
SCG2	CHCHD2	SEPT11	CROT
STMN2	HSPD1	FAU	GPC3
MAF	EEF1D	HSPE1	WLS
COL1A2	MT.ND1	LRRC75A.AS1	STMN2
CFAP45	MT.RNR1	PFDN5	EZR
CELF4	PEG10	RP11.475C16.1	ANXA5

NSG1	CSRP2	RP11.889L3.1	RTN4
CKS1B	CRABP1	UBA52	PTTG1
MKI67	CKB	COL14A1	TUBA1A
CACNA2D1	GULP1	TFPI	OTX2
CENPK	CENPK	DMKN	NSG1
KIAA0101	KIAA0101	ROBO2	CDK6
MTRNR2L1	MTRNR2L1	THSD7A	GPM6A
NLRP2	NLRP2	ZNF117	MAPT
SFRP2	SFRP2	KIF1A	RSPO2
TPM2	TPM2	SYDE2	RTN1
GPM6A	MTHFD2	CHN2	TUBB2A
MAPT	PKIB	CLGN	COL4A5
RSPO2	PLOD2	RP1.102E24.1	PLXDC2
RTN1	C12ORF57	NCALD	C1ORF54
TUBB2A	PSMB5	WASF2	TCF7L2
RSPO3	CCT3	AC009362.2	TPBG
TFF3	DST	RP11.478C6.4	EIF2AK2
ZC2HC1A	HINT1	SESN3	ID3
AC144530.1	HNRNPDL	TOP2B	ODC1
AP5M1	HSP90AB1	BSG	PON2
TMEM47	LMAN1	EEF2	SOX2
ZNF385D	NREP	PABPC1P3	
ZNF503	NUCKS1	PHPT1	
NRG1	PRDX1	PLEKHA5	
BLM	SNRPD2	SH3BGRL	
DHFR	TUBA1B	TLE4	
FST	TXNIP	ZFAND5	
LIN28A	NRG1	TAF1D	
EIF2AK2	BLM	CCT7	
ATAD2	DHFR	CTB.63M22.1	
LYAR	FST	SNHG1	
VRK1	LIN28A	ATP5G2	
ASPM	SPRY1	PSMB2	
COTL1	FOXP1	RP11.371A22.1	
RANP1	SLC39A8	RP11.641D5.1	
TGIF1	WNT5A	RP3.417G15.1	
	RP11.778D9.4	AB019441.29	
	ATAD5	CNBP	
	CRNDE	COX4I1	
	GOLGA8B	HSP90AA1	
	SULF2	MYEF2	
	KCNQ1OT1	NACA	

	PPM1K	RP1.278E11.3	
	RGS2	RP11.114H7.1	
	ITGB1	RP11.314A20.1	
	TIA1	RP11.488C13.1	
	ALCAM	RP13.258O15.1	
	BTG1	RP3.486I3.4	
	GPCPD1	SNU13	
	PABPC3	TOMM7	
	YBX1	UBL5	
	UQCRH		

Figure S5 *List of DEGs for Set 1 (Days 8, 18, 25, 32, 37), Set 2 (Days 8, 18) and Set 3 (Days 25, 32, 37) between PINK1 and control cell lines.*

DEGs core (13)	Gene functions
CCND1 *MDK* *MT.RNR2* *NEFL* *SNHG5* *NAP1L1* *VIM* *EIF1AY* *RP4.765C7.2* *VCAN* *FAM162A* *LIX1* *SLIT2*	*glycosaminoglycan catabolic process* *regulation of RNA stability* *regulation of mRNA catabolic process* *snRNA 3'-end processing* *RNA surveillance* *nuclear RNA surveillance* *exosome (RNase complex)* *exoribonuclease complex* *snRNA processing* *nuclear-transcribed mRNA catabolic process, exonucleolytic* *exoribonuclease activity* *exoribonuclease activity, producing 5'-phosphomonoesters* *ncRNA catabolic process* *3'-5' exonuclease activity* *snRNA metabolic process* *ncRNA 3'-end processing* *sulfur compound catabolic process* *exonuclease activity, active with either ribo- or deoxyribonucleic acids and producing 5'-phosphomonoesters* *aminoglycan catabolic process* *nuclear-transcribed mRNA catabolic process, deadenylation-dependent decay* *exonuclease activity* *mucopolysaccharide metabolic process* *ribonuclease activity* *rRNA processing* *glycosaminoglycan metabolic process*

	aminoglycan metabolic process *RNA 3'-end processing* *carbohydrate derivative catabolic process* *nuclease activity* *rRNA metabolic process* *nuclear-transcribed mRNA catabolic process* *rRNA 3'-end processing* *maturation of 5.8S rRNA from tricistronic rRNA transcript (SSU-rRNA, 5.8S rRNA, LSU-rRNA)* *maturation of 5.8S rRNA* *intermediate filament cytoskeleton organization* *cleavage involved in rRNA processing* *regulation of neutrophil chemotaxis* *neutrophil chemotaxis* *regulation of neutrophil migration* *intermediate filament-based process* *regulation of granulocyte chemotaxis* *RNA phosphodiester bond hydrolysis* *glycosaminoglycan biosynthetic process* *snoRNA 3'-end processing* *dermatan sulfate metabolic process* *dermatan sulfate proteoglycan biosynthetic process* *snoRNA processing*

Figure S6 *List of our core of 13 DEGs common to Set 1, 2 and 3 (first column), and relative shared biological functions (second column).*

List of common genes between DEGs and DAPs (90)		Gene functions
MT1H	PALLD	*DNA replication* *DNA-dependent DNA replication* *chromosomal region* *nuclear chromosome segregation* *cell cycle G1/S phase transition* *chromosome segregation* *sister chromatid segregation* *nuclear DNA replication* *cell cycle DNA replication* *DNA conformation change* *mitotic nuclear division* *axonogenesis*
TAGLN	MCM4	
GDF3	PTPN13	
CDK6	CNN2	
DSP	TPM2	
SEMA6A	GGH	
SPG20	RRM2	
SCRN1	MTHFD2	
SLC25A24	CACNA2D1	
LAMB1	RTN1	
PLOD2	MCM6	
H2AFY2	UFM1	

EPCAM	FBN2
L1TD1	KIF4A
KIF21A	COLEC12
WLS	EVL
TRIO	PLIN2
RBP1	PLOD2
ALCAM	SCG2
SLIT2	TPBG
KIF11	SYNE2
EPHA4	PCNA
HELLS	CALB1
CENPF	TJP1
SPATS2L	WLS
MCM7	ABCA8
NCAM1	BASP1
SMC2	GAP43
PCNA	RTN4
MCM2	SYT1
TAGLN3	NCAM1
SMC4	**NEFL**
FAM84B	PAK3
INA	NRCAM
PGM2L1	VAMP2
ALCAM	HSPB1
DCLK1	SYNE2
NBEA	PCSK1
GJA1	CNN3
MCM3	CA2
GAP43	TFPI2
ELAVL4	CALD1
WDHD1	PLS3
CDK6	P4HA1
DCX	STMN2

protein-DNA complex
mitotic sister chromatid segregation
protein-DNA complex assembly
protein-DNA complex subunit organization
DNA recombination
chromosome, telomeric region
recombinational repair
catalytic activity, acting on DNA
ATPase activity
double-strand break repair
DNA replication preinitiation complex
double-strand break repair via homologous recombination
condensed chromosome
neuron projection guidance
developmental growth
DNA strand elongation
DNA-dependent ATPase activity
DNA packaging
brain development
chromosome condensation
axon guidance
helicase activity
neuron projection extension
cell recognition
negative regulation of cell projection organization
developmental cell growth
developmental growth involved in morphogenesis
actin filament-based movement
mitotic DNA replication
neuron recognition
DNA helicase activity
DNA packaging complex
replication fork
DNA duplex unwinding
DNA geometric change
axon extension
actin-mediated cell contraction
cell adhesion mediator activity
pallium development
DNA replication initiation
neuron projection fasciculation
cerebral cortex cell migration
cerebral cortex development

	telencephalon cell migration *forebrain cell migration*

Figure S7 *List of overlapping 90 genes between DEGs and DAPs including all time points (first column) and of related biological processes (second column). In bold, NEFL and SLIT2 which are also included in the top 13 DEGs core.*

GO Biological Processes (STRING) – **D0** *(DAPs FC1)*

#term ID	term description	observed gene count	background gene count	strength	false discovery rate
GO:0006520	Cellular amino acid metabolic process	18	278	0.95	6.08e-08
GO:0019752	Carboxylic acid metabolic process	27	853	0.64	9.62e-07
GO:0009987	Cellular process	136	15024	0.1	1.17e-06
GO:0043436	Oxoacid metabolic process	28	944	0.61	1.17e-06
GO:1901605	Alpha-amino acid metabolic process	14	191	1.0	1.17e-06
GO:0044281	Small molecule metabolic process	35	1684	0.46	2.22e-05
GO:0009063	Cellular amino acid catabolic process	10	124	1.05	7.51e-05
GO:0006575	Cellular modified amino acid metabolic process	11	180	0.93	0.00018
GO:1901606	Alpha-amino acid catabolic process	9	104	1.08	0.00018
GO:1901607	Alpha-amino acid biosynthetic process	7	58	1.22	0.00050
GO:0009064	Glutamine family amino acid metabolic process	7	69	1.15	0.0013
GO:0048513	Animal organ development	46	3197	0.3	0.0021
GO:0009065	Glutamine family amino acid catabolic process	5	27	1.41	0.0026
GO:0009066	Aspartate family amino acid metabolic process	6	50	1.22	0.0026
GO:0046395	Carboxylic acid catabolic process	11	260	0.77	0.0033
GO:0043648	Dicarboxylic acid metabolic process	7	93	1.02	0.0054
GO:0046686	Response to cadmium ion	6	63	1.12	0.0067
GO:0042221	Response to chemical	54	4333	0.23	0.0090
GO:0044282	Small molecule catabolic process	13	424	0.63	0.0100
GO:0042398	Cellular modified amino acid biosynthetic process	5	45	1.18	0.0165
GO:0070887	Cellular response to chemical stimulus	40	2919	0.28	0.0215
GO:0000904	Cell morphogenesis involved in differentiation	14	566	0.53	0.0395
GO:0070831	Basement membrane assembly	3	9	1.66	0.0395

GO Biological Processes (STRING) – **D8** *(DAPs FC1)*

#term ID	term description	observed gene count	background gene count	strength	false discovery rate
GO:0044281	Small molecule metabolic process	33	1684	0.49	4.09e-05
GO:0019752	Carboxylic acid metabolic process	22	853	0.61	0.00014

GO:0006928	Movement of cell or subcellular component	29	1501	0.49	0.00021
GO:0006575	Cellular modified amino acid metabolic process	9	180	0.9	0.0063
GO:0009987	Cellular process	114	15024	0.08	0.0063
GO:0040011	Locomotion	23	1251	0.47	0.0063
GO:0044237	Cellular metabolic process	72	7513	0.18	0.0074
GO:0019637	Organophosphate metabolic process	18	870	0.52	0.0130
GO:0008152	Metabolic process	76	8298	0.16	0.0146
GO:0016477	Cell migration	18	896	0.5	0.0160
GO:0010043	Response to zinc ion	5	53	1.18	0.0305
GO:1902533	Positive regulation of intracellular signal transduction	19	1041	0.46	0.0305
GO:0032989	Cellular component morphogenesis	14	614	0.56	0.0329
GO:0070887	Cellular response to chemical stimulus	36	2919	0.29	0.0329
GO:0042221	Response to chemical	47	4333	0.24	0.0330
GO:0051716	Cellular response to stimulus	62	6489	0.18	0.0436
GO:0006520	Cellular amino acid metabolic process	9	278	0.71	0.0498
GO:0009636	Response to toxic substance	8	219	0.76	0.0498
GO:0009967	Positive regulation of signal transduction	24	1654	0.36	0.0498
GO:0031175	Neuron projection development	14	680	0.52	0.0498
GO:0043405	Regulation of map kinase activity	10	342	0.67	0.0498
GO:0044283	Small molecule biosynthetic process	13	572	0.56	0.0498
GO:0048812	Neuron projection morphogenesis	12	495	0.59	0.0498
GO:0050896	Response to stimulus	72	8046	0.15	0.0498
GO:0120036	Plasma membrane bounded cell projection organization	19	1122	0.43	0.0498

GO Biological Processes (STRING) – **D18** *(DAPs FC1)*

#term ID	term description	observed gene count	background gene count	strength	false discovery rate
GO:0009987	Cellular process	228	15024	0.07	0.00022
GO:0007275	Multicellular organism development	104	5023	0.21	0.00027
GO:0019318	Hexose metabolic process	14	157	0.84	0.00027
GO:0032502	Developmental process	116	5841	0.19	0.00027
GO:0048731	System development	95	4426	0.22	0.00027
GO:0048856	Anatomical structure development	110	5402	0.2	0.00027
GO:0071840	Cellular component organization or biogenesis	112	5633	0.19	0.00027
GO:0016043	Cellular component organization	108	5447	0.19	0.00045
GO:0044281	Small molecule metabolic process	47	1684	0.34	0.00072
GO:0007399	Nervous system development	59	2371	0.29	0.00075
GO:0048812	Neuron projection morphogenesis	22	495	0.54	0.00090
GO:0030029	Actin filament-based process	24	592	0.5	0.0011
GO:0007010	Cytoskeleton organization	35	1126	0.38	0.0015
GO:0009653	Anatomical structure morphogenesis	54	2165	0.29	0.0015
GO:0030036	Actin cytoskeleton organization	21	516	0.5	0.0036

GO:0044237	Cellular metabolic process	132	7513	0.13	0.0036
GO:0030154	Cell differentiation	77	3702	0.21	0.0044
GO:0032989	Cellular component morphogenesis	23	614	0.46	0.0044
GO:0035295	Tube development	28	851	0.41	0.0044
GO:0008652	Cellular amino acid biosynthetic process	8	75	0.92	0.0057
GO:0000902	Cell morphogenesis	25	726	0.43	0.0061
GO:0031175	Neuron projection development	24	680	0.44	0.0061
GO:0048666	Neuron development	27	827	0.4	0.0061
GO:2000145	Regulation of cell motility	29	929	0.38	0.0062
GO:0048468	Cell development	42	1629	0.3	0.0065
GO:0007409	Axonogenesis	17	384	0.54	0.0067
GO:0008152	Metabolic process	140	8298	0.12	0.0082
GO:0001655	Urogenital system development	15	315	0.57	0.0087
GO:0009991	Response to extracellular stimulus	19	483	0.48	0.0087
GO:0019752	Carboxylic acid metabolic process	27	853	0.39	0.0087
GO:0022008	Neurogenesis	42	1657	0.29	0.0087
GO:0044283	Small molecule biosynthetic process	21	572	0.45	0.0087
GO:0051270	Regulation of cellular component movement	30	1009	0.36	0.0087
GO:0072001	Renal system development	14	280	0.59	0.0087
GO:0006928	Movement of cell or subcellular component	39	1501	0.3	0.0088
GO:0030182	Neuron differentiation	30	1019	0.36	0.0090
GO:0048667	Cell morphogenesis involved in neuron differentiation	18	445	0.5	0.0090
GO:0006006	Glucose metabolic process	9	116	0.78	0.0093
GO:0044085	Cellular component biogenesis	57	2583	0.23	0.0098
GO:0007015	Actin filament organization	13	254	0.6	0.0112
GO:0009888	Tissue development	43	1760	0.28	0.0114
GO:0022607	Cellular component assembly	53	2359	0.24	0.0116
GO:0043436	Oxoacid metabolic process	28	944	0.36	0.0126
GO:0016477	Cell migration	27	896	0.37	0.0128
GO:0048699	Generation of neurons	39	1551	0.29	0.0133
GO:0071704	Organic substance metabolic process	131	7755	0.12	0.0133
GO:0035239	Tube morphogenesis	22	656	0.42	0.0140
GO:0000904	Cell morphogenesis involved in differentiation	20	566	0.44	0.0150
GO:0044238	Primary metabolic process	125	7332	0.12	0.0150
GO:0006950	Response to stress	70	3485	0.19	0.0156
GO:0030334	Regulation of cell migration	26	865	0.37	0.0160
GO:0001822	Kidney development	13	271	0.57	0.0161
GO:0007422	Peripheral nervous system development	7	75	0.86	0.0176
GO:0072359	Circulatory system development	26	872	0.36	0.0176
GO:0014044	Schwann cell development	5	31	1.1	0.0178
GO:0040011	Locomotion	33	1251	0.31	0.0184

GO:0048513	Animal organ development	65	3197	0.2	0.0196
GO:0022603	Regulation of anatomical structure morphogenesis	30	1095	0.33	0.0200
GO:0006004	Fucose metabolic process	4	16	1.29	0.0201
GO:0031667	Response to nutrient levels	17	449	0.47	0.0201
GO:0055114	Oxidation-reduction process	27	939	0.35	0.0203
GO:0042552	Myelination	8	111	0.75	0.0261
GO:0015800	Acidic amino acid transport	6	58	0.9	0.0289
GO:1901607	Alpha-amino acid biosynthetic process	6	58	0.9	0.0289
GO:0032879	Regulation of localization	57	2740	0.21	0.0290
GO:0043933	Protein-containing complex subunit organization	37	1539	0.27	0.0352
GO:0097435	Supramolecular fiber organization	17	480	0.44	0.0370
GO:0050793	Regulation of developmental process	55	2648	0.21	0.0384
GO:0048588	Developmental cell growth	7	90	0.78	0.0386
GO:0051128	Regulation of cellular component organization	51	2402	0.22	0.0398
GO:0009058	Biosynthetic process	57	2788	0.2	0.0410
GO:1901605	Alpha-amino acid metabolic process	10	191	0.61	0.0410
GO:0060429	Epithelium development	29	1109	0.31	0.0438
GO:0010586	miRNA metabolic process	4	22	1.15	0.0453
GO:0034330	Cell junction organization	17	493	0.43	0.0453
GO:0007411	Axon guidance	12	275	0.53	0.0476

GO Biological Processes (STRING) – **D25** *(DAPs FC2)*

#term ID	term description	observed gene count	background gene count	strength	false discovery rate
GO:0006267	Pre-replicative complex assembly involved in nuclear cell cycle dna replication	6	7	2.32	8.12e-08
GO:0033260	Nuclear dna replication	8	43	1.66	9.38e-08
GO:0000727	Double-strand break repair via break-induced replication	6	11	2.13	9.63e-08
GO:0006261	DNA-dependent DNA replication	9	119	1.27	4.59e-06
GO:0000082	G1/S transition of mitotic cell cycle	9	128	1.24	7.33e-06
GO:0071840	Cellular component organization or biogenesis	48	5633	0.32	8.71e-06
GO:0006270	DNA replication initiation	6	32	1.66	1.10e-05
GO:0006260	DNA replication	10	205	1.08	1.81e-05
GO:0061564	Axon development	13	421	0.88	2.03e-05
GO:0000278	Mitotic cell cycle	16	695	0.75	2.09e-05
GO:1903047	Mitotic cell cycle process	15	616	0.77	2.78e-05
GO:0007409	Axonogenesis	12	384	0.88	5.36e-05
GO:0016043	Cellular component organization	45	5447	0.31	7.39e-05
GO:0048812	Neuron projection morphogenesis	13	495	0.81	9.18e-05
GO:0032989	Cellular component morphogenesis	14	614	0.75	0.00013
GO:1902969	Mitotic dna replication	4	11	1.95	0.00018

GO:0022402	Cell cycle process	17	976	0.63	0.00021
GO:0031175	Neuron projection development	14	680	0.7	0.00036
GO:0006268	DNA unwinding involved in DNA replication	4	15	1.81	0.00045
GO:0048666	Neuron development	15	827	0.65	0.00060
GO:0000902	Cell morphogenesis	14	726	0.67	0.00068
GO:0007399	Nervous system development	26	2371	0.43	0.00068
GO:0086065	Cell communication involved in cardiac conduction	5	44	1.44	0.00068
GO:0006271	DNA strand elongation involved in DNA replication	4	18	1.74	0.00071
GO:0007411	Axon guidance	9	275	0.9	0.00088
GO:1902975	Mitotic dna replication initiation	3	4	2.26	0.00088
GO:0030182	Neuron differentiation	16	1019	0.58	0.0011
GO:0007049	Cell cycle	18	1313	0.53	0.0015
GO:0022008	Neurogenesis	20	1657	0.47	0.0025
GO:0120036	Plasma membrane bounded cell projection organization	16	1122	0.54	0.0030
GO:0035637	Multicellular organismal signaling	6	137	1.03	0.0065
GO:0030029	Actin filament-based process	11	592	0.66	0.0079
GO:0048699	Generation of neurons	18	1551	0.45	0.0114
GO:0006996	Organelle organization	29	3450	0.31	0.0138
GO:0086064	Cell communication by electrical coupling involved in cardiac conduction	3	16	1.66	0.0138
GO:0071103	DNA conformation change	8	328	0.78	0.0151
GO:0086001	Cardiac muscle cell action potential	4	50	1.29	0.0153
GO:0048468	Cell development	18	1629	0.43	0.0192
GO:0006928	Movement of cell or subcellular component	17	1501	0.44	0.0230
GO:0007010	Cytoskeleton organization	14	1126	0.48	0.0388
GO:0035583	Sequestering of tgfbeta in extracellular matrix	2	4	2.09	0.0488
GO:0086019	Cell-cell signaling involved in cardiac conduction	3	27	1.43	0.0488

GO Biological Processes (STRING) – **D32** *(DAPs FC2)*

#term ID	term description	observed gene count	background gene count	strength	false discovery rate
GO:0048731	System development	40	4426	0.43	5.51e-07
GO:0007275	Multicellular organism development	42	5023	0.39	6.88e-07
GO:0032501	Multicellular organismal process	49	6933	0.32	7.00e-07
GO:0032502	Developmental process	45	5841	0.36	7.00e-07
GO:0048856	Anatomical structure development	43	5402	0.37	7.00e-07
GO:0048513	Animal organ development	32	3197	0.47	3.16e-06
GO:0001654	Eye development	12	365	0.99	7.51e-06
GO:0043010	Camera-type eye development	11	318	1.01	1.50e-05
GO:0030705	Cytoskeleton-dependent intracellular transport	9	195	1.14	3.07e-05
GO:0001822	Kidney development	10	271	1.04	3.43e-05
GO:0009888	Tissue development	22	1760	0.57	3.71e-05
GO:0010970	Transport along microtubule	8	155	1.18	6.21e-05

GO:0016043	Cellular component organization	39	5447	0.33	9.17e-05
GO:0120036	Plasma membrane bounded cell projection organization	17	1122	0.65	0.00010
GO:0098840	Protein transport along microtubule	6	67	1.42	0.00011
GO:0033036	Macromolecule localization	25	2473	0.48	0.00012
GO:0007154	Cell communication	38	5320	0.33	0.00013
GO:0051179	Localization	39	5591	0.32	0.00014
GO:0009653	Anatomical structure morphogenesis	23	2165	0.5	0.00015
GO:0071702	Organic substance transport	23	2173	0.5	0.00016
GO:0007155	Cell adhesion	15	925	0.68	0.00017
GO:0035735	Intraciliary transport involved in cilium assembly	5	40	1.57	0.00017
GO:0051641	Cellular localization	27	2967	0.43	0.00017
GO:0051649	Establishment of localization in cell	24	2375	0.48	0.00017
GO:0023052	Signaling	37	5239	0.32	0.00019
GO:0060429	Epithelium development	16	1109	0.63	0.00025
GO:2000026	Regulation of multicellular organismal development	22	2096	0.49	0.00027
GO:0035295	Tube development	14	851	0.69	0.00029
GO:0009790	Embryo development	15	1002	0.65	0.00034
GO:0008104	Protein localization	22	2139	0.48	0.00035
GO:0072359	Circulatory system development	14	872	0.68	0.00036
GO:0071705	Nitrogen compound transport	20	1823	0.51	0.00045
GO:0046907	Intracellular transport	18	1520	0.55	0.00059
GO:0120031	Plasma membrane bounded cell projection assembly	10	433	0.84	0.00060
GO:0015800	Acidic amino acid transport	5	58	1.41	0.00062
GO:0050896	Response to stimulus	46	8046	0.23	0.00072
GO:0050793	Regulation of developmental process	24	2648	0.43	0.00073
GO:0050804	Modulation of chemical synaptic transmission	10	446	0.82	0.00073
GO:0046903	Secretion	15	1097	0.61	0.00078
GO:0120035	Regulation of plasma membrane bounded cell projection organization	12	687	0.71	0.00078
GO:0048598	Embryonic morphogenesis	11	571	0.76	0.00082
GO:0009887	Animal organ morphogenesis	14	967	0.63	0.00086
GO:0044782	Cilium organization	9	360	0.87	0.00086
GO:0032940	Secretion by cell	14	979	0.63	0.00096
GO:0051234	Establishment of localization	32	4479	0.33	0.0010
GO:0051716	Cellular response to stimulus	40	6489	0.26	0.0010
GO:0006886	Intracellular protein transport	14	999	0.62	0.0011
GO:0007399	Nervous system development	22	2371	0.44	0.0012
GO:0030326	Embryonic limb morphogenesis	6	127	1.15	0.0012
GO:0014047	Glutamate secretion	4	32	1.57	0.0013
GO:0006928	Movement of cell or subcellular component	17	1501	0.53	0.0015
GO:0006810	Transport	31	4353	0.32	0.0016
GO:0015833	Peptide transport	17	1518	0.52	0.0016

GO:0071692	Protein localization to extracellular region	6	137	1.11	0.0016
GO:0035721	Intraciliary retrograde transport	3	10	1.95	0.0018
GO:0007165	Signal transduction	33	4876	0.3	0.0019
GO:0007507	Heart development	10	522	0.75	0.0019
GO:0010646	Regulation of cell communication	27	3514	0.36	0.0020
GO:0006835	Dicarboxylic acid transport	5	86	1.24	0.0023
GO:0023051	Regulation of signaling	27	3553	0.35	0.0024
GO:0034613	Cellular protein localization	17	1610	0.5	0.0030
GO:0022607	Cellular component assembly	21	2359	0.42	0.0031
GO:0030198	Extracellular matrix organization	8	338	0.85	0.0031
GO:0060271	Cilium assembly	8	339	0.84	0.0031
GO:0035272	Exocrine system development	4	46	1.41	0.0035
GO:0051239	Regulation of multicellular organismal process	25	3227	0.36	0.0038
GO:0015031	Protein transport	16	1486	0.5	0.0040
GO:0009987	Cellular process	63	15024	0.09	0.0056
GO:0060445	Branching involved in salivary gland morphogenesis	3	17	1.72	0.0056
GO:0051094	Positive regulation of developmental process	15	1389	0.51	0.0069
GO:0065008	Regulation of biological quality	28	4042	0.31	0.0071
GO:0007166	Cell surface receptor signaling pathway	20	2325	0.41	0.0073
GO:0010975	Regulation of neuron projection development	9	510	0.72	0.0073
GO:0031346	Positive regulation of cell projection organization	8	391	0.78	0.0073
GO:0050789	Regulation of biological process	54	11475	0.14	0.0073
GO:0010976	Positive regulation of neuron projection development	7	288	0.86	0.0075
GO:0023061	Signal release	6	197	0.96	0.0078
GO:0042733	Embryonic digit morphogenesis	4	61	1.29	0.0084
GO:0051960	Regulation of nervous system development	12	942	0.58	0.0087
GO:0060284	Regulation of cell development	12	956	0.57	0.0098
GO:0050794	Regulation of cellular process	52	10932	0.15	0.0107
GO:0030154	Cell differentiation	26	3702	0.32	0.0110
GO:0044087	Regulation of cellular component biogenesis	12	971	0.56	0.0110
GO:0051962	Positive regulation of nervous system development	9	547	0.69	0.0112
GO:0007417	Central nervous system development	12	988	0.56	0.0126
GO:0060830	Ciliary receptor clustering involved in smoothened signaling pathway	2	3	2.3	0.0126
GO:0045597	Positive regulation of cell differentiation	12	993	0.55	0.0130
GO:0006836	Neurotransmitter transport	5	139	1.03	0.0137
GO:0007224	Smoothened signaling pathway	4	72	1.22	0.0137
GO:0065007	Biological regulation	55	12171	0.13	0.0178
GO:0035583	Sequestering of tgfbeta in extracellular matrix	2	4	2.17	0.0179
GO:0050803	Regulation of synapse structure or activity	6	239	0.87	0.0185
GO:0048646	Anatomical structure formation involved in morphogenesis	11	883	0.57	0.0189

GO:0032879	Regulation of localization	21	2740	0.36	0.0190
GO:0002790	Peptide secretion	5	152	0.99	0.0192
GO:1901652	Response to peptide	8	476	0.7	0.0217
GO:0001656	Metanephros development	4	84	1.15	0.0224
GO:0050769	Positive regulation of neurogenesis	8	479	0.69	0.0224
GO:0001657	Ureteric bud development	4	86	1.14	0.0240
GO:0021532	Neural tube patterning	3	35	1.41	0.0274
GO:0022603	Regulation of anatomical structure morphogenesis	12	1095	0.51	0.0274
GO:0048468	Cell development	15	1629	0.44	0.0282
GO:0060249	Anatomical structure homeostasis	7	380	0.74	0.0294
GO:0048048	Embryonic eye morphogenesis	3	37	1.38	0.0305
GO:0031076	Embryonic camera-type eye development	3	39	1.36	0.0351
GO:0040012	Regulation of locomotion	11	969	0.53	0.0357
GO:0043434	Response to peptide hormone	7	394	0.72	0.0357
GO:0060831	Smoothened signaling pathway involved in dorsal/ventral neural tube patterning	2	7	1.93	0.0357
GO:0120032	Regulation of plasma membrane bounded cell projection assembly	5	181	0.91	0.0361
GO:0031589	Cell-substrate adhesion	5	182	0.91	0.0364
GO:0045595	Regulation of cell differentiation	16	1874	0.4	0.0364
GO:0007269	Neurotransmitter secretion	4	102	1.07	0.0386
GO:0048666	Neuron development	10	827	0.55	0.0387
GO:0050767	Regulation of neurogenesis	10	828	0.55	0.0388
GO:0050770	Regulation of axonogenesis	5	187	0.9	0.0393
GO:0048732	Gland development	7	410	0.7	0.0410
GO:0033260	Nuclear dna replication	3	43	1.32	0.0412
GO:0046942	Carboxylic acid transport	6	293	0.78	0.0413
GO:1905515	Non-motile cilium assembly	3	45	1.3	0.0455
GO:0030182	Neuron differentiation	11	1019	0.51	0.0474
GO:0000302	Response to reactive oxygen species	5	198	0.87	0.0476
GO:1900264	Positive regulation of dna-directed dna polymerase activity	2	9	1.82	0.0476
GO:0048729	Tissue morphogenesis	8	561	0.63	0.0483

GO Biological Processes (STRING) – **D57** *(DAPs FC2)*

#term ID	term description	observed gene count	background gene count	strength	false discovery rate
GO:0071840	Cellular component organization or biogenesis	177	5633	0.26	3.85e-15
GO:0016043	Cellular component organization	169	5447	0.25	1.17e-13
GO:0031175	Neuron projection development	46	680	0.59	5.95e-11
GO:0034330	Cell junction organization	39	493	0.66	5.95e-11
GO:0048666	Neuron development	51	827	0.55	5.95e-11
GO:0007399	Nervous system development	90	2371	0.34	1.65e-09
GO:0120036	Plasma membrane bounded cell projection organization	57	1122	0.47	1.65e-09

GO:0030182	Neuron differentiation	53	1019	0.48	3.83e-09
GO:0048699	Generation of neurons	67	1551	0.4	8.81e-09
GO:0065008	Regulation of biological quality	124	4042	0.25	2.08e-08
GO:0051128	Regulation of cellular component organization	87	2402	0.32	2.63e-08
GO:0048812	Neuron projection morphogenesis	34	495	0.6	3.35e-08
GO:0022008	Neurogenesis	68	1657	0.37	3.81e-08
GO:0099504	Synaptic vesicle cycle	17	120	0.91	1.35e-07
GO:0006996	Organelle organization	108	3450	0.26	1.63e-07
GO:0007010	Cytoskeleton organization	52	1126	0.43	1.63e-07
GO:0032879	Regulation of localization	91	2740	0.28	3.70e-07
GO:0050808	Synapse organization	24	283	0.69	3.70e-07
GO:0061564	Axon development	29	421	0.6	5.13e-07
GO:0009987	Cellular process	304	15024	0.07	5.17e-07
GO:0032989	Cellular component morphogenesis	35	614	0.52	9.55e-07
GO:0048468	Cell development	63	1629	0.35	1.17e-06
GO:0048667	Cell morphogenesis involved in neuron differentiation	29	445	0.58	1.44e-06
GO:0000902	Cell morphogenesis	38	726	0.48	1.48e-06
GO:0000904	Cell morphogenesis involved in differentiation	33	566	0.53	1.48e-06
GO:0051179	Localization	148	5591	0.18	1.48e-06
GO:0048856	Anatomical structure development	143	5402	0.18	3.21e-06
GO:0120035	Regulation of plasma membrane bounded cell projection organization	36	687	0.48	3.55e-06
GO:0007409	Axonogenesis	26	384	0.59	3.85e-06
GO:0033036	Macromolecule localization	81	2473	0.28	5.23e-06
GO:0010975	Regulation of neuron projection development	30	510	0.53	5.27e-06
GO:0050804	Modulation of chemical synaptic transmission	27	446	0.54	1.60e-05
GO:0001505	Regulation of neurotransmitter levels	19	231	0.68	2.02e-05
GO:0007155	Cell adhesion	41	925	0.41	2.25e-05
GO:0007275	Multicellular organism development	132	5023	0.18	2.37e-05
GO:0016192	Vesicle-mediated transport	63	1805	0.3	2.98e-05
GO:0006810	Transport	118	4353	0.19	3.37e-05
GO:0051641	Cellular localization	89	2967	0.24	3.55e-05
GO:0051640	Organelle localization	31	598	0.48	3.57e-05
GO:0048731	System development	119	4426	0.19	4.22e-05
GO:0071702	Organic substance transport	71	2173	0.28	4.27e-05
GO:0032502	Developmental process	146	5841	0.16	5.82e-05
GO:0098693	Regulation of synaptic vesicle cycle	13	114	0.82	6.75e-05
GO:0051049	Regulation of transport	61	1776	0.3	7.20e-05
GO:0051234	Establishment of localization	119	4479	0.19	7.32e-05
GO:0008104	Protein localization	69	2139	0.27	9.64e-05
GO:1990778	Protein localization to cell periphery	18	237	0.64	9.85e-05
GO:0044087	Regulation of cellular component biogenesis	40	971	0.38	0.00015
GO:0016358	Dendrite development	12	112	0.79	0.00032

GO:0019752	Carboxylic acid metabolic process	36	853	0.39	0.00032
GO:0032501	Multicellular organismal process	163	6933	0.13	0.00032
GO:0071705	Nitrogen compound transport	60	1823	0.28	0.00032
GO:0015800	Acidic amino acid transport	9	58	0.95	0.00040
GO:0017156	Calcium-ion regulated exocytosis	8	42	1.04	0.00040
GO:0006836	Neurotransmitter transport	13	139	0.73	0.00043
GO:0030154	Cell differentiation	100	3702	0.19	0.00043
GO:0051046	Regulation of secretion	31	686	0.42	0.00043
GO:0044281	Small molecule metabolic process	56	1684	0.28	0.00050
GO:0051588	Regulation of neurotransmitter transport	12	120	0.76	0.00052
GO:1901698	Response to nitrogen compound	41	1070	0.34	0.00052
GO:0060284	Regulation of cell development	38	956	0.36	0.00053
GO:0072659	Protein localization to plasma membrane	15	193	0.65	0.00055
GO:0016079	Synaptic vesicle exocytosis	9	62	0.92	0.00058
GO:0042221	Response to chemical	112	4333	0.17	0.00058
GO:1903530	Regulation of secretion by cell	29	630	0.42	0.00058
GO:0007269	Neurotransmitter secretion	11	102	0.79	0.00062
GO:0014047	Glutamate secretion	7	32	1.1	0.00062
GO:0099612	Protein localization to axon	5	10	1.46	0.00062
GO:0022604	Regulation of cell morphogenesis	25	498	0.46	0.00063
GO:0048278	Vesicle docking	9	64	0.91	0.00064
GO:0051649	Establishment of localization in cell	71	2375	0.24	0.00064
GO:0050767	Regulation of neurogenesis	34	828	0.37	0.00078
GO:0051960	Regulation of nervous system development	37	942	0.36	0.00078
GO:0043436	Oxoacid metabolic process	37	944	0.35	0.00080
GO:0006865	Amino acid transport	12	131	0.72	0.00095
GO:0043269	Regulation of ion transport	30	696	0.4	0.0011
GO:0070727	Cellular macromolecule localization	53	1616	0.28	0.0011
GO:0031346	Positive regulation of cell projection organization	21	391	0.49	0.0012
GO:0050803	Regulation of synapse structure or activity	16	239	0.59	0.0012
GO:0140029	Exocytic process	9	71	0.86	0.0012
GO:0006928	Movement of cell or subcellular component	50	1501	0.28	0.0013
GO:0071205	Protein localization to juxtaparanode region of axon	4	5	1.66	0.0013
GO:0098657	Import into cell	13	164	0.66	0.0015
GO:0099536	Synaptic signaling	23	463	0.46	0.0015
GO:0033043	Regulation of organelle organization	45	1306	0.3	0.0016
GO:0036465	Synaptic vesicle recycling	8	56	0.92	0.0016
GO:0051129	Negative regulation of cellular component organization	30	713	0.39	0.0016
GO:0010243	Response to organonitrogen compound	37	987	0.34	0.0017
GO:0034613	Cellular protein localization	52	1610	0.27	0.0017
GO:0045184	Establishment of protein localization	51	1564	0.27	0.0017

GO:0010769	Regulation of cell morphogenesis involved in differentiation	18	309	0.53	0.0018
GO:0051493	Regulation of cytoskeleton organization	25	546	0.42	0.0021
GO:1901652	Response to peptide	23	476	0.45	0.0021
GO:0044085	Cellular component biogenesis	73	2583	0.21	0.0023
GO:0006904	Vesicle docking involved in exocytosis	7	43	0.97	0.0025
GO:0010976	Positive regulation of neuron projection development	17	288	0.53	0.0025
GO:0040011	Locomotion	43	1251	0.3	0.0025
GO:0030029	Actin filament-based process	26	592	0.4	0.0027
GO:0010807	Regulation of synaptic vesicle priming	4	7	1.52	0.0028
GO:0030913	Paranodal junction assembly	4	7	1.52	0.0028
GO:0060996	Dendritic spine development	6	29	1.08	0.0028
GO:0097479	Synaptic vesicle localization	7	44	0.96	0.0028
GO:0046942	Carboxylic acid transport	17	293	0.52	0.0029
GO:0000226	Microtubule cytoskeleton organization	23	492	0.43	0.0031
GO:0045216	Cell-cell junction organization	13	180	0.62	0.0031
GO:0046928	Regulation of neurotransmitter secretion	10	106	0.74	0.0032
GO:0015031	Protein transport	48	1486	0.27	0.0033
GO:0060341	Regulation of cellular localization	37	1027	0.32	0.0033
GO:0006835	Dicarboxylic acid transport	9	86	0.78	0.0037
GO:0061024	Membrane organization	31	796	0.35	0.0037
GO:1901699	Cellular response to nitrogen compound	27	645	0.38	0.0037
GO:0048488	Synaptic vesicle endocytosis	7	48	0.93	0.0040
GO:0007212	Dopamine receptor signaling pathway	6	32	1.03	0.0041
GO:0050770	Regulation of axonogenesis	13	187	0.6	0.0041
GO:0098609	Cell-cell adhesion	23	505	0.42	0.0041
GO:0007411	Axon guidance	16	275	0.53	0.0042
GO:1901605	Alpha-amino acid metabolic process	13	191	0.59	0.0049
GO:0034329	Cell junction assembly	16	280	0.52	0.0050
GO:1901700	Response to oxygen-containing compound	49	1567	0.26	0.0053
GO:0071417	Cellular response to organonitrogen compound	25	590	0.39	0.0055
GO:0023051	Regulation of signaling	91	3553	0.17	0.0056
GO:0043270	Positive regulation of ion transport	16	285	0.51	0.0059
GO:0043254	Regulation of protein-containing complex assembly	21	451	0.43	0.0061
GO:0023061	Signal release	13	197	0.58	0.0062
GO:0050807	Regulation of synapse organization	14	228	0.55	0.0067
GO:0099637	Neurotransmitter receptor transport	6	36	0.98	0.0067
GO:0009112	Nucleobase metabolic process	6	37	0.97	0.0075
GO:0043434	Response to peptide hormone	19	394	0.44	0.0083
GO:0048813	Dendrite morphogenesis	7	56	0.86	0.0084
GO:0015711	Organic anion transport	21	465	0.42	0.0086
GO:0051050	Positive regulation of transport	33	923	0.31	0.0086

GO:0007017	Microtubule-based process	28	727	0.35	0.0089
GO:0070887	Cellular response to chemical stimulus	77	2919	0.18	0.0091
GO:0010977	Negative regulation of neuron projection development	11	151	0.62	0.0092
GO:0050896	Response to stimulus	174	8046	0.1	0.0092
GO:0010646	Regulation of cell communication	89	3514	0.16	0.0093
GO:1901607	Alpha-amino acid biosynthetic process	7	58	0.84	0.0097
GO:0009653	Anatomical structure morphogenesis	61	2165	0.21	0.0098
GO:0031345	Negative regulation of cell projection organization	12	181	0.58	0.0101
GO:0051648	Vesicle localization	13	210	0.55	0.0102
GO:0022607	Cellular component assembly	65	2359	0.2	0.0103
GO:2000300	Regulation of synaptic vesicle exocytosis	8	80	0.76	0.0104
GO:1903421	Regulation of synaptic vesicle recycling	5	25	1.06	0.0112
GO:0030036	Actin cytoskeleton organization	22	516	0.39	0.0119
GO:0007417	Central nervous system development	34	988	0.3	0.0124
GO:0006520	Cellular amino acid metabolic process	15	278	0.49	0.0127
GO:0045666	Positive regulation of neuron differentiation	18	377	0.44	0.0127
GO:0010033	Response to organic substance	78	3011	0.17	0.0132
GO:0014070	Response to organic cyclic compound	32	911	0.31	0.0133
GO:0030168	Platelet activation	10	135	0.63	0.0148
GO:0032535	Regulation of cellular component size	18	383	0.43	0.0148
GO:0095500	Acetylcholine receptor signaling pathway	5	27	1.03	0.0148
GO:0017157	Regulation of exocytosis	13	222	0.53	0.0157
GO:0035637	Multicellular organismal signaling	10	137	0.62	0.0163
GO:0072657	Protein localization to membrane	21	495	0.39	0.0168
GO:0009719	Response to endogenous stimulus	44	1447	0.24	0.0187
GO:0002175	Protein localization to paranode region of axon	3	5	1.54	0.0190
GO:0051590	Positive regulation of neurotransmitter transport	5	29	1.0	0.0190
GO:0032880	Regulation of protein localization	32	934	0.3	0.0191
GO:0140056	Organelle localization by membrane tethering	11	170	0.57	0.0205
GO:0006897	Endocytosis	19	433	0.4	0.0213
GO:0006206	Pyrimidine nucleobase metabolic process	4	16	1.16	0.0229
GO:0051962	Positive regulation of nervous system development	22	547	0.37	0.0230
GO:0019748	Secondary metabolic process	6	49	0.85	0.0235
GO:0060627	Regulation of vesicle-mediated transport	22	550	0.36	0.0244
GO:1902903	Regulation of supramolecular fiber organization	17	368	0.43	0.0244
GO:0006887	Exocytosis	28	789	0.31	0.0260
GO:0031585	Regulation of inositol 1,4,5-trisphosphate-sensitive calcium-release channel activity	3	6	1.46	0.0260
GO:0046907	Intracellular transport	45	1520	0.23	0.0260
GO:0050769	Positive regulation of neurogenesis	20	479	0.38	0.0261
GO:0006820	Anion transport	23	593	0.35	0.0265

GO:0001508	Action potential	8	97	0.68	0.0290
GO:0010771	Negative regulation of cell morphogenesis involved in differentiation	8	98	0.67	0.0308
GO:0031113	Regulation of microtubule polymerization	6	53	0.82	0.0324
GO:0046903	Secretion	35	1097	0.27	0.0324
GO:0009725	Response to hormone	29	849	0.29	0.0351
GO:0016185	Synaptic vesicle budding from presynaptic endocytic zone membrane	3	7	1.39	0.0351
GO:0009611	Response to wounding	21	532	0.36	0.0362
GO:0007213	G protein-coupled acetylcholine receptor signaling pathway	4	19	1.08	0.0364
GO:0051656	Establishment of organelle localization	17	385	0.41	0.0367
GO:0055114	Oxidation-reduction process	31	939	0.28	0.0383
GO:0065007	Biological regulation	240	12171	0.06	0.0391
GO:0140352	Export from cell	33	1028	0.27	0.0403
GO:0046112	Nucleobase biosynthetic process	4	20	1.06	0.0418
GO:0030334	Regulation of cell migration	29	865	0.29	0.0442
GO:0045665	Negative regulation of neuron differentiation	12	222	0.49	0.0442
GO:0007223	Wnt signaling pathway, calcium modulating pathway	5	38	0.88	0.0484
GO:0048489	Synaptic vesicle transport	5	38	0.88	0.0484
GO:0060322	Head development	27	788	0.3	0.0484
GO:0099175	Regulation of postsynapse organization	8	107	0.64	0.0484
GO:1902414	Protein localization to cell junction	7	82	0.69	0.0489

Disease-associated genes **D57**

#term ID	term description	observed gene count	background gene count	strength	false discovery rate
DOID:331	Central nervous system disease	47	1107	0.39	0.00011
DOID:0060037	Developmental disorder of mental health	28	514	0.5	0.00032
DOID:1059	Intellectual disability	25	412	0.54	0.00032
DOID:150	Disease of mental health	33	689	0.44	0.00032
DOID:1826	Epilepsy	20	274	0.62	0.00032
DOID:936	Brain disease	34	739	0.42	0.00033
DOID:4	Disease	145	5921	0.15	0.00058
DOID:863	Nervous system disease	66	2132	0.25	0.0015
DOID:7	Disease of anatomical entity	108	4452	0.15	0.0377

Figure S8 *List of biological processes (from STRING database) for the DAPs for each time point between PINK1 versus control cell line. In the last table, the list of diseases already associated in literature to the DAPs at Day 57 of neuronal differentiation.*

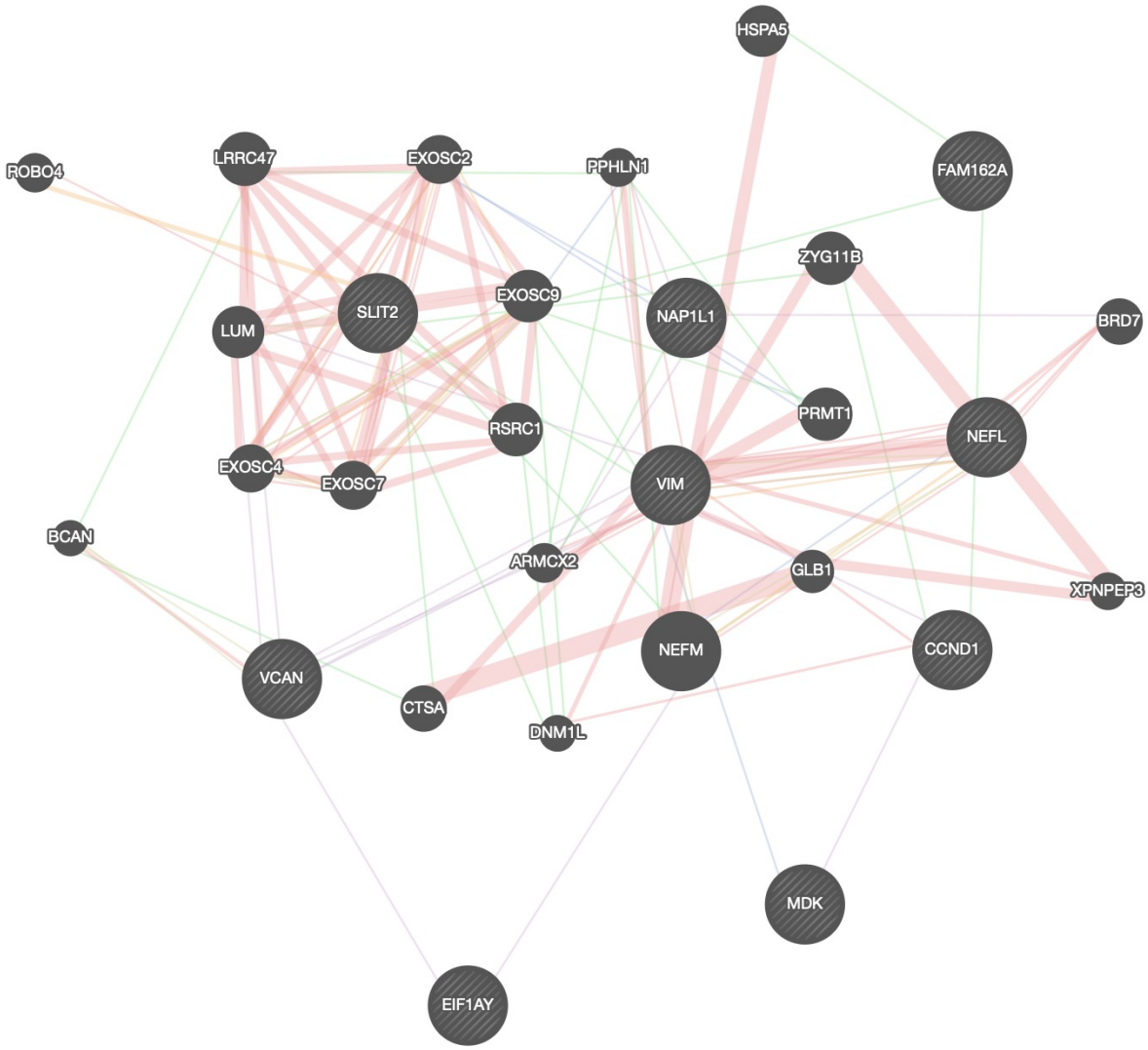

Figure S9 *Gene network analysis (from GeneMANIA) on the top 13 DEGs shows that NEFL and SLIT2, which are also found strongly dysregulated in the proteomics analysis, form important nodes.*

gene	max_pval	Avg	gene	max_pval	Avg	gene	max_pval	Avg	gene	max_pval	Avg	gene	max_pval	Avg
MTRNR2L1	3.71E-21	-6.33E-01	PTMAP5	2.02E-10	-1.85E-01	RP11.676M6	9.09E-05	-1.16E-01	CCT8	6.49E-03	1.40E-01	FAM126A	2.86E-03	2.33E-01
S100A6	8.08E-18	-5.19E-01	ARGLU1	2.98E-04	-1.84E-01	CHD2	1.63E-03	-1.13E-01	TCTN3	5.20E-03	1.40E-01	TUBGCP5	3.34E-08	2.33E-01
ZNF280D	2.49E-17	-5.01E-01	IRX3	5.15E-05	-1.73E-01	SFSWAP	1.89E-03	-1.11E-01	IQCB1	6.27E-04	1.41E-01	PGD	6.71E-07	2.35E-01
PLCB4	6.73E-03	-4.84E-01	AZI2	4.11E-04	-1.72E-01	TTC6	4.37E-03	-1.11E-01	PHB	3.06E-03	1.43E-01	SMARCA4	2.97E-06	2.37E-01
VWA5A	9.85E-06	-4.45E-01	GOLGA8B	3.36E-03	-1.71E-01	RP11.64B16.	1.15E-03	-1.07E-01	UQCRFS1	2.72E-03	1.44E-01	CTSB	2.31E-06	2.38E-01
TCEAL5	6.78E-14	-4.07E-01	RSRC2	4.62E-10	-1.67E-01	HNRNPCP2	5.82E-04	-1.06E-01	LANCL1	1.78E-03	1.45E-01	NIPA2	2.62E-08	2.41E-01
RP11.692N5.	3.69E-10	-4.07E-01	MAGI2.AS3	5.03E-04	-1.67E-01	SOD1	1.95E-04	-1.05E-01	CAMK2D	7.48E-04	1.46E-01	MED15	1.26E-05	2.41E-01
GOPC	5.87E-20	-3.75E-01	CSRP1	2.14E-06	-1.65E-01	RP4.796I17.5	5.89E-03	-1.03E-01	POU6F2	1.73E-03	1.54E-01	CD164	2.83E-03	2.43E-01
NLRP2	1.91E-09	-3.62E-01	ZNF75A	8.42E-07	-1.63E-01	TBRG1	9.37E-03	-1.03E-01	ABLIM1	1.31E-03	1.54E-01	PEG10	3.82E-04	2.47E-01
RALGPS2	5.42E-04	-3.55E-01	ARMC2	4.94E-04	-1.62E-01	SMARCB1	1.47E-04	-1.02E-01	SC5D	8.78E-03	1.56E-01	ZNF880	5.11E-08	2.56E-01
MLF1	1.34E-17	-3.52E-01	FNBP1L	1.26E-03	-1.59E-01	TRMT1L	1.29E-03	-1.00E-01	GHITM	2.46E-05	1.56E-01	LMAN1	7.77E-08	2.57E-01
CALM2P2	1.65E-22	-3.43E-01	CAT	8.06E-03	-1.57E-01	SNX9	9.90E-03	1.01E-01	LSM3	6.57E-03	1.56E-01	ZNF37A	3.66E-09	2.60E-01
BBS2	2.76E-15	-3.38E-01	NSA2	4.67E-05	-1.56E-01	DAB1	4.30E-05	1.02E-01	WDR11	9.94E-03	1.57E-01	ACTN1	3.91E-10	2.64E-01
MORF4L1P1	1.39E-11	-3.29E-01	MGMT	8.83E-03	-1.56E-01	FTH1	3.41E-04	1.03E-01	RPN2	3.88E-03	1.59E-01	CYCS	5.25E-04	2.66E-01
FOS	6.99E-13	-3.23E-01	SMARCE1P6	1.86E-05	-1.56E-01	NAA20	9.72E-03	1.04E-01	SRA1	5.11E-05	1.59E-01	OSBPL8	1.55E-08	2.68E-01
RSRP1	5.42E-13	-3.08E-01	MT.CYB	1.51E-08	-1.55E-01	CEP350	7.93E-03	1.06E-01	GOLT1B	6.52E-04	1.59E-01	MYL12A	1.52E-12	2.70E-01
PHYH	6.13E-05	-3.04E-01	MT.CO3	1.28E-08	-1.55E-01	CTC.444N24.	9.77E-03	1.10E-01	C21ORF91	4.03E-03	1.60E-01	GABPB1.AS1	2.90E-04	2.89E-01
NAP1L5	4.87E-12	-2.82E-01	KIF27	6.39E-03	-1.55E-01	FZD7	7.11E-03	1.10E-01	IARS	4.71E-03	1.60E-01	HSPA1A	3.35E-03	2.92E-01
MT.ND5	1.36E-17	-2.82E-01	CECR1	1.54E-07	-1.53E-01	AK6	4.24E-03	1.10E-01	RRP7A	2.19E-04	1.60E-01	C6ORF48	4.00E-20	2.93E-01
ZNF528.AS1	2.88E-13	-2.77E-01	SLC7A8	2.66E-03	-1.52E-01	NUDT21	1.83E-03	1.10E-01	CNN3	2.49E-04	1.61E-01	PCBP1	1.10E-03	2.97E-01
RP4.765C7.2	5.86E-08	-2.77E-01	LUC7L3	4.10E-04	-1.52E-01	FGFR1	4.69E-03	1.12E-01	CHAC1	8.92E-10	1.64E-01	CD59	1.96E-08	2.99E-01
MALAT1	8.50E-09	-2.67E-01	PSMA4	1.86E-03	-1.52E-01	IFI27L1	6.12E-03	1.12E-01	RRAGD	4.30E-03	1.65E-01	C19ORF53	5.42E-06	3.00E-01
CROT	6.31E-05	-2.67E-01	RP11.288E14	4.65E-05	-1.51E-01	CCNB1IP1	3.00E-03	1.13E-01	XPOT	1.54E-03	1.66E-01	SNHG8	5.67E-09	3.01E-01
ADGRG7	2.23E-07	-2.65E-01	ANKRD36	2.43E-03	-1.49E-01	UBE2D2	1.20E-03	1.13E-01	CCT4	5.01E-07	1.66E-01	CSTB	1.31E-03	3.04E-01
CALR	1.08E-08	-2.64E-01	TTC12	4.30E-05	-1.48E-01	ABCA5	5.45E-04	1.13E-01	THUMPD3	2.66E-03	1.67E-01	PALLD	4.80E-08	3.06E-01
PTGR1	1.97E-08	-2.57E-01	AKAP8L	8.47E-03	-1.48E-01	TET3	2.94E-03	1.15E-01	SPRED1	8.51E-05	1.69E-01	MYL6	1.24E-19	3.07E-01
CMTM8	3.02E-08	-2.56E-01	ZCCHC11	3.46E-05	-1.48E-01	HLA.B	1.25E-04	1.15E-01	YPEL1	2.24E-03	1.71E-01	CRYZ	1.31E-11	3.10E-01
ZNF528	8.01E-10	-2.55E-01	RNPC3	5.86E-03	-1.46E-01	WBSCR22	7.45E-04	1.15E-01	NDUFB6	1.30E-03	1.73E-01	SNAP29	2.12E-04	3.12E-01
TTC3	4.16E-08	-2.53E-01	SEPT02	1.52E-04	-1.45E-01	SREK1IP1	4.88E-03	1.16E-01	CSRP2	4.69E-03	1.75E-01	CYFIP1	1.47E-10	3.13E-01
AC009245.3	2.69E-07	-2.52E-01	FBXO9	1.03E-03	-1.43E-01	CSNK1G3	7.96E-04	1.17E-01	CUL3	1.58E-06	1.75E-01	EGLN3	5.56E-03	3.20E-01
NCALD	1.74E-06	-2.50E-01	NDUFB11	1.46E-03	-1.42E-01	GXYLT1	4.33E-03	1.17E-01	PTPRZ1	2.10E-03	1.77E-01	RANBP1	1.73E-16	3.42E-01
DNAJC15	2.13E-05	-2.50E-01	FGD4	7.85E-03	-1.42E-01	ATG101	2.79E-04	1.18E-01	TCEAL7	5.01E-11	1.77E-01	TAGLN	3.67E-03	3.47E-01
SHH	2.05E-04	-2.46E-01	NKD1	3.76E-03	-1.40E-01	NR1D2	7.71E-05	1.18E-01	PSMB5	1.02E-03	1.77E-01	COMT	1.25E-11	3.55E-01
MINOS1P3	2.08E-08	-2.42E-01	MRPS21	3.39E-03	-1.39E-01	EIF3A	2.83E-03	1.20E-01	EMP2	1.06E-08	1.81E-01	SLC25A4	1.61E-13	3.66E-01
EFCAB2	1.23E-07	-2.39E-01	DAAM1	9.04E-03	-1.39E-01	RAB9A	6.09E-03	1.20E-01	ABRACL	3.57E-03	1.85E-01	TYW3	1.73E-14	3.92E-01
RP11.488C13	3.83E-04	-2.37E-01	CCNL1	5.81E-05	-1.37E-01	RPA3	4.76E-03	1.22E-01	PSMD7	3.85E-03	1.85E-01	EPHA4	1.45E-06	4.02E-01
RP11.475C16	8.30E-10	-2.34E-01	STK33	4.87E-03	-1.37E-01	SHROOM3	3.03E-03	1.22E-01	TIMELESS	2.26E-05	1.86E-01	RP11.122G18	1.54E-05	4.14E-01
NME4	4.13E-06	-2.30E-01	NKX6.1	3.63E-04	-1.36E-01	USP49	3.50E-03	1.22E-01	ANXA5	2.16E-09	1.90E-01	HSPA8	4.07E-10	4.44E-01
GPATCH8	6.37E-03	-2.24E-01	TRA2A	8.89E-04	-1.35E-01	MRPL17	9.86E-03	1.24E-01	HNRNPA3	5.41E-06	1.90E-01	PCSK1	3.39E-05	4.45E-01
TMEM132C	8.05E-07	-2.19E-01	MAP3K12	3.47E-04	-1.35E-01	EIF3B	1.52E-03	1.25E-01	RP11.298C3.	2.98E-06	1.91E-01	LGI1	2.79E-09	5.00E-01
TSPYL5	2.51E-11	-2.16E-01	FAM208A	7.79E-05	-1.34E-01	MRPL15	1.83E-03	1.26E-01	HSPA1B	1.21E-04	1.91E-01	PGK1	8.78E-31	5.12E-01
TCF25	5.59E-13	-2.16E-01	NSMCE1	1.87E-05	-1.33E-01	RTCB	5.00E-04	1.26E-01	C14ORF119	3.53E-05	1.92E-01	GPC3	2.49E-17	5.13E-01
RP11.641D5.	4.00E-13	-2.14E-01	ZNF83	1.99E-04	-1.33E-01	MYO10	4.23E-03	1.26E-01	PKP2	4.26E-06	1.92E-01	CCDC144NL.A	2.27E-09	7.13E-01
EEF1A1	1.88E-03	-2.12E-01	NONO	4.82E-03	-1.33E-01	RBM12	1.06E-03	1.29E-01	IPO5	6.10E-05	1.93E-01	SNHG5	2.84E-40	1.04E+00
TMEM38B	3.98E-03	-2.10E-01	NAALAD2	1.08E-03	-1.31E-01	CNTNAP2	6.80E-04	1.29E-01	IPO7	3.09E-07	1.95E-01	DLK1	8.21E-25	1.17E+00
PRTG	2.00E-11	-2.08E-01	C6ORF118	9.31E-04	-1.30E-01	IPO9	2.84E-03	1.31E-01	NME1	2.74E-04	1.97E-01			
PDIA6	4.07E-06	-2.08E-01	CHCHD2	5.40E-03	-1.29E-01	MCL1	4.96E-03	1.32E-01	EXOC5	3.08E-09	1.98E-01			
THAP9.AS1	4.34E-04	-2.07E-01	RP11.76E16.	8.54E-04	-1.29E-01	NUP62	2.75E-03	1.32E-01	SLK	8.24E-03	1.98E-01			
KIAA1211	8.03E-03	-2.07E-01	PSMD5.AS1	5.92E-03	-1.29E-01	SUGT1	4.58E-03	1.33E-01	GNB1	2.04E-03	2.08E-01			
RBM39	1.82E-03	-2.06E-01	PPP1R21	3.23E-03	-1.26E-01	WDR34	2.01E-03	1.33E-01	FRA10AC1	2.39E-04	2.09E-01	**Genes identified only at four**		
HNRNPC	1.95E-08	-2.05E-01	PHTF1	6.29E-03	-1.26E-01	ZNF593	2.38E-03	1.34E-01	MYL9	2.32E-05	2.10E-01	**timepoints iPSCs, D6, D15, D21**		
CBX3P9	1.01E-07	-2.04E-01	SH3YL1	7.01E-04	-1.25E-01	BTN2A2	1.35E-03	1.34E-01	PLIN2	2.15E-11	2.11E-01	RP13.258O15	3.39E-03	-2.49E-01
GTF2I	7.03E-05	-2.03E-01	SPATA7	1.74E-03	-1.25E-01	ANKRD11	1.98E-03	1.35E-01	ENAH	5.29E-09	2.13E-01	HNRNPCP1	2.93E-03	-1.69E-01
CLHC1	1.97E-03	-2.02E-01	FAM184A	2.20E-03	-1.24E-01	ELOVL5	1.14E-03	1.37E-01	HIC2	2.23E-06	2.13E-01	SRSF9	4.05E-03	-1.43E-01
HMGN1P38	3.95E-12	-1.98E-01	RAB4A	9.50E-04	-1.22E-01	NDUFA12	1.14E-04	1.37E-01	PFKP	4.80E-03	2.13E-01	HSD17B4	2.97E-03	-1.34E-01
ZSCAN30	2.36E-03	-1.95E-01	LINC00909	1.52E-03	-1.20E-01	THAP7	2.82E-08	1.37E-01	BRCA2	9.99E-07	2.15E-01	RNF26	2.65E-03	1.13E-01
EIF5P1	1.70E-04	-1.94E-01	VPS39	5.83E-03	-1.19E-01	RFWD3	1.13E-05	1.39E-01	EIF1AY	3.64E-04	2.16E-01	KMT2A	5.37E-03	1.42E-01
LRIG3	6.90E-06	-1.90E-01	PDAP1	4.93E-03	-1.18E-01	GNAS	2.74E-03	1.39E-01	CENPW	5.06E-10	2.18E-01	IWS1	7.26E-04	1.39E-01
CBX1	1.56E-03	-1.86E-01	ANKRD26	8.88E-04	-1.18E-01	PSMC3IP	8.07E-03	1.39E-01	DPH3	1.47E-04	2.18E-01			
PSMG3	1.90E-03	-1.86E-01	RRAGB	9.27E-04	-1.16E-01	AK4	1.80E-03	1.39E-01	CRKL	1.44E-10	2.24E-01			

Figure S10 *Group D, 284 genes. Repeating the analysis as in Group C, but using only timepoints D6, D15 and D21 identified a total of 286 DEGs (Group D). In black: genes of group D only. In blue: genes of group D that are also part of group C. In green: six genes of group C that were not included in Group D, hence, even though group D consists of 286 genes, the total number used in the network analysis was 292 (Novak et al., 2022).*

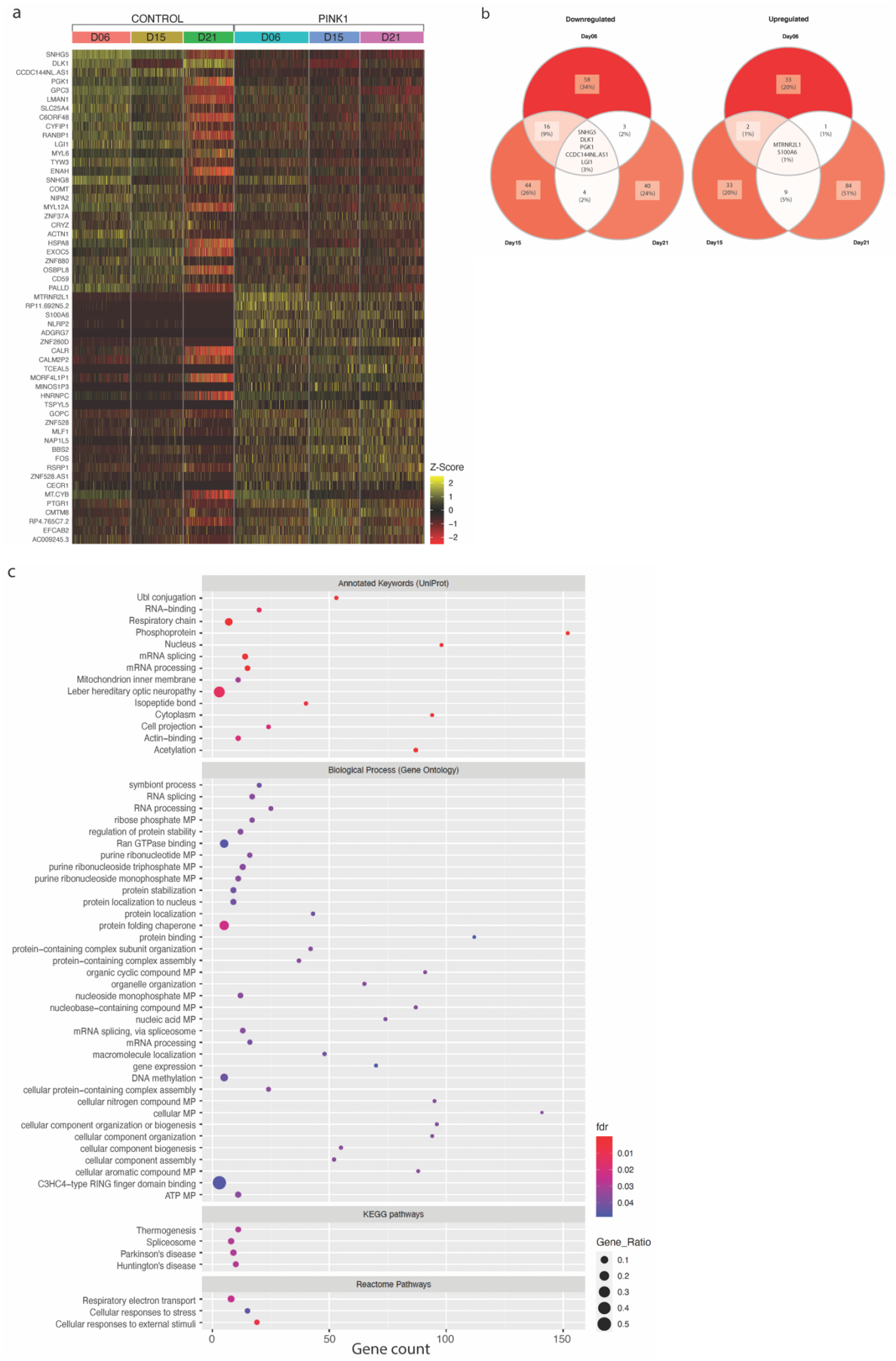

Figure S11 *Fig. 4.9 in higher resolution (See Subsection 4.2.1).*

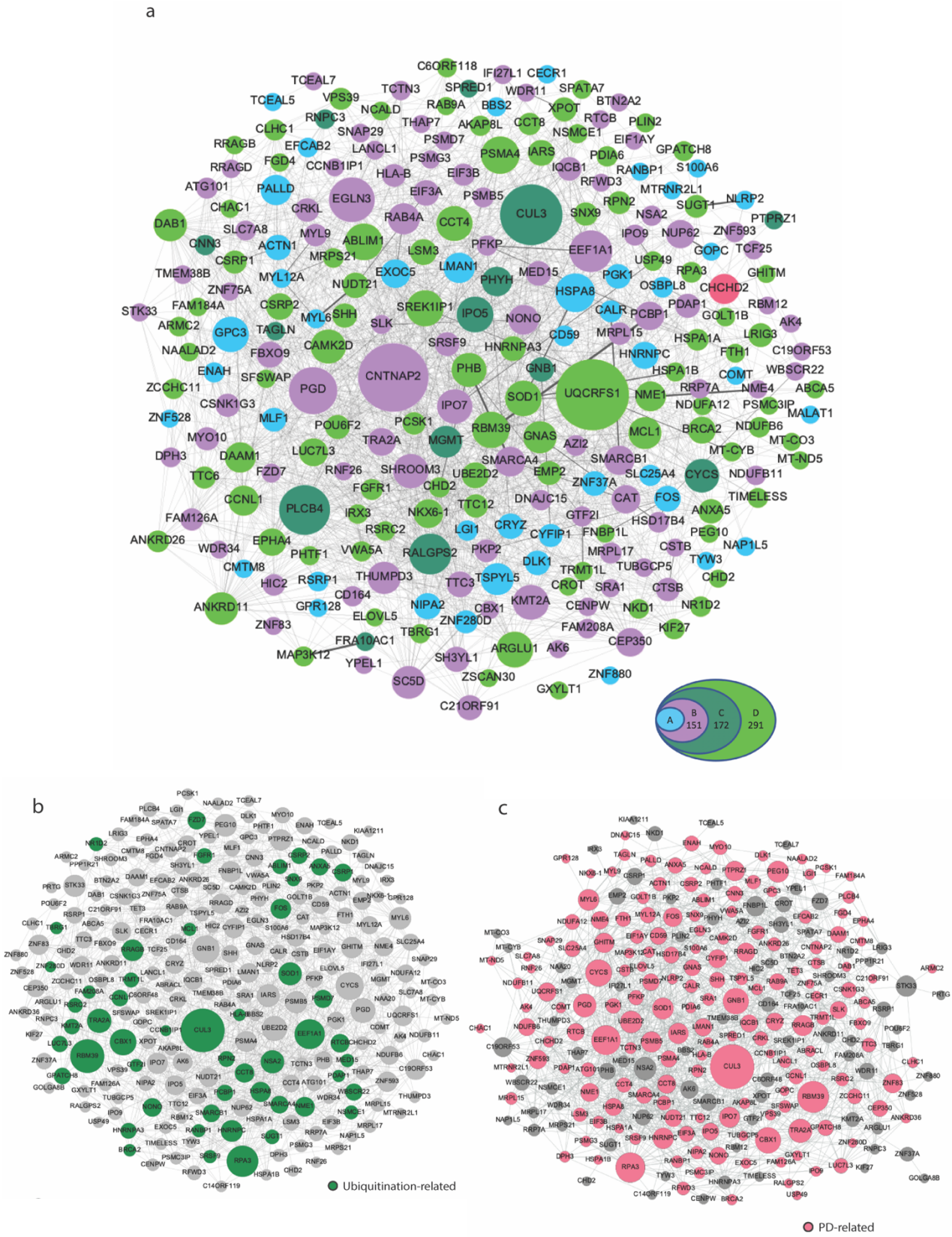

Figure S12 *Fig. 4.10 in higher resolution (See Subsection 4.2.3).*

8. Appendix B: Published Manuscripts

Stem Cell Research 61 (2022) 102765

Contents lists available at ScienceDirect

Stem Cell Research

journal homepage: www.elsevier.com/locate/scr

Lab Resource: Multiple Cell Lines

Generation of two human induced pluripotent stem cell lines from fibroblasts of Parkinson's disease patients carrying the ILE368ASN mutation in *PINK1* (LCSBi002) and the R275W mutation in *Parkin* (LCSBI004)

Gabriela Novak [a,b,*], Steven Finkbeiner [b], Gaia Skibinski [b], Michela Bernini [a], Cristina Donato [a], Alexander Skupin [a]

[a] The Integrative Cell Signalling Group, Luxembourg Centre for Systems Biomedicine (LCSB), University of Luxembourg, Esch-sur-Alzette, Luxembourg
[b] Center for Systems and Therapeutics, Gladstone Institutes and the Departments of Neurology and Physiology, University of California, San Francisco, CA 94158, USA

A B S T R A C T

Mutations in *PINK1* and *Parkin* are two of the main causes of recessive early-onset Parkinson's disease (PD). We generated human induced pluripotent stem cells (hiPSCs) from fibroblasts of a 64-year-old male patient with a homozygous ILE368ASN mutation in *PINK1*, who experienced disease onset at 33 years, and from fibroblasts of a 61-year-old female patient heterozygous for the R275W mutation in *Parkin*, who experienced disease onset at 44 years. Array comparative genomic hybridization (aCGH) determined genotypic variation in each line. The cell lines were successfully used to generate midbrain dopaminergic neurons, the neuron type primarily affected in PD.

1. Resource table

Unique stem cell lines identifier	LCSBi002-B LCSBi002-C LCSBi004-A LCSBi004-B
Alternative names of stem cell lines	ND40066-PINK1-ILE368ASN-clone 7 (LCSBi002-B) ND40066-PINK1-ILE368ASN-clone 8 (LCSBi002-C)ND29369-PARKIN/PARK2-R275W-clone 1 (LCSBi004-A) ND29369-PARKIN/PARK2-R275W-clone 4 (LCSBi004-B)
Institution	Gladstone Institutes, CA, USA
Contact information of distributor	Gabriela Novak gabriela.novak@alumni.utoronto.ca Alexander Skupin alexander.skupin@uni.lu
Type of cell lines	iPSC
Origin	Human
Cell Source	Fibroblasts
Clonality	Clonal
Method of reprogramming	CytoTune-iPS Sendai Reprogramming kit (ThermoFisher Scientific). transgenes/vectors used:CytoTuneTM 2.0 KOS (Sox2) CytoTuneTM 2.0 hc-Myc CytoTuneTM 2.0 hKlf4 Clearance was confirmed using Scorecard, which detects the presence of Sendai virus, passage number is listed in Fig. 1d.
Multiline rationale	Mutations in two genes known to interact, leading to the same disease
Gene modification	YES
Type of modification	Familial, spontaneous mutation
Associated disease	Parkinson's disease
Gene/locus	PINK1 (PARK6) ILE368ASN 1p36.12 PARKIN/PARK2-R275W 6q26
Method of modification	N/A
Name of transgene or resistance	N/A
Inducible/constitutive system	N/A
Date archived/stock date	2016
Cell line repository/bank	https://hpscreg.eu/cell-line/LCSBi002-B https://hpscreg.eu/cell-line/LCSBi002-C https://hpscreg.eu/cell-line/LCSBi004-A https://hpscreg.eu/cell-line/LCSBi004-B
Ethical approval	Samples were collected in accordance with the US Government guidelines and are subject to MTA issued by Coriell Institute for Medical Research NINDS Cell Repository. The iPSC reprogramming protocol was approved by the Committee on Human Research at the University of California, San Francisco.

* Corresponding author.
E-mail address: gabriela.novak@alumni.utoronto.ca (G. Novak).

https://doi.org/10.1016/j.scr.2022.102765
Received 22 July 2021; Received in revised form 19 March 2022; Accepted 26 March 2022
Available online 29 March 2022

2. Resource utility

Parkinson's disease (PD) leads to the death of midbrain dopaminergic (mDA) neurons. This poses a major obstacle to the study of the disease. Differentiating neurons from iPSCs of patients who carry PD-related mutations provides an almost unlimited source of mDA neurons and an invaluable resource for the study of PD.

3. Resource details

Parkinson's disease (PD) is one of the most prevalent neurodegenerative disorder, second only to Alzheimer's disease. It is characterized by the loss of midbrain dopaminergic (mDA) neurons (Ando et al., 2017; Madsen et al., 2021; Novak et al., 2022; Zhu et al., 2018). The pathological mechanisms of PD are only partly understood, and there is no treatment able to reverse its progression. By the end stage of the disease, about 90% of mDA neurons die, posing a major obstacle to the study of human mDA neurons affected by PD. Technological advancements in somatic cell reprogramming into iPSCs and directed differentiation into mDA neurons has created an essential resource for PD research. We can now generate patient-based iPSCs from skin cells of PD patients who carry PD-associated mutations (Novak et al., 2022). Hence, the mechanism of disease development due to individual mutations can be studied in genetic backgrounds shown to be permissive to disease development. The aCGH analysis was used to identify the gene variants each patient carries, to allow for the investigation of the effects of genetic background (Supplement and a resource details file "CGH data") (see Table 1 and 2).

When mitochondria become damaged, PINK1 recruits Parkin to the outer mitochondrial membrane, which initiates mitophagy (Ando et al., 2017). The fact that a mutation in either *PINK1* or *Parkin* leads to PD underscores the importance of this pathway in PD development. The *PINK1* ILE368ASN mutation interferes with mitophagy by reducing the interaction of PINK1 with its chaperone, HSP90, which destabilizes PINK1 at the mitochondrial membrane, and by reducing its ubiquitin kinase activity through deformation of its substrate binding pocket (Ando et al., 2017). Mutations in *Parkin* are one of the most common causes of recessive juvenile onset Parkinson's disease and of sporadic early-onset PD (Zhu et al., 2018). However, Parkin participates in multiple pathways within the cell, making it challenging to identify the specific effects of *Parkin* mutations in PD (Zhu et al., 2018).

Fibroblasts homozygous for the *PINK1* mutation ILE368ASN were obtained from a 64-year-old male patient with disease onset at 33 years (ND40066, Coriell Institute), and fibroblasts heterozygous for the R275W missense mutation in exon 7 of *Parkin*, which falls within the RING finger 1 domain of the Parkin protein (Madsen et al., 2021), were obtained from a 61-year-old female patient with disease onset at 44 years (LCSBi004, ND29369) (Madsen et al., 2021). Fibroblasts were reprogrammed using the Sendai virus reprogramming method, which should not introduce changes into the genome. Expression of the iPSC markers Oct3/4 and Tra-1-60 was shown by immunocytochemistry, alongside transmitted light (TL) images of iPSC colonies (Fig. 1a, Supplement) and the expression of iPSC status markers *OCT4* (*POU5F1*), *SOX2* and *NANOG* was determined by qPCR (Fig. 1b). In Fig. 1b, the 29542-3 and 29542-7 stand for the cell line ND29542, clones 3 and 7, respectively, which are previously published well classified clones of the ND29542 cell line (Novak et al., 2021). The 40066-7 and 40066-8 stand

Table 2
Characterization and validation.

Classification	Test	Result	Data
Morphology	Photography	normal	Fig. 1 panel a and Supplement
Phenotype	Qualitative analysis: Immunocytochemistry	Confirmed by staining for pluripotency markers: Oct4 & Tra-1-60	Fig. 1 panel a Supplement
	Quantitative analysis: *RT-qPCR*	Determined by expression of iPSC-specific transcripts via qPCR (*OCT4*, *NANOG*, *SOX2*), by Scorecard and by FACS (staining for SSEA4 with more than 90% cells positive).	Fig. 1 panel b Fig. 1 panel d FACS – Supplement
Genotype	Karyotype	ND 40066: 46, XY normal human male karyotype ND27760: 46, XX, normal female karyotype, also confirmed in iPSCs.	Attached as supplementary figure
Identity	Array comparative genomic hybridization STR analysis	aCGH Probes: Pass SNP Probes: Pass submitted	Attached as supplementary figure Submitted in archive with journal *
Mutation analysis	Sequencing	Homozygous PINK1 mut. Heterozygous PARKIN mut.	Fig. 1 panel c and Supplement
Microbiology and virology	Mycoplasma	Mycoplasma testing: Negative	Supplement
Differentiation potential	Scorecard	Embryonic bodies show ability to differentiate into all three lineages	Fig. 1 panel d, and Supplement
Donor screening (OPTIONAL)	HIV 1 + 2 Hepatitis B, Hepatitis C	All samples negative for HIV 1, Hepatitis B, & Hepatitis C	Supplement
Genotype additional info (OPTIONAL)	Blood group genotyping	N/A	
	HLA tissue typing	N/A	

*Parental line was not included, however, a full aCGH analysis and a STR analysis were performed for all ND40066 clones and their profiles match. and we confirmed the presence of the mutation by sequencing all ND40066 clones. Both ND29369 clones were confirmed to carry the PARKIN R275W mutation and their STR profiles match.

Table 1
Summary of lines.

iPSC line names	Abbreviation in figures	Gender	Age	Ethnicity	Genotype of locus	Disease
ND40066-PINK1-clone 7 (LCSBi002-B)	ND40066-7	Male	64	Caucasian	ILE368ASN	Parkinson's disease
ND40066-PINK1-clone 8 (LCSBi002-C)	ND40066-8					
ND29369-PARKIN-clone 1 (LCSBi004-A)	ND29369-1	Female	61	Hispanic	R275W	Parkinson's disease
ND29369-PARKIN-clone 4 (LCSBi004-B)	ND29369-4					

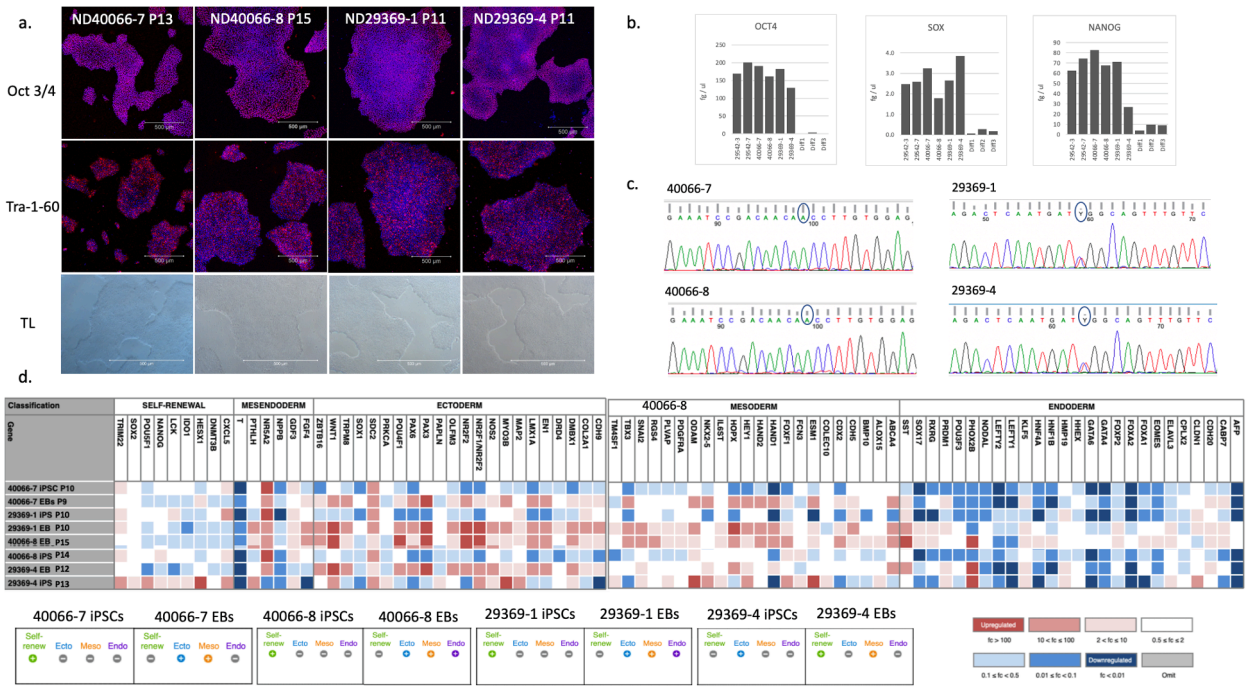

Fig. 1.

for the *PINK1* mutation-carrying cell line ND40066 clones 7 and 8, respectively. The 29369-1 and 29369-4 stand for the *PARKIN* mutation-carrying cell line ND29369 clones 1 and 4, respectively. Diff 1, 2 and 3 are samples of neurons differentiated from ND40066-8 via protocol published in (Novak et al., 2022), to illustrate loss of *OCT4* (*POU5F1*), *SOX2* and *NANOG* upon differentiation. The ND40066 clone 8 is in itself a well-classified cell line (Novak et al., 2022). The iPSC status of this cell line was determined at the single cell level, as described in (Novak et al., 2022). Furthermore, the iPSC status of the ND40066-7, ND40066-8, ND29369-1 and ND29369-4 cell lines was determined by comparison of the expression of an iPSC marker panel by these cells to a library of well classified iPSC cell lines using Scorecard analysis (Supplement, section "Scorecard - iPSC marker expression"). Presence of the mutations was confirmed by sequencing (Fig. 1c, Supplement). The iPSC status and trilineage differentiation capacity of the clones was determined using Scorecard (Fig. 1d, Supplement). Scorecard uses TaqMan probes to several iPSC status markers to determine the iPSC status of each cell line. To analyse each cell line's trilineage potential, the expression of markers for each of the three early germ layers, the endoderm, the ectoderm, and the mesoderm, is determined. These layers are generated by allowing the iPSCs to spontaneously differentiate into embryonic bodies (EBs). Genotypic variation was determined by aCGH analysis (Supplement). It should be noted that comparative genomic hybridization (CGH) array does not detect translocations or inversions, alterations in chromosome structure, mosaicism or polyploidy. Both cell lines were screened and found negative for HIV 1, Hepatitis B, and Hepatitis C and mycoplasma (Supplement).

Both cell lines were used to successfully generate mDA neurons in our laboratory, which were analysed by single cell RNA seq analysis (Novak et al., 2022).

4. Materials and methods

Fibroblasts were obtained from the Coriell Institute and were cultured as described in recently published methods section pertaining to cells processed in parallel (Novak et al., 2021).

4.1. Karyotype and aCGH analysis

Live adherent fibroblasts of the ND40066 cell line were karyotyped and the genotypic variation of the iPSCc clones 7 and 8 of this cell line was analysed using Array Comparative Genomic Hybridization (aCGH), a high resolution karyotype analysis for the detection of unbalanced structural and numerical chromosomal alterations (Supplement) (Cell Line Genetics, Madison, WI, USA) as described previously (Novak et al., 2021). Live adherent fibroblasts of the ND29369 cell line were subjected to aCGH analysis (Cell Line Genetics, Madison, WI, USA) to determine this cell line's genotypic variation and the normal karyotype of the iPSCs reprogrammed from this cell line was confirmed in the ND29369 clones 1 and 4 (Cell Line Genetics, Madison, WI, USA) (Supplement) as described previously (Novak et al., 2021).

4.2. Reprogramming

Reprogramming of fibroblasts into pluripotent stem cells was done using Sendai virus at the Yale Human Embryonic Stem Cell Core, New Haven CT, USA. Early passage iPSCs were then passaged and characterized as described previously (Novak et al., 2021).

4.3. iPSC clone classification

The iPSC status was confirmed by immunocytochemistry (Fig. 1a and Supplement), as described previously (Novak et al., 2021). The primary antibodies used were anti-POU5F1 (also known as Oct3/4) and anti-Tra-1-60, and the secondary antibody was Donkey anti-Mouse IgG, Alexa Fluor Plus 555 (Table 3). The *PINK1* ILE368ASN mutation (rs774647122, NM_032409.3: 1194 T > A) in the cell line ND40066 (LCSBi002) and the *PARKIN* R275W mutation (rs34424986, NM_004562.3: 921C > T) in the cell line ND29369 (LCSBi004) were confirmed as described earlier (Novak et al., 2021), using primers listed in Table 3 (Fig. 1c and Supplement). Expression analysis was performed using quantitative PCR (qPCR) as described earlier (Novak et al., 2021) (Fig. 1b) using primers listed in Table 3. The expression is in fg/ul of cDNA sample, where 1 ul of sample represents 0.01ug of total RNA converted to cDNA, as described previously (Novak et al., 2021). The

Table 3
Reagents detail.

Antibodies used for immunocytochemistry			
	Antibody	Dilution	Company Cat # and RRID
Pluripotency Markers	Mouse anti-Human POU5F1 (Oct3/4)	*1:500*	Santa Cruz Biotechnology sc-5279 RRID AB_628051
	Mouse anti-Human Tra-1-60	*1:500*	Merck Millipore MAB4360 RRID AB_2119183
Secondary antibodies	Donkey anti-**Mouse** IgG, Alexa Fluor Plus **555**	1:1000	ThermoFisher A32773 RRID AB_2762848
Nuclear stain	DAPI	300 nM	Thermofisher D1306
Primers	Target	Forward/Revers e primer (5′- 3′)	
Sequencing primers	*PINK1* ILE368ASN	5′-AACTATCCCTGTACCCTGCG-3′ 5′-CCAAAATCTGCGATCACCAGC-3′	
Sequencing primers	*PARKIN* R275W	5′-CCGCCACGTGATTTGCTTAG-3′ 5′-TCTGCAGGACACACTCCTCT-3′	
qPCR primers	*OCT4*	5′-TCGAGAACCGAGTGAGAGG-3′ 5′-GAACCACACTCGGACCACA-3′	
qPCR primers	*SOX2*	5′-GCCGAGTGGAAACTTTGTCG-3′ 5′-GCAGCGTGTACTTATCCTTCTT-3′	
qPCR primers	*NANOG*	5′-TTCCCTCCTCCATGGATCTG-3′ 5′-TGTTTCTTGACTGGGACCTTGTC-3′	
qPCR primers	*B2M* Beta-2-microglobulin	5′-GAGTATGCCTGCCGTGTG-3′ 5′-AATCCAAATGCGGCATCT-3′	
Trilineage markers			
Trilineage markers (qPCR)	Ectoderm, Mesoderm, Endoderm	Scorecard – Thermofisher – A15870	

iPSC status and trilineage potential was further confirmed by a TaqMan iPSC Scorecard Assay (ThermoFisher Scientific, Fig. 1d and Supplement) according to the manufacturer's protocol and as described previously (Novak et al., 2021).

5. Additional information

For additional methodological details, including mDA neuron differentiation, and for single cell RNAseq analysis data, please see (Novak et al., 2022).

Declaration of Competing Interest

The authors declare that they have no known competing financial interests or personal relationships that could have appeared to influence the work reported in this paper.

Acknowledgements

This work was made possible in part by support of S.F. from the Michael J Fox Foundation through Head Start Program and National Institutes of Health (NIH) grants R01 NS124848, RF1 AG058476, R37 NS101996, and P01 AG054407.

Appendix A. Supplementary data

Supplementary data to this article can be found online at https://doi.org/10.1016/j.scr.2022.102765.

References

Ando, M., Fiesel, F.C., Hudec, R., Caulfield, T.R., Ogaki, K., Górka-Skoczylas, P., Koziorowski, D., Friedman, A., Chen, L.i., Dawson, V.L., Dawson, T.M., Bu, G., Ross, O.A., Wszolek, Z.K., Springer, W., 2017. The PINK1 p.I368N mutation affects protein stability and ubiquitin kinase activity. Mol. Neurodegeneration 12 (1).

Madsen, D.A., Schmidt, S.I., Blaabjerg, M., Meyer, M., 2021. Interaction between Parkin and α-synuclein in PARK2-mediated Parkinson's disease. Cells 10, 283. https://doi.org/10.3390/cells10020283.

Novak, G., Finkbeiner, S., Skibinski, G., Skupin, A., 2021. Generation of two human induced pluripotent stem cell lines from fibroblasts of unrelated Parkinson's patients carrying the G2019S mutation in the LRRK2 gene (LCSBi005, LCSBi006). Stem Cell Res. 57, 102569.

Novak, G., Kyriakis, D., Grzyb, K., Bernini, M., Rodius, S., Dittmar, G., Finkbeiner, S., Skupin, A., 2022. Single-cell transcriptomics of human iPSC differentiation dynamics reveal a core molecular network of Parkinson's disease. Commun. Biol. 5, 49. https://doi.org/10.1038/s42003-021-02973-7.

Zhu, M., Cortese, G.P., Waites, C.L., 2018. Parkinson's disease-linked Parkin mutations impair glutamatergic signaling in hippocampal neurons. BMC Biol. 16, 100. https://doi.org/10.1186/s12915-018-0567-7.

communications biology

ARTICLE

https://doi.org/10.1038/s42003-021-02973-7 OPEN

Single-cell transcriptomics of human iPSC differentiation dynamics reveal a core molecular network of Parkinson's disease

Gabriela Novak[1,2,3✉], Dimitrios Kyriakis[1], Kamil Grzyb[1], Michela Bernini[1], Sophie Rodius[4], Gunnar Dittmar[4,5], Steven Finkbeiner[3] & Alexander Skupin[1,6✉]

Parkinson's disease (PD) is the second-most prevalent neurodegenerative disorder, characterized by the loss of dopaminergic neurons (mDA) in the midbrain. The underlying mechanisms are only partly understood and there is no treatment to reverse PD progression. Here, we investigated the disease mechanism using mDA neurons differentiated from human induced pluripotent stem cells (hiPSCs) carrying the ILE368ASN mutation within the *PINK1* gene, which is strongly associated with PD. Single-cell RNA sequencing (RNAseq) and gene expression analysis of a *PINK1*-ILE368ASN and a control cell line identified genes differentially expressed during mDA neuron differentiation. Network analysis revealed that these genes form a core network, members of which interact with all known 19 protein-coding Parkinson's disease-associated genes. This core network encompasses key PD-associated pathways, including ubiquitination, mitochondrial function, protein processing, RNA metabolism, and vesicular transport. Proteomics analysis showed a consistent alteration in proteins of dopamine metabolism, indicating a defect of dopaminergic metabolism in *PINK1*-ILE368ASN neurons. Our findings suggest the existence of a network onto which pathways associated with PD pathology converge, and offers an inclusive interpretation of the phenotypic heterogeneity of PD.

[1] The Integrative Cell Signalling Group, Luxembourg Centre for Systems Biomedicine (LCSB), University of Luxembourg, Esch-sur-Alzette, Luxembourg. [2] Luxembourg Institute of Health (LIH), Esch-sur-Alzette, Luxembourg. [3] Center for Systems and Therapeutics, the Gladstone Institutes and Departments of Neurology and Physiology, University of California, San Francisco, San Francisco, CA 94158, USA. [4] Department of Infection and Immunity, Luxembourg Institute of Health, Strassen, Luxembourg. [5] Department of Life Sciences and Medicine, University of Luxembourg, Belvaux, Luxembourg. [6] University of California San Diego, La Jolla, CA 92093, USA. ✉email: gabriela.novak@alumni.utoronto.ca; alexander.skupin@uni.lu

Parkinson's disease (PD) is one of the most prevalent neurological disorders, second only to Alzheimer's disease, with a prevalence of 1.8%, among persons over the age of 65 and 2.6% in the 85 to 89 age group[1–3]. As the average age of the population increases, PD is expected to pose an increasing burden to society. PD is characterized by the death of the midbrain dopaminergic (mDA) neurons found in the substantia nigra region of the brain, which are selectively sensitive to Parkinson's disease-associated neuronal cell death[4–7]. This results in the development of motor deficits, including bradykinesia, rigidity, and tremor, but many patients also develop non-motor symptoms, such as depression or dementia[8]. Unfortunately, current treatments only temporarily ameliorate the motor symptoms and do not reverse or slow down the progression of PD[4].

Most of our understanding of PD pathology at the molecular level is based on mutations known to cause PD, although these account for only 3–5% of PD cases, the remaining cases being idiopathic[2]. Despite the small fraction of cases they explain, these mutations provide an important window into the underlying molecular mechanisms of PD because they identify pathways which, when disrupted, are able to cause the disease. Many of these mutations converge on mitochondrial homeostasis, repair, and mitophagy. Hence, mitochondrial dysfunction likely plays a key role in the pathophysiology of PD[9]. An important group of these mutations lies within the *PINK1* gene. The PINK1 protein is expressed ubiquitously throughout the brain, in all cell types, where it localizes to the mitochondrial membrane[10]. PINK1 is a mitochondrial ubiquitin kinase and, together with the cytosolic ubiquitin ligase PARKIN, it targets damaged mitochondria for degradation via mitophagy, performing a mitochondrial quality control function needed to prevent accumulation of damaged mitochondria, which otherwise results in neuronal cell death[11–13]. The ILE368ASN mutation interferes with this process by reducing the interaction of PINK1 with its chaperone, HSP90, and destabilizing PINK1 at the mitochondrial membrane[11]. It also reduces its ubiquitin kinase activity through the deformation of its substrate-binding pocket and substrate misalignment[11]. Even though multiple publications have shown the involvement of PINK1 in mitophagy, its function is much broader. The targets of this kinase are involved in many cellular functions, including neuronal maturation[14], neurite outgrowth[15], suppression of mitophagy[16], and cell cycle modulation[17]. The broader impact on these pathways of loss-of-function mutations in this important kinase has not yet been fully elucidated[18].

One of the main obstacles to the study of Parkinson's disease is the death of mDA neurons and the resulting shortage of available postmortem samples. By the time of diagnosis, 60% of these neurons have disappeared and about 90% die by the late stage of the disease[6]. One approach is to study PD-associated mutations in animal models[19], but human-like mutations in animals often do not lead to the development of comparable pathology due to species differences in expression of key genes[20,21]. Thankfully, the development of cellular reprogramming allows nowadays for the conversion of somatic cells into induced pluripotent stem cells (iPSCs), which can subsequently be differentiated into neurons. This enables us to generate iPSCs from the skin cells of PD patients[22] and differentiate them into mDA neurons carrying disease-associated mutations[23–25]. Differentiating mDA neurons from iPSCs provides an almost unlimited source of neurons that allow for deep phenotyping and the elucidation of the cellular mechanisms underlying PD pathology.

Here, we generated iPSCs from the fibroblasts of a patient homozygous for the PD-associated mutation ILE368ASN (p.I368N) in the *PINK1* gene[2]. We used an optimized differentiation protocol to specifically generate mDA neurons, as this cell type displays a unique susceptibility to cell death in PD;[23,25,26] the effect of PD on other types of DA neurons is variable[6,27].

The mDA neurons are unique and distinct from other DA neurons. Their development diverges from that of other DA neurons even before they commit to neural fate[28]. During early neural development, neural tube stem cells generate neurons and glia, the two basic building blocks of the brain. While other DA neurons follow this direct path, which is determined by the expression of the PAX6 transcription factor, mDA neurons develop from radial glial cells of the floor plate and their development is driven by early exposure to high levels of the SHH transcription factor[29], which prevents expression of the PAX6 transcription factor[30] and sets these cells on an entirely different developmental path[25,28]. As a result, mDA neuronal precursors follow a very unique signaling cascade, leading to the expression of a transcriptome that greatly differs from that of other DA neurons[21,25–28,31–35]. Their distinct identity is reflected in their function and current research indicates that this leads to their unique susceptibility to death in PD, which in turn has been directly associated with the classic movement symptoms of the disease[6,26–28,36]. This is also supported by the observation that gene expression differences between murine and human mDA neurons, which translate into subtle functional differences, lead to incomplete PD phenotype in animal models[19,21].

To investigate the disease mechanisms linked to the *PINK1* mutation, we performed extensive single-cell RNA sequencing (SC-RNAseq) analysis using Drop-Seq[37] at four different timepoints during mDA neuron differentiation[23–25]. We generated four pairs of samples, each consisting of a *PINK1*-ILE368ASN and a control (17608/6[38]) cell line differentiated in parallel. The pairs were differentiated in succession so that they would be at a different stage of differentiation on the collection day (Fig. 1). This also means that they represent four independent biological replicates. Pairwise differential expression analysis was then performed between the *PINK1*-ILE368ASN and control cell line of each pair, with a constraint that genes must be strongly and consistently dysregulated in all pairs, hence at all timepoints, to be considered in our analysis. The reasons for this are listed in the discussion section. Using databases of known protein-protein interactions, we show that these genes form a network and that its members directly interact with all 19 protein-coding PARK genes associated with PD. This suggests that other PD-associated mutations may also be acting through this common network of genes. Furthermore, the pathway most strongly associated with the genes of this network is the Parkinson's disease KEGG pathway. Subsequent proteomics analysis of differentiated cells confirmed the manifestation of the transcriptional modifications at the protein level. Our results point to the existence of a common disease mechanism that potentially underlies idiopathic PD and may represent a unifying perspective on PD progression that will guide future intervention strategies.

Results

We performed a systematic differential expression analysis at a single-cell resolution between an iPSC line carrying the PD-associated ILE368ASN mutation in the *PINK1* gene and age- and sex-matched control cell line (control 1–2 in ref. [38]) during their parallel differentiation into mDA neurons (Fig. 1 and Supplementary Tables 1, 2). After preprocessing and quality-filtering, we used 4495 cells and 18,097 genes in our downstream analysis (Methods). For data integration, we performed a network analysis to identify the underlying key mechanisms of PD progression.

Fibroblasts were isolated from a 64-year-old male with PD symptom onset at 33 years of age who was homozygous for the ILE368ASN (P.I368N/P.I368N) mutation in the *PINK1* gene

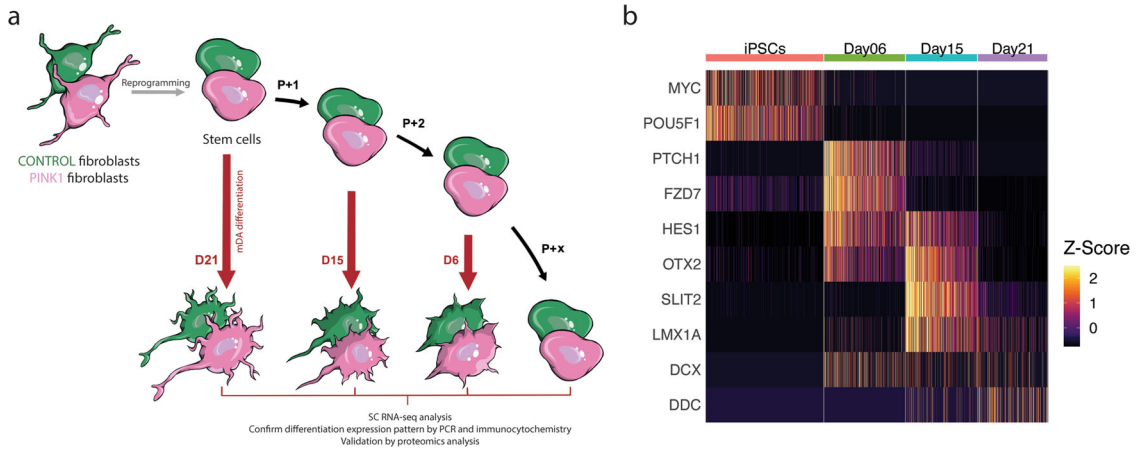

Fig. 1 Experimental design. a Fibroblasts were used to generate human induced pluripotent stem cells (iPSCs), which were then used to generate mDA neurons. Differentiation was initiated concurrently in a *PINK1*-ILE368ASN and a control cell line, at three different timepoints, to obtain cells which reach different stages of differentiation on the same collection day (generating four independent pairs). The samples were collected and processed for SC-RNAseq at the same time to avoid batch effects. "P + 1" indicates that the iPSCs were passaged before new differentiation was initiated. Since D10 was not used in the pairwise analysis, we indicated "P + 2" between D15 and D6 differentiation initiation. **b** Heatmap illustrating the transitions in gene expression from iPSC markers (*MYC* and *POU5F1-OCT3/4*), to genes associated with mDA differentiation (*PTCH1, FZDZ, HES1, OTX2, SLIT1*, and *LMX1A*), and finally to an early expression of mature mDA markers (*DCX* and *DDC*). This is discussed in more detail in the text and in Figs. 3 and 4. The gene expression matrix used here consists of 4495 cells (39,194 genes). Colors correlate to normalized counts (*z*-score, centered, and scaled) of the indicated gene.

(Coriell Institute, Cat. No. ND40066). The fibroblasts were confirmed to have a normal karyotype (Supplementary Fig. 1). Reprogramming was done at Yale Human Embryonic Stem Cell Core (New Haven CT) using the Sendai virus. The normal karyotype of iPSCs was confirmed (Supplementary Fig. 2 and Supplementary Tables 9, 10). Their iPSC status was ascertained by staining for the POU5F1 (also known as OCT4)[39–42] and the TRA-1-80[42,43] iPSC markers (Fig. 2a), by expression of key iPSC status markers using sc-RNAseq (Fig. 2b), and by the TaqMan iPSC Scorecard Assay[44,45], which also confirmed the trilineage potential of the cell line[44] (Fig. 2c).

Single-cell RNAseq (sc-RNAseq) analysis reveals gene expression panel for direct classification of iPSCs' stemness or pluripotency. Staining for OCT/TRA proteins and Scorecard are common approaches for determining iPSC status (reviewed by Smith and Stein)[42]. Here we show that a panel of genes indicative of iPSC status is readily detectable by single-cell analysis and can be used to indicate iPSC status directly in the cells used in an sc-RNAseq experiment, rather than by staining or expression analysis of an independent sample, which in some cases may not reflect the iPSC status of the experimental sample. Furthermore, this may be useful in cases where the samples are no longer available, such as for data obtained from an sc-RNAseq data repository. In our dataset, we quantified the expression of genes commonly used to ascertain iPSC status (*MYC*[46] and *POU5F1*[39–42]) and showed that these can be readily detected by sc-RNAseq analysis (Fig. 2b). However, sc-RNAseq analysis comes with some limitations. In particular, it is not able to detect genes which are naturally expressed at low levels. We, therefore, created a list of genes associated with high stemness, i.e., expressed selectively in iPSCs exhibiting full stem cell phenotype, which are readily detectable in sc-RNAseq data, creating a link between an iPSC state characterized by standard techniques and a signature visible in sc-RNAseq data. The heatmap of top genes differentially expressed during the transition between iPSC and subsequent differentiation stages shows that the iPSCs express several genes associated with stemness (Fig. 2b). For instance, we detected the expression of *TDGF-1*, which was shown to be expressed by stem cells with the highest expression of stemness markers[41]. Additional genes expressed by the iPSCs were *L1TD1*, *USP44*, *POLR3G*, and *TERF1* (essential for the maintenance of pluripotency in human stem cells[47–50]), as well as *IFITM1*, *DPPA4*, and *PRDX1* (associated with stemness[51–53]).

Based on our observations, we propose that the following panel of genes should provide a reliable indication of stemness in single-cell experiments: *MYC (cMyc), POU5F1 (Oct4), LIN28A, TDGF-1, L1TD1, USP44, POLR3G*, and *TERF1* (Fig. 2b).

In vitro differentiation of iPSC-derived mDA neurons recapitulates the in vivo process. As stated by Bjorklund & Dunnett "expression of TH is not in itself sufficient to prove that a neuron is catecholaminergic, let alone dopaminergic"[35]. Hence, we made great effort to confirm that the neurons generated by our protocol display a true mDA phenotype.

To confirm that our differentiation protocol (Supplementary Table 1) recapitulates the in vivo mDA differentiation path, we identified genes that are essential and specific to the in vivo mDA differentiation process (*OTX2, EN1, LMX1B, LMX1A, FOXA2, MSX1, NR4A2, PITX*3, and others) (Supplementary Table 3)[25–28,33–35] and analyzed their expression during the development of the control cell line at timepoints D0 (iPSCs), D6, D10, D15, D21 D26, D35, and D50, which represent the major developmental steps of the protocol (Fig. 3).

We first imaged cells at timepoints Day 25 and Day 35, as at this stage the cells should have developed mDA characteristics. Staining for key mDA protein markers TH, PITX3, LMX1A, and DAT, with MAP2 as a neuronal marker, confirmed the mDA phenotype (Fig. 3a). (The co-expression of these mDA markers with TH is shown in Fig. 4a.) At D25, neuronal cells possess only short processes and generally low mDA marker expression, but by D35 their axons are far longer and mDA marker expression is more defined and more robust. The mRNA expression of *TH, LMX1A*, and *ALDHA1A* was further validated by qPCR, and the trajectory of these genes' expression indicated the development of mDA characteristics by Day 21 (Fig. 3b), in agreement with the imaging results at Day 25 (Fig. 3a).

To characterize the differentiation process in more detail, we performed the sc-RNAseq analysis at eight timepoints of the differentiation process. Analysis of differentially expressed genes

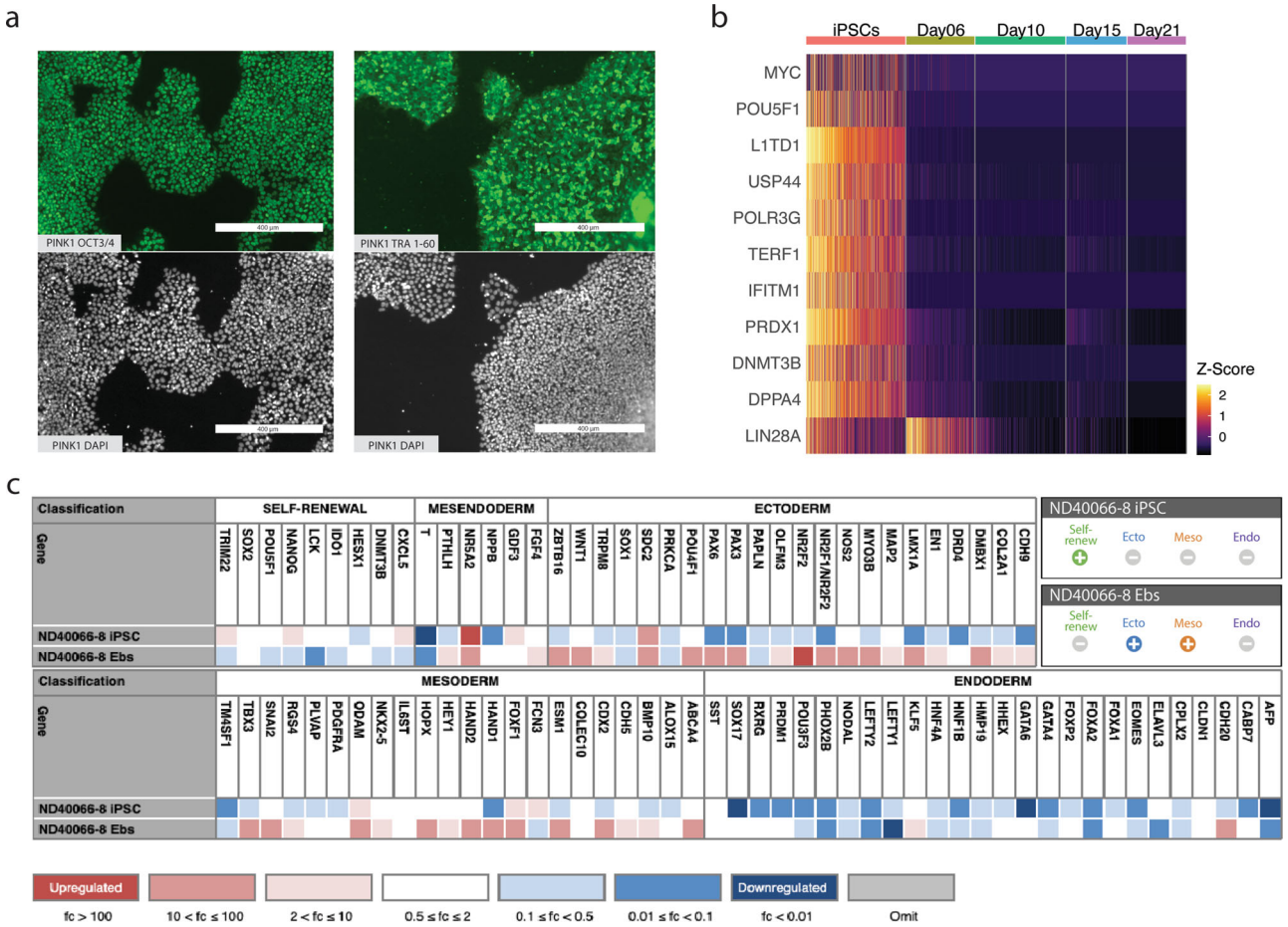

Fig. 2 Classification of iPSC status. a Immunocytochemistry (ICC). Staining for the iPSC markers POU5F1 (more commonly known as OCT3/4) and TRA-1-60 of iPSC colonies, prior to differentiation. DAPI was used to stain cell nuclei as a reference. **b** Expression of genes known to indicate iPSC status (*MYC* and *POU5F1*) and of genes identified by a differential expression analysis between iPSCs and differentiating cells (also see Supplementary Fig. 12). Colors correlate to normalized counts (*z*-score, centered, and scaled) of the indicated genes. *TDGF-1* is expressed in iPS cells of high stemness;[41] *L1TD1*, *USP44*, *POLR3G*, and *TERF1* are essential for the maintenance of pluripotency in human stem cells;[47–50] *IFITM1*, *PRDX1*, *DNMT3B*, *DPPA4*, and *LIN28A* and are associated with stemness[51–53,137,138]. **c** Results of Scorecard analysis of iPSCs and embryonic bodies (EBs)[44,45]. iPSCs are expected to show high expression of self-renewal genes and low expression of mesoderm, ectoderm, and endoderm markers. EBs are cells at an early stage of spontaneous differentiation. Scorecard analysis of EBs determines the iPSC line's potential to differentiate into the three germ layers, hence, EBs are expected to express few or no self-renewal genes and to show expression of some mesoderm, ectoderm and endoderm markers: Ecto±, Meso±, Endo±.

across timepoints revealed the expression of specific differentiation stage modules (Supplementary Fig. 12), in accordance with known in vivo stage-specific expression patterns (Fig. 3c and Supplementary Table 3). For example, in vivo, the development of mDA phenotype depends on the early high expression of Sonic Hedgehog (SHH), followed by the induction of Wnt signaling and the expression mDA-specific downstream pathways[25,26,28] (Fig. 3c and Supplementary Table 3). Consistent with these in vivo differentiation steps, *PTCH1*, a receptor for *SHH*, and *FZD7*, a receptor for Wnt proteins (Fig. 3c) were among the highest-expressed genes on day 6 (D6) of the differentiation protocol. The presence of *EN1* as a key entity was confirmed by qPCR (Supplementary Fig. 15), as its expression level was too low for detection by sc-RNAseq. The sc-RNAseq analysis again revealed that at Day 21 many factors that are specific to the mDA differentiation path, such as *TCF12, ALCAM, PITX2, ASCL1*, and *DDC*[27,54–57], were among the most highly expressed genes (Fig. 3c and Supplementary Fig. 12). Overall, these observations confirm that our in vitro differentiation protocol does indeed recapitulate the in vivo differentiation of mDA neurons and produces genuine mDA neurons (PAX6-, ALDH1A1+, PITX3+, KCNH6/GIRK2+, NR4A2/NURR1+, and LMX1A+), rather than other types of DA neurons (PAX6+ and ALDH1A3+) (Table 1 and Supplementary Fig. 3).

However, this assessment of the differentiation process of human mDAs was mostly based on the pattern of mDA differentiation gene expression in murine brains. We, therefore, compared our data with the recently outlined pattern of gene expression during human mDA[21,58]. The pattern of gene expression during our in vitro differentiation of human iPSCs into mDA neurons matched the pattern of human mDA differentiation[21] more closely than that of murine neurons, confirming the validity of our differentiation protocol.

Using the gene expression groups associated with different stages of maturation, from radial glia (Rgl), progenitors (Prog), to neural progenitors (NProg), and finally to mDA neurons (DA)[21] (Supplementary Table 3), we could characterize the differentiation trajectory by the level of gene expression (Fig. 3d). We then used these gene groups to characterize individual cells with respect to their most likely cell type and determined the population dynamics by the percentage of cell types present at each timepoint (Fig. 3e). The analysis showed fast differentiation from iPSC state to a neuronal lineage by Day 6, and the subsequent maturation towards an mDA phenotype starting at

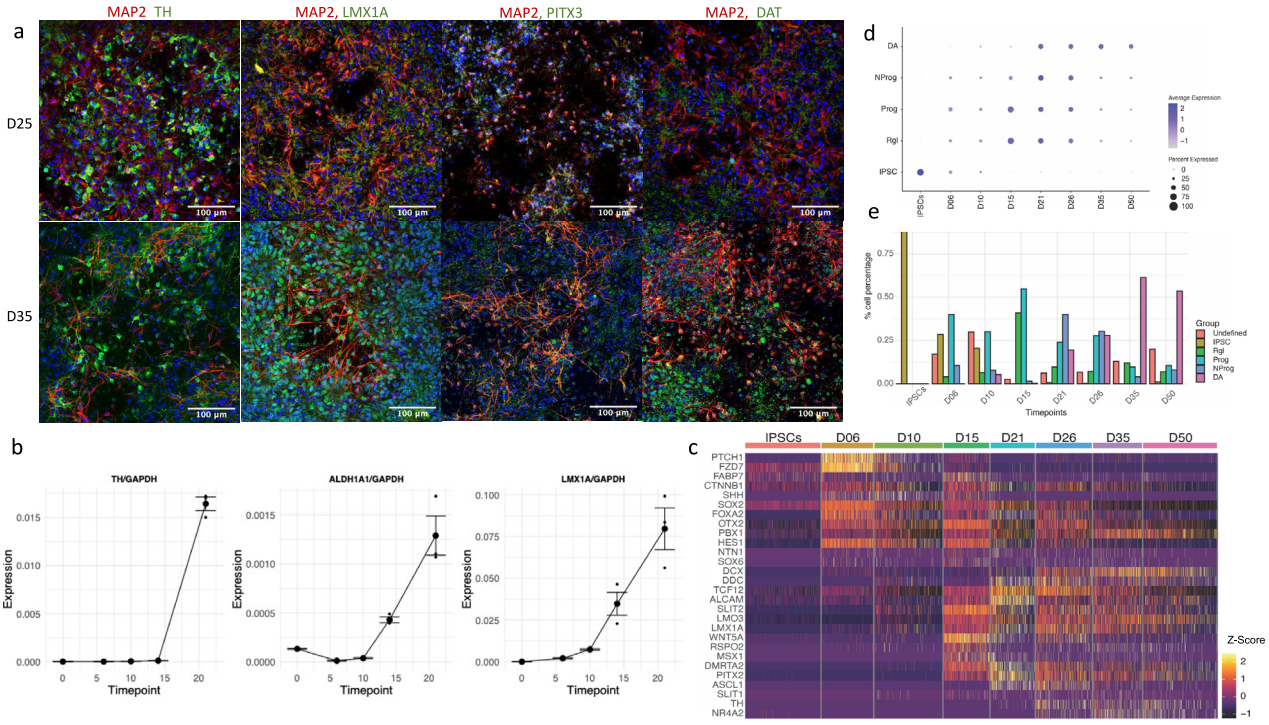

Fig. 3 In vitro differentiation of iPSC-derived mDA neurons recapitulates the in vivo process. a To illustrate the maturation of neuronal morphology and mDA status, differentiated neurons were stained at D25 and D35 for a neuronal marker MAP2 (red) and mDA markers (green): TH, PITX3, LMX1A, and DAT. While D25 neurons show short processes and low expression of mDA markers, D35 neurons show much longer axons and well-defined expression of mDA markers (green/red overlap resulting on orange/yellow). **b** Quantitation of mDA markers *TH, ALDH1A1*, and *LMX1A*, using absolute quantitation via qPCR. Each timepoint represents three independently differentiated biological replicates, amplified in duplicate. Standard error (SE) bars are the SE of biological replicates. The expression levels are standardized to total RNA and to the expression of the housekeeping gene *GAPDH* (see Methods). **c** Heatmap showing the expression of genes known from the literature to be involved and necessary for mDA neuron differentiation (Supplementary Table 3). Colors correlate to normalized counts (*z*-score, centered, and scaled) of the indicated genes. **d** The mDA differentiation gene expression profile recently published by Ásgrímsdóttir and Arenas (2020)[21] was used to show the progression during differentiation, from iPSCs to radial glia (Rgl), to progenitors (Prog) and neuroprogenitors (NProg), and to early mDA neurons (DA). Genes used to determine the expression modules are listed in Supplementary Table 3. **e** Proportions of cells expressing the various phenotypes illustrated in (**d**). The gene expression matrix obtained by SC-RNAseq used here consists of 4495 cells (see Methods section).

Day 21, accompanied by the increasing prevalence of DA phenotype, from 20% at Day 21, to 28% at Day 26, and 61% at D35, after which it seemed to stabilize (Fig. 3d). This characterization further confirms that early mDA differentiation is achieved around Day 21.

The PINK1-ILE368ASN mutation is associated with persistently dysregulated expression of nearly 300 loci. To investigate the effect of the *PINK1* mutation on mDA development, we differentiated the control and the *PINK1*-ILE368ASN cell lines in parallel (Figs. 1, 4) and focused on the early differentiation period, to increase our chances of finding the direct effects of *PINK1*-ILE368ASN, as described below. Co-staining of TH positive neurons with the midbrain dopaminergic markers PITX3, LMX1A, and DAT in both the control and PINK1 cell lines identified neurons at day D21 as early postmitotic mDA neurons[25] with clearly neuronal morphology and no major differences between the cell lines (Fig. 4a).

To investigate potential underlying mechanisms of the PINK1 mutation, differential expression between the two, in parallel differentiated, cell lines at each timepoint was determined and genes that were identified as differentially expressed at all four timepoints were identified. Each timepoint is an independent biological replicate, initiated at a different time and with cells of a different passage number. Control and *PINK1*- ILE368ASN cells co-clustered together based on their differentiation stage, from iPSCs, to day 6 (D6), D15, and D21 (Fig. 4b), indicating that overall RNA expression was specific to differentiation stages, and rather uniform between cell lines, which was amenable to the identification of subtle gene expression differences due to the presence of a mutation in the *PINK1*- ILE368ASN cell line.

The *PINK1*- ILE368ASN cells at D10 showed low viability, hence the D10 timepoint was not included in the pairwise analysis. After preprocessing and quality-filtering (Methods and Supplementary Fig. 4), a total of 4495 cells (2518 control and 1977 PINK1 cells) and 18,097 genes were included in our analysis. UMAP analysis of the single-cell data revealed that gene expression was rather similar between the cell lines and mainly defined by differentiation stage, rather than by cell line origin (Fig. 4b). In accordance with the staining results (Figs. 3a, 4a), we observed the onset of expression of the mature mDA markers *TH* and *KCNH6* (also known as *GIRK2*) on D21 (Fig. 4c).

The analysis of pairwise differential expression at each timepoint (adjusted p values (p_{adj}) <0.01 fold changes (FC) >0.1) (Fig. 5a) identified 14 genes that were upregulated and 13 genes that were significantly downregulated in the *PINK1*-ILE368ASN cell line compared to control (Fig. 5b and Table 2, indicated by "X"). Because iPSCs are very different from differentiating neuronal precursors, we next tested whether including iPSCs had disproportionately affected the results by excluding neuron-specific genes. Repeating the analysis on D6,

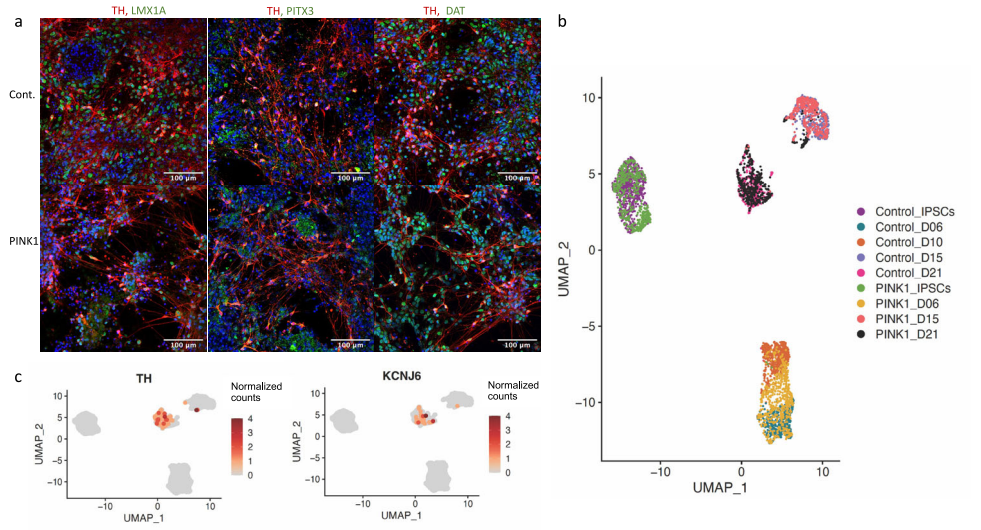

Fig. 4 Classification of mDA status. a TH positive neurons co-express mDA markers PITX3, LMX1A, and DAT in control (top) and PINK1 cell line (bottom), at D35. For images of individual targets see Supplementary Fig. 13 and for colorblind-friendly images see Supplementary Fig. 14. **b** Based on our SC-RNAseq data, cell lines cluster according to differentiation stage, indicating that gene expression is very homogenous between the control and the *PINK1*-ILE368ASN cell lines, which allows for the detection of even subtle alteration induced the presence of the PINK1 mutation. **c** Trajectory of expression of *TH* and *KCNJ6* (*GIRK2*), two mDA neuron markers. At D21 neurons begin to show *TH* expression, together with an expression of other mDA markers, which indicates that they are becoming early postmitotic mDA neurons[25]. Similar observations can also be made from an expression heatmap shown in Supplementary Fig. 12. The scale represents normalized counts.

Table 1 DA neuron heterogeneity: mDA and non-mDA markers.

Dopaminergic neuron type	TH	DDC AADC	SLC6A3 DAT	SLC18a2 VMAT	PAX6	Other	
A8–10 midbrain dopaminergic neurons	+	+	+	+	-	**ALDH1A1**	
A11 periventricular nucleus (PVN)	+	+	-	+	-	**ALDH1A3**	
A12 arcuate nucleus (endocrine)	+	+	+	+	-	**ALDH1A3**	Dlx1
A13 medial zona incerta	+	+	-	+	+*	**ALDH1A3**	Dlx1, SST
A14 preoptic periventricular nucleus	+	+	-	+	+*	**ALDH1A3**	
A15 preoptic & endopeduncular area	+	-	-	+?	+	**ALDH1A3**	
A16 periglomerular cells, olfactory bulb	+	+	+	-	+	**ALDH1A1**	
A17 interplexiform cells in the retina	+	+	+			**NKR**	

When studying PD, it is important to ascertain that the DA neurons are in fact mDA neurons. In an in vitro differentiation system, simple marker combinations that normally distinguish mDA neurons, such as positional and anatomical information, are missing. We relied instead on molecular markers culled from the literature to monitor our differentiation protocols. (* A13 and A14 PAVH express PAX6 transiently during development. PAX6 is expressed early in development, whereas the remaining markers are expressed later and are markers of mature DA neurons. "?" indicates that the literature regarding the expression is not unanimous.)[25,34,35,139–144].

D15 and D21 only identified 28 genes that were upregulated and 27 genes that were downregulated at all three timepoints, including all genes previously identified (Table 2). As expected, excluding iPSCs resulted in the identification of a broader range of genes because genes that are differentially expressed only in the neuronal lineage were previously excluded due to the requirement that DEGs be dysregulated at all timepoints. However, both sets are equally valuable, as genes dysregulated even in iPSCs are likely to participate in systemic PD pathology, regardless of cell type, and may be relevant to a broader spectrum of PD pathology than the death of mDA neurons. Interestingly, most of the differentially expressed genes are already linked to PD, other PD mutations, or neurodegeneration (Table 2).

For an alternative definition of differentially expressed genes (DEGs), we used the maximum adjusted p value in a pairwise combination as an adjusted p value, and the average fold change that occurred in the pairwise comparison as a fold change threshold. With this approach, we retained only genes dysregulated in the same direction at all timepoints. This analysis led to 151 DEGs (named Group B, Supplementary Table 4), which included the previously identified genes of Group A, and of which 65 were upregulated and 86 downregulated compared with controls ($p_{adj} < 0.01$ and FC > 0.1). Taking the mean of FC of the different timepoints enhanced the identification of DEGs because it reduced the effect of the variability between pairs due to their different differentiation states. Repeating the same analysis for the four timepoints (iPSCs, D6, D15, and D21), but taking into account only the absolute degree of change in iPSCs, yielded 172 genes (Group C, Supplementary Table 5). Repeating the analysis using only timepoints D6, D15, and D21 identified a total of 286 DEGs (Group D) (also see Fig. 6a and Supplementary Data 1). Together, when all analyses were pooled, we obtained 292 DEGs (six genes in Group C depended on the inclusion of iPSCs and did not appear in Group D, see Supplementary Data 1).

Enrichment analysis reveals a strong association with the KEGG Parkinson pathway. Enrichment analysis was performed using the STRING[59] database (Fig. 5c). The highest-associated KEGG pathways were the Parkinson's, Huntington's, and spliceosome pathways. Details are listed in Supplementary Data 5. Biological processes most strongly associated with the DEGs were C3HC4-type RING finger domain binding, Ran GTPase binding, and protein

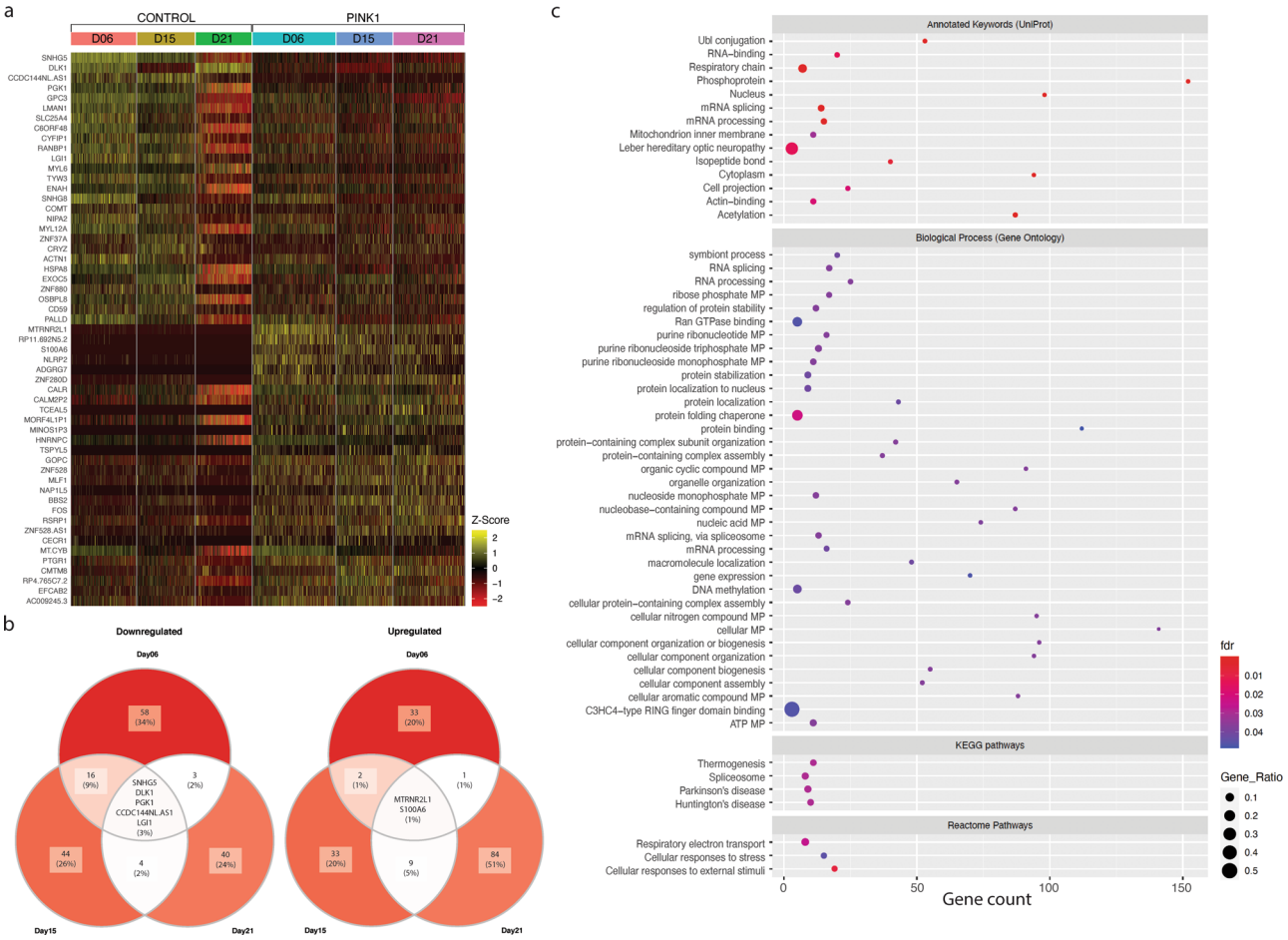

Fig. 5 Differentially expressed genes (DEGs) in a cell line homozygous for a mutation in the *PINK1* gene, compared to a control cell line, at three timepoints during the differentiation of mDA neurons (D6, D15, and D21). a Heatmap of the top DEGs. Each column corresponds to a timepoint for either control or PINK1 cells; each row shows the expression of one gene in individual cells. Colors correlate to normalized counts (*z*-score, centered, and scaled) of the indicated genes. **b** Top DEGs. The minimum fold change was increased to highlight the top differentially expressed genes. We identified the top 56 genes as our group A (Table 2); here we show the top five upregulated genes (left Venn diagram) and the top three downregulated genes (right Venn diagram). **c** Enrichment analysis performed using the STRING[59] database. The top KEGG pathway associated with this dataset is Parkinson's disease. The other three KEGG pathways identified were Spliceosome, Huntington's disease, and Thermogenesis. Details are listed in Supplementary Data 5. The gene expression matrix used for the downstream analysis consisted of 4495 cells (39,194 genes) and differential expression analysis resulted in 292 DEGs, which were used to perform the enrichment analysis.

folding chaperones. Respiratory chain transport was the most strongly associated Reactome pathway.

Data integration reveals a common PD network. To integrate the expression analysis and identify underlying disease mechanisms, we generated a network of interactions between the DEGs via Gephi[60], using protein–protein interaction (PPI) information obtained from the STRING and GeneMANIA databases[59,61]. The network we obtained includes 246 of the 292 DEGs, since pseudogenes and non-coding RNAs could not be integrated into a protein–protein interaction network (Fig. 6), and 2122 interactions (Supplementary Data 2). The curated network contains only DEGs and any genes that were automatically added by the databases were removed to ensure a reliable core network based solely on DEG data. Based on known protein–protein interactions, the DEGs integrate into a close-knit core network in which several DEGs form central nodes (Fig. 6). To evaluate the importance of the DEG-based PPI network produced by STRINGdb (v10)[59], we compared the DEG-based network with corresponding random networks generated from sets of 292 randomly chosen genes excluding DEGs. Based on 50 random networks, we show that the DEG-based network includes significantly more protein-coding genes and interactions than by chance (Supplementary Fig. 5) and that the network structure in terms of degree distribution is significantly distinct as evaluated by the Wilcoxon test ($p = 2.22e\text{-}16$) and indicates the mechanistic character of the network.

The network of genes dysregulated by the presence of the *PINK1*-ILE368ASN mutation includes genes related to other PD-associated pathways, which is intriguing since it was generally assumed that each PD-associated mutation leads to PD pathology via an independent, characteristic path. For example, two DEGs, *GOPC*, and *GPC3*[62,63] interact with the PD-associated gene *DJ-1* (*PARK7*)[2,64]. The DEG network also includes genes of the *LRRK2 (PARK8)* network[2,64], namely *ENAH, HSPA8, MYL6, MALAT1*, and *SNHG5* (Supplementary Fig. 6). *SNHG5* and *MALAT1* interact with *LRRK2* via *miR-205-5p*[44,45]. DLK1 and MALAT1 mediate α-synuclein accumulation[65,66]. In fact, the DLK1-NURR1 interaction involved in this process may be mDA neuron-specific[67], highlighting the necessity to use mDA neurons for the study of PD-related pathways. Additionally, MALAT1 was shown to increase α-synuclein protein expression[68]. In short, this suggests that interactions leading to PD pathology are more

Table 2 The top genes dysregulated consistently in PINK1 vs. control cells across differentiation stages.

Upregulated in PINK1					Downregulated in PINK1				
GENE	**incl. iPSCs**	**excl. in STRING**	**PD association**	**Ref.**	**GENE**	**incl. iPSCs**	**excl. in STRING**	**PD association**	**Ref.**
AC009245.3	X	Pseudogene			*ACTN1*			PD	145
ADGRG7	X		rare var., mito	146	*C6ORF48*	X			
BBS2					*CCDC144NL.AS1*	X	RNA		
CALM2P2	X	Pseudogene			*CD59*	X		PD	147
CALR			PD	148	*COMT*			PD	149
CECR1					*CRYZ*	X		GWAS, PD Gene	63
CMTM8			GWAS, PD	63	*CYFIP1*	X		(via mTOR)	150
EFCAB2	X		microarray	151	*DLK1*			PD	152
FOS			rat, L-DOPA	153	*ENAH*			GWAS, *LRRK2*	154
GOPC			*PARK7 (DJ-1)*	63	*EXOC5*			Parkinson Dis.Map	155
HNRNPC	X		binds Parkin	101	*GPC3*			reduced in *DJ-1* mut.	62
MALAT1			PD	156	*HSPA8*	X		PD, *LRRK2*	157
MINOS1P3	X	Pseudogene			*LGI1*			PD	119
MLF1			via *HTRA2*	158	*LMAN1*			Parkin transloc.	104
MORF4L1P1	X	Pseudogene			*MYL12A*			binds Parkin	101
MT-CYB			mito	159	*MYL6*	X		interacts with LRRK2	160
MTRNR2L1	X		binds Parkin	101	*NIPA2*	X		tremor	161
NAP1L5					*OSBPL8*			via ZNF746, Biogrid	162
NLRP2	X		inflammasome	163	*PALLD*			PD	164
PTGR1					*PGK1*	X		PD	165
RP11.692N5.2	X	Pseudogene			*RANBP1*				
RP4.765C7.2	X	Pseudogene			*SLC25A4*			binds Parkin	101
RSRP1					*SNHG5*	X	RNA	via miR-205, LRRK2	166
S100A6	X		PD	167	*SNHG8*		RNA		
TCEAL5	X				*TYW3*	X			
TSPYL5			Ubiquit.	168	*ZNF37A*	X			
ZNF280D	X		GWAS*	169	*ZNF880*	X			
ZNF528									
ZNF528.AS1		RNA Gene							

Pairwise differential expression analysis of each timepoint (iPSCs, D6, D15, and D21), resulted in 14 genes that were upregulated and 13 genes that were downregulated in the *PINK1*-ILE368ASN cell line, compared to control (p_val_adj <0.01 and abs(avg_logFC) >0.1); these genes are marked with "x" in column "Incl. iPSCs". Twenty-nine additional genes were identified in an analysis that included D6, D15, and D21, but not iPSCs. The "Excluded" column explains why a gene was not included in the protein–protein interaction network. These 56 top DEGs are later referred to as Group A. The gene expression matrix used for the downstream analysis consisted of 4495 cells (39,194 genes). * rs11060180.

complex than one mutation - one path to PD, as generally thought. It also indicates that many druggable targets may be useful in treating PD and that these may be universally effective for PD caused by several different mutations, and perhaps even for idiopathic PD. For example, terazosin, which is already in clinical use, was found to be associated with slower disease progression, likely by enhancing the activity of phosphoglycerate kinase 1 (PGK1)[69], one of the top DEGs identified in our study.

For the evaluation of the relative importance of each node within the network, we applied betweenness centrality[60] (Fig. 6a), an approach that reveals the overall connectedness of each gene. Genes onto which several other genes converge are shown as large circles or nodes, their size being proportional to the number of interactions they form. Interestingly, the major nodes of this network are genes already known to play an important role in ubiquitination (Fig. 6b) and PD pathology (Fig. 6c and Table 3). Next, we built a correlation network (p value < 0.05, $r > 0.1$) of the 246 DEGs based on the normalized counts. By extracting the common interactions of these two networks, we obtained a network with 297 interactions (Supplementary Table 6), which highlights protein–protein connections that correlate with differential expression of the genes. This analysis further supports the role of the connections between these genes in mediating the resulting differential expression in the presence of the *PINK1*-ILE368ASN mutation. STRING was subsequently used to highlight functional pathways represented within the DEG network (Supplementary Fig. 7 and Supplementary Data 3). Several pathways known to play a role in PD pathology are strongly represented within the network, notably ubiquitination[19,70], mitochondrial pathways[9,71], cellular response to stress[72], lysosomal proteins[73], protein metabolism (localization, modification, transport, folding, and stability), RNA processing[74], aromatic compound metabolism[75–78], vesicle-mediated transport and exocytosis[79], and cellular catabolic processes[72,73] (Supplementary Fig. 7). Importantly, the strongest-associated pathway is the KEGG-PD[59] pathway (Supplementary Fig. 9a). The CHCHD2 gene was identified as a dysregulated gene through our analysis, but it was also recently identified as a PD-associated gene and named *PARK22*[64,80,81] (Fig. 6a).

To investigate further how the identified network relates to other known PD mechanisms, PD-associated genes, also known as PARK genes (Supplementary Table 6 and Supplementary Fig. 9), were added to the DEG network. Next, PARK–PARK interactions were removed and only PARK–DEG interactions were retained to test how PARK genes integrate into the network. All 19 protein-coding PARK genes[2,64] interact directly with at least one, but usually several DEGs (Supplementary Fig. 9). The degree of interaction of PARK genes with the DEGs of the network is illustrated by coloring (in pink) DEGs that directly interact with a PARK gene. The darker the color, the greater the number of PARK genes the DEG interacts with. The preexisting central nodes of the network generally interact with several PARK genes, suggesting that they play a central role in linking the PARK genes to the network, but also that PARK genes may mediate PD

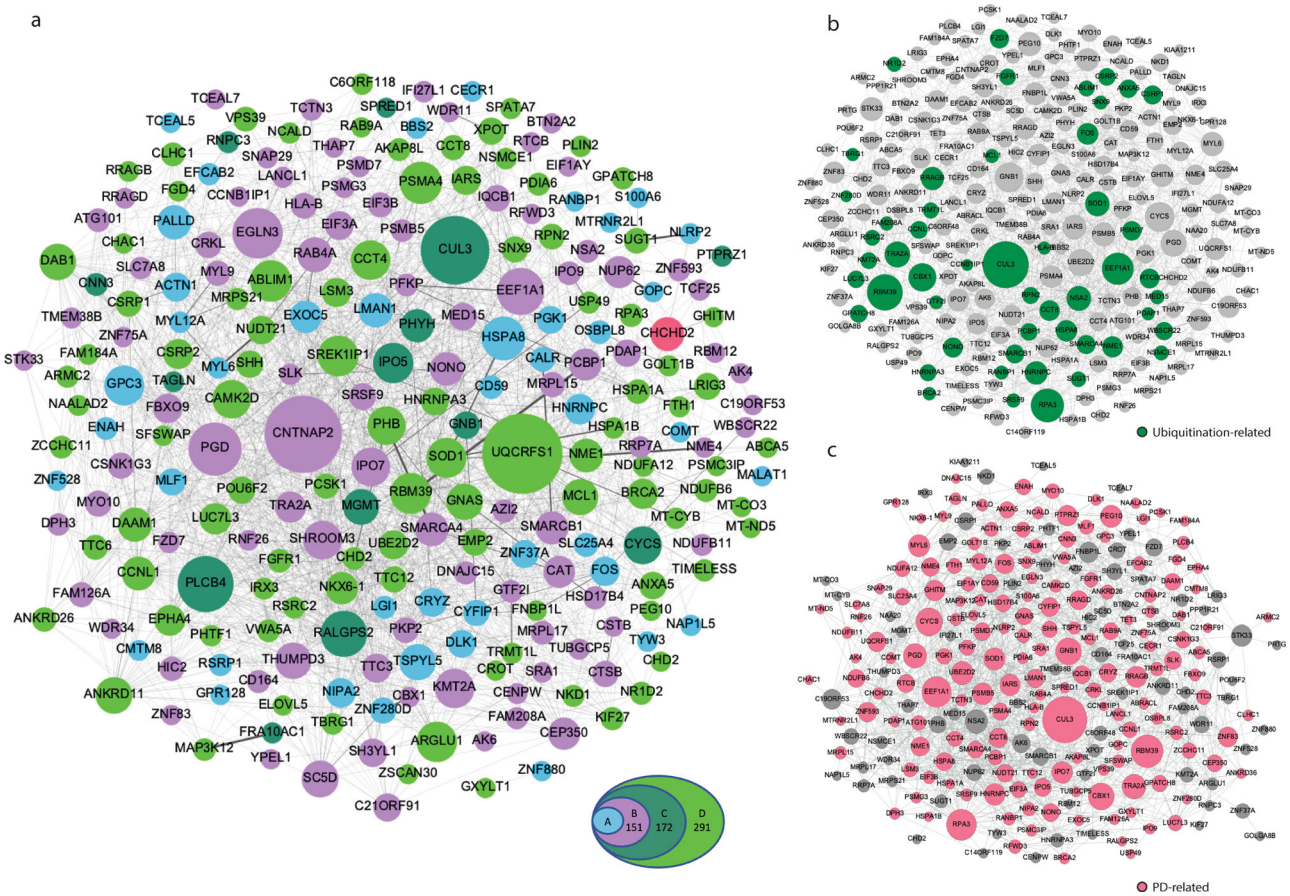

Fig. 6 Network analysis. a Protein–protein interaction network based on known interactions available through the STRING[59] and GeneMANIA[61] databases. Only strong interactions were retained, predicted interactions or text associations were omitted (see Methods). Betweenness centrality was used to illustrate the relative importance of each node within the network through the level of its connectedness to other proteins. The larger the circle, the more partners the node is connected to. The colors represent the four DEG sets, with the top 56 DEGs (group A) in light blue, group B in purple, group C in dark green, and group D in light green. Each set consists of genes of the previous set plus additional genes identified by the new parameters. *CHCHD2* (pink, part of group B) is a DEG, which has recently been identified as a PARK gene. Random selection of genes from genes detected by sc-RNAseq did not lead to a network formation (Supplementary Fig. 5). **b** DEGs which play a role in ubiquitination. Additional functional pathways are listed in Supplementary Fig. 7 and Supplementary Data 3. Specific connections to ubiquitination proteins are shown in Supplementary Fig. 8. **c** Based on the literature, 68% of the DEGs of this network are already known to be associated with PD (for references see Supplementary Data 4). Supplementary Fig. 9 shows which genes/proteins of the network directly interact with PARK genes through known protein–protein interactions. The topology of all three networks is the same, the different appearance is a result of a separate analysis run, but the connections and size of the nodes remain identical.

pathology through a few central pathways of this network, and that the effects of different PARK genes converge on the same set of pathways (Supplementary Fig. 9).

Further analysis revealed that a large number of the DEGs interact with genes associated with mitochondria or ubiquitination (Fig. 6b and Supplementary Fig. 8). For this analysis, we used BioGRID[61,82] to identify interactions with mitochondrial or ubiquitination proteins for the top 172 DEGs (groups A–C). These interactions were used to create a network illustrating that many of the DEGs in our study directly interact with genes involved in mitochondrial function and in ubiquitination. Only direct DEG to mitochondrial gene or DEG to ubiquitination gene interactions were included and PARK genes were added for reference (Supplementary Fig. 8). Based on manual literature search, we determined that at least 68% of the DEGs (174 of 255 genes, not including pseudogenes and RNA genes) are already directly associated with PD, either experimentally, or linked through GWAS-PD, or by PD expression studies (Fig. 6c and Supplementary Data 4). This is particularly true for the major nodes of the network (Table 3 and Fig. 6c).

Proteomics analysis confirms impaired neuronal phenotype in *PINK1*-ILE368ASN mutant line. To investigate how the identified transcriptional modifications manifest in the neuronal phenotypes, we performed proteomics analysis at an early (day 25) and later maturation stage (day 40). The analysis identified 39 differentially abundant proteins in *PINK1*-ILE368ASN cells as compared to controls, based on biological duplicates with a log2 fold change larger than 1 (Fig. 7a). Of these, four differ at both timepoints (D25 and D40). Overall, 31 proteins were differentially abundant at D25, including CSRP2 and VWASA, which were also identified by sc-RNAseq as differentially expressed at the mRNA level at D6, D15, and D21 (Fig. 7b and Supplementary Table 8). At D40, 12 proteins were found to be differentially abundant, including four also identified at D25, namely TH, DDC, NES, and VIM. We performed a network analysis based on the differentially abundant proteins (Fig. 7b). The resulting network again connects PD-related nodes and exhibits a good overlap with the transcriptional-derived network. This consistent result indicates that the observed transcriptional modification led to an impaired neuronal phenotype, despite the subtle differences

Table 3 Central nodes of the DEG network are associated with PD (Fig. 6c).

Node gene	Role in Parkinson's disease
HSPA8 (also known as *HSP73, HSC70*)	Disaggregation of α-synuclein amyloid fibrils[85] Autophagy, part of the catabolic pathway for α-synuclein[86] Mediates mitophagy by regulating the stability of PINK1 protein[87] Impaired gene expression in sporadic PD[88]
EEF1A1	Mediates activation of heat-shock transcription factor HSF1, prevents α-synuclein aggregation[90] Interacts with Parkin (PARK2)[82]
HNRNPC	Interacts with Parkin (PARK2)[82] Part of the poly ADP-ribose (PAR) cell death pathway accountable for selective dopaminergic neuronal loss[99]
PSMA4	Part of the Parkinson's disease KEGG pathway[92,93] Interacts with Parkin (PARK2) and FBX07 (PARK15)[82]
CYCS	Role in aggregation of alpha-synuclein[170] CTD gene-disease associations - Parkinson disease gene set[63]
ACTN1	Interacts with DJ-1 (PARK7)[82] It is a binding partner of mitochondrial-shaping proteins[171]
PGK1	PGK1 mutation causes vulnerability to parkinsonism[172] Activation of PGK1 partially restored motor function and slowed disease progression[69]
PHB	Regulates dopaminergic cell death in substantia nigra[173]
SHH	Play a role in neuroinflammatory response in the MPTP model of Parkinson's disease[174]
BRCA2	Deubiquitinase plays a role in neuronal inflammation[175]
VPS39	It is part of the endocytic membrane trafficking pathway involved in PD and its methylation rates are associated with Parkinson's disease risk[176] Plays complex functions in endocytic and autophagic pathways[177]
UQCRFS1	KEGG pathway, Parkinson disease[92,93]
CNTNAP2	Differentially expressed in the presence of *LRRK2* G2019S mutation, associated with PD[97] GWASdb SNP-disease associations, Parkinson's disease gene set[63] Plays a role in the formation of protein aggregates and PD[95,96]
CUL3	Ubiquitin ligase, a potential drug target for Parkinson's disease[84]
PLCB4	GWAS - Parkinson's disease[63] Motor defect consistent with ataxia in Plcb4-null mice[100]
EGLN3	GEO signatures of differentially expressed genes for diseases—Parkinson's Disease_Substantia Nigra[63] Prolyl hydroxylase targets substrates for ubiquitination[178]
RALGPS2	Targets include Nurr1, which is associated with Parkinson disease[63]

Central nodes were determined using the Gephi visualization platform. They represent points of convergence of the network (Supplementary Fig. 5). Since these nodes have already been linked to PD pathways, many more DEGs might also contribute to PD pathology through these pathways. These nodes not only provide a point of convergence for DEGs identified in our study, but they also interact with several PARK genes, suggesting that PARK proteins may also converge on the pathways identified here (Supplementary Fig. 7).

in expression, and further highlights the importance of the proposed PD Core network.

Discussion

The aim of this study was to identify genes that were differentially expressed as a result of a mutation in the *PINK1* gene, using mDA neurons differentiated from patient-derived iPSCs, a model relevant to PD. We focused on the analysis of early timepoints of the differentiation protocol, on cells undergoing neural differentiation up to the state of early postmitotic mDA neurons (D21), as these are not expected to display the activation of damage-control pathways induced by neurotoxicity, but are likely to reveal pathways that lead to primary pathology of PD. Because genetic background can potentially influence the severity and course of the disease[12,83], we chose a cell line homozygous for the ILE368ASN-*PINK1* mutation. This mutation imparts a very strong drive towards PD, resulting in full penetrance and an early onset of the disease, hence its impact is expected to diminish the effect of genetic background[12].

By including four different differentiation timepoints and requiring each DEG to be altered at every timepoint, we excluded pathways associated with mDA differentiation, as the expression of such genes changes between each step (Supplementary Fig. 12). The limitation of using an early time period is that we could not identify pathways associated with PD pathology in mature and aging neurons, however, this was intentional. We focused on the identification of pathways prior to damage onset, in order to eliminate the identification of pathways secondary to the disease, ones induced by damage and associated with cell death. Extension of the timeline to mature and aging neurons is the focus of our future experiments.

Figure 4b shows that samples clustered according to the differentiation stage, rather than cell line identity. Therefore, while the requirement for expression at all timepoints allowed us to identify changes independent of cell state transition, pairwise comparison excluded genes commonly expressed at any particular timepoint, with remaining expression changes being specific to the presence of the PD-associated mutation. The single-cell expression data were analyzed in several layers. First, we identified the most strongly DEGs consistently altered in the same direction at all four timepoints including iPSCs (Fig. 6a and Table 2). This led to a list of genes dysregulated by the *PINK1*-ILE368ASN mutation independent of the cell type (iPSCs, neuronal precursors, or neurons) (Table 2, Group A "incl. iPSCs", marked by "X"). Second, we applied an approach, in which the iPSC timepoint was excluded, leading to an expanded gene list, which included genes more likely to be dysregulated specifically in a neural cell type (Table 2 and Fig. 6, Group A, 56 genes). Using an approach that reduced the effect of variability between pairs due to different differentiation states expanded the list to 151 genes dysregulated in the same direction at all timepoints (Fig. 6a—Group B and Supplementary Table 4), while taking into account only the absolute degree of change in iPSCs expanded the list further, to 172 non-neuron-specific DEGs (incl. iPSCs, Fig. 6a—group C and Supplementary Table 5). Excluding iPSCs from

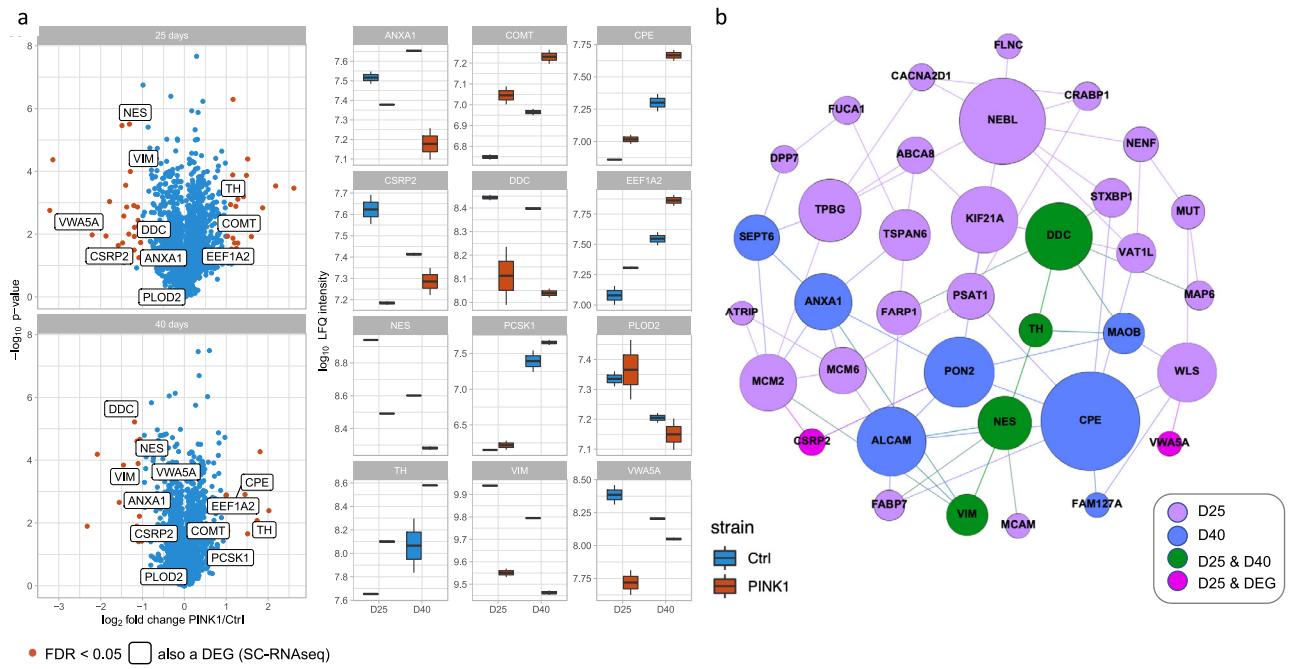

Fig. 7 Comparative proteomics analysis between CTRL and *PINK1*-ILE368ASN cell line at D25 and D40 validates the manifestation of the transcriptional phenotype. Results of proteomic analysis at D25 and D40 of the differentiation protocol. **a** The volcano plot shows significantly differentially abundant proteins (FDR <0.05, fold change larger than 2 or −2) as red points, with remaining datapoints shown in blue. The names of proteins that were detected as both top differentially abundant at the protein level by the proteomics analysis and as differentially expressed at the mRNA level by SC-RNAseq are highlighted using a textbox. The data shows results at two timepoints, D25 and D40, in two biological replicates per timepoint. Box plots further highlight the expression of genes shown in textboxes of the volcano plot (interquartile range, showing the expression at D25 and D40, in the PINK1 cell line and in control (IQR, 25–75% q1–q3), with bars indicating Q1 ± 1.5 IQR). **b** This figure shows a network of proteins differentially expressed between a control and a PINK1 mutation-carrying cell line, at D25 and D40. Proteins which are differentially expressed at both D25 and D40 are highlighted in green and point to a dysfunction of the dopaminergic system. D25 differentially abundant proteins are in purple, D40 in blue, proteins also identified as by SC-RNAseq differentially expressed at the mRNA level are in pink. For a table of proteins see Supplementary Table 8. Betweenness centrality was used to illustrate the relative connectedness of each node within the network, the greater the number of documented interactions with other nodes, the larger the circle.

this analysis again expanded this list by neuron-specific DEGs, to a total of 285 (Fig. 6a—group D and Supplementary Data 1). Creating a protein–protein interaction network based on these groups of DEGs demonstrated that genes of all groups formed important nodes within the interaction network. Furthermore, genes of all groups were frequently associated with PD. Overall, this indicates that all the selection criteria levels identified relevant targets (Fig. 6 and Supplementary Data 4).

Analysis of the network shows that certain DEGs are points of convergence within the protein network and form major nodes (Fig. 6 and Supplementary Fig. 9), namely CUL3, HSPA8, EEF1A1, UQCRFS1, CNTNAR2, PSMA4, HNRNPC, and PLCB4. The proteins forming the major nodes are already known to play an important role in PD pathology (Fig. 6c and Table 3). CUL3 has been linked to PD by GWAS studies and is considered a potential PD drug target[84]. HSPA8 (also known as HSP73 and HSC70), disaggregates α-synuclein amyloid fibrils and plays a role in autophagy and the catabolic pathway for α-synuclein, mediates mitophagy by regulating the stability of the PINK1 protein, and its expression was shown to be impaired in sporadic PD[85–88]. In fact, HSPA8 is by far the most important node in the network generated with data from the STRING[59] database, which is preferentially based on functional interaction (Supplementary Fig. 9a, b). It is also one of the most highly dysregulated genes in our dataset. EEF1A1 Translation Elongation Factor mediates activation of the heat-shock transcription factor HSF1, a key player in PD[89], and prevents α-synuclein aggregation, as well as interacting with Parkin (PARK2) and HTRA2 (PARK13)[82,90] (Supplementary Fig. 9). UQCRFS1 is a mitochondrial electron transport chain ubiquinol-cytochrome c reductase[91], a member of the KEGG-PD pathway (Entry K00411[92,93]), and has been identified as a PD risk gene[94]. CNTNAP2, which belongs to the neurexin superfamily, plays a role in triggering protein aggregates[95,96], was found to be differentially expressed in the blood of PD patients with *LRRK2* mutation[97], and was also associated with PD by GWAS[63]. PSMA4, a proteasome subunit, is part of the KEGG-PD pathway (hsa05012, bta05012, and K02728)[92,93] and is a member of the ubiquitin-proteasomal pathway, which plays a key role in Parkinson's disease[98]. It also interacts with Parkin (PARK2) and FBXO7 (PARK15)[82]. HNRNPC interacts with both PARK2 and members of the Poly (ADP-ribose)-dependent cell death pathway implicated in PD[99]. *PLCB4* has been linked to PD[63] and knock-out mice show motor defects consistent with ataxia[100]. However, many of the less conspicuous nodes are also known to play a role in PD, including EGLN3, IPO5, IPO7, PALLD, PGD, RALGPS2, CYCS, SHH, BRCA2, and others (Fig. 6c and Table 3).

Hence, the network derived from our analysis of the ILE368ASN-*PINK1* mutation is revealing the convergence of many known key PD-associated pathways. This convergence suggests that different mutations may feed into the same PD pathology-associated routes and that each mutation can act through several pathways. A good example of such previously unexplored interaction complexity are the interactions between two prominent PD partners, PINK1 and PARKIN. The PINK1 protein is known to interact with PARKIN directly and together

they target damaged mitochondria for degradation[11–13]. However, our data indicates that the presence of the ILE368ASN-*PINK1* mutation results in the dysregulation of several other genes that are possibly upstream of *PARKIN*[101], including *HNRNPC*[99], *MTRNR2L1*[102], *MYL12A*, and *SLC25A4*[103], as well as *LMAN1*, a membrane mannose-binding lectin, which was shown to play a role in PARKIN translocation[104]. This suggests that the direct interaction between PINK1 and PARKIN is not the only means by which PINK1 interacts with the PARKIN pathway.

A strength of our network analysis is that it might shed light on PD-associated genes whose function is so far poorly understood. An example is the mitochondria-localized CHCHD2 protein[105], also called PARK22. Mutations in its gene are linked with autosomal dominant PD, but the precise mechanism is unknown[106]. One hypothesis is that CHCHD2 colocalizes with the mitochondrial contact site and cristae organizing system (MICOS)[106]. However, in the DEG-based protein network, CHCHD2 directly interacts with at least three other proteins, SLC25A4/ANT1 (STRING[59]), GHITM (STRING[59] and GeneMANIA[61]), and NME4 (GeneMANIA[61]). Evidence suggests that *GHITM* plays a role in PINK1-mediated neurodegeneration[107] and *NME4* was shown to be downregulated in PD[75]. SLC25A4 (also known as ANT1) plays an essential role in mitophagy and has been linked to PD pathology[103,108]. Hence, when it comes to mediating pathological changes in CHCHD2-associated PD, the interaction of CHCHD2 with SLC25A4 (ANT1), GHITM, and NME4 may be more relevant than its previously proposed interaction with MICOS in (Fig. 6, in pink).

We also analyzed the correlation of expression between various gene pairs. This correlation may indicate that the genes and their proteins are targets of the same regulatory pathway, or are otherwise related. In our dataset, the expression of several interaction partners shows high correlation, namely PLCB4-RALGPS-TTC3-ZNF37A, EIF3B-HSPA8 (a major network node, ubiquitination pathway)-PCBP1 (ubiquitination pathway). Another cluster centers on MT-CYB and involves both mitochondrial and ubiquitination pathways by NME1–MT-CYB–MT-ND5–MT-CO3–MRPS21 interactions. Among the top pairs are also PSMD7-PSMB5, TAGLN-MYL9, and VWA5A- ZCCHC11 (Supplementary Figs. 16, 17). The interactions of these proteins may, therefore, play a key role in PINK1-mediated PD pathology. To further investigate the involvement of this network in PD, we performed a manual search and found that 68% of the DEGs are already known to be associated with PD (Fig. 7b and Supplementary Data 4), with nearly all major nodes having strong PD association (Table 3 and Fig. 7b). This indicates that these nodes may be key points of integration of the effects of PD pathology, an idea further substantiated by the convergence of the added PARK genes onto these nodes (Supplementary Fig. 9). Furthermore, these nodes form a link between different functional pathways known to be involved in PD. In particular, this is true for CUL3, HSPA8, and PSMA4 (Supplementary Fig. 7 and Supplementary Data 3).

To see whether a reciprocal approach leads to the same conclusion, we looked at whether some of the known PARK proteins directly interact with the network (Supplementary Fig. 9 and Supplementary Table 6). This has revealed that all 19 protein-coding PARK genes form direct interactions with the network, often with several DEGs, as indicated by the size of the node they form when included in the network (Supplementary Fig. 9b, d, DEGs that directly interact with PARK proteins are in pink). Not surprisingly, PARKIN, a known PINK1 partner, was the most strongly associated member of the PARK group with the DEG-based network. The *CHCHD2* gene (*PARK22*) was itself identified as one of the DEGs. The resulting network illustrates that, in spite of the very different nature of PD-associated mutations, the molecular pathways through which the different PARK genes mediate PD pathology are interconnected. In fact, it is often the central nodes which directly interact with proteins of the PARK genes (Supplementary Table 6), which suggests that PD-associated mutations converge on the same network of central nodes, which then mediate common aspects of PD pathology and would explain why mutations in so many genes lead to a similar outcome[109]. As a corollary, any mutation can lead to pathology via several molecular paths. This allows for the involvement of a network which contains many potential modifiers and underscores the role genetic background plays in PD penetrance and severity, as alleles of several network genes may reduce or amplify the effect of any given mutation[12,83].

Another line of supporting evidence for the network's role in PD is that, based on the STRING[59] database search, the most strongly associated KEGG pathway of this dataset is the Parkinson's disease KEGG pathway (Fig. 5c). CYCS, an important node of the network, is part of the KEGG Parkinson's pathway (Supplementary Fig. 9 and Supplementary Data 5). The other three KEGG pathways identified were spliceosome, Huntington's disease, and thermogenesis, in order of decreasing strength of association (Fig. 5c and Supplementary Data 5).

A surprising finding from our work, which examined neurons during their differentiation and up to their early postmitotic state, is that pathways known to play a key role in PD are profoundly and consistently dysregulated at all timepoints examined, far before the onset of PD pathology. This is in line with current research suggesting that pathology far precedes the onset of notable mDA neuron cell death and observable PD motor symptoms[19,110]. For example, the CHCHD2 protein is part of the purine metabolic pathway that produces DNA, RNA, nucleosides, and nucleotides and has been shown to be altered in PD[75–78]. The DEG network illustrates that the expression of a large number of interconnected genes in the aromatic compound metabolic pathway is altered in cells carrying the *PINK1*-ILE368ASN mutation (Supplementary Fig. 7b). In total, 39 genes of the nitrogen compound metabolic process (Ncmp) and 88 genes specific to the aromatic compound metabolic process (Acmp, a subgroup of the Ncmp) are differentially expressed in our dataset (Supplementary Data 3). Many of the DEGs identified in our study are part of more than one pathway and, therefore, interconnect the various pathways known to play a role in PD, including stress and catabolic processes[72,73], aromatic compound metabolism[75], vesicle-mediated transport and exocytosis[79], RNA metabolism[74], protein transport, localization, folding, stability, and ubiquitination[70] (Supplementary Fig. 7a–g and Supplementary Data 3). This confirms observations that PD pathology involves many different pathways[111] and suggests that the final stage is a result of long-term untreated pathology. It also points to possible early alterations which may be detectable and used as a diagnostic tool, as well as to targets for early treatment and prevention of the disease.

To investigate whether the observed transcriptional modifications lead to functional deficits that would further support the relevance of this model, we performed a proteomics analysis at D25 and D40 of the protocol. D21 represents early postmitotic neurons, while D25 represents early mature neurons and D40 mature neurons. Our first analysis showed dysregulation of dopaminergic metabolism at D25 and D40 of differentiation (Fig. 7b and Supplementary Table 8). The list of differentially abundant proteins identified by proteomics analysis exhibits an overlap with the DEGs identified in the sc-RNAseq analysis (Fig. 7b and Supplementary Table 8) and many of these proteins are already known to be involved in PD[112]. Importantly, two proteins that were differentially expressed at both D25 and D40, DDC and TH, are key enzymes involved in dopamine metabolism and closely associated with PD[113,114]. Altogether, four proteins were differentially expressed at both timepoints, in two

independent biological replicates per timepoint (Fig. 7b and Supplementary Table 8). The other two proteins are the cytoskeletal proteins VIM (Vimentin)[115] and NES (Nestin), the latter is co-expressed with the PD-associated gene DJ-1 (PARK7)[116]. These were found to be abnormal also by other studies, and are involved in cytoskeletal transport, which represents a key aspect of PD pathology[112]. Performing a network analysis based on the proteome phenotype revealed a proteomics network related to the transcriptional network (Fig. 7b). In all, these data show a consistent abnormality in the levels of enzymes needed for DA metabolism, which indicates that cells carrying the *PINK1*-ILE368ASN mutation have a functional deficit of the DA metabolic pathway that eventually can lead to neuronal loss of mDA.

The next important step will be to investigate gene expression alterations in aging neurons and how this leads to neurodegeneration in the presence of PD-associated mutations. Genetic background likely plays a greater role in PD caused by mutations with lower penetrance or in idiopathic cases. Therefore, in the future, we will explore the potential overlap between the network identified in this study and the pathways altered by idiopathic disease, as well as the effect of genetic background, by investigating isogenic controls together with cell lines carrying PD mutations. The challenge is that idiopathic cases can be caused by interactions between genes of small effect and the environment, or between environmental factors alone, which potentially broadens the spectrum of pathways involved in the development of PD in these cases[117,118]. Many of these pathways are unlikely to be strongly altered by gene mutations and are likely difficult to distinguish from background noise generated by natural variation in PD-unrelated pathways. Therefore, we first focused to understand the effect of PD-associated mutations of strong effect, in order to detect a core network of pathways distinctly altered in PD.

It will be of great interest to see if cells from idiopathic patients show dysregulation of this integrated network. In fact, our analysis has identified genes, which are known to be associated with sporadic PD, but which had no known connection to molecular mechanisms underlying PD pathology. Knowing how they integrate into the network may point to the mechanism by which they cause PD pathology. For example, one of the top DEGs is *LGI1*[119]. The development of antibodies to the LGI1 protein leads to immunomodulated Parkinsonism, yet there is no known mechanism linking it to PD pathology[119]. In the network, *LGI1* directly interacts with several neighbors (Supplementary Fig. 10). Its most important interaction is its co-expression with CNTNAP2, which is part of the neurexin family and is required for axon organization, and MGMT, which repairs the methylated nucleobase in DNA[59]. From GeneMANIA alone, the strongest evidence is for interaction with GOLT1B, which plays a role in Golgi transport[120]. Hence, LGI1-associated pathology leading to PD symptoms may be mediated through pathways, which are also dysregulated by the presence of the *PINK1*-ILE368ASN mutation. *CNTNAP2* is another very good candidate, as it was shown to be dysregulated in PD patients carrying a mutation in the *LRRK2* gene, providing additional evidence that it likely plays a role in PD pathology[97].

The fact that so many genes which belong to other PD mutation-related pathways were dysregulated by the presence of the *PINK1*-ILE368ASN mutation suggests that pathways involved in PD pathology are far more interconnected than previously thought. It is likely that PD pathology is more a disease with a characteristic network fingerprint than a disease caused by independent mutations acting through unrelated pathways (Fig. 6a). This and future studies will hopefully provide a picture of how various mutations feed into this network and cause its dysregulation. If idiopathic PD is shown to also be mediated by the dysregulation of this network, then we may finally be able to understand the cause of idiopathic PD, which represents 80–85% of all PD cases[2].

Methods

Generation of iPSC cell lines. Fibroblasts (cat. No. ND40066) isolated from a 64-year-old male with PD symptom onset at 33 years of age who carried a homozygous mutation ILE368ASN (P.I368N/P.I368N) (Supplementary Fig. 11) in the *PINK1* gene were obtained from the Coriell Institute (Cat. No. ND40066). Samples were collected in accordance with the US Government guidelines and are subject to an MTA issued by Coriell Institute for Medical Research NINDS Cell Repository. Conditions for use of the NINDS Materials are governed by the Rutgers University Institution Review Board (IRB) and must be in compliance with the Office of Human Research Protection (OHRP), Department of Health and Human Services (DHHS), regulations for the protection of human subjects found at 45 CFR Part 46. Patient consent was obtained before collection as per NINDS requirements, described in Supplementary file "NINDS sample submission guidelines & consent" under the section "Sample Submission". Fibroblasts were cultured on gelatin-coated plates (10% gelatin in PBS, coated for 10 min at room temperature) in KO DMEM + 10% FBS + 1% penicillin/streptomycin (stock was 10,000 units penicillin and 10 mg streptomycin ml^{-1}) at standard culture conditions (37 °C, 5% CO2).

Live adherent fibroblasts in culture media were sent to be karyotyped by Cell Line Genetics, Madison, WI, USA (Supplementary Fig. 1) and confirmed to have a normal karyotype. The reprogramming of fibroblasts into pluripotent stem cells was done at Yale Human Embryonic Stem Cell Core (New Haven CT) using the Sendai virus. The iPSC clone was again analyzed using Array Comparative Genomic Hybridization (aCGH), a high-resolution karyotype analysis for the detection of unbalanced structural and numerical chromosomal alterations and confirmed to be normal (Supplementary Fig. 2 and Supplementary Tables 9, 10). To confirm the presence of homozygous *PINK1* (P.I368N/P.I368N) mutation, PCR was performed using GoTaq (Promega), Cycling: 95oC 30 s, 36x (95oC 15 s, 60oC 20 s, 68oC 15 s), 68oC 5 min. Primers are listed in Supplementary Table 7 (designed using Primer3Plus and synthesized by Eurogentec). The PCR was confirmed by electrophoresis to produce only one band, the remaining reaction was cleaned using a PCR cleaning kit (Pure Link PCR Micro Kit Cat. 310050). The PCR fragment was sequenced by Eurofins Genomics and sequencing results are listed in Supplementary Fig. 11a, b (the sequence underlying Supplementary Fig. 11 has been deposited to NCBI under the accession OK050183.1). The resulting iPSC cell lines were maintained on Geltrex matrix (Gibco) in mTeSR™1 media (StemCell Technologies) under standard incubator conditions of 5% CO2 and humidity. The protocol was approved by the Committee on Human Research at the University of California San Francisco. The control cell line (also known as 17608/6) is described in ref. [38], it was stained for Oct 3/4 and Tra-1-60 in parallel to the PINK1 cell line. The source is the dermal fibroblasts of a healthy 67-year-old male.

Analysis of iPSC status and trilineage potential by TaqMan iPSC Scorecard assay. To confirm the iPSC status of reprogrammed donor fibroblasts, we performed a TaqMan iPSC Scorecard Assay[44], which also confirmed the cells' trilineage potential (Fig. 2b). We followed the protocol described by the manufacturer of the TaqMan hPSC Scorecard Assay (Thermo Fisher Scientific).

Stem cells were cultured on Geltrex matrix (Gibco) in mTeSR™1 media (StemCell Technologies) under standard incubator conditions of 5% CO2 and humidity. On the day of analysis, the cells were dissociated using Accutase and pelleted by centrifugation. RNA was extracted using a Qiagen extraction kit and cDNA was synthesized as per Scorecard kit instructions. Embryonic bodies were generated as per Scorecard kit instructions, RNA was extracted and cDNA synthesized in the same way as for iPSC pellets. The TaqMan hPSC Scorecard Kit 384w plate was amplified using Lightcycler 480 (Roche Diagnostics) and the data were uploaded to the hPSC Scorecard analysis software available online from Thermo Fisher Scientific. The resulting graphs were downloaded and included in Fig. 2.

Immunocytochemistry. A 24-well cell culture plate was seeded with iPSCs, one or two wells per cell line, and the IPSCs were then allowed to form colonies. At least a dozen colonies were present in each well and images were taken of several representative stained colonies. This was performed prior to any major experiment, to confirm the status of the cell line. Any evidence of differentiation identified by a loss of iPSC marker expression was documented. These adherent colonies were fixed in 4% PFA for 10 min, washed and permeabilized with 0.1% Triton X-100 in 1X PBS for 15 min, then washed and incubated in a blocking solution of 2% BSA in 1X PBS for 1 h. They were then incubated with a primary antibody for POU5F1 (also known as Oct 3/4, Santa Cruz Biotechnology, sc-5279) and TRA-1-60 (MAB4360, Merck Millipore) at 1/500 dilution in blocking solution, overnight at 4 °C (Fig. 2a). The next day they were washed three times with PBS and a secondary antibody (AlexaFluor 488, Thermo Fisher) was applied at a 1/1000 dilution in blocking solution and incubated for 1 h at room temperature. The cells were then washed three times with PBS and imaged. Differentiated cells were stained for microtubule-associated protein 2 (MAP2, MAB3418, Merck Millipore), tyrosine hydroxylase (TH, Pel-Freez Biologicals P40101), PAX6 (901301, Imtec diagnostics) at 1/500 dilution, PITX3 (Sigma-Aldrich, HPA044639), LMX1A (Abcam,

ab139726) and SLC6A3/DAT (Thermo fisher, PA1-4656). (Supplementary Table 7 and Supplementary Figs. 3, 13, 14). Images were captured using a confocal Zeiss Laser Scanning Microscope 710 with a 20x air objective and processed using ZEISS ZEN Microscope Software. The same preset parameters were used for the acquisition of images. Images were converted from.czi format to.tiff format and scale bars were added using Fiji open-source software[121].

Differentiation of iPSCs into mDA neurons. The protocol used to differentiate iPSCs into mDA neurons was modified from refs. [24,122] (Table 1). The iPSCs were grown to 95% confluence, dissociated using accutase, and 1.5 wells were combined into one well at day −1. They were allowed to recover in the presence of ROCK inhibitor for about 8 h and then in mTeSR without ROCK inhibitor for about 16 h. After this, day 0 media were applied (Table 1). Both control and *PINK1*-ILE368ASN cell lines were differentiated at the same time so that they would be subject to the same conditions. Different timepoints were generated by repeating the differentiation protocol on a later date, as described in Supplementary Table 2.

Cells were fed fresh media daily, 36 ml per six-well plate or as needed, judging consumption from media color, and replacing media whenever it started to turn yellow, using the appropriate media and factor mix for that day.

Real-time quantitative PCR of mDA and non-mDA markers. Total RNA was extracted from a cell pellet of a 12-well plate well using the RNeasy Plus Universal Kit Mini (50), Catalog no. 73404), as per manufacturer instructions. The RNA concentration was determined through absorption at 260 nm using the Nanodrop instrument (Fisher Scientific). The Superscript IIITM First-Strand Synthesis System for RT-PCR (Invitrogen) was used to prepare cDNA, using oligo(dT)20 and 2 ug of total RNA as per manufacturer instructions. The cDNA was stored at −20 °C.

Primers were designed using Primer Blast[123] and synthesized by Eurogentec Belgium. The primers used are listed in Supplementary Table 7. Standard templates of 90–150 bp in length were generated by PCR, purified using Invitrogen Pure Link PCR Micro Kit (K310050), and their concentration determined using NanoDrop Spectrophotometer. These were then diluted to generate a series of standards of known concentration, from 200 to 0.002 fg μl^{-1}. The cDNA levels within samples were determined using quantitative real-time PCR (QRT-PCR) on a Roche Lightcycler 480 using the Maxima® SYBR Green/ROX qPCR Master Mix (2×) (cat. #K0223) using absolute quantitation by generating a standard curve based on the standards of known concentration and extrapolating the concentration of the unknowns (samples). The parameters were: initial denaturation at 95 °C for 10 min., followed by 40 cycles of 95 °C for 15 s, 60 °C for 30 s, and 72 °C for 35 s. This was followed by a dissociation curve to confirm that only one PCR product was present. Each absolute concentration of a particular gene was then divided by the absolute concentration of a housekeeping gene, in this case, *GAPDH*. In previous experiments, *GAPDH* has been identified as the most stable housekeeping gene in iPSCs and in iPSCs differentiating using our protocol. The values were, therefore, standardized per total RNA of the sample, since 2 ug of total RNA was used for every sample, as well as per expression *GAPDH*.

Statistics and reproducibility. In real-time qPCR graphs, each timepoint consists of at least three independently differentiated samples, seeded at the same time, hence representing biological replicates. The sample concentration was determined by absolute quantitation, comparing the sample concentration to a known concentration of a standard template identical to the one being amplified. The value was standardized to total RNA, by cDNA synthesizing each cDNA sample from a standard amount of total RNA for each sample. This value was then divided by the concentration of *GAPDH* obtained for that particular sample, thus standardizing to *GAPDH* levels and generating a unitless number denoting expression relative to the expression of the housekeeping gene *GAPDH*. *GAPDH* was selected from among a number of possible housekeeping genes, as it showed the best ability to normalize gene expression in a population of untreated samples. A detailed description of this rationale and approach is in Novak et al.[124]. Each of the samples was amplified in duplicate. Each sample value was an average of the experimental duplicate. Standard error was calculated as the standard deviation of the three biological replicates, divided by the square root of the number of samples[125].

To allow for reproducibility through independent analysis, all datasets were made accessible and can be accessed from repositories listed in the Code availability and Data availability sections.

Single-cell RNA sequencing. On the day of collection, cells were dissociated using accutase. The single-cell suspension was spun down and cells were washed with (PBS, 2% BSA) twice, then passed through a 40 µm filter to remove larger cell clumps. The sample was then counted and viability was determined using (Vi-CELL XR, Cell Counter, Beckman Coulter). Cells were required to have at least a 95% viability. The samples were then diluted in PBS with 2% BSA to a final concentration of 190,000 cells ml^{-1}. About 3 ml were then used for single-cell analysis. Subsequently, cells were processed by the Drop-Seq approach[37,126,127] and sequenced.

Microfluidics fabrication for single-cell RNAseq. Microfluidics devices were generated on-site, using a technique described below, which is based on an earlier Drop-Seq protocol[37,128,129]. Soft lithography was performed using SU-8 2050 photoresist (MicroChem) on a 4″ silicon substrate, to generate a 90 µm aspect depth feature. The wafer masks were subjected to silanization overnight using chlorotrimethylsilane (Sigma), before being used for the fabrication of microfluidics. Silicon-based polymerization chemistry was used to fabricate the Drop-Seq chips. In short, we prepared a 1:10 ration mix of polydimethylsiloxane (PDMS) base and cross-linker (Dow Corning), which was degassed and poured onto the Drop-Seq master template. PDMS was cured on the master template, at 70 °C for 2 h. After cooling, PDMS monoliths were cut and 1.25 mm biopsy punchers (World Precision Instruments) were used to punch out the inlet/outlet ports. Using a Harrick plasma cleaner, the PDMS monolith was then plasma bonded to a clean microscope glass slide. After the pairing of the PDMS monolith's plasma-treated surfaces with the glass slide, we subjected the flow channels to a hydrophobicity treatment using 1H,1H,2H,2H-perfluorodecyltri-chlorosilane (in 2% v/v in FC-40 oil; Alfa Aesar/Sigma) for 5 min of treatment. Excess silane was removed by being blown through the inlet/outlet ports. Chips were then incubated at 80 °C for 15 min.

Single-cell isolation and RNA capturing. We determined experimentally that, when using the microfluidics chips, a bead concentration of 180 beads/µL is optimal for an efficient co-encapsulation of the synthesized barcoded beads (ChemGenes Corp., USA) and cells, inside droplets containing lysis reagents in Drop-Seq lysis buffer medium. Barcoded oligo (dT) handles synthesized on the surface of the beads were used to capture cellular mRNA.

For cell encapsulation, we loaded into one syringe each, 1.5 ml of bead suspensions (BD) and the cell suspension. Micro-stirrer was used (VP Scientific) to keep beads in homogenous suspension. For the droplet generation, a QX200 carrier oil (Bio-Rad) was loaded into a 20-ml syringe and used as a continuous phase. To create droplets, we used KD Scientific Legato Syringe Pumps to generate 2.5 and 11 ml/h flowrates for the dispersed and continuous phase flows, respectively. After the droplet formation was optimal and stable, the droplet suspension was collected into a 50-ml Falcon tube. In total, 1 ml of the single-cell suspension was collected. Bright-field microscopy using INCYTO C-Chip Disposable Hemacytometer (Thermo Fisher Scientific) was used to evaluate droplet consistency and stability. To avoid multiple beads per droplet, bead formation and occupancy within individual droplets was monitored throughout the collection process.

The subsequent steps of droplet breakage, bead harvesting, reverse transcription, and exonuclease treatment were carried out as described below, in accordance with the Drop-Seq protocol[37]. The RT buffer was premixed as follows, 1× Maxima RT buffer, 4% Ficoll PM-400 (Sigma), 1 µM dNTPs (Thermo Fisher Scientific), 1 U/ml RNase Inhibitor (Lucigen), 2.5 µM Template Switch Oligo, and 10 U/ml Maxima H-RT (Thermo Fisher Scientific). After Exo-I treatment, INCYTO C-Chip Disposable Hemacytometer was used to estimate the bead counts, and 10,000 beads were aliquoted in 0.2 ml Eppendorf PCR tubes. We then added 50 µl of PCR mix, consisting of 1× HiFi HotStart ReadyMix (Kapa Biosystems) and a 0.8 mM Template Switch PCR primer. The thermocycling program of the PCR was 95 °C (3 min), four cycles of 98 °C (20 s), 65 °C (45 s), 72 °C (3 min) and 9 cycles of 98 °C (20 s), 67 °C (20 s), 72 °C (3 min), and a final extension step of 72 °C for 5 min. After PCR amplification, 0.6× Agencourt AMPure XP beads (Beckman Coulter) were used for library purification according to the manufacturer's protocol. The purified libraries were eluted in 10 µl RNase/DNase-free Molecular Grade Water. We used the Bioanalyzer High Sensitivity Chip (Agilent Technologies) to analyze the quality and concentration of the sequencing libraries.

NGS preparation for Drop-seq libraries. The 3′ end-enriched cDNA libraries were prepared by tagmentation reaction of 600 pg cDNA library using the standard Nextera XT tagmentation kit (Illumina). Reactions were performed according to the manufacturer's instructions. The PCR amplification cycling program used was 95 °C 30 s, and 12 cycles of 95 °C (10 s), 55 °C (30 s), and 72 °C (30 s), followed by a final extension step of 72 °C (5 min). Libraries were purified twice to reduce primers and short DNA fragments with 0.6× and 1× Agencourt AMPure XP beads (Beckman Coulter), respectively, in accordance with the manufacturer's protocol. Finally, purified libraries were eluted in 10 µl Molecular Grade Water. Quality and quantity of the tagmented cDNA library were evaluated using Bioanalyzer High Sensitivity DNA Chip. The average size of the tagmented libraries prior to sequencing was between 400 and 700 bps.

Purified Drop-seq cDNA libraries were sequenced using Illumina NextSeq 500 with the recommended sequencing protocol except for 6 pM of custom primer (GCCTGTCCGCGGAAGCAGTGGTATCAACGCAGAGTAC) applied for priming of read 1. Paired-end sequencing of 20 bases (covering the 1–12 bases of random cell barcode and the remaining 13–20 bases of random unique molecular identifier (UMI)) was performed for read 1, and of 50 bases of the genes for read 2 (Supplementary Fig. 4).

Bioinformatics processing and data analysis. The FASTQ files were assembled from the raw BCL files using Illumina's bcl2fastq converter and run through the

FASTQC codes (Babraham bioinformatics; https://www.bioinformatics.babraham.ac.uk/projects/fastqc/) to check for consistency in library qualities. The monitored quality assessment parameters monitored were (i) per-base sequence quality (especially for the read 2 of the gene), (ii) per-base N content, (iii) per-base sequence content, and (iv) over-represented sequences. The FASTQ files were then merged and converted into binaries using PICARD's FastqToSam algorithm. The sequencing reads were converted into a digital gene expression matrix using the Drop-seq bioinformatics pipeline[37].

Single-cell RNAseq data analysis. The identification of low-quality cells was done separately for each dataset. In order to select only the highest quality data, we sorted the cells by their cumulative gene expression. Only cells with the highest cumulative expression were considered for the analysis[130].

In addition to this filtering, we defined cells as low-quality based on three criteria for each cell. The number of expressed genes must be more than 200 and 2 median absolute- deviations

(MADs) above the median; the total number of counts has to be 2 MADs above or below the median, and the percentage of counts to mitochondrial genes has to be 1.5 MADs above the median. Cells failing at least one criteria were considered as low-quality cells and filtered out from the further analysis. Similar to the cell filtering, we filtered out low-quality genes, identified by being expressed in less than ten cells in the data.

The integration of the filtered matrices of the different datasets was performed using scTransform[131] on a Seurat object[132] based on the treatment. The final gene expression matrix, which was used for the downstream analysis, consisted of 4495 cells and 39,194 genes with a median total number of mRNA counts of 7750 and a median number of expressed genes of 3521. Principal component analysis (PCA) was computed using the 5000 most variable genes of the integrated data. The clustering of data were performed using Louvain clustering. The resolution of the clustering was selected based on the best silhouette score of the different resolutions[133]. A shortlist of manually curated markers was used to validate the different stages of the differentiation process.

We then performed differential expression analysis between the two treatments (control and PINK1) at each timepoint. The differential expression analysis was done using MAST[132] (default parameters) on the normalized counts using the total number of transcripts in each cell as a covariate and the Bonferroni correction to correct for multiple hypothesis testing (Padj). In addition, we tried to find conserved markers among the different timepoints using MAST again and the total number of transcripts in each cell as a latent variable. Genes with fold changes of the same sign in the fold change were then identified across the different timepoints and the average fold change was calculated. The genes with average fold change > 0.1 and maximum adjusted p value < 0.01 were selected as differentially expressed.

The first analysis of pairwise differential expression at each timepoint (adjusted p values (p_{adj}) <0.01 fold changes (FC) >0.1) was performed to identify genes that were upregulated and downregulated in the PINK1 cell line compared to control (see Results section). The analysis was repeated with the exclusion of iPSCs and using only D6, D15, and D21 timepoints. We then used the maximum adjusted p value in a pairwise combination as an adjusted p value, and the average fold change that occurred in the pairwise comparison as fold change threshold hence retained only genes dysregulated in the same direction at all timepoints (Group B). We then took the mean of FC of the different timepoints to reduce the effect of the variability between pairs due to their different differentiation states. The analysis was performed for the four timepoints (iPSCs, D6, D15, and D21), taking into account only the absolute degree of change in iPSCs (Group C). The analysis was then repeated using only timepoints D6, D15, and D21 (Group D).

Network analysis. We extracted protein–protein interaction information between the DEGs from STRING[59] and from GeneMANIA[61]. We excluded indirect association, such as text mining, co-occurrence, and neighborhood from STRING, and co-expression, colocalization, shared protein domains, and predicted interactions from GeneMANIA, retaining only genetic interactions, pathways, and physical interactions (2122 interactions in total). We deleted any genes or interactions that were added by these databases, in order to only focus on DEGs and interactions among them. The network diameter was calculated and betweenness centrality was used to illustrate the relative importance of each node within the network. As a control, we selected the same number of genes at random, using the list of genes detected by our RNAseq analysis, excluding DEGs. This control set did not produce a network and led to a mostly disconnected array of genes (Supplementary Fig. 5). Networks were also generated using the STRING and GeneMANIA inputs independently (Supplementary Fig. 9). We constructed a correlation network based on the correlation of expression of DEGs (p value <0.05, correlation >0.1) and identify edges that are common to the two networks. This network consisted of 860 interactions (Supplementary Fig. 16). We then extracted shared interactions of these two networks, which amounted to 297 interactions (Supplementary Fig. 17a).

In order to validate the PPI network produced by STIRNGdb (v10), we created 50 PPI (protein–protein interaction) networks using 292 random genes (same as the number of DEGs). We then compared the number of detected proteins, the number of interactions between the genes, and the distribution of the node degrees. We performed the Wilcoxon test to access if the two-degree distributions are different from one another in a statistically significant manner, which showed a statistically significant difference ($p = 2.22e-16$) (Supplementary Fig. 17b).

Proteome analysis. Cell pellets were lysed in 1% sodium deoxycholate in 50 mM sodium bicarbonate pH8. After sonication, samples were incubated on ice for 30 min and centrifuged at 4 °C for 30 min at 16,000×g. Supernatants were recovered and quantified using PierceTM BCA Protein Assay Kit (23225, Thermo Scientific). Protein extracts (10 µg) were reduced with 10 mM DTT for 45 min at 37 °C, incubated for 15 min at room temperature, then alkylated with 25 mM iodoacetamide for 30 min at room temperature in darkness. Proteins were further digested overnight at 37 °C with 0.2 µg of trypsin/Lys-C Mix (V507A, Promega). Samples were acidified in 1% formic acid and centrifuged for 10 min at 12,000 × g. Supernatants were recovered and peptides were desalted on Sep-Pak tC18 µElution Plates (Waters, 186002318), dried by vacuum centrifugation, and reconstituted in 25 µl of 1% Acetonitrile/0.05% trifluoroacetic acid.

Following quantification by nanodrop, each sample (200 ng) was analysed by mass spectrometry. The LCMS setup consisted of a Dionex Ultimate 3000 RSLC chromatography system configured in column switching mode. The mobile phases A and B consisted of 0.1% formic acid in water and 0.1% formic acid in acetonitrile, respectively. The loading phase consisted of 0.05% trifluoroacetic acid and 1% acetonitrile in water. The LC system was operated with a Thermo pepmap100 C18 (2 µm particles) 75 µm × 15 cm analytical column (loading 5 ul min^{-1}; analytical 300 nl min^{-1}). The loading column consisted of Thermo pepmap100 C18 (3 µm particles) 75 µm × 2 cm. Samples were separated by a linear gradient ranging from 2% B to 35% B 66 min and sprayed into the mass spectrometer using a Nanospray Flex (Thermo Scientific) ion source. MS acquisition was performed on Q Exactive-HF (Thermo Scientific) operated in data-dependent acquisition mode. MS cycle (AGC MS1 3e6; AGC MS2 1e5) consisted of a high-resolution survey scan (60,000 at 200 m/z) followed by the fragmentation of the top 12 most intense peptides at a resolution of 15,000 at 200 m/z. Dynamic exclusion of already fragmented peptide ions was set to 20 s.

Analysis was performed with the MaxQuant software package version 1.6.17.0[134]. The minimum ratio for LFQ was set to 2. An FDR <1% was applied for peptides and proteins. A human Uniprot database (July 2018) was used to perform the Andromeda search[135]. Oxidized methionine and acetylated N-termini were set as variable modifications while carbamidomethylation on cysteine was set as a fixed modification. Peptide tolerance was 20 ppm. MS intensities were normalized by the MaxLFQ algorithm[136] implemented in MaxQuant while using the match-between-runs feature.

Ethics. Patient-derived cell lines were handled according to the ethics guidelines set out by the National Ethics Board of Luxembourg, (Comité National d'Ethique dans la Recherche; CNER). The use of these cell lines is governed by a materials transfer agreement (MTA) with the NINDS (fibroblast supplier), which states that the conditions for use of the NINDS Materials are governed by the Rutgers University Institution Review Board (IRB) and must be in compliance with the Office of Human Research Protection (OHRP), Department of Health and Human Services (DHHS), regulations for the protection of human subjects found at 45 CFR Part 46. Patient consent was obtained before collection as per NINDS requirements. Samples are collected with informed consent (under IRB approval) and the process is described in Supplementary file "NINDS sample submission guidelines & consent" under the section "Sample Submission". https://catalog.coriell.org/1/NINDS/About/NINDS-Repository-FAQ; https://stemcells.nindsgenetics.org/?line=ND40066

Reporting Summary. Further information on research design is available in the Nature Research Reporting Summary linked to this article.

Data availability

The sequence underlying Supplementary Fig. 11 has been deposited to NCBI under the accession OK050183.1. Single-cell RNAseq data is available through the Gene Expression Omnibus (GEO), accession number GSE183248. The proteomics data is available via the Proteomics Identification Database (PRIDE), identifier PXD028283. The proteomics dataset is available at https://r3lab.uni.lu/frozen/cca2-s098, with a https://doi.org/10.17881/cca2-s098.

Code availability

All analysis scripts are publicly available via: https://gitlab.lcsb.uni.lu/ICS-lcsb/ipscs_pink1.

Received: 15 September 2020; Accepted: 14 December 2021;
Published online: 13 January 2022

References

1. Mayeux, R. Epidemiology of neurodegeneration. *Annu. Rev. Neurosci.* **26**, 81–104 (2003).

2. Klein, C. & Westenberger, A. Genetics of Parkinson's disease. *Cold Spring Harb. Perspect. Med.* **120**, 1297–1305 (2012) https://doi.org/10.1101/cshperspect.a008888.
3. Abbas, M. M., Xu, Z. & Tan, L. C. S. Epidemiology of Parkinson's disease—East versus west. *Mov. Disord. Clin. Pract.* **5**, 14–28 (2018) https://doi.org/10.1002/mdc3.12568.
4. Verschuur, C. V. M. et al. Randomized delayed-start trial of levodopa in Parkinson's disease. *N. Engl. J. Med.* **380**, 315–324 (2019).
5. Brichta, L. & Greengard, P. Molecular determinants of selective dopaminergic vulnerability in Parkinson's disease: an update. *Front. Neuroanat.* **8**, 152 (2014) https://doi.org/10.3389/fnana.2014.00152.
6. Giguère, N., Nanni, S. B. & Trudeau, L. E. On cell loss and selective vulnerability of neuronal populations in Parkinson's disease. *Front. Neurol.* **9**, 455 (2018) https://doi.org/10.3389/fneur.2018.00455.
7. Surmeier, D. J., Obeso, J. A. & Halliday, G. M. Selective neuronal vulnerability in Parkinson disease. *Nat. Rev. Neurosci.* **18**, 101–113 (2017).
8. Chaudhuri, K. R., Healy, D. G. & Schapira, A. H. V. Non-motor symptoms of Parkinson's disease: diagnosis and management. *Lancet Neurol.* **5**, 235–245 (2006) https://doi.org/10.1016/S1474-4422(06)70373-8.
9. Larsen, S. B., Hanss, Z. & Krüger, R. The genetic architecture of mitochondrial dysfunction in Parkinson's disease. *Cell Tissue Res.* https://doi.org/10.1007/s00441-017-2768-8 **373**, 21–37 (2018).
10. Gandhi, S. PINK1 protein in normal human brain and Parkinson's disease. *Brain* **129**, 1720–1731 (2006).
11. Ando, M. et al. The PINK1 p.I368N mutation affects protein stability and ubiquitin kinase activity. *Mol. Neurodegener.* **12**, 32 (2017).
12. Schneider, S. A. & Klein, C. *PINK1* type of young-onset Parkinson disease. *GeneReviews®* (1993).
13. Rakovic, A. et al. PINK1-dependent mitophagy is driven by the UPS and can occur independently of LC3 conversion. *Cell Death Differ.* **26**, 1428–1441 (2019).
14. Furlong, R. M. et al. The Parkinson's disease gene PINK1 activates Akt via PINK1 kinase-dependent regulation of the phospholipid PI(3,4,5)P3. *J. Cell Sci.* **132**, jcs233221 (2019).
15. Dagda, R. K. et al. Beyond the mitochondrion: cytosolic PINK1 remodels dendrites through protein kinase A. *J. Neurochem.* **128**, 864–877 (2014) https://doi.org/10.1111/jnc.12494.
16. Steer, E. K., Dail, M. K. & Chu, C. T. Beyond mitophagy: cytosolic PINK1 as a messenger of mitochondrial health. *Antioxid. Redox Signal.* **22**, 1047–1059 (2015).
17. Sarraf, S. A. et al. PINK1/parkin influences cell cycle by sequestering TBK1 at damaged mitochondria, inhibiting mitosis. *Cell Rep.* **29**, 225–235 (2019).
18. Pryde, K. R., Smith, H. L., Chau, K. Y. & Schapira, A. H. V. PINK1 disables the anti-fission machinery to segregate damaged mitochondria for mitophagy. *J. Cell Biol.* **213**, 163–171 (2016) https://doi.org/10.1083/jcb.201509003.
19. Le, W., Sayana, P. & Jankovic, J. Animal models of Parkinson's disease: a gateway to therapeutics? *Neurotherapeutics* **11**, 92–110 (2014) https://doi.org/10.1007/s13311-013-0234-1.
20. Konnova, E. A. & Swanberg, M. *Parkinson's Disease: Pathogenesis and Clinical Aspects* (Codon Publications, 2018).
21. Ásgrímsdóttir, E. S. & Arenas, E. Midbrain dopaminergic neuron development at the single cell level: in vivo and in stem cells. *Front. Cell Dev. Biol.* **8**, 463 (2020).
22. Tanabe, K., Takahashi, K. & Yamanaka, S. Induction of pluripotency by defined factors. *Proc. Jpn. Acad. Ser. B Phys. Biol. Sci.* **90**, 83–96 (2014) https://doi.org/10.2183/pjab.90.83.
23. Kriks, S. et al. Floor plate-derived dopamine neurons from hESCs efficiently engraft in animal models of PD. *Nature* https://doi.org/10.1038/nature10648.Floor (2012).
24. Kriks, S. *et al.* Dopamine neurons derived from human ES cells efficiently engraft in animal models of Parkinson's disease. *Nature* https://doi.org/10.1038/nature10648 (2011).
25. Arenas, E., Denham, M. & Villaescusa, J. C. How to make a midbrain dopaminergic neuron. *Development* https://doi.org/10.1242/dev.097394 (2015).
26. Hegarty, S. V., Sullivan, A. M. & O'Keeffe, G. W. Midbrain dopaminergic neurons: a review of the molecular circuitry that regulates their development. *Dev. Biol.* https://doi.org/10.1016/j.ydbio.2013.04.014 (2013).
27. Anderegg, A., Poulin, J. F. & Awatramani, R. Molecular heterogeneity of midbrain dopaminergic neurons - Moving toward single cell resolution. *FEBS Lett.* https://doi.org/10.1016/j.febslet.2015.10.022 (2015).
28. Blaess, S. & Ang, S. L. Genetic control of midbrain dopaminergic neuron development. *Wiley Interdiscip. Rev. Dev. Biol.* https://doi.org/10.1002/wdev.169 (2015).
29. Wurst, W., Bally-Cuif, L. & Bally-Cuif, L. Neural plate patterning: upstream and downstream of the isthmic organizer. *Nat. Rev. Neurosci.* https://doi.org/10.1038/35053516 (2001).
30. Corbin, J. G., Rutlin, M., Gaiano, N. & Fishell, G. Combinatorial function of the homeodomain proteins Nkx2.1 and Gsh2 in ventral telencephalic patterning. *Development* https://doi.org/10.1242/dev.00717 (2003).
31. Tiklová, K. et al. Single-cell RNA sequencing reveals midbrain dopamine neuron diversity emerging during mouse brain development. *Nat. Commun.* https://doi.org/10.1038/s41467-019-08453-1 (2019).
32. Przybilla, J., Rohlf, T., Loeffler, M. & Galle, J. Understanding epigenetic changes in aging stem cells - a computational model approach. *Aging Cell* https://doi.org/10.1111/acel.12177 (2014).
33. Bonilla, S. et al. Identification of midbrain floor plate radial glia-like cells as dopaminergic progenitors. *Glia* https://doi.org/10.1002/glia.20654 (2008).
34. Ang, S. L. Transcriptional control of midbrain dopaminergic neuron development. *Development* https://doi.org/10.1242/dev.02501 (2006).
35. Björklund, A. & Dunnett, S. B. Dopamine neuron systems in the brain: an update. *Trends Neurosci.* https://doi.org/10.1016/j.tins.2007.03.006 (2007).
36. Roeper, J. Dissecting the diversity of midbrain dopamine neurons. *Trends Neurosci.* https://doi.org/10.1016/j.tins.2013.03.003 (2013).
37. Macosko, E. Z. et al. Highly parallel genome-wide expression profiling of individual cells using nanoliter droplets. *Cell* https://doi.org/10.1016/j.cell.2015.05.002 (2015).
38. Schöndorf, D. C. et al. IPSC-derived neurons from GBA1-associated Parkinson's disease patients show autophagic defects and impaired calcium homeostasis. *Nat. Commun.* https://doi.org/10.1038/ncomms5028 (2014).
39. Pesce, M. & Schöler, H. R. Oct-4: gatekeeper in the beginnings of mammalian development. *Stem Cells* **19**, 271–278 (2001).
40. Niwa, H., Miyazaki, J. & Smith, A. G. Quantitative expression of Oct-3/4 defines differentiation, dedifferentiation or self-renewal of ES cells. *Nat. Genet.* **24**, 372–376 (2000).
41. Hough, S. R., Laslett, A. L., Grimmond, S. B., Kolle, G. & Pera, M. F. A continuum of cell states spans pluripotency and lineage commitment in human embryonic stem cells. *PLoS ONE* https://doi.org/10.1371/journal.pone.0007708 (2009).
42. Smith, K. P., Luong, M. X. & Stein, G. S. Pluripotency: toward a gold standard for human ES and iPS cells. *J. Cell. Physiol.* **220**, 21–29 (2009).
43. Bhattacharya, B. et al. Gene expression in human embryonic stem cell lines: unique molecular signature. *Blood* **103**, 2956–2964 (2004).
44. Tsankov, A. M. et al. A qPCR ScoreCard quantifies the differentiation potential of human pluripotent stem cells. *Nat. Biotechnol.* **33**, 1182–1192 (2015).
45. Bock, C. et al. Reference maps of human ES and iPS cell variation enable high-throughput characterization of pluripotent cell lines. *Cell* **144**, 439–452 (2011).
46. Fagnocchi, L. & Zippo, A. Multiple roles of MYC in integrating regulatory networks of pluripotent stem cells. *Front. Cell Dev. Biol.* **5**, 7 (2017).
47. Emani, M. R. et al. The L1TD1 protein interactome reveals the importance of post-transcriptional regulation in human pluripotency. *Stem Cell Reports* https://doi.org/10.1016/j.stemcr.2015.01.014 (2015).
48. Lund, R. J. et al. RNA polymerase III subunit POLR3G regulates specific subsets of polyA+ and smallRNA transcriptomes and splicing in human pluripotent stem cells. *Stem Cell Reports* https://doi.org/10.1016/j.stemcr.2017.04.016 (2017).
49. Liu, Q. et al. The miR-590/Acvr2a/Terf1 axis regulates telomere elongation and pluripotency of mouse iPSCs. *Stem Cell Reports* https://doi.org/10.1016/j.stemcr.2018.05.008 (2018).
50. Suresh, B., Lee, J., Kim, H. & Ramakrishna, S. Regulation of pluripotency and differentiation by deubiquitinating enzymes. *Cell Death Differ.* https://doi.org/10.1038/cdd.2016.53 (2016).
51. Fu, Y. et al. IFITM1 suppresses expression of human endogenous retroviruses in human embryonic stem cells. *FEBS Open Bio.* https://doi.org/10.1002/2211-5463.12246 (2017).
52. Madan, B. et al. The pluripotency-associated gene Dppa4 is dispensable for embryonic stem cell identity and germ cell development but essential for embryogenesis. *Mol. Cell. Biol.* https://doi.org/10.1128/mcb.01970-08 (2009).
53. Kwon, S. C. et al. The RNA-binding protein repertoire of embryonic stem cells. *Nat. Struct. Mol. Biol.* https://doi.org/10.1038/nsmb.2638 (2013).
54. Bye, C. R., Rytova, V., Alsanie, W. F., Parish, C. L. & Thompson, L. H. Axonal growth of midbrain dopamine neurons is modulated by the cell adhesion molecule ALCAM through trans-heterophilic interactions with L1cam, Chl1, and semaphorins. *J. Neurosci.* https://doi.org/10.1523/JNEUROSCI.0278-19.2019 (2019).
55. Hoekstra, E. J. et al. Lmx1a encodes a rostral set of mesodiencephalic dopaminergic neurons marked by the Wnt/B-catenin signaling activator R-spondin 2. *PLoS ONE* https://doi.org/10.1371/journal.pone.0074049 (2013).
56. Mesman, S. & Smidt, M. P. Tcf12 is involved in early cell-fate determination and subset specification of midbrain dopamine neurons. *Front. Mol. Neurosci.* https://doi.org/10.3389/fnmol.2017.00353 (2017).
57. Raina, A., Mahajani, S., Bähr, M. & Kügler, S. Neuronal trans-differentiation by transcription factors Ascl1 and Nurr1: induction of a dopaminergic

neurotransmitter phenotype in cortical GABAergic neurons. *Mol. Neurobiol.* https://doi.org/10.1007/s12035-019-01701-x (2020).
58. La Manno, G. et al. Molecular diversity of midbrain development in mouse, human, and stem cells. *Cell* https://doi.org/10.1016/j.cell.2016.09.027 (2016).
59. Szklarczyk, D. et al. STRING v11: protein-protein association networks with increased coverage, supporting functional discovery in genome-wide experimental datasets. *Nucleic Acids Res.* https://doi.org/10.1093/nar/gky1131 (2019).
60. Bastian, M., Heymann, S. & Jacomy, M. Gephi: an open source software for exploring and manipulating networks. *Third Int. AAAI Conf. Weblogs Soc. Media* https://doi.org/10.1136/qshc.2004.010033 (2009).
61. Warde-Farley, D. et al. The GeneMANIA prediction server: biological network integration for gene prioritization and predicting gene function. *Nucleic Acids Res.* https://doi.org/10.1093/nar/gkq537 (2010).
62. Qiu, B. et al. DJ-1 promotes development of DEN-induced hepatocellular carcinoma and proliferation of liver cancer cells. *Oncotarget* https://doi.org/10.18632/oncotarget.14293 (2017).
63. Rouillard, A. D. et al. The harmonizome: a collection of processed datasets gathered to serve and mine knowledge about genes and proteins. *Database* https://doi.org/10.1093/database/baw100 (2016).
64. Puschmann, A. New genes causing hereditary Parkinson's disease or Parkinsonism. *Curr. Neurol. Neurosci. Rep.* https://doi.org/10.1007/s11910-017-0780-8 (2017).
65. Oliveira, L. M. A. et al. Elevated α-synuclein caused by SNCA gene triplication impairs neuronal differentiation and maturation in Parkinson's patient-derived induced pluripotent stem cells. *Cell Death Dis.* https://doi.org/10.1038/cddis.2015.318 (2015).
66. Cruz-Monteagudo, M. et al. Efficient and biologically relevant consensus strategy for Parkinson's disease gene prioritization. *BMC Med. Genomics* https://doi.org/10.1186/s12920-016-0173-x (2016).
67. Volakakis, N. et al. Nurr1 and retinoid X receptor ligands stimulate ret signaling in dopamine neurons and can alleviate α-synuclein disrupted gene expression. *J. Neurosci.* https://doi.org/10.1523/JNEUROSCI.1155-15.2015 (2015).
68. Zhang, Q. S. et al. Beta-asarone protects against MPTP-induced Parkinson's disease via regulating long non-coding RNA MALAT1 and inhibiting α-synuclein protein expression. *Biomed. Pharmacother.* https://doi.org/10.1016/j.biopha.2016.06.017 (2016).
69. Cai, R. et al. Enhancing glycolysis attenuates Parkinson's disease progression in models and clinical databases. *J. Clin. Invest.* https://doi.org/10.1172/JCI129987 (2019).
70. Walden, H. & Muqit, M. M. K. Ubiquitin and Parkinson's disease through the looking glass of genetics. *Biochem. J.* https://doi.org/10.1042/BCJ20160498 (2017).
71. Matheoud, D. et al. Parkinson's disease-related proteins PINK1 and parkin repress mitochondrial antigen presentation. *Cell* https://doi.org/10.1016/j.cell.2016.05.039 (2016).
72. Puspita, L., Chung, S. Y. & Shim, J. W. Oxidative stress and cellular pathologies in Parkinson's disease. *Mol. Brain* https://doi.org/10.1186/s13041-017-0340-9 (2017).
73. Lin, K. J. et al. The overcrowded crossroads: mitochondria, alpha-synuclein, and the endo-lysosomal system interaction in Parkinson's disease. *Int. J. Mol. Sci.* https://doi.org/10.3390/ijms20215312 (2019).
74. Martin, I. Decoding Parkinson's disease pathogenesis: the role of deregulated mRNA translation. *J. Parkinsons Dis.* https://doi.org/10.3233/JPD-150738 (2016).
75. Garcia-Esparcia, P., Hernández-Ortega, K., Ansoleaga, B., Carmona, M. & Ferrer, I. Purine metabolism gene deregulation in Parkinson's disease. *Neuropathol. Appl. Neurobiol.* https://doi.org/10.1111/nan.12221 (2015).
76. Krupke, D. M., Begley, D. A., Sundberg, J. P., Bult, C. J. & Eppig, J. T. The mouse tumor biology database. *Nat. Rev. Cancer* https://doi.org/10.1038/nrc2390 (2008).
77. Bult, C. J. et al. Mouse genome database (MGD) 2019. *Nucleic Acids Res.* https://doi.org/10.1093/nar/gky1056 (2019).
78. Finger, J. H. et al. The mouse Gene Expression Database (GXD): 2011 update. *Nucleic Acids Res.* https://doi.org/10.1093/nar/gkq1132 (2011).
79. Ebanks, K., Lewis, P. A. & Bandopadhyay, R. Vesicular dysfunction and the pathogenesis of Parkinson's disease: clues from genetic studies. *Front. Neurosci.* **13**, 1381 (2020).
80. Funayama, M. *et al.* CHCHD2 mutations in autosomal dominant late-onset Parkinson's disease: a genome-wide linkage and sequencing study. *Lancet Neurol.* https://doi.org/10.1016/S1474-4422(14)70266-2 (2015).
81. Lee, R. G. et al. Early-onset Parkinson disease caused by a mutation in CHCHD2 and mitochondrial dysfunction. *Neurol. Genet.* https://doi.org/10.1212/nxg.0000000000000276 (2018).
82. Stark, C. BioGRID: a general repository for interaction datasets. *Nucleic Acids Res.* https://doi.org/10.1093/nar/gkj109 (2006).
83. Zanon, A., Pramstaller, P. P., Hicks, A. A. & Pichler, I. Environmental and genetic variables influencing mitochondrial health and Parkinson's disease penetrance. *Parkinsons Dis.* https://doi.org/10.1155/2018/8684906 (2018).
84. Canning, P. & Bullock, A. N. New strategies to inhibit KEAP1 and the Cul3-based E3 ubiquitin ligases. *Biochem. Soc. Trans.* https://doi.org/10.1042/BST20130215 (2014).
85. Gao, X. et al. Human Hsp70 disaggregase reverses Parkinson's-linked α-synuclein amyloid fibrils. *Mol. Cell* https://doi.org/10.1016/j.molcel.2015.07.012 (2015).
86. Sala, G. et al. Rotenone down-regulates HSPA8/hsc70 chaperone protein in vitro: a new possible toxic mechanism contributing to Parkinson's disease. *Neurotoxicology* https://doi.org/10.1016/j.neuro.2016.04.018 (2016).
87. Zheng, Q. et al. Hsp70 participates in PINK1-mediated mitophagy by regulating the stability of PINK1. *Neurosci. Lett.* https://doi.org/10.1016/j.neulet.2017.10.051 (2018).
88. Mandel, S. et al. Gene expression profiling of sporadic Parkinson's disease substantia nigra pars compacta reveals impairment of ubiquitin-proteasome subunits, SKP1A, aldehyde dehydrogenase, and chaperone HSC-70. *Ann. N. Y. Acad. Sci.* https://doi.org/10.1196/annals.1344.031 (2005).
89. Liangliang, X. et al. Dominant-positive HSF1 decreases alpha-synuclein level and alpha-synuclein-induced toxicity. *Mol. Biol. Rep.* https://doi.org/10.1007/s11033-009-9623-2 (2010).
90. Ekimova, I. V. et al. New HSF1 inducer as a therapeutic agent in a rodent model of Parkinson's disease. *Exp. Neurol.* https://doi.org/10.1016/j.expneurol.2018.04.012 (2018).
91. Hernandez, S. M., Tikhonova, E. B. & Karamyshev, A. L. Protein-protein interactions in alpha-synuclein biogenesis: new potential targets in Parkinson's disease. *Front. Aging Neurosci.* **12**, 72 (2020).
92. Kanehisa, M. KEGG: Kyoto Encyclopedia of genes and genomes. *Nucleic Acids Res.* https://doi.org/10.1093/nar/28.1.27 (2000).
93. Kanehisa, M., Sato, Y., Furumichi, M., Morishima, K. & Tanabe, M. New approach for understanding genome variations in KEGG. *Nucleic Acids Res.* https://doi.org/10.1093/nar/gky962 (2019).
94. Feng, Y. & Wang, X. Systematic analysis of microarray datasets to identify Parkinson's disease-associated pathways and genes. *Mol. Med. Rep.* https://doi.org/10.3892/mmr.2017.6124 (2017).
95. La Cognata, V., Morello, G., D'Agata, V. & Cavallaro, S. Copy number variability in Parkinson's disease: assembling the puzzle through a systems biology approach. *Human Genet.* https://doi.org/10.1007/s00439-016-1749-4 (2017).
96. Varea, O. et al. Synaptic abnormalities and cytoplasmic glutamate receptor aggregates in contactin associated protein-like 2/Caspr2 knockout neurons. *Proc. Natl. Acad. Sci. USA* https://doi.org/10.1073/pnas.1423205112 (2015).
97. Infante, J. et al. Identification of candidate genes for Parkinson's disease through blood transcriptome analysis in LRRK2-G2019S carriers, idiopathic cases, and controls. *Neurobiol. Aging* https://doi.org/10.1016/j.neurobiolaging.2014.10.039 (2015).
98. Chung, K. K., Dawson, V. L. & Dawson, T. M. The role of the ubiquitin-proteasomal pathway in Parkinson's disease and other neurodegenerative disorders. *Trends Neurosci.* https://doi.org/10.1016/s0166-2236(00)01998-6 (2001).
99. Lee, Y. et al. Poly (ADP-ribose) in the pathogenesis of Parkinson's disease. *BMB Reports* https://doi.org/10.5483/BMBRep.2014.47.8.119 (2014).
100. Kim, D. et al. Phospholipase C isozymes selectively couple to specific neurotransmitter receptors. *Nature* https://doi.org/10.1038/38508 (1997).
101. Zanon, A. et al. Profiling of Parkin-binding partners using tandem affinity purification. *PLoS ONE* https://doi.org/10.1371/journal.pone.0078648 (2013).
102. Guo, B. et al. Humanin peptide suppresses apoptosis by interfering with Bax activation. *Nature* https://doi.org/10.1038/nature01627 (2003).
103. Hoshino, A. et al. The ADP/ATP translocase drives mitophagy independent of nucleotide exchange. *Nature* https://doi.org/10.1038/s41586-019-1667-4 (2019).
104. Hasson, S. A. et al. High-content genome-wide RNAi screens identify regulators of parkin upstream of mitophagy. *Nature* https://doi.org/10.1038/nature12748 (2013).
105. Kee, T. R. et al. Mitochondrial CHCHD2: disease-associated mutations, physiological functions, and current animal models. *Front. Aging Neurosci.* **13**, 660843 (2021).
106. Zhou, W. et al. PD-linked CHCHD2 mutations impair CHCHD10 and MICOS complex leading to mitochondria dysfunction. *Hum. Mol. Genet.* https://doi.org/10.1093/hmg/ddy413 (2019).
107. Sen, N. E. et al. Search for SCA2 blood RNA biomarkers highlights Ataxin-2 as strong modifier of the mitochondrial factor PINK1 levels. *Neurobiol. Dis.* https://doi.org/10.1016/j.nbd.2016.09.002 (2016).
108. Martin, L. J., Semenkow, S., Hanaford, A. & Wong, M. The mitochondrial permeability transition pore regulates Parkinson's disease development in mutant α-synuclein transgenic mice. *Neurobiol. Aging* https://doi.org/10.1016/j.neurobiolaging.2013.11.008 (2014).

109. Inamdar, N., Arulmozhi, D., Tandon, A. & Bodhankar, S. Parkinsons disease: genetics and beyond. *Curr. Neuropharmacol.* **5**, 99–113 (2007).
110. Chaudhuri, K. R., Odin, P., Antonini, A. & Martinez-Martin, P. Parkinson's disease: the non-motor issues. *Parkinsonism Relat. Disord.* **17**, 717–723 (2011).
111. Agarwal, D. et al. A single-cell atlas of the human substantia nigra reveals cell-specific pathways associated with neurological disorders. *Nat. Commun.* **11**, 4183 (2020).
112. Clark, E. H., de la Torre, A. V., Hoshikawa, T. & Briston, T. Targeting mitophagy in Parkinson's disease. *J. Biol. Chem.* **296**, 100209 (2021).
113. Burkhard, P., Dominici, P., Borri-Voltattorni, C., Jansonius, J. N. & Malashkevich, V. N. Structural insight into Parkinson's disease treatment from drug-inhibited DOPA decarboxylase. *Nat. Struct. Biol.* **8**, 963–967 (2001).
114. Tabrez, S. et al. A synopsis on the role of tyrosine hydroxylase in Parkinson's disease. *CNS Neurol. Disord. Drug Targets* **11**, 395–409 (2012).
115. Siciliano, R. A. et al. Decreased amount of vimentin N-terminal truncated proteolytic products in parkin-mutant skin fibroblasts. *Biochem. Biophys. Res. Commun.* **521**, 693–698 (2020).
116. Yan, H. & Pu, X.-P. Expression of the Parkinson's disease-related protein DJ-1 during neural stem cell proliferation. *Biol. Pharm. Bull.* **33**, 18–21 (2010).
117. Chen, H. & Ritz, B. The search for environmental causes of Parkinson's disease: Moving forward. *Journal of Parkinson's Disease* (2018) https://doi.org/10.3233/JPD-181493.
118. Gwinn, K. et al. Parkinson's disease biomarkers: perspective from the NINDS Parkinson's disease biomarkers program. *Biomark. Med.* **11**, 451–473 (2017).
119. Kurtis, M. M., Toledano, R., García-Morales, I. & Gil-Nagel, A. Immunomodulated parkinsonism as a presenting symptom of LGI1 antibody encephalitis. *Parkinsonism Relat. Disord.* https://doi.org/10.1016/j.parkreldis.2015.08.014 (2015).
120. Lin, A., Wang, R. T., Ahn, S., Park, C. C. & Smith, D. J. A genome-wide map of human genetic interactions inferred from radiation hybrid genotypes. *Genome Res.* https://doi.org/10.1101/gr.104216.109 (2010).
121. Schindelin, J. et al. Fiji: an open-source platform for biological-image analysis. *Nat. Methods* **9**, 676–682 (2012).
122. Tomishima, M. *StemBook* (Harvard Stem Cell Institute, 2012).
123. Ye, J. et al. Primer-BLAST: a tool to design target-specific primers for polymerase chain reaction. *BMC Bioinformatics* https://doi.org/10.1186/1471-2105-13-134 (2012).
124. Novak, G. & Tallerico, T. Nogo A, B and C expression in schizophrenia, depression and bipolar frontal cortex, and correlation of Nogo expression with CAA/TATC polymorphism in 3'-UTR. *Brain Res.* **1120**, 161–171 (2006).
125. Novak, G., Fan, T., O'Dowd, B. F. & George, S. R. Striatal development involves a switch in gene expression networks, followed by a myelination event: implications for neuropsychiatric disease. *Synapse* **67**, 179–188 (2013).
126. Trapnell, C. et al. The dynamics and regulators of cell fate decisions are revealed by pseudotemporal ordering of single cells. *Nat. Biotechnol.* https://doi.org/10.1038/nbt.2859 (2014).
127. Sousa, C. et al. Single-cell transcriptomics reveals distinct inflammation-induced microglia signatures. *EMBO Rep.* https://doi.org/10.15252/embr.201846171 (2018).
128. Sousa, C. et al. Single-cell transcriptomics reveals distinct inflammation-induced microglia signatures. *EMBO Rep.* https://doi.org/10.15252/embr.201846171 (2018).
129. Dirkse, A. et al. Stem cell-associated heterogeneity in glioblastoma results from intrinsic tumor plasticity shaped by the microenvironment. *Nat. Commun.* **10**, 1787 (2019).
130. James, N. A. & Matteson, D. S. ecp: an R package for nonparametric multiple change point analysis of multivariate data. *J. Stat. Softw.* https://doi.org/10.18637/jss.v062.i07 (2015).
131. Butler, A., Hoffman, P., Smibert, P., Papalexi, E. & Satija, R. Integrating single-cell transcriptomic data across different conditions, technologies, and species. *Nat. Biotechnol.* https://doi.org/10.1038/nbt.4096 (2018).
132. Finak, G. et al. MAST: A flexible statistical framework for assessing transcriptional changes and characterizing heterogeneity in single-cell RNA sequencing data. *Genome Biol.* https://doi.org/10.1186/s13059-015-0844-5 (2015).
133. Rousseeuw, P. J. Silhouettes: a graphical aid to the interpretation and validation of cluster analysis. *J. Comput. Appl. Math.* https://doi.org/10.1016/0377-0427(87)90125-7 (1987).
134. Cox, J. & Mann, M. MaxQuant enables high peptide identification rates, individualized p.p.b.-range mass accuracies and proteome-wide protein quantification. *Nat. Biotechnol.* **26**, 1367–1372 (2008).
135. Cox, J. et al. Andromeda: a peptide search engine integrated into the MaxQuant environment. *J. Proteome Res.* **10**, 1794–1805 (2011).
136. Cox, J. et al. Accurate proteome-wide label-free quantification by delayed normalization and maximal peptide ratio extraction, termed MaxLFQ. *Mol. Cell. Proteom.* **13**, 2513–2526 (2014).
137. Wongtrakoongate, P., Li, J. & Andrews, P. W. DNMT3B inhibits the re-expression of genes associated with induced pluripotency. *Exp. Cell Res.* **321**, 231–239 (2014).
138. Zhang, J. et al. LIN28 regulates stem cell metabolism and conversion to primed pluripotency. *Cell Stem Cell* **19**, 66–80 (2016).
139. Vitalis, T., Cases, O., Engelkamp, D., Verney, C. & Price, D. J. Defects of tyrosine hydroxylase-immunoreactive neurons in the brains of mice lacking the transcription factor Pax6. *J. Neurosci.* https://doi.org/10.1523/jneurosci.20-17-06501.2000 (2000).
140. Cliburn, R. A. et al. Immunochemical localization of vesicular monoamine transporter 2 (VMAT2) in mouse brain. *J. Chem. Neuroanat.* https://doi.org/10.1016/j.jchemneu.2016.11.003 (2017).
141. Campbell, J. N. et al. A molecular census of arcuate hypothalamus and median eminence cell types. *Nat. Neurosci.* https://doi.org/10.1038/nn.4495 (2017).
142. Sharma, S., Kim, L. H., Mayr, K. A., Elliott, D. A. & Whelan, P. J. Parallel descending dopaminergic connectivity of A13 cells to the brainstem locomotor centers. *Sci. Rep.* https://doi.org/10.1038/s41598-018-25908-5 (2018).
143. Sánchez-González, M. Á., García-Cabezas, M. Á., Rico, B. & Cavada, C. The primate thalamus is a key target for brain dopamine. *J. Neurosci.* https://doi.org/10.1523/JNEUROSCI.0968-05.2005 (2005).
144. Koblinger, K. et al. Characterization of A11 neurons projecting to the spinal cord of mice. *PLoS ONE* https://doi.org/10.1371/journal.pone.0109636 (2014).
145. Malty, R. H. et al. A map of human mitochondrial protein interactions linked to neurodegeneration reveals new mechanisms of redox homeostasis and NF-κB signaling. *Cell Syst.* https://doi.org/10.1016/j.cels.2017.10.010 (2017).
146. Gaare, J. J. et al. Rare genetic variation in mitochondrial pathways influences the risk for Parkinson's disease. *Mov. Disord.* https://doi.org/10.1002/mds.64 (2018).
147. Carpanini, S. M., Torvell, M. & Morgan, B. P. Therapeutic inhibition of the complement system in diseases of the central nervous system. *Front. Immunol.* https://doi.org/10.3389/fimmu.2019.00362 (2019).
148. Kuang, X. L. et al. Reductions of the components of the calreticulin/calnexin quality-control system by proteasome inhibitors and their relevance in a rodent model of Parkinson's disease. *J. Neurosci. Res.* https://doi.org/10.1002/jnr.23413 (2014).
149. Klebe, S. et al. The Val158Met COMT polymorphism is a modifier of the age at onset in Parkinson's disease with a sexual dimorphism. *J. Neurol. Neurosurg. Psychiatry* https://doi.org/10.1136/jnnp-2012-304475 (2013).
150. Hoeffer, C. A. et al. Altered mTOR signaling and enhanced CYFIP2 expression levels in subjects with fragile X syndrome. *Genes Brain Behav.* https://doi.org/10.1111/j.1601-183X.2012.00768.x (2012).
151. Tan, C., Liu, X. & Chen, J. Microarray analysis of the molecular mechanism involved in Parkinson's disease. *Parkinsons. Dis.* https://doi.org/10.1155/2018/1590465 (2018).
152. Jacobs, F. M. J. et al. Identification of Dlk1, Ptpru and Klhl1 as novel Nurr1 target genes in meso-diencephalic dopamine neurons. *Development* https://doi.org/10.1242/dev.037556 (2009).
153. Lindenbach, D., Conti, M. M., Ostock, C. Y., Dupre, K. B. & Bishop, C. Alterations in primary motor cortex neurotransmission and gene expression in hemi-parkinsonian rats with drug-induced dyskinesia. *Neuroscience* https://doi.org/10.1016/j.neuroscience.2015.09.018 (2015).
154. Lavoy, S., Chittoor-Vinod, V. G., Chow, C. Y. & Martin, I. Genetic modifiers of neurodegeneration in a drosophila model of parkinson's disease. *Genetics* https://doi.org/10.1534/genetics.118.301119 (2018).
155. Martin-Urdiroz, M., Deeks, M. J., Horton, C. G., Dawe, H. R. & Jourdain, I. The exocyst complex in health and disease. *Front. Cell .Dev. Biol.* https://doi.org/10.3389/fcell.2016.00024 (2016).
156. Chen, Q., Huang, X. & Li, R. Lncrna MALAT1/miR-205-5p axis regulates MPP+-induced cell apoptosis in MN9d cells by directly targeting LRRK2. *Am. J. Transl. Res.* **10**, 563–572 (2018).
157. Loeffler, D. A., Smith, L. M., Coffey, M. P., Aasly, J. O. & LeWitt, P. A. CSF Nrf2 and HSPA8 in Parkinson's disease patients with and without LRRK2 gene mutations. *J. Neural Transm.* https://doi.org/10.1007/s00702-015-1479-0 (2016).
158. Sun, Y. et al. MLF1 is a proapoptotic antagonist of HOP complex-mediated survival. *Biochim. Biophys. Acta - Mol. Cell Res.* https://doi.org/10.1016/j.bbamcr.2017.01.016 (2017).
159. Emmanuele, V. et al. A novel mutation in the mitochondrial DNA cytochrome b gene (MTCYB) in a patient with mitochondrial encephalomyopathy, lactic acidosis, and strokelike episodes syndrome. *J. Child Neurol.* https://doi.org/10.1177/0883073812445787 (2013).
160. Meixner, A. et al. A QUICK screen for Lrrk2 interaction partners - Leucine-rich repeat kinase 2 is involved in actin cytoskeleton dynamics. *Mol. Cell. Proteomics* https://doi.org/10.1074/mcp.M110.001172 (2011).
161. Odgerel, Z. et al. Whole genome sequencing and rare variant analysis in essential tremor families. *PLoS ONE* https://doi.org/10.1371/journal.pone.0220512 (2019).

162. Kang, H. & Shin, J. H. Repression of rRNA transcription by PARIS contributes to Parkinson's disease. *Neurobiol. Dis*. https://doi.org/10.1016/j.nbd.2014.10.003 (2015).
163. Mamik, M. K. & Power, C. Inflammasomes in neurological diseases: emerging pathogenic and therapeutic concepts. *Brain* https://doi.org/10.1093/brain/awx133 (2017).
164. Itoh, Y. & Voskuhl, R. R. Cell specificity dictates similarities in gene expression in multiple sclerosis, Parkinson's disease, and Alzheimer's disease. *PLoS ONE* https://doi.org/10.1371/journal.pone.0181349 (2017).
165. Morales-Briceño, H. et al. Parkinsonism in PGK1 deficiency implicates the glycolytic pathway in nigrostriatal dysfunction. *Park. Relat. Disord*. https://doi.org/10.1016/j.parkreldis.2019.04.004 (2019).
166. He, B., Bai, Y., Kang, W., Zhang, X. & Jiang, X. LncRNA SNHG5 regulates imatinib resistance in chronic myeloid leukemia via acting as a CeRNA against MiR-205-5p. *Am. J. Cancer Res*. 7, 1704–1713 (2017).
167. Lippolis, R. et al. Altered protein expression pattern in skin fibroblasts from parkin-mutant early-onset Parkinson's disease patients. *Biochim. Biophys. Acta Mol. Basis Dis*. https://doi.org/10.1016/j.bbadis.2015.06.015 (2015).
168. Epping, M. T. et al. TSPYL5 suppresses p53 levels and function by physical interaction with USP7. *Nat. Cell Biol*. https://doi.org/10.1038/ncb2142 (2011).
169. Buniello, A. et al. The NHGRI-EBI GWAS Catalog of published genome-wide association studies, targeted arrays and summary statistics 2019. *Nucleic Acids Res*. **47**, D1005–D1012 (2019).
170. Hashimoto, M., Takeda, A., Hsu, L. J., Takenouchi, T. & Masliah, E. Role of cytochrome c as a stimulator of α-synuclein aggregation in Lewy body disease. *J. Biol. Chem*. https://doi.org/10.1074/jbc.274.41.28849 (1999).
171. Rocha, S. et al. Biological implications of differential expression of mitochondrial-shaping proteins in Parkinson's disease. *Antioxidants* https://doi.org/10.3390/antiox7010001 (2018).
172. Sakaue, S. et al. Early-onset parkinsonism in a pedigree with phosphoglycerate kinase deficiency and a heterozygous carrier: do PGK-1 mutations contribute to vulnerability to parkinsonism? *npj Park. Dis*. https://doi.org/10.1038/s41531-017-0014-4 (2017).
173. Dutta, D. et al. Low levels of prohibitin in substantia nigra makes dopaminergic neurons vulnerable in Parkinson's disease. *Mol. Neurobiol*. https://doi.org/10.1007/s12035-016-0328-y (2017).
174. Lee, J. H. et al. Injury-stimulated Sonic hedgehog expression in microglia contributes to neuroinflammatory response in the MPTP model of Parkinson's disease. *Biochem. Biophys. Res. Commun*. https://doi.org/10.1016/j.bbrc.2016.11.144 (2017).
175. Cheng, X. et al. The BRCC3 regulated by Cdk5 promotes the activation of neuronal NLRP3 inflammasome in Parkinson's disease models. *Biochem. Biophys. Res. Commun*. https://doi.org/10.1016/j.bbrc.2019.11.141 (2020).
176. Bandres-Ciga, S. et al. The endocytic membrane trafficking pathway plays a major role in the risk of Parkinson's disease. *Mov. Disord*. https://doi.org/10.1002/mds.27614 (2019).
177. Zhen, Y. & Li, W. Impairment of autophagosome-lysosome fusion in the buff mutant mice with the VPS33AD251E mutation. *Autophagy* https://doi.org/10.1080/15548627.2015.1072669 (2015).
178. Fu, J., Menzies, K., Freeman, R. S. & Taubman, M. B. EGLN3 prolyl hydroxylase regulates skeletal muscle differentiation and myogenin protein stability. *J. Biol. Chem*. https://doi.org/10.1074/jbc.M608748200 (2007).

Acknowledgements

We thank Dr. Rudi Balling for stimulating discussions. We would like to acknowledge the excellent support by the LCSB Bio-Imaging Facility through Aymeric d'Hérouël, his advice was essential for the analytical part of this manuscript, as well as for the imaging sections, and the outstanding service by the LCSB-Sequencing Platform through Rashi Halder. We thank Francoise Chanut for her very thorough and effective feedback. D.K. and M.B. were financially supported by the PRIDE program of the Luxembourg National Research Fund through PRIDE17/12244779/PARK-QC and PRIDE/10907093/CRITICS, respectively. This work was also made possible in part by the support of S.F. from the Michael J Fox Foundation through Head Start Program and Parkin Consortium grants and from the National Institutes on Aging (RF1 AG058476 and P01 AG54407).

Author contributions

G.N. and A.S. designed the project. G.N. generated the iPS cell lines and performed iPSC characterization, as well as mDA differentiation, sample preparation for single-cell RNAseq, qPCR experiments, and ICC. K.G. performed scRNAseq experiments. D.K. designed the bioinformatic analysis pipeline, performed the bioinformatic analysis, and rendered figures. M.B. artistically rendered article figures, assisted with cell culture, and supplied PAX6 staining figures. G.N. designed and performed the network analysis. G.N. and A.S. supervised the work and wrote the manuscript. The iPSC cell lines were generated under the supervision of S.F., who also helped edit the manuscript. G.D. and S.R. performed proteome analysis. G.N. performed interpretation of the proteomics data.

Competing interests

The authors declare no competing interests.

Additional information

Supplementary information The online version contains supplementary material available at https://doi.org/10.1038/s42003-021-02973-7.

Correspondence and requests for materials should be addressed to Gabriela Novak or Alexander Skupin.

Peer review information *Communications Biology* thanks the anonymous reviewers for their contribution to the peer review of this work. Primary Handling Editor: George Inglis. Peer reviewer reports are available.

Reprints and permission information is available at http://www.nature.com/reprints

Publisher's note Springer Nature remains neutral with regard to jurisdictional claims in published maps and institutional affiliations.